R4 and R12 subfamily RGS proteins – Structures, functions, and emerging chemical biology

Adam Jordan Kimple

A dissertation submitted to the faculty of the University of North Carolina at Chapel Hill in partial fulfillment of the requirements for the degree of Doctor of Philosophy in the School of Medicine (Pharmacology)

Chapel Hill
2010

Approved by:

Advisor: Dr. David P. Siderovski

Reader: Dr. Marion E. Couch

Reader: Dr. Henrik G. Dohlman

Reader: Dr. T. Kendall Harden

Reader: Dr. Franck Polleux

ABSTRACT

ADAM JORDAN KIMPLE:
R4 and R12 subfamily RGS proteins –
Structures, functions, and emerging chemical biology
(Under the direction of Dr. David Peter Siderovski)

It is essential that cells respond to their extracellular environment with appropriate intracellular changes. Many environmental cues are received at the cell membrane, by a family of G-protein coupled receptors (GPCRs) and their heterotrimeric G-proteins, composed of Gα, Gβ and Gγ subunits. Upon binding of a hormone, neurotransmitter, tastant, or small molecule agonist at the membrane-bound GPCR, the receptor catalyzes the exchange of GDP for GTP on the heterotrimeric Gα subunit. This change results in the release of Gβγ from the Gα subunit. The dissociated Gα and Gβγ dimer can each signal to downstream effectors until the Gα hydrolyzes GTP, resulting in the reassociation of the Gαβγ heterotrimer. The duration of effector activation is therefore controlled by the duration of the Gα subunit in its GTP-bound state. The state of Gα as a GTP-bound protein is short-lived, however, given that the protein has an intrinsic ability to hydrolyze GTP to GDP and inorganic phosphate – an activity that can be greatly accelerated by Regulator of G-protein Signaling (RGS) proteins, which are known to act as GTPase-accelerating proteins (GAPs) for Gα subunits. The work described herein represents series of studies aimed at furthering our understanding of the molecular determinants of RGS protein/Gα interaction specificity, facilitating the identification of small molecule modulators of RGS protein activity, and understanding the biochemical function and physiological roles of RGS21.

Toward the first aim, I performed mutagenesis on residues predicted to change the Gα specificity of RGS2 and extensively characterized these mutants using GTP hydrolysis assays and Gα interaction assays employing surface plasmon resonance and *in vitro* FRET. To comprehensively understand the role that each mutation was playing in allowing RGS2 to bind to a non-native Gα binding partner, I solved a crystal structure of a mutant RGS2 in complex with $G\alpha_i$.

Toward the second aim, facilitating the identification of small molecule modulators of RGS protein function, I used a variety of biophysical tools to determine the mechanism of action of the first commercially available RGS protein inhibitor – which was ultimately determined to be a non-specific, thiol-reactive compound. In order to identify new small molecule modulators of RGS protein function, I developed and validated a high-throughput screen for the RGS12/$G\alpha_{i1}$ interaction. This screen was run against several compound libraries, both locally and at the NIH Chemical Genomics Center (NCGC); however, no hits were subsequently validated as *in vivo* inhibitors of the RGS12/$G\alpha_{i1}$ interaction. Given these setbacks, we rethought how we were screening for RGS protein inhibitors and developed a completely novel, enzymatic-based assay that can be used for high-throughput screening.

Toward the final aim, we confirmed the disputed report by von Buchholtz *et al.* that RGS21 is expressed only in chemosensory cells; however, we were also able to identify *RGS21* transcripts in sensory digestive and pulmonary epithelia. Using biochemical methods, we demonstrated that RGS21 exhibits high affinity binding toward a variety of Gα substrates and that it can accelerate their GTP hydrolysis *in vitro*. We also present data that endogenous RGS21 expression serves to negatively regulate tastant receptor signal transduction in a cellular model of gustation.

I dedicate my work:

To my parents and grandparents who taught me the value of hard work and to never give up.

To my brother Randy who always set the bar high.

To my wife Kelly for her loving support.

And to Marley for her endless enthusiasm.

ACKNOWLEDGEMENTS

I would like to express my sincere gratitude to my dissertation advisor, Professor David Siderovski, who first convinced me to come to Chapel Hill and work in a "wetlab." His enthusiasm for science and his attention to detail have nurtured my development as a scientist. He always made the time for my questions and generously provided me with gallons of red ink. Also, I would like to extend my deepest thanks to Dr. Francis Willard, whose unwavering patience and love of science were also critical to my development as a scientist. His depth of understanding of the field and his constant willingness to help continually awes me.

I would like to thank the other members of the Siderovski laboratory, Dr. Melinda Willard, Dr. Chris Johnston, Robin Muller, Susan Siderovski, Stephanie Hutsell, Dr. Patrick Giguere, Dr. Genevieve Laroche, Dr. Emily Oestrich, Dr. Staci Cohen, and Dustin Bosch, who have not only helped me grow as a scientist but also provided friendship:

I would like to thank my MD/PhD classmates, in particular, Lillian Brown, Jason Simmons, Nate Sowa, and Kwun Wah Wen for their support and encouragement on this long journey as well as the "The Program" – notably, Dr. Eugene Orringer, Liz Garman, Alison Regan, and Carol Herion, Linnea Engblom for their help along the way.

I would like to thank the entire staff of the Pharmacology Department, especially Kathy Justice, Tangi Covington, Eddie Gill, Alfred Dolge, Arlene Sandaval and Chris Turner

for all their help over the years in submitting grants, spending grants, and their expertise in navigating “the system.”

Finally and importantly, I would like to thank the members of my dissertation committee: Dr. T Kendall Harden, Dr. Marion Couch, Dr. Franck Polleux, and Dr. Henrik Dohlman for sharing time in their busy schedules to guide my personal and scientific development.

TABLE OF CONTENTS

LIST OF TABLES

Table:

LIST OF FIGURES

ABBREVIATIONS

Å	Angstrom
AGS	activator of G-protein signaling
AlF_4^-	Aluminum tetrafluoride (or tetrafluoroaluminate) ion
C (Cys)	cysteine
C-terminus	carboxyl terminus
C. elegans	Caenorhabditis elegans
Ca^{2+}	calcium ion
cAMP	cyclic adenosine monophosphate
cDNA	complementary DNA
CFP	cyan fluorescent protein
CFTF	cystic fibrosis transmembrane conductance regulator
D (Asp)	aspartic acid
DAG	diacylglycerol
DEP	Dishevelled/EGL-10/Pleckstrin homology
DMEM	Dulbecco's modified eagles medium
DNA	Deoxyribonucleic acid
E (Glu)	glutamic acid
EDTA	ethylenediaminetetraacetic acid
ELISA	Enzyme-linked immunosorbent assay
F (Phe)	phenylalanine
FBS	fetal bovin serum
Fmoc	fluoromethoxy-carbonyl
FP	Fluorescence polarization
FRET	fluorescence resonance energy transfer
g	acceleration by gravity

G (Gly)	glycine
G-protein	Guanine nucleotide binding protein
GAP	GTPase accelerating protein
GDI	guanine nucleotide dissociation inhibitor
GDP	guanosine-5'-diphosphate
GEF	guanine exchange factor
GGL	G-gamma like
GGL domain	G protein gamma subunit like domain
GoLoco	Gi/o-Loco interaction motif
GPCR	G-protein coupled receptor
GRK	G-protein receptor kinase
GST	glutathione S transferrase
GTP	guanosine-5'-triphosphate
GTPase	GTP hydrolase
Gα	alpha subunit of heterotrimeric G protein
$G\alpha_i$	“inhibitory” G protein of adenylyl cyclase
$G\alpha_o$	“other”; most abundant G protein in bovine brain
$G\alpha_q$	“queer”; G protein that is not a substrate for ADP-ribosylation
$G\alpha_s$	“stimulatory” G protein of adenylyl cyclase
$G\alpha_t$	“transducin”; abundant G protein in retinal photoreceptor cells
Gβ	beta subunit of heterotrimeric G protein
Gβγ	beta/gamma subunits of heterotrimeric G protein
Gγ	gamma subunit of heterotrimeric G protein
HA	hemagluttinin epitope tag
HEPES	4-(2-hydroxyethyl)-1-piperazineethanesulfonic acid
His_6	hexahistidine epitope tag
I (Ile)	isoleucine

IP_3	inositol 1,4,5-trisphosphate
IPTG	isopropyl-beta-D-thiogalactopyranoside
K (Lys)	lysine
K_D	dissociation constant
kD (kDa)	kilodalton
koff	dissociation rate constant
kon	association rate contant
LARG	leukemia associated Rho GEF
M	molar
MAPK	mitogen activated protein kinase
Mg^{2+}	magnesium ion
N (Asn)	asparagine
N-terminus	amino terminus
Na^{+}	sodium ion
NaCl	sodium chloride
NCGC	National Chemical Genomic Consortium
NH^{3+}	free amino group
NHS	N-Hydroxysuccinimide
Ni^{2+}	nickel ion
nm	nanometers
nM	nanomolar
NTA	nickel-nitrilotriacetic acid
P (Pro)	proline
Pcp2	purkinje cell protein 2
PCR	Polymerase chain reaction
PDB	Protein Data Bank
PDZ	PSD-95/Dlg/ZO-1 homology domain

PKA	protein kinase A
PLC	phospholipase-C
PTB	phosphotyrosine binding domain
PTX	pertussis toxin
Q (Gln)	glutamine
R (Arg)	arginine
RBD	Ras binding domain
RGS	regulator of G-protein signaling
RIKEN	Rikagaku Kenkyūsho (Japanese Natural Science Research Institute)
RMSD	Root mean square deviation
RU	resonance units
S (Ser)	serine
S. cerevisiae	Saccharomyces cerevisiae
S200	sephadex 200 gel exclusion column
SDS	sodium dodecyl sulfate
SDS/PAGE	SDS polyacrylamide gel electrophoresis
SGC	Structural Genomic Consortium
SPR	surface plasmon resonance
T (Thr)	threonine
TBS	tris-buffered saline
TBS-T	TBS with 0.001% tween-20
TEV	tobacco etch virus
TPR	tetratricopeptide repeat
TRIS	tris(hydroxymethyl)aminomethane
UNC	University of North Carolina at Chapel Hill
V (Val)	valine
w/v	weight-to-volume

w/w	weight-to-weight
Y (Tyr)	tyrosine
YFP	yellow fluorescent protein

CHAPTER 1

GENERAL INTRODUCTION

Overview: *G-protein coupled receptors and heterotrimeric G-proteins are critical to relaying information from the extracellular environment into the intracellular compartment. This chapter provides a broad overview of GPCR signaling, Regulators of G-protein Signaling (RGS proteins), and Guanine nucleotide Dissociation Inhibitors (GDIs) of heterotrimeric G-proteins.*

Elements of this work referenced in this chapter have been published in:

> Siderovski, D. P., Kimple, A. J., Willard, F. S. Large G-Proteins. Ed. Begley, T. P. Wiley Encyclopedia of Chemical Biology. Hoboken, N.J.: John Wiley & Sons, 2009.

1.1 PHARMACEUTICAL AND BIOLOGICAL IMPORTANCE OF G-PROTEIN COUPLED RECEPTOR SIGNALING

In order for a cell to adapt to its environment, it must be able to receive extracellular cues and then elicit an intracellular response. While there are multiple receptor families (*i.e.*, receptor tyrosine kinases, ion channels, nuclear receptors), G-protein coupled receptors (GPCRs) represent the largest and most pharmacologically important family. Approximately 1% of the human genome is dedicated to these receptors [1, 2] and over 50% of the pharmaceuticals prescribed annually target one or more of these receptors [3, 4]. In addition to being the largest component of the druggable proteome, GPCRs are also responsible for our ability to perceive the visual, olfactory, and gustatory cues in our environment. Missense and truncation mutations in individual codons in genes encoding GPCRs results in a myriad of pathologies including color blindness, retinitis pigmentosa, pseudohermaphrotidism, and Hirschsprung's disease [5]. Because of the importance of GPCRs in both pathology and treatment of disease, it is critical we comprehensively understand these receptors and their downstream components.

At the most basic level, GPCRs consist of seven α-helical transmembrane stretches with an extracellular N-terminus and an intracellular C-terminus. These diverse receptors can be further divided into subfamilies named by their hallmark member: glutamate-, rhodopsin-, adhesion-, frizzled-, and secretin-like [1, 6]. While the precise mechanism of activation of the heterotrimeric G-protein varies from family to family and remains elusive, in simplest terms upon binding of a hormone, neurotransmitter, ion, or other stimuli, the GPCR undergoes conformation changes that allow the activation of the Gα(GDP)/Gβγ complex.

Upon ligand binding, the GPCR catalyzes the release of GDP and subsequent binding of GTP on the Gα subunit [7-9].

1.2 THE CLASSIC GUANINE NUCLEOTIDE CYCLE

Heterotrimeric G-proteins act as molecular switches that are in the off state when bound to GDP and are activated when GTP bound. In the basal state, the GDP bound Gα-subunit is bound to the Gβγ subunit (Figure 1.1). The Gα/Gβγ interaction serves to enhance localization to the membrane, to enhance coupling, and to slow the spontaneous dissociation of GDP (reducing constitutive activity) [10-13]. Upon an agonist-induced conformational change, the receptor acts as a guanine nucleotide exchange factor resulting in the displacement of GDP and subsequent binding of GTP. The nucleotide pocket of the heterotrimeric G-protein alpha subunit is surrounded by three flexible switch regions that undergo dramatic conformational changes depending on nucleotide state [14, 15]. The binding of GTP and subsequent change in the switch regions results in the dissociation of the GTP-bound Gα from Gβγ. At this point, the activated Gα subunit and the Gβγ obligate heterodimer are able to interact with effectors such as adenylyl cyclase, phospholipase C isoforms, RhoGEFs, and ion channels [7, 16-21].

1.3 G-PROTEIN SUBUNITS

1.3.1 Gα

The Gα subunit, in its inactive state, binds GDP within a nucleotide-binding pocket circumscribed by residues derived from both of its constituent domains: a Ras-like domain (resembling the structural fold of small G-proteins) and an all α-helical domain unique to the

large Gα family, comprising a structurally distinct six-helix bundle (Figure 1.2A). An extended N-terminal α-helix is modified by covalent attachment of the fatty acids myristate and/or palmitate, which facilitates membrane targeting as well as assembly with Gβγ subunits [22]. Exchange of GDP for GTP is catalyzed in a poorly understood process by an activated GPCR which acts as a guanine nucleotide exchange factor for the Gα·GDP/Gβγ heterotrimer [8, 9] and causes a structural rearrangement within three switch regions (I-III) of Gα (Figure 1.2B) that results from nucleotide-pocket residues interacting with the γ-phosphate of the newly-bound GTP [23, 24]. The particular conformations of these three switch regions are critical to the protein/protein interactions that Gα makes with its nucleotide-selective binding partners such as Gβγ, effectors, RGS proteins, and GoLoco motifs [14, 15, 25, 26].

1.3.2 Gβγ

Gβ and Gγ subunits form tightly associated heterodimers (Figure 1.3). Gβ begins with an extended N-terminal α-helix and is composed mainly of a β-propeller fold formed by seven individual segments of a ~40-amino acid sequence known as the WD-40 repeat. Gγ is an extended stretch of two α-helices joined by an intervening loop. Assuming no significant tertiary structure on its own, the N-terminus of Gγ participates in a coiled-coil interaction with the N-terminal α-helix of Gβ (Figure 1.3); much of the remainder of Gγ binds along the outer edge of the Gβ toroid [27, 28]. Gγ is prenylated posttranslationally on a cysteine residue that is four amino acids from the C-terminus: Most Gγ subunits receive a 20-carbon geranylgeranyl group at this position (Fig 1.3), whereas Gγ1, Gγ8, and Gγ11 alternatively receive a 15-carbon farnesyl group [22]. This lipid modification aids in the resultant

membrane localization of the Gβγ heterodimer that is important to receptor coupling. Gβγ and GDP-bound Gα form the G-protein heterotrimer via two principal sites of interaction: 1) extensive burial of the β3/α2 loop and α2 helix (switch II) of Gα within six of the seven WD repeats of Gβ, and 2) contact between the side of the first β-propeller blade of Gβ and the extended N-terminal helix of Gα [14, 15]. These extensive interactions form the basis for competition for Gβγ binding between Gα·GDP and βγ-effectors. Structures of Gβγ bound to the βγ-effector GRK2, the regulatory protein phosducin, and SIGK (a peptide capable of disrupting effector activation) have shown that the effector-binding site on Gβγ overlaps significantly with the region responsible for binding switch II of Gα near the central pore of the Gβ toroid [29-31].

1.4 GTP HYDROLYSIS

The mechanism of GTP hydrolysis by Gα has been discerned from x-ray diffraction crystallographic structures of the Gα transition state-mimetic form (Gα bound to GDP and AlF_4^-) [32], as well as hydrolysis reaction intermediates including Gα bound to guanosine 5'-(βγ-imido)triphosphate (GppNHp) or GDP plus inorganic phosphate [33, 34]. The GTP hydrolysis reaction is mediated by three conserved Gα amino acids (Figure 1.4; residues numbered as found in $G\alpha_{i1}$). Glutamine-204 in switch II coordinates the critical nucleophilic water molecule responsible for hydrolysis of the γ-phosphate, whereas arginine-178 and threonine-181 (both from switch I) help to stabilize the leaving group (as mimicked by the planar anion AlF_4^-), with the latter coordinating a bound Mg^{2+} ion [32].

1.5 GTPase ACCELERATING PROTEINS

Intrinsic GTP hydrolysis was initially thought to control the lifetime of G-protein alpha subunits in their GTP bound state and the *in vitro* kinetics of GTP hydrolysis by $G\alpha_s$ supported this hypothesis [35]; however, intrinsic rates of GTP hydrolysis measured *in vitro* could not account for the fast deactivation kinetics seen with other G-proteins in the cellular context. For instance, purified transducin, which is the heterotrimeric G-protein that couples to the photoreceptor rhodopsin, hydrolyzes GTP with a $t_{½}$ of ~15 seconds; however, the rate of retinal deactivation is <1 sec [36]. Additionally, G-protein coupled inwardly-rectifying potassium channels (GIRKs), which are activated by $G\beta\gamma$ freed from $G\alpha_i$ subunits, are deactivated 100 times faster than would be predicted based on the intrinsic GTP hydrolysis rate exhibited by $G\alpha_i$ subunits *in vitro* [37, 38]. The first evidence that the cycle of nucleotide binding and hydrolysis could be modulated by binding partners other than $G\beta\gamma$ came from the report of Berstein *et al*. demonstrating that the $G\alpha_{q/11}$ effector PLC-β1 could also increase the rate of GTP hydrolysis by $G\alpha_{q/11}$ [39]. While PLC-β1 seemed to have paradoxical roles being both an effector and a GTPase Accelerating Protein (GAP) for $G\alpha_{q/11}$, this report provided the first demonstration of a GAP for heterotrimeric G-proteins, although GAPs had been known for Ras-family GTPases for at least five years previously [40]. The first evidence of non-effector GAPs for heterotrimeric G-proteins came from a yeast-based genetic screen for mutants that increased sensitivity of *Saccharomyces cerevisiae* to α-factor pheromone. These screens identified two primary factors that made yeast supersensitive to α-factor, supersensitive 1 (Sst1) and supersensitive 2 (Sst2) [41, 42]. In these initial studies, Sst1 acted as a "barrier" inhibiting the diffusion of α-factor in solution [42]. Consistent with this initial description, Sst1 (also known as Bar1) is now known to encode an extracellular

protease that degrades α-factor in the environment [43]. While the molecular details of Sst2's function remained enigmatic for seven more years, unlike Sst1 it was speculated to inhibit the pheromone response in the intracellular compartment [42]. Once the components of the pheromone pathway had been rigorously elucidated [44-47], work by Dr. Henrik Dohlman and colleagues demonstrated that the overexpression of the yeast Gα subunit (GPA1) suppressed the supersensitivity of Sst2 mutant yeast but overexpression of Gβ subunit (Ste4) was not able to suppress the phenotype [48]. While these experiments were not able to demonstrate conclusively a binary interaction between Sst2 and GPA1, it helped establish the groundwork for the discovery of a novel family of negative regulators of G-protein coupled receptor signaling by multiple groups [49-55].

This newly identified family of proteins, the Regulators of G-protein Signaling (RGS proteins), is characterized by the presence of a nine α-helical bundle that binds selectively to the Gα transition state for GTP hydrolysis [25, 56]. The nine helices can be subdivided into two subdomains, the first of which is composed of helices αI, II, III, VIII and IX while the remaining subdomain is comprised of helices αIV, V, VI, and VII, with each subdomain arranged in antiparallel helical bundles (Figure 1.5A). Unlike the GAPs for small G-proteins [57], RGS proteins do not contribute any single residue to the nucleotide binding pocket that is necessary for the catalytic mechanism. Their catalytic activity has been established by x-ray diffraction crystallography and NMR structures of isolated RGS proteins, as well as RGS protein/Gα protein complexes [25, 56, 58-61]. RGS proteins are selective for binding most avidly to the transition state of Gα(GTP→GDP) which can be mimicked by Gα(GDP) bound with the planar ion aluminium tetrafluoride (AlF_4^-) [49, 62, 63]. Three critical contacts are formed between RGS proteins and their Gα partners [25, 60, 61]. The amide of

Asn 122 (residue numbered as in human RGS8) forms a hydrogen bond with the critical glutamine of Gα responsible for GTP hydrolysis, *e.g.*, Gln 204 of $G\alpha_{i3}$. This helps orient the glutamine residue to stabilize the terminal phosphate that is being hydrolyzed from GTP (as mimicked by the AlF_4^- ion). A second Asn (e.g. Asn of RGS8) contacts the side chain hydroxyl of a Switch I threonine (Thr 182 in $G\alpha_{i3}$) allowing the side chain hydroxyl to contact the Switch II Lys (Lys 210 in $G\alpha_{i3}$). This locks Switch I and Switch II into their transition state conformations. Additionally an aspartate residue in the C terminus of the RGS domain (Asp 157 in RGS8), which is conserved in all RGS proteins except RGS2, serves to stabilize the backbone amine of the Gα Switch I Thr 182 (allowing the neighboring Thr 181 side chain hydroxyl group to stabilize the Mg^{2+} cation (Figure 1.6). The numerous contacts made by Thr 182 highlight the importance of this switch I region in Gα in stabilizing the RGS domain/Gα interaction and, in addition, explain the profound loss of binding and GAP activity that occurs when the neighboring glycine (Gly 183 in $G\alpha_{i3}$) is subtly changed to serine. This "RGS-insensitivity" point mutation (Gly 183 to serine) was originally identified by Dohlman and colleagues in Gpa1, the Gα subunit of the yeast *Saccharomyces cerevisiae* [64], functions equivalently in mammalian Gα subunits such as $G\alpha_{i1}$, $G\alpha_o$, and $G\alpha_q$ [65, 66], and additionally has been shown to leave all other functions of Gα intact, including intrinsic nucleotide binding and hydrolysis activities, as well as coupling to Gβγ, receptor, and effectors [65, 67-70].

Thirty-seven RGS proteins are encoded by gene loci in the human genome – a collection of related proteins which can be divided into 10 different subfamilies (Figure 1.7). The largest is known as the R4 family and contains 10 members: RGS1, -2, -3, -4, -5, -8, -13, -16, -18, and -21. R4 family members are the smallest and simplest of the RGS proteins and,

with the exception of RGS3, consist of a single RGS domain with minimal additional amino acids at their N- and C-termini. With the exception of RGS2 [59, 71], members of this family accelerate the hydrolysis of GTP by both G_i and G_q family Gα subunits (Figure 1.8) [56, 72]. With little biochemical selectivity between $G\alpha_{i1}$, $G\alpha_{i2}$, $G\alpha_{i3}$, $G\alpha_o$, and $G\alpha_q$ substrates, and no additional regions containing obvious domain structures, members of this subfamily would be predicted to act promiscuously as negative regulators of Gi- and Gq-coupled GPCRs; however, early work of Wilkie and Muallem demonstrated that the N-termini of R4 family members, outside of the canonical RGS domain, can provide specificity to the *in vivo* potency of R4 protein GAP activity on specific receptors [73, 74]. While it is not entirely clear how these terminal extensions on R4 family RGS domains enhance specificity, it has been suggested that selectivity towards particular GPCR signaling pathways is mediated by the binding of adaptor proteins such as spinophilin [75] or through direct interactions with receptors [74, 76, 77]. In addition to receptor specificity that is dependent on the N-terminus, point mutations have been identified that affect the overall *in vivo* stability of RGS protein in overexpression studies [78]. The physiological relevance of the N-terminus in regulating degradation of RGS proteins is supported by the identification of a hypertensive cohort who had a single nucleotide polymorphism in the gene loci of RGS2 that results in a Gln-2-Leu mutation resulting in destabilization of RGS2 and subsequent hypertension [79].

While the biochemical role of RGS proteins as GTPase-accelerating proteins has been well characterized [49, 56, 80, 81], and the cellular role of RGS proteins in attenuating GPCR-mediated signaling is also established [82-85], it has remained a more arduous task to characterize the specific roles of RGS proteins in animal models. Of the R4 family members,

five mouse knockout models have been published to date. Using a RGS1-deficient mouse strain, the Kehrl laboratory reported on the observed importance of RGS1 in negatively regulating CXCR4 and CXCR5 chemokine receptor signaling in B-lymphocytes and the necessity of RGS1 expression for the proper maturation of germinal centers [86]. A different immune system phenotype was identified by the Druey lab in RGS13-deficient mice. Their research demonstrated that loss of RGS13 resulted in increased mast cell degranulation and anaphylaxis. Classically, deregulation occurs when the antigen-bound immunoglobulin E (IgE) interacts with the IgE receptor (FcεRI) which is not a G-protein coupled receptor [87-90]; however, Druey and colleagues showed that RGS13 acts in a GAP-independent manner to negatively regulate IgE-mediated degranulation. They determined the amino-terminal 51 amino acids (outside of the RGS domain) bind the p85α regulatory subunit of phosphatidylinositol-3-OH kinase preventing the activation of antigen-induced, PI(3)K-mediated, degranulation [91]. In addition to their role in B-cells and mast cells, RGS proteins have been shown to be important in response to immune system function. RGS2 was originally identified as a gene upregulated upon activation of blood mononuclear cells by the plant lectin ConA or treated with cycloheximide [92-94]. In studies of RGS2-deficient mice, the Siderovski and Penninger labs were able to show that, unlike RGS1-deficient mice, RGS2-deficient mice have normal B cell quantities and differentiation; however, RGS2-deficient mice were unable to mount a robust T-cell mediated immune response. RGS2-deficient T-cells, when compared to wildtype T-cells, were impaired in their ability to proliferate in response to T-cell receptor engagement, to treatment with phorbol myristate acetate (PMA) and Ca^{2+}-ionophores, or to anti-CD3ε cross-linking, with or without CD28 co-receptor engagement [95]. Additionally, T-cells had an impaired ability to secrete

interleukin-2 (IL-2) in response to an immune challenge. While the diminished IL-2 secretion could account for the decreased proliferation [96], supplementation of IL-2 was unable to stimulate T-cell proliferation to levels seen in wildtype T-cells, suggesting that the observed phenotype was not the result of decreased IL-2 production [95].

In addition to their roles in modulating immune responses, R4 family RGS proteins have been shown to regulate vascular development and physiology [97]. Maintenance of vascular perfusion of the entire body is a delicate balance. On one hand, if arterial pressure is significantly decreased, regional hypoxia and coagulative necrosis will destroy tissue; however, if arterial pressure is elevated, the risk of heart failure, stroke, and kidney disease are dramatically increased [98]. One crucial component to maintaining normotension is vascular resistance, which is dynamically modulated by the vascular smooth muscle that lines blood vessels. Given that vessel resistance (R) is inversely proportional to vessel radius (r) to the fourth power ($R \propto 1/r^4$), small changes in the lumen of a vessel can have dramatic change in the resistance and thus the vascular pressure [99]. GPCRs are crucial mediators of vasodilation and vasoconstriction [100]; for example, angiotensin II, norepinephrine, vasopressin, and acetylcholine cause vasocontriction by activating GPCRs coupled to $G\alpha_{q/11}$ which subsequently activate phospholipase C (PLC) [100]

The *in vitro* specificity of RGS2 toward $G\alpha_q$ [59, 71] and the multitude of $G\alpha_q$ coupled GPCRs that control vasoconstriction suggest that RGS2 might be an important negative regulator in inhibiting vascular smooth muscle constriction. The first demonstration of the importance of RGS2 in regulating blood pressure came from studies of RGS2-deficient mice [95] that characterized RGS2-deficient animals as having constitutive hypertension [101-103]. Further evidence supporting the role of RGS2 in maintaining normo-static blood

pressure has come from human population-based studies of hypertensive cohorts. These studies have identified single nucleotide polymorphisms within the coding region of RGS2 that results in a decrease of proper localization of RGS2 to the plasma membrane and a resultant decrease of its inhibitory influence on $G\alpha_q$-mediated vasoconstrictive hormone signal transduction [79, 101]. While the loss of RGS2 results in constitutive hypertension, mice deficient in RGS5, which is highly expressed in pericytes, exhibit constitutive *hypotension*, suggesting that RGS5 might be a critical negative regulator of vasodilatory signaling or vascular development [104]. While the mechanism by which RGS5 assists in the maintenance of normal blood pressure remains to be established, RGS5 has been observed to be highly expressed in vascular smooth muscle and pericytes [105, 106]. The high expression of RGS5 in pericytes of angiogenic tumor vessels [107] led Hamzah and colleagues to cross RGS5-deficient mice with a tumorgenic mouse strain which rapidly develops insulinomas [108]. The tortuosity and dilated nature of the vessels characteristic of insulinomas derived from wild–type mice were lost in the RGS5-deficient line. Instead, the blood supply in RGS5-deficient insulinomas had a regular appearance with normal branching reminiscent of normal developmental angiogenesis in organs [108, 109]. While the precise role that RGS5 is playing in the neovascularization of tumors is unclear, it is apparent that RGS5 is a critical component of maintaining normal blood pressure and proper angiogenesis.

An additional RGS-deficient mouse model identified to have a cardiovascular phenotype is the RGS4-deficient mouse [110]. In this mouse, the RGS4 promoter was used to drive the expression of beta-galactosidase allowing expression of the *Rgs4* gene to be characterized by histochemical staining. The authors reported high levels of expression of the *Rgs4* gene locus in the sinoatrial node [111], an anatomical region of the heart which serves to initiate and

control the timing of cardiac contractions [112]. In the absence of RGS4 expression, basal heart rates were identical to wildtype; however, upon activation of the parasympathetic system by the administration of carbachol, RGS4-deficient mice had an exaggerated decrease in heart rate as compared to wildtype controls [111]. In examining isolated sinoatrial myocytes from RGS4-deficient and control animals, Cifelli and colleagues also observed a decreased frequency of action potential initiation in response to activation of the parasympathetic nervous system by carbachol administration [111].

While R4-family members have been implicated in the modulation of cardiovascular function through these mouse knockout studies [110, 111], it was also expected that RGS4-deficient mice would also have altered pre-pulse inhibition of acoustic startle (an animal model of schizophrenia), based on human population studies of gene transcripts found decreased in schizophrenia [113]; however, the *Rgs4* knockout mouse strain has not yet produced a significant phenotype relating to experimental tests of schizophrenia [110]. While it is possible that RGS4 is not involved in the pathogenesis of schizophrenia, it is equally possible that developmental compensation by other R4 family members has masked phenotypes that could otherwise have been observed in the absence of RGS4 expression. To overcome the limitations of knocking out individual RGS proteins and looking for phenotypes in the presence of developmental compensation, Wyeth Laboratories produced two transgenic rat strains that overexpressed either wild-type $G\alpha_q$ or RGS-insensitive $G\alpha_q$ using a pan-neuron Thy1.2 promoter [106-110]. Inhibition of the $G\alpha_q$ coupled serotonin receptor 5-HT_{2C} is associated with weight gain associated with atypical anti-psychotic medications [114-116], which antagonize a wide range of dopamine and serotonin receptors [117-119]. RGS-insensitive $G\alpha_q$ transgenic rats exhibited lower basal weight as well as a

greater decrease in food intake upon the administration of the 5-HT_{2C} agonist Ro 60-175 [120]. While these results are suggestive that an unidentified RGS protein negatively regulates activation of the 5-HT_{2C}, additional studies are required to identify the specific RGS protein involved in regulating this system. Additionally, these studies should be verified in an animal model that expresses RGS-insensitive $G\alpha_q$ at endogenous levels. Systemic administration of (±)-2,5-dimethoxy-4-iodoamphetamine (DOI), a 5-HT_{2A} specific agonist, leads to increased secretion of oxytocin, corticosterone, ACTH, and prolactin by the hypothalamus [121]. Using the same rat RGS-insensitive $G\alpha_q$ transgenic model, Shi and colleagues reported a role of endogenous RGS proteins in regulating serotonin-induced oxytocin release yet having no effect on serotonin-induced ACTH release [122].

Such transgenic studies are not ideal because one has to deconvolute the changes in phenotypes induced by overexpression of additional Gα from the expression of RGS-insensitive Gα. To overcome these difficulties, Neubig and colleagues have made knock-in mice expressing RGS-insensitive $G\alpha_o$ or $G\alpha_{i2}$ [123], thereby providing endogenous levels of Gα subunit expression. Goldstein *et al*. demonstrated that the loss of RGS-mediated GAP activity on $G\alpha_o$ results in greater therapeutic effects of epinephrine and norepinephine in inhibiting epileptiform activity in hippocampal slices [123]. Huang *et al*. showed that RGS-insensitive $G\alpha_{i2}$ mice are resistant to weight gain when provided a high fat diet and are additionally protected from developing insulin resistance [124]. While these studies are powerful in that they can identify RGS protein GAP activity-mediated phenotypes specific to a particular Gα subunit (*e.g*., $G\alpha_{i2}$ or $G\alpha_o$), these results will require extensive follow-up studies with single RGS protein knockouts (or other strategies) to identify the particular RGS protein(s) functional in these physiological signaling pathways.

While the cellular effects of R4 family members can generally be attributed to their ability to accelerate Gα GTP hydrolysis [85], in recent years it has become apparent that RGS domain-containing proteins can also serve as complex scaffolds for assembling signaling nodes [125-127]. In contrast to the numerous membership of the R4 family with substrate promiscuity across $G\alpha_i$ and $G\alpha_q$ subunits, the R12 subfamily consists only of three members (RGS10, -12, and -14), each of which has a central RGS domain that interacts with $G\alpha_i$ and not $G\alpha_q$ subunits [56]. RGS12 and RGS14, both originally cloned by the Siderovski lab [128], also have additional protein domains known to interact with Ras-superfamily small GTPases, receptor tyrosine kinases, and classical components of the mitogen-activated protein kinase (MAPK) cascade [126]. Relating more directly to heterotrimeric G-protein signaling, the R12 family members RGS12 and RGS14 also contain a unique 19 amino acid motif, distinct from the RGS domain, that interacts with $G\alpha_{i1,2,3}$ subunits in the ground state (GDP bound) and inhibits their spontaneous dissociation of GDP (*i.e.*, guanine nucleotide dissociation inhibitor or "GDI" activity).

1.6 GUANINE NUCLEOTIDE DISSOCIATION INHIBITORS

Before the discovery of GDI activity within R12-family RGS proteins, the original guanine nucleotide dissociation inhibitor described for heterotrimeric G-proteins was the Gβγ subunit which, when bound to Gα, prevents the release of GDP [10, 12]. In a gene-trap experiment for glial cell-specific genes, Granderath and colleagues identified Loco, the *Drosophila* homologue of RGS12. Loss of this gene results in a significant reduction of offspring viability and, in viable offspring, a severe impairment of locomotor activity [129].

Granderath and colleagues were surprised when subsequent experiments revealed Loco could interact with *Drosophila* $G\alpha_i$ in the absence of the RGS domain. Our lab used this puzzling finding to identify a highly conserved 19 amino acid motif present in the *Drosophila* gene Loco protein, its mammalian paralogues RGS12 and RGS14, as well as in the Gα-interacting protein LGN [130, 131]. Ponting simultaneously discovered the same motif in this collection of proteins using similar bioinformatic arguments [132]. Given its initial discovery in the Loco protein and the ability of this motif to interact with $G\alpha_{i/o}$-family Gα subunits, the Siderovski lab named this 19 amino acid motif the "GoLoco" motif [131]. In addition to its presence in RGS12 and RGS14, single GoLoco motifs have also been identified in Rap1GAP, a negative regulator of Ras-family GTPases [133], and in the *C. elegans* proteins GPR-1/-2 [134]. Additionally several proteins have been identified that contain multiple tandem repeats of GoLoco motifs such as AGS3, LGN, Pcp-2, and AGS4/G18 (*a.k.a.* GPSM3) (reviewed in [26]) (Figure 1.9).

The structure of RGS14 bound to the GoLoco motif (amino acids 496-531) revealed that the first 13 amino acids adopt an α-helical secondary structure and bind between the α3-helix and switch II of the Ras-like domain of $G\alpha_{i1}$ [135, 136] (Figure 1.9). The binding of the RGS14 GoLoco motif results in a distortion of the Gβγ-binding interface; in agreement with this structural distortion, it has been demonstrated biochemically that Gα(GDP) subunits can bind to either Gβγ or a GoLoco motif but not both [137-139]. The C-terminus of the GoLoco motif invariantly consists of an acidic-glutamine-arginine triad (Figure 1.9), the terminal arginine of which extends into the nucleotide binding pocket (in a similar manner to the catalytic Arg finger essential to Ras-family GAPs [140, 141]) and makes contact with the α- and β-phosphates of the bound guanine nucleotide. Arg-178 within Switch I of $G\alpha_{i1}$ is

usually in contact with the α- and β-phosphate oxygens [142]; however, upon binding the GoLoco motif, Arg-178 is displaced by the arginine of the GoLoco terminal triad, causing it to form a new contact with the hydroxyl of the ribose sugar and a salt bridge with Glu-43 of $G\alpha_{i1}$. Substitution of the terminal Arg of the GoLoco triad with phenylalanine results in complete loss of Gα binding [143-145].

While it is clear that GoLoco motifs bind $G\alpha_i$ subunits *in vitro* in a nucleotide dependent manner [135, 143, 144] and that these motifs are crucial in determining the subcellular localization of the proteins which have them [125, 126, 146-148], their precise role in normal physiology remains obscure and there is little evidence supporting their role in modulating GPCR signaling.

Work by the Knoblich and Chia laboratories provided the first evidence that the GoLoco motifs within the protein Partner of Inscuteable (Pins) were critical in establishing asymmetric cell division in *Drosophilia* neuroblasts [149, 150]. The *Drosophila* $G\alpha_i$, Pins, and Inscuteable proteins form an apical complex that is necessary for apical/basal asymmetry [151] and the loss of any of these components results in the loss of appropriate spindle orientation and a reduction in the asymmetry of neuroblast division that is normally critical for establishing different daughter cell fates [149, 150, 152]. Consistent with the nucleotide dependent binding of the GoLoco motifs, overexpression of wildtype Gα, but not constitutively active Gα, results in the loss of the apical/basal patterning of cell fate determinants that is dependent on GoLoco/Gα(GDP) interactions [153].

Corroborating the importance of GoLoco motif proteins to asymmetric cell division in *Drosophila*, extensive work has also been done in the nematode worm. In *C. elegans*, the Pins homologues GPR-1 and GPR-2 segregate to the posterior cortex of the zygote and are

necessary for the asymmetric positioning of the mitotic spindle that is required for the proper first division of the embryo [134]. Studies by Colombo *et al*. demonstrated that, upon severing the spindle, the posterior spindle pole's velocity is ~40% greater than the anterior spindle pole, and that RNAi-mediated depletion of GPR-1 and GPR-2 or of the Gα subunits GOA-1 and GPA-16 results in an equalization of spindle velocity and symmetric division [134]. These studies have supported the idea that GoLoco motif proteins, by forming a complex with Gα subunits at the cell cortex in an asymmetrically distributed fashion, control spindle orientation and pulling forces that lead to asymmetric cell division.

1.7 SMALL MOLECULE MODULATORS OF RGS FUNCTION

GPCRs are the single largest target of currently prescribed pharmaceuticals and RGS proteins are potent negative regulators of GPCR-mediated signaling. RGS proteins thus provide an attractive target to either modulate the action of currently prescribed pharmaceuticals or modulate tonic signaling in a pathway-dependent manner [154-157]. While a small molecule that binds to the surface of an RGS protein and blocks its interaction with Gα would be an invaluable proof-of-principle for this concept, it is would be equally useful to have a small molecule that could allosterically enhance the GAP function of endogenous RGS proteins.

Bioinformatic methods [158] and mutagenesis [159] have implicated a region between helix IV-V (Figure 1.10) as the allosteric site on the RGS domain responsible for the influences of phosphatidylinositol-3,4,5-trisphosphate (PIP_3) and Ca^{2+}/calmodulin on GAP activity. This allosteric site (B-site) is distinct from the Gα-interacting "A-site" (Figure 1.10) and, upon binding of PIP_3, decreases GAP activity *in vitro*. In a Ca^{2+} dependent manner, calmodulin (CaM) can competitively inhibit PIP_3-mediated GAP inhibition [159-161].

Modulation of GAP activity via PIP_3 and Ca^{2+}/CaM is also seen in cellular assays using cardiac myocytes in electrophysiological recordings of GPCR signaling to ion channel gating [161-163]. Based on sequence conservation in the B-site, it is possible that the allosteric modulation of RGS1, -2, -10, and -19 also occurs; however, this remains to be experimentally validated. This site could potentially be exploited by small molecules to either mimic the effect of PIP_3 in inhibiting GAP activity, or mimic the effect of Ca^{2+}/CaM in preventing the allosteric inhibition of GAP activity.

Currently the only way to disrupt the RGS domain/Gα interaction is via point mutations on either protein's interaction surface. Single amino acid substitutions on either side of the interface can completely abolish binding and the catalytic activity of RGS proteins [59, 64, 164]. The ability to disrupt this large protein/protein interface (1290 $Å^2$ [25]) with single point mutations suggests that the small perturbations in the topology of the surface by virtue of a bound small molecule could have dramatic results in inhibiting RGS domain GAP activity. The current dearth of small molecule modulators of RGS proteins only makes discovering the first *in vivo*-acting RGS protein modulator more exciting.

Measuring RGS domain-mediated acceleration of GTP hydrolysis *in vitro,* for example as part of a compound library screening campaign, is difficult because GDP release by Gα (not GTP hydrolysis) is the rate-limiting step [12, 165]. Thus, to quantify the effects of RGS domain GAP activity, one typically preloads radiolabelled GTP and measures the one round of hydrolysis in a so-called "single-turnover" assay [49]. This experimental design requires one to establish a pool of Gα([γ-^{32}P]GTP), initiate the assay at time zero with the addition of Mg^{2+}, sample aliquots over time, precipitate all unhydrolyzed GTP with charcoal, separate the charcoal, and then quantify the inorganic phosphate that was produced (and

resides in the supernatant) using liquid scintillation. This cumbersome assay design is not suitable to automation, so our group and others have developed alternative assays that are more suitable for high throughput screening of compound libraries (see Chapters 4 and 5).

Wyeth Laboratory published yeast two-hybrid based screening method for identifying RGS4 or RGS20 inhibitors [166, 167]. While their screen was reported to have identified small molecule inhibitors, these compounds were never made public and the screening program has been disbanded (Dr. David Siderovski, personal communications).

In a functional screen to identify novel treatments for urinary incontinence using *ex vivo* rat bladder smooth muscle cultures, a Bristol-Myers Squibb group identified two compounds (BMS-192364 and BMS-195270) that had no known molecular target yet resulted in relaxation of bladder [168]. Using a nematode genetics approach to identifying the target of these two drugs, this group concluded that these two compounds targeted the Gα/RGS domain interaction and specifically locked the pair in an unproductive complex [168]. While they did not provide direct biochemical evidence for this proposed mechanism of action, there is precedence that brefeldin A, a naturally-occurring antibiotic, can trap the Ras-family GTPase ARF1 in an unproductive complex with the ARF1 GEF, Sec7 [169]. Currently, no one has yet reported being able to confirm that these two BMS compounds target the RGS/Gα interaction; the Siderovski lab obtained both of these compounds but was unable to test them in single-turnover assays owing to compound solubility problems (Dr. Francis Willard; personal communication). In addition to the efforts that are ongoing by the pharmaceutical industry, our laboratory as well as the Neubig lab at the University of Michigan have been developing novel high throughput screening assays for the RGS domain/Gα interaction target and searching for small molecule modulators of RGS protein GAP activity.

Neubig and colleagues have described a high-throughput flow cytometry method to screen for small molecules that can disrupt the binding of RGS proteins to Gα subunits. Their assay design uses fluorescently-labeled Gα protein and a LumAvidin® microsphere-coupled RGS protein to look for compounds that disrupted their interaction. The advantage of this assay is the ability to multiplex different biotinylated RGS proteins to different LumAvidin® microspheres [170, 171]. The results of an initial "in house" screening of a ~3,000 compound collection from ChemBridge were published by Roman *et al*. [171]; ultimately, they only identified one reactive compound that non-specifically modifies cysteines, including a critical surface-exposed cysteine in the RGS4 A-site [172] (Chapter 3). Both the Wyeth yeast two-hybrid screen and the flow cytometry-based screen were unable to measure the actual catalytic activity of RGS proteins *in vitro*. Instead, it has been common practice in RGS protein assays and screens to use binding of Gα to the RGS domain as an indirect indicator of GAP activity. Based on the mechanism by which RGS proteins stabilize the switch regions in their transition state conformation, this is a valid assumption; however, using binding as a surrogate for GAP activity has two potential pitfalls. The first deficit is that a compound such as brefeldin A that traps the G-protein in an unproductive complex with its regulatory partner would be missed. It is possible that, for the RGS/Gα target, a small molecule might inhibit RGS domain-mediated stabilization of the switch regions in a conformation that facilitates hydrolysis or otherwise traps the RGS/Gα complex. Additionally, it is possible that, relying on binding rather than enzymatic activity in a compound library screen, one may have false negatives given weak binding of an inhibitor that would be lost to the noise of the assay. Instead, if one were able to read out successive rounds of GTP hydrolysis by Gα, and acceleration of that hydrolysis by the RGS protein, the

effects of such weak inhibitors may become apparent. The current efforts of our laboratory in developing high throughput screening assays for RGS/Gα targets will be further discussed in Chapters 4 and 5 and both use fluorescence polarization as the primary readout.

1.8 FLUORESCENCE POLARIZATION

Fluorescence occurs when the absorption of light causes a molecule's electronic configuration to enter an excited state and the spontaneous return to the ground state results in the emission of a photon of lower energy (higher wavelength) than the incident photon [173]. The ability to label proteins with fluorescent dyes or naturally-fluorescent proteins has allowed scientists to track changes in location of proteins in real time, to measure the subcellular compartments where proteins are activated *in vivo*, and to monitor protein-protein interactions in real time [174, 175]. Generally when a dye is excited with a excitation beam from a non-laser excitation source, the dye is excited by a random orientation of incident photons. It was noted in 1926 by Francis Perrin that, if an immobilized fluorophore is excited with plane-polarized light, the emission is polarized in the same plane; however, if the fluorophore is in solution, the emission becomes random [176]. This phenomenon has been extremely useful in the biological sciences to track single nucleotide polymorphisms, peptide/protein interactions, DNA/protein interactions, phosphorylation events and photolytic cleavages [177-181]. Two different, but interchangeable, methods are commonly used to quantify this phenomenon: anisotropy *(r)* or polarization (*P*). In general, biophysicists prefer to use anisotropy because the loss of light due to the polarizer is corrected by the factor of 2 in the denominator of the equation, while polarization (*P*) has become the standard in the biological sciences [182]. Both anisotropy and polarization measurements are made by

quantifying the intensity of the fluorescence emission perpendicular ($I_{\perp}$) and parallel ($I_{\parallel}$) to the plane of excitation (Equation 1.1; Figure 1.11); the value of anisotropy and polarization can be easily interconverted (Equation 1.2). The remainder of the text will refer to polarization in terms of (*P*) which, while technically unitless, is commonly expressed in the literature as milliP (mP).

(1.1) $$r = \frac{I_{\parallel} - I_{\perp}}{I_{\parallel} + 2I_{\perp}} \qquad P = \frac{I_{\parallel} - I_{\perp}}{I_{\parallel} + I_{\perp}}$$

(1.2) $$r = \frac{2(P)}{3 - P}$$

Given that excitation, relaxation, and subsequent emission do not occur instantaneously, if a fluorescent dye is undergoing rotational motion, a polarized excitation source will be depolarized if the rotational motion of the dye is faster than its fluorescence lifetime. Polarization measurements provide an index of the average angular displacement of a fluorophore that occurs between absorption and emission of a photon. The angular displacement and, thus, the polarization is dependent on the rotational velocity of the molecule (rotational correlation time; θ), the delay of the fluorophore from excitation to emission (fluorescence lifetime; τ), and the fundamental polarization for a particular dye (physical constant for a particular dye; P_0), as set forth by the classic Perrin equation (Equation 1.3) [176, 182].

(1.3) $$\left(\frac{1}{P} - \frac{1}{3}\right) = \left(\frac{1}{P_0} - \frac{1}{3}\right)\left(1 + \tau/\theta\right)$$

The rotational correlation time (θ) is dependent on the viscosity (η) of the environment and the apparent molecular weight of the fluorescent dye or dye-conjugate (*M*). For a globular

protein, the rotational correlation time (θ) is directly related to the molecular weight of the protein by the formula:

$$\theta = \frac{\eta M}{RT}(\bar{v} + h) \tag{1.4}$$

Typically in the biological sciences, fluorescence polarization is used for measuring binding reactions in which viscosity of the solution remains unchanged. Therefore, the only variable that is commonly changing the rotational correlation time (θ) is the apparent molecular weight of the dye. The most widely used dye for fluorescence polarization is fluorescein isothicyanate (FITC) and its derivatives which have a fluorescence lifetime (τ) of ~4 ns. This fundamental property of the dye limits the types of molecular interactions that can be monitored using fluorescence polarization (Figure 1.12) [182]. For instance, a FITC-labelled molecular probe in general must have a molecular weight below 5,000 Da and bind to an interactor of greater than 10,000 Da in order to obtain a sufficient signal by fluorescence polarization (Figure 1.12). While there are no commercial fluorophores available with fluorescence lifetimes that allow the detection of interactions between two large macromolecules, several publications exist describing novel dyes capable of monitoring binding interactions between albumin and antibodies [183-185].

While fluorescence polarization assays require that the molecular weight of the probe must be much less than the molecular weight of the bound complex, this limitation is offset by several advantages that fluorescence polarization offers compared to traditional methods for monitoring protein/ligand and protein/protein interactions. First, no radioactive waste is generated while the probe concentration can remain low, typically in the picomolar to nanomolar range. Second, fluorescence polarization assays are homogeneous and do not require additional steps after the reaction is established for separating the tracer from the

reaction mixture. In addition to equilibrium binding analyses, fluorescence polarization allows the experimenter to set up experiments so that kinetic data can be obtained from multiple samples (including 96 well, 384 well, and 1536 well formats). Given that the polarization signal is not dependent on the absolute intensity of the fluorophore, these fluorescence polarization assays are able to accommodate day-to-day variations in probe concentration, as well as loss of probe due to decay, and are generally robust to instrument changes such as drift, gain settings, and lamp changes [186]. In Chapters 4 and 5, I describe my use of fluorescence polarization in developing two different assays, namely the binding of $G\alpha_{i1}$(GDP) to the GoLoco motif of RGS12, and the production of GDP by RGS4-accelerated $G\alpha_{i1}$(GTP) in multiple rounds of GTP hydrolysis.

1.9 REFERENCES

1. Fredriksson, R., M.C. Lagerstrom, L.G. Lundin, and H.B. Schioth, *The G-protein-coupled receptors in the human genome form five main families. Phylogenetic analysis, paralogon groups, and fingerprints*. Mol Pharmacol, 2003. **63**(6): p. 1256-72.

2. Takeda, S., S. Kadowaki, T. Haga, H. Takaesu, and S. Mitaku, *Identification of G protein-coupled receptor genes from the human genome sequence*. FEBS Lett, 2002. **520**(1-3): p. 97-101.

3. Jacoby, E., R. Bouhelal, M. Gerspacher, and K. Seuwen, *The 7 TM G-protein-coupled receptor target family*. ChemMedChem, 2006. **1**(8): p. 761-82.

4. Lundstrom, K., *Latest development in drug discovery on G protein-coupled receptors*. Curr Protein Pept Sci, 2006. **7**(5): p. 465-70.

5. Spiegel, A.M. and L.S. Weinstein, *Inherited diseases involving g proteins and g protein-coupled receptors*. Annu Rev Med, 2004. **55**: p. 27-39.

6. Perez, D.M., *The evolutionarily triumphant G-protein-coupled receptor*. Mol Pharmacol, 2003. **63**(6): p. 1202-5.

7. Gilman, A.G., *G proteins: transducers of receptor-generated signals*. Annu Rev Biochem, 1987. **56**: p. 615-49.

8. Johnston, C.A. and D.P. Siderovski, *Receptor-mediated activation of heterotrimeric G-proteins: current structural insights*. Mol Pharmacol, 2007. **72**(2): p. 219-30.

9. Oldham, W.M. and H.E. Hamm, *Heterotrimeric G protein activation by G-protein-coupled receptors*. Nat Rev Mol Cell Biol, 2008. **9**(1): p. 60-71.

10. Brandt, D.R. and E.M. Ross, *GTPase activity of the stimulatory GTP-binding regulatory protein of adenylate cyclase, Gs. Accumulation and turnover of enzyme-nucleotide intermediates*. J Biol Chem, 1985. **260**(1): p. 266-72.

11. Evanko, D.S., M.M. Thiyagarajan, D.P. Siderovski, and P.B. Wedegaertner, *Gbeta gamma isoforms selectively rescue plasma membrane localization and palmitoylation of mutant Galphas and Galphaq*. J Biol Chem, 2001. **276**(26): p. 23945-53.

12. Higashijima, T., K.M. Ferguson, P.C. Sternweis, M.D. Smigel, and A.G. Gilman, *Effects of Mg2+ and the beta gamma-subunit complex on the interactions of guanine nucleotides with G proteins*. J Biol Chem, 1987. **262**(2): p. 762-6.

13. Robillard, L., N. Ethier, M. Lachance, and T.E. Hebert, *Gbetagamma subunit combinations differentially modulate receptor and effector coupling in vivo*. Cell Signal, 2000. **12**(9-10): p. 673-82.

14. Wall, M.A., B.A. Posner, and S.R. Sprang, *Structural basis of activity and subunit recognition in G protein heterotrimers*. Structure, 1998. **6**(9): p. 1169-83.

15. Bohm, A., R. Gaudet, and P.B. Sigler, *Structural aspects of heterotrimeric G-protein signaling*. Curr Opin Biotechnol, 1997. **8**(4): p. 480-7.

16. Exton, J.H., *Regulation of phosphoinositide phospholipases by hormones, neurotransmitters, and other agonists linked to G proteins*. Annu Rev Pharmacol Toxicol, 1996. **36**: p. 481-509.

17. Kammermeier, P.J., V. Ruiz-Velasco, and S.R. Ikeda, *A voltage-independent calcium current inhibitory pathway activated by muscarinic agonists in rat sympathetic neurons requires both Galpha q/11 and Gbeta gamma*. J Neurosci, 2000. **20**(15): p. 5623-9.

18. Kozasa, T., X. Jiang, M.J. Hart, P.M. Sternweis, W.D. Singer, A.G. Gilman, G. Bollag, and P.C. Sternweis, *p115 RhoGEF, a GTPase activating protein for Galpha12 and Galpha13*. Science, 1998. **280**(5372): p. 2109-11.

19. Pitcher, J.A., N.J. Freedman, and R.J. Lefkowitz, *G protein-coupled receptor kinases*. Annu Rev Biochem, 1998. **67**: p. 653-92.

20. Rhee, S.G., *Regulation of phosphoinositide-specific phospholipase C*. Annu Rev Biochem, 2001. **70**: p. 281-312.

21. Simonds, W.F., *G protein regulation of adenylate cyclase*. Trends Pharmacol Sci, 1999. **20**(2): p. 66-73.

22. Wedegaertner, P.B., P.T. Wilson, and H.R. Bourne, *Lipid modifications of trimeric G proteins*. J Biol Chem, 1995. **270**(2): p. 503-6.

23. Lambright, D.G., J.P. Noel, H.E. Hamm, and P.B. Sigler, *Structural determinants for activation of the alpha-subunit of a heterotrimeric G protein*. Nature, 1994. **369**(6482): p. 621-8.

24. Posner, B.A., M.B. Mixon, M.A. Wall, S.R. Sprang, and A.G. Gilman, *The A326S mutant of Gialpha1 as an approximation of the receptor-bound state*. J Biol Chem, 1998. **273**(34): p. 21752-8.

25. Tesmer, J.J., D.M. Berman, A.G. Gilman, and S.R. Sprang, *Structure of RGS4 bound to AlF4--activated G(i alpha1): stabilization of the transition state for GTP hydrolysis*. Cell, 1997. **89**(2): p. 251-61.

26. Willard, F.S., R.J. Kimple, and D.P. Siderovski, *Return of the GDI: the GoLoco motif in cell division*. Annu Rev Biochem, 2004. **73**: p. 925-51.

27. Sondek, J., A. Bohm, D.G. Lambright, H.E. Hamm, and P.B. Sigler, *Crystal structure of a G-protein beta gamma dimer at 2.1A resolution*. Nature, 1996. **379**(6563): p. 369-74.

28. Wall, M.A., D.E. Coleman, E. Lee, J.A. Iniguez-Lluhi, B.A. Posner, A.G. Gilman, and S.R. Sprang, *The structure of the G protein heterotrimer Gi alpha 1 beta 1 gamma 2*. Cell, 1995. **83**(6): p. 1047-58.

29. Bonacci, T.M., J.L. Mathews, C. Yuan, D.M. Lehmann, S. Malik, D. Wu, J.L. Font, J.M. Bidlack, and A.V. Smrcka, *Differential targeting of Gbetagamma-subunit signaling with small molecules*. Science, 2006. **312**(5772): p. 443-6.

30. Gaudet, R., A. Bohm, and P.B. Sigler, *Crystal structure at 2.4 angstroms resolution of the complex of transducin betagamma and its regulator, phosducin*. Cell, 1996. **87**(3): p. 577-88.

31. Lodowski, D.T., J.A. Pitcher, W.D. Capel, R.J. Lefkowitz, and J.J. Tesmer, *Keeping G proteins at bay: a complex between G protein-coupled receptor kinase 2 and Gbetagamma*. Science, 2003. **300**(5623): p. 1256-62.

32. Coleman, D.E., A.M. Berghuis, E. Lee, M.E. Linder, A.G. Gilman, and S.R. Sprang, *Structures of active conformations of Gi alpha 1 and the mechanism of GTP hydrolysis*. Science, 1994. **265**(5177): p. 1405-12.

33. Coleman, D.E. and S.R. Sprang, *Structure of Gialpha1.GppNHp, autoinhibition in a galpha protein-substrate complex*. J Biol Chem, 1999. **274**(24): p. 16669-72.

34. Raw, A.S., D.E. Coleman, A.G. Gilman, and S.R. Sprang, *Structural and biochemical characterization of the GTPgammaS-, GDP.Pi-, and GDP-bound forms of a GTPase-deficient Gly42 --> Val mutant of Gialpha1*. Biochemistry, 1997. **36**(50): p. 15660-9.

35. Cassel, D., F. Eckstein, M. Lowe, and Z. Selinger, *Determination of the turn-off reaction for the hormone-activated adenylate cyclase*. J Biol Chem, 1979. **254**(19): p. 9835-8.

36. Vuong, T.M. and M. Chabre, *Deactivation kinetics of the transduction cascade of vision*. Proc Natl Acad Sci U S A, 1991. **88**(21): p. 9813-7.

37. Breitwieser, G.E. and G. Szabo, *Mechanism of muscarinic receptor-induced K+ channel activation as revealed by hydrolysis-resistant GTP analogues*. J Gen Physiol, 1988. **91**(4): p. 469-93.

38. Yatani, A., R. Mattera, J. Codina, R. Graf, K. Okabe, E. Padrell, R. Iyengar, A.M. Brown, and L. Birnbaumer, *The G protein-gated atrial K+ channel is stimulated by three distinct Gi alpha-subunits*. Nature, 1988. **336**(6200): p. 680-2.

39. Berstein, G., J.L. Blank, D.Y. Jhon, J.H. Exton, S.G. Rhee, and E.M. Ross, *Phospholipase C-beta 1 is a GTPase-activating protein for Gq/11, its physiologic regulator*. Cell, 1992. **70**(3): p. 411-8.

40. Trahey, M. and F. McCormick, *A cytoplasmic protein stimulates normal N-ras p21 GTPase, but does not affect oncogenic mutants*. Science, 1987. **238**(4826): p. 542-5.

41. Chan, R.K. and C.A. Otte, *Isolation and genetic analysis of Saccharomyces cerevisiae mutants supersensitive to G1 arrest by a factor and alpha factor pheromones*. Mol Cell Biol, 1982. **2**(1): p. 11-20.

42. Chan, R.K. and C.A. Otte, *Physiological characterization of Saccharomyces cerevisiae mutants supersensitive to G1 arrest by a factor and alpha factor pheromones*. Mol Cell Biol, 1982. **2**(1): p. 21-9.

43. MacKay, V.L., S.K. Welch, M.Y. Insley, T.R. Manney, J. Holly, G.C. Saari, and M.L. Parker, *The Saccharomyces cerevisiae BAR1 gene encodes an exported protein with homology to pepsin*. Proc Natl Acad Sci U S A, 1988. **85**(1): p. 55-9.

44. Dietzel, C. and J. Kurjan, *The yeast SCG1 gene: a G alpha-like protein implicated in the a- and alpha-factor response pathway*. Cell, 1987. **50**(7): p. 1001-10.

45. Hartwell, L.H., *Mutants of Saccharomyces cerevisiae unresponsive to cell division control by polypeptide mating hormone*. J Cell Biol, 1980. **85**(3): p. 811-22.

46. Miyajima, I., M. Nakafuku, N. Nakayama, C. Brenner, A. Miyajima, K. Kaibuchi, K. Arai, Y. Kaziro, and K. Matsumoto, *GPA1, a haploid-specific essential gene, encodes a yeast homolog of mammalian G protein which may be involved in mating factor signal transduction*. Cell, 1987. **50**(7): p. 1011-9.

47. Nakayama, N., Y. Kaziro, K. Arai, and K. Matsumoto, *Role of STE genes in the mating factor signaling pathway mediated by GPA1 in Saccharomyces cerevisiae*. Mol Cell Biol, 1988. **8**(9): p. 3777-83.

48. Dohlman, H.G., D. Apaniesk, Y. Chen, J. Song, and D. Nusskern, *Inhibition of G-protein signaling by dominant gain-of-function mutations in Sst2p, a pheromone desensitization factor in Saccharomyces cerevisiae*. Mol Cell Biol, 1995. **15**(7): p. 3635-43.

49. Berman, D.M., T.M. Wilkie, and A.G. Gilman, *GAIP and RGS4 are GTPase-activating proteins for the Gi subfamily of G protein alpha subunits*. Cell, 1996. **86**(3): p. 445-52.

50. De Vries, L., M. Mousli, A. Wurmser, and M.G. Farquhar, *GAIP, a protein that specifically interacts with the trimeric G protein G alpha i3, is a member of a protein family with a highly conserved core domain*. Proc Natl Acad Sci U S A, 1995. **92**(25): p. 11916-20.

51. Druey, K.M., K.J. Blumer, V.H. Kang, and J.H. Kehrl, *Inhibition of G-protein-mediated MAP kinase activation by a new mammalian gene family*. Nature, 1996. **379**(6567): p. 742-6.

52. Hunt, T.W., T.A. Fields, P.J. Casey, and E.G. Peralta, *RGS10 is a selective activator of G alpha i GTPase activity*. Nature, 1996. **383**(6596): p. 175-7.

53. Koelle, M.R. and H.R. Horvitz, *EGL-10 regulates G protein signaling in the C. elegans nervous system and shares a conserved domain with many mammalian proteins*. Cell, 1996. **84**(1): p. 115-25.

54. Siderovski, D.P., A. Hessel, S. Chung, T.W. Mak, and M. Tyers, *A new family of regulators of G-protein-coupled receptors?* Curr Biol, 1996. **6**(2): p. 211-2.

55. Watson, N., M.E. Linder, K.M. Druey, J.H. Kehrl, and K.J. Blumer, *RGS family members: GTPase-activating proteins for heterotrimeric G-protein alpha-subunits*. Nature, 1996. **383**(6596): p. 172-5.

56. Soundararajan, M., F.S. Willard, A.J. Kimple, A.P. Turnbull, L.J. Ball, G.A. Schoch, C. Gileadi, O.Y. Fedorov, E.F. Dowler, V.A. Higman, S.Q. Hutsell, M. Sundstrom, D.A. Doyle, and D.P. Siderovski, *Structural diversity in the RGS domain and its interaction with heterotrimeric G protein alpha-subunits*. Proc Natl Acad Sci U S A, 2008. **105**(17): p. 6457-62.

57. Vetter, I.R. and A. Wittinghofer, *The guanine nucleotide-binding switch in three dimensions*. Science, 2001. **294**(5545): p. 1299-304.

58. Moy, F.J., P.K. Chanda, M.I. Cockett, W. Edris, P.G. Jones, K. Mason, S. Semus, and R. Powers, *NMR structure of free RGS4 reveals an induced conformational change upon binding Galpha*. Biochemistry, 2000. **39**(24): p. 7063-73.

59. Kimple, A.J., M. Soundararajan, S.Q. Hutsell, A.K. Roos, D.J. Urban, V. Setola, B.R. Temple, B.L. Roth, S. Knapp, F.S. Willard, and D.P. Siderovski, *Structural determinants of G-protein alpha subunit selectivity by regulator of G-protein signaling 2 (RGS2)*. J Biol Chem, 2009. **284**(29): p. 19402-11.

60. Slep, K.C., M.A. Kercher, W. He, C.W. Cowan, T.G. Wensel, and P.B. Sigler, *Structural determinants for regulation of phosphodiesterase by a G protein at 2.0 A*. Nature, 2001. **409**(6823): p. 1071-7.

61. Slep, K.C., M.A. Kercher, T. Wieland, C.K. Chen, M.I. Simon, and P.B. Sigler, *Molecular architecture of Galphao and the structural basis for RGS16-mediated deactivation*. Proc Natl Acad Sci U S A, 2008. **105**(17): p. 6243-8.

62. Popov, S., K. Yu, T. Kozasa, and T.M. Wilkie, *The regulators of G protein signaling (RGS) domains of RGS4, RGS10, and GAIP retain GTPase activating protein activity in vitro*. Proc Natl Acad Sci U S A, 1997. **94**(14): p. 7216-20.

63. Sondek, J., D.G. Lambright, J.P. Noel, H.E. Hamm, and P.B. Sigler, *GTPase mechanism of Gproteins from the 1.7-A crystal structure of transducin alpha-GDP-AIF-4*. Nature, 1994. **372**(6503): p. 276-9.

64. DiBello, P.R., T.R. Garrison, D.M. Apanovitch, G. Hoffman, D.J. Shuey, K. Mason, M.I. Cockett, and H.G. Dohlman, *Selective uncoupling of RGS action by a single point mutation in the G protein alpha-subunit*. J Biol Chem, 1998. **273**(10): p. 5780-4.

65. Lan, K.L., N.A. Sarvazyan, R. Taussig, R.G. Mackenzie, P.R. DiBello, H.G. Dohlman, and R.R. Neubig, *A point mutation in Galphao and Galphai1 blocks interaction with regulator of G protein signaling proteins*. J Biol Chem, 1998. **273**(21): p. 12794-7.

66. Clark, M.J. and J.R. Traynor, *Assays for G-protein-coupled receptor signaling using RGS-insensitive Galpha subunits*. Methods Enzymol, 2004. **389**: p. 155-69.

67. Fu, Y., H. Zhong, M. Nanamori, R.M. Mortensen, X. Huang, K. Lan, and R.R. Neubig, *RGS-insensitive G-protein mutations to study the role of endogenous RGS proteins*. Methods Enzymol, 2004. **389**: p. 229-43.

68. Day, P.W., J.J. Tesmer, R. Sterne-Marr, L.C. Freeman, J.L. Benovic, and P.B. Wedegaertner, *Characterization of the GRK2 binding site of Galphaq*. J Biol Chem, 2004. **279**(51): p. 53643-52.

69. Ikeda, S.R. and S.W. Jeong, *Use of RGS-insensitive Galpha subunits to study endogenous RGS protein action on G-protein modulation of N-type calcium channels in sympathetic neurons*. Methods Enzymol, 2004. **389**: p. 170-89.

70. Chen, H., M.A. Clark, and N.A. Lambert, *Endogenous RGS proteins regulate presynaptic and postsynaptic function: functional expression of RGS-insensitive Galpha subunits in central nervous system neurons*. Methods Enzymol, 2004. **389**: p. 190-204.

71. Heximer, S.P., N. Watson, M.E. Linder, K.J. Blumer, and J.R. Hepler, *RGS2/G0S8 is a selective inhibitor of Gqalpha function*. Proc Natl Acad Sci U S A, 1997. **94**(26): p. 14389-93.

72. Arshavsky, V.Y., T.D. Lamb, and E.N. Pugh, Jr., *G proteins and phototransduction*. Annu Rev Physiol, 2002. **64**: p. 153-87.

73. Zeng, W., X. Xu, S. Popov, S. Mukhopadhyay, P. Chidiac, J. Swistok, W. Danho, K.A. Yagaloff, S.L. Fisher, E.M. Ross, S. Muallem, and T.M. Wilkie, *The N-terminal domain of RGS4 confers receptor-selective inhibition of G protein signaling*. J Biol Chem, 1998. **273**(52): p. 34687-90.

74. Xu, X., W. Zeng, S. Popov, D.M. Berman, I. Davignon, K. Yu, D. Yowe, S. Offermanns, S. Muallem, and T.M. Wilkie, *RGS proteins determine signaling specificity of Gq-coupled receptors*. J Biol Chem, 1999. **274**(6): p. 3549-56.

75. Wang, X., W. Zeng, A.A. Soyombo, W. Tang, E.M. Ross, A.P. Barnes, S.L. Milgram, J.M. Penninger, P.B. Allen, P. Greengard, and S. Muallem, *Spinophilin regulates Ca2+ signalling by binding the N-terminal domain of RGS2 and the third intracellular loop of G-protein-coupled receptors*. Nat Cell Biol, 2005. **7**(4): p. 405-11.

76. Bernstein, L.S., S. Ramineni, C. Hague, W. Cladman, P. Chidiac, A.I. Levey, and J.R. Hepler, *RGS2 binds directly and selectively to the M1 muscarinic acetylcholine receptor third intracellular loop to modulate Gq/11alpha signaling*. J Biol Chem, 2004. **279**(20): p. 21248-56.

77. Wang, Q., L.Y. Liu-Chen, and J.R. Traynor, *Differential modulation of mu- and delta-opioid receptor agonists by endogenous RGS4 protein in SH-SY5Y cells*. J Biol Chem, 2009. **284**(27): p. 18357-67.

78. Bodenstein, J., R.K. Sunahara, and R.R. Neubig, *N-terminal residues control proteasomal degradation of RGS2, RGS4, and RGS5 in human embryonic kidney 293 cells*. Mol Pharmacol, 2007. **71**(4): p. 1040-50.

79. Yang, J., K. Kamide, Y. Kokubo, S. Takiuchi, C. Tanaka, M. Banno, Y. Miwa, M. Yoshii, T. Horio, A. Okayama, H. Tomoike, Y. Kawano, and T. Miyata, *Genetic variations of regulator of G-protein signaling 2 in hypertensive patients and in the general population*. J Hypertens, 2005. **23**(8): p. 1497-505.

80. Snow, B.E., R.A. Hall, A.M. Krumins, G.M. Brothers, D. Bouchard, C.A. Brothers, S. Chung, J. Mangion, A.G. Gilman, R.J. Lefkowitz, and D.P. Siderovski, *GTPase activating specificity of RGS12 and binding specificity of an alternatively spliced PDZ (PSD-95/Dlg/ZO-1) domain*. J Biol Chem, 1998. **273**(28): p. 17749-55.

81. Apanovitch, D.M., K.C. Slep, P.B. Sigler, and H.G. Dohlman, *Sst2 is a GTPase-activating protein for Gpa1: purification and characterization of a cognate RGS-Galpha protein pair in yeast*. Biochemistry, 1998. **37**(14): p. 4815-22.

82. Doupnik, C.A., N. Davidson, H.A. Lester, and P. Kofuji, *RGS proteins reconstitute the rapid gating kinetics of gbetagamma-activated inwardly rectifying K+ channels*. Proc Natl Acad Sci U S A, 1997. **94**(19): p. 10461-6.

83. Saitoh, O., Y. Kubo, Y. Miyatani, T. Asano, and H. Nakata, *RGS8 accelerates G-protein-mediated modulation of K+ currents*. Nature, 1997. **390**(6659): p. 525-9.

84. He, W., C.W. Cowan, and T.G. Wensel, *RGS9, a GTPase accelerator for phototransduction*. Neuron, 1998. **20**(1): p. 95-102.

85. Lambert, N.A., C.A. Johnston, S.D. Cappell, S. Kuravi, A.J. Kimple, F.S. Willard, and D.P. Siderovski, *Regulators of G-protein Signaling accelerate GPCR signaling kinetics and govern sensitivity solely by accelerating GTPase activity*. Proc Natl Acad Sci U S A.

86. Moratz, C., J.R. Hayman, H. Gu, and J.H. Kehrl, *Abnormal B-cell responses to chemokines, disturbed plasma cell localization, and distorted immune tissue architecture in Rgs1-/- mice*. Mol Cell Biol, 2004. **24**(13): p. 5767-75.

87. Gilfillan, A.M. and J. Rivera, *The tyrosine kinase network regulating mast cell activation*. Immunol Rev, 2009. **228**(1): p. 149-69.

88. Kinet, J.P., *The high-affinity IgE receptor (Fc epsilon RI): from physiology to pathology*. Annu Rev Immunol, 1999. **17**: p. 931-72.

89. Metz, M. and M. Maurer, *Mast cells--key effector cells in immune responses*. Trends Immunol, 2007. **28**(5): p. 234-41.

90. Rivera, J. and A.M. Gilfillan, *Molecular regulation of mast cell activation*. J Allergy Clin Immunol, 2006. **117**(6): p. 1214-25; quiz 1226.

91. Bansal, G., Z. Xie, S. Rao, K.H. Nocka, and K.M. Druey, *Suppression of immunoglobulin E-mediated allergic responses by regulator of G protein signaling 13*. Nat Immunol, 2008. **9**(1): p. 73-80.

92. Siderovski, D.P., S. Blum, R.E. Forsdyke, and D.R. Forsdyke, *A set of human putative lymphocyte G0/G1 switch genes includes genes homologous to rodent cytokine and zinc finger protein-encoding genes*. DNA Cell Biol, 1990. **9**(8): p. 579-87.

93. Siderovski, D.P., S.P. Heximer, and D.R. Forsdyke, *A human gene encoding a putative basic helix-loop-helix phosphoprotein whose mRNA increases rapidly in cycloheximide-treated blood mononuclear cells*. DNA Cell Biol, 1994. **13**(2): p. 125-47.

94. Heximer, S.P., A.D. Cristillo, and D.R. Forsdyke, *Comparison of mRNA expression of two regulators of G-protein signaling, RGS1/BL34/1R20 and RGS2/G0S8, in cultured human blood mononuclear cells*. DNA Cell Biol, 1997. **16**(5): p. 589-98.

95. Oliveira-Dos-Santos, A.J., G. Matsumoto, B.E. Snow, D. Bai, F.P. Houston, I.Q. Whishaw, S. Mariathasan, T. Sasaki, A. Wakeham, P.S. Ohashi, J.C. Roder, C.A. Barnes, D.P. Siderovski, and J.M. Penninger, *Regulation of T cell activation, anxiety, and male aggression by RGS2*. Proc Natl Acad Sci U S A, 2000. **97**(22): p. 12272-7.

96. Cantrell, D.A. and K.A. Smith, *The interleukin-2 T-cell system: a new cell growth model*. Science, 1984. **224**(4655): p. 1312-6.

97. Manzur, M. and R. Ganss, *Regulator of G protein signaling 5: a new player in vascular remodeling*. Trends Cardiovasc Med, 2009. **19**(1): p. 26-30.

98. Harris, D.M., H.I. Cohn, S. Pesant, and A.D. Eckhart, *GPCR signalling in hypertension: role of GRKs*. Clin Sci (Lond), 2008. **115**(3): p. 79-89.

99. Levy, M.N., A.J. Pappano, and R.M. Berne, *Cardiovascular physiology*. 9th ed. Mosby physiology monograph series. 2007, Philadelphia, PA: Mosby Elsevier. xiv, 269 p.

100. Brinks, H.L. and A.D. Eckhart, *Regulation of GPCR signaling in Hypertension*. Biochim Biophys Acta.

101. Gu, S., S. Tirgari, and S.P. Heximer, *The RGS2 gene product from a candidate hypertension allele shows decreased plasma membrane association and inhibition of Gq*. Mol Pharmacol, 2008. **73**(4): p. 1037-43.

102. Heximer, S.P., R.H. Knutsen, X. Sun, K.M. Kaltenbronn, M.H. Rhee, N. Peng, A. Oliveira-dos-Santos, J.M. Penninger, A.J. Muslin, T.H. Steinberg, J.M. Wyss, R.P. Mecham, and K.J. Blumer, *Hypertension and prolonged vasoconstrictor signaling in RGS2-deficient mice*. J Clin Invest, 2003. **111**(4): p. 445-52.

103. Tang, K.M., G.R. Wang, P. Lu, R.H. Karas, M. Aronovitz, S.P. Heximer, K.M. Kaltenbronn, K.J. Blumer, D.P. Siderovski, Y. Zhu, and M.E. Mendelsohn, *Regulator of G-protein signaling-2 mediates vascular smooth muscle relaxation and blood pressure*. Nat Med, 2003. **9**(12): p. 1506-12.

104. Cho, H., C. Park, I.Y. Hwang, S.B. Han, D. Schimel, D. Despres, and J.H. Kehrl, *Rgs5 targeting leads to chronic low blood pressure and a lean body habitus*. Mol Cell Biol, 2008. **28**(8): p. 2590-7.

105. Bondjers, C., M. Kalen, M. Hellstrom, S.J. Scheidl, A. Abramsson, O. Renner, P. Lindahl, H. Cho, J. Kehrl, and C. Betsholtz, *Transcription profiling of platelet-derived growth factor-B-deficient mouse embryos identifies RGS5 as a novel marker for pericytes and vascular smooth muscle cells*. Am J Pathol, 2003. **162**(3): p. 721-9.

106. Cho, H., T. Kozasa, C. Bondjers, C. Betsholtz, and J.H. Kehrl, *Pericyte-specific expression of Rgs5: implications for PDGF and EDG receptor signaling during vascular maturation*. FASEB J, 2003. **17**(3): p. 440-2.

107. Berger, M., G. Bergers, B. Arnold, G.J. Hammerling, and R. Ganss, *Regulator of G-protein signaling-5 induction in pericytes coincides with active vessel remodeling during neovascularization*. Blood, 2005. **105**(3): p. 1094-101.

108. Hamzah, J., M. Jugold, F. Kiessling, P. Rigby, M. Manzur, H.H. Marti, T. Rabie, S. Kaden, H.J. Grone, G.J. Hammerling, B. Arnold, and R. Ganss, *Vascular normalization in Rgs5-deficient tumours promotes immune destruction*. Nature, 2008. **453**(7193): p. 410-4.

109. Ryschich, E., J. Schmidt, G.J. Hammerling, E. Klar, and R. Ganss, *Transformation of the microvascular system during multistage tumorigenesis*. Int J Cancer, 2002. **97**(6): p. 719-25.

110. Grillet, N., A. Pattyn, C. Contet, B.L. Kieffer, C. Goridis, and J.F. Brunet, *Generation and characterization of Rgs4 mutant mice*. Mol Cell Biol, 2005. **25**(10): p. 4221-8.

111. Cifelli, C., R.A. Rose, H. Zhang, J. Voigtlaender-Bolz, S.S. Bolz, P.H. Backx, and S.P. Heximer, *RGS4 regulates parasympathetic signaling and heart rate control in the sinoatrial node*. Circ Res, 2008. **103**(5): p. 527-35.

112. Lilly, L.S. and Harvard Medical School., *Pathophysiology of heart disease : a collaborative project of medical students and faculty*. 3rd ed. 2003, Philadelphia: Lippincott Williams & Wilkins. xiii, 445 p.

113. Mirnics, K., F.A. Middleton, G.D. Stanwood, D.A. Lewis, and P. Levitt, *Disease-specific changes in regulator of G-protein signaling 4 (RGS4) expression in schizophrenia*. Mol Psychiatry, 2001. **6**(3): p. 293-301.

114. Kirk, S.L., J. Glazebrook, B. Grayson, J.C. Neill, and G.P. Reynolds, *Olanzapine-induced weight gain in the rat: role of 5-HT2C and histamine H1 receptors*. Psychopharmacology (Berl), 2009. **207**(1): p. 119-25.

115. Reynolds, G.P., M.J. Hill, and S.L. Kirk, *The 5-HT2C receptor and antipsychoticinduced weight gain - mechanisms and genetics*. J Psychopharmacol, 2006. **20**(4 Suppl): p. 15-8.

116. Reynolds, G.P., Z.J. Zhang, and X.B. Zhang, *Association of antipsychotic drug-induced weight gain with a 5-HT2C receptor gene polymorphism*. Lancet, 2002. **359**(9323): p. 2086-7.

117. Meltzer, H.Y., S. Matsubara, and J.C. Lee, *Classification of typical and atypical antipsychotic drugs on the basis of dopamine D-1, D-2 and serotonin2 pKi values*. J Pharmacol Exp Ther, 1989. **251**(1): p. 238-46.

118. Roth, B.L., R.D. Ciaranello, and H.Y. Meltzer, *Binding of typical and atypical antipsychotic agents to transiently expressed 5-HT1C receptors*. J Pharmacol Exp Ther, 1992. **260**(3): p. 1361-5.

119. Meltzer, H.Y., *Role of serotonin in the action of atypical antipsychotic drugs*. Clin Neurosci, 1995. **3**(2): p. 64-75.

120. Rosenzweig-Lipson, S., M. Brandt, K. Williams, E. Shukhina, D. Howland, K. Young, and K. Marquis, *Potentiation of 5-HT2C and 5-HT2A mediated effects in transgenic RGS-insensitive Gq (G188S) mutant rats*., in *Society for Neuroscience*. 2000: New Orleans.

121. Van de Kar, L.D., A. Javed, Y. Zhang, F. Serres, D.K. Raap, and T.S. Gray, *5-HT2A receptors stimulate ACTH, corticosterone, oxytocin, renin, and prolactin release and activate hypothalamic CRF and oxytocin-expressing cells*. J Neurosci, 2001. **21**(10): p. 3572-9.

122. Shi, J., K.J. Damjanoska, B. Zemaitaitis, F. Garcia, G. Carrasco, N.R. Sullivan, Y. She, K.H. Young, G. Battaglia, L.D. Van De kar, D.S. Howland, and N.A. Muma, *Alterations in 5-HT2A receptor signaling in male and female transgenic rats over-expressing either Gq or RGS-insensitive Gq protein*. Neuropharmacology, 2006. **51**(3): p. 524-35.

123. Goldenstein, B.L., B.W. Nelson, K. Xu, E.J. Luger, J.A. Pribula, J.M. Wald, L.A. O'Shea, D. Weinshenker, R.A. Charbeneau, X. Huang, R.R. Neubig, and V.A. Doze, *Regulator of G protein signaling protein suppression of Galphao protein-mediated alpha2A adrenergic receptor inhibition of mouse hippocampal CA3 epileptiform activity*. Mol Pharmacol, 2009. **75**(5): p. 1222-30.

124. Huang, X., R.A. Charbeneau, Y. Fu, K. Kaur, I. Gerin, O.A. MacDougald, and R.R. Neubig, *Resistance to diet-induced obesity and improved insulin sensitivity in mice with a regulator of G protein signaling-insensitive G184S Gnai2 allele*. Diabetes, 2008. **57**(1): p. 77-85.

125. Willard, F.S., M.D. Willard, A.J. Kimple, M. Soundararajan, E.A. Oestreich, X. Li, N.A. Sowa, R.J. Kimple, D.A. Doyle, C.J. Der, M.J. Zylka, W.D. Snider, and D.P. Siderovski, *Regulator of G-protein signaling 14 (RGS14) is a selective H-Ras effector*. PLoS One, 2009. **4**(3): p. e4884.

126. Willard, M.D., F.S. Willard, X. Li, S.D. Cappell, W.D. Snider, and D.P. Siderovski, *Selective role for RGS12 as a Ras/Raf/MEK scaffold in nerve growth factor-mediated differentiation*. EMBO J, 2007. **26**(8): p. 2029-40.

127. Shu, F.J., S. Ramineni, and J.R. Hepler, *RGS14 is a multifunctional scaffold that integrates G protein and Ras/Raf MAPkinase signalling pathways*. Cell Signal. **22**(3): p. 366-76.

128. Snow, B.E., L. Antonio, S. Suggs, H.B. Gutstein, and D.P. Siderovski, *Molecular cloning and expression analysis of rat Rgs12 and Rgs14*. Biochem Biophys Res Commun, 1997. **233**(3): p. 770-7.

129. Granderath, S., A. Stollewerk, S. Greig, C.S. Goodman, C.J. O'Kane, and C. Klambt, *loco encodes an RGS protein required for Drosophila glial differentiation*. Development, 1999. **126**(8): p. 1781-91.

130. Mochizuki, N., G. Cho, B. Wen, and P.A. Insel, *Identification and cDNA cloning of a novel human mosaic protein, LGN, based on interaction with G alpha i2*. Gene, 1996. **181**(1-2): p. 39-43.

131. Siderovski, D.P., M. Diverse-Pierluissi, and L. De Vries, *The GoLoco motif: a Galphai/o binding motif and potential guanine-nucleotide exchange factor*. Trends Biochem Sci, 1999. **24**(9): p. 340-1.

132. Ponting, C.P., *Raf-like Ras/Rap-binding domains in RGS12- and still-life-like signalling proteins*. J Mol Med, 1999. **77**(10): p. 695-8.

133. Willard, F.S., A.B. Low, C.R. McCudden, and D.P. Siderovski, *Differential G-alpha interaction capacities of the GoLoco motifs in Rap GTPase activating proteins*. Cell Signal, 2007. **19**(2): p. 428-38.

134. Colombo, K., S.W. Grill, R.J. Kimple, F.S. Willard, D.P. Siderovski, and P. Gonczy, *Translation of polarity cues into asymmetric spindle positioning in Caenorhabditis elegans embryos*. Science, 2003. **300**(5627): p. 1957-61.

135. Kimple, R.J., M.E. Kimple, L. Betts, J. Sondek, and D.P. Siderovski, *Structural determinants for GoLoco-induced inhibition of nucleotide release by Galpha subunits*. Nature, 2002. **416**(6883): p. 878-81.

136. Sammond, D.W., Z.M. Eletr, C. Purbeck, R.J. Kimple, D.P. Siderovski, and B. Kuhlman, *Structure-based protocol for identifying mutations that enhance protein-protein binding affinities*. J Mol Biol, 2007. **371**(5): p. 1392-404.

137. Bernard, M.L., Y.K. Peterson, P. Chung, J. Jourdan, and S.M. Lanier, *Selective interaction of AGS3 with G-proteins and the influence of AGS3 on the activation state of G-proteins*. J Biol Chem, 2001. **276**(2): p. 1585-93.

138. Natochin, M., K.G. Gasimov, and N.O. Artemyev, *Inhibition of GDP/GTP exchange on G alpha subunits by proteins containing G-protein regulatory motifs*. Biochemistry, 2001. **40**(17): p. 5322-8.

139. Webb, C.K., C.R. McCudden, F.S. Willard, R.J. Kimple, D.P. Siderovski, and G.S. Oxford, *D2 dopamine receptor activation of potassium channels is selectively decoupled by Galpha-specific GoLoco motif peptides*. J Neurochem, 2005. **92**(6): p. 1408-18.

140. Rittinger, K., P.A. Walker, J.F. Eccleston, K. Nurmahomed, D. Owen, E. Laue, S.J. Gamblin, and S.J. Smerdon, *Crystal structure of a small G protein in complex with the GTPase-activating protein rhoGAP*. Nature, 1997. **388**(6643): p. 693-7.

141. Scheffzek, K., M.R. Ahmadian, W. Kabsch, L. Wiesmuller, A. Lautwein, F. Schmitz, and A. Wittinghofer, *The Ras-RasGAP complex: structural basis for GTPase activation and its loss in oncogenic Ras mutants*. Science, 1997. **277**(5324): p. 333-8.

142. Mixon, M.B., E. Lee, D.E. Coleman, A.M. Berghuis, A.G. Gilman, and S.R. Sprang, *Tertiary and quaternary structural changes in Gi alpha 1 induced by GTP hydrolysis*. Science, 1995. **270**(5238): p. 954-60.

143. Kimple, A.J., A. Yasgar, M. Hughes, A. Jadhav, F.S. Willard, R.E. Muller, C.P. Austin, J. Inglese, G.C. Ibeanu, D.P. Siderovski, and A. Simeonov, *A high throughput fluorescence polarization assay for inhibitors of the GoLoco motif/G-alpha interaction*. Comb Chem High Throughput Screen, 2008. **11**(5): p. 396-409.

144. Kimple, R.J., L. De Vries, H. Tronchere, C.I. Behe, R.A. Morris, M. Gist Farquhar, and D.P. Siderovski, *RGS12 and RGS14 GoLoco motifs are G alpha(i) interaction sites with guanine nucleotide dissociation inhibitor Activity*. J Biol Chem, 2001. **276**(31): p. 29275-81.

145. Peterson, Y.K., M.L. Bernard, H. Ma, S. Hazard, 3rd, S.G. Graber, and S.M. Lanier, *Stabilization of the GDP-bound conformation of Gialpha by a peptide derived from the G-protein regulatory motif of AGS3*. J Biol Chem, 2000. **275**(43): p. 33193-6.

146. Willard, F.S., Z. Zheng, J. Guo, G.J. Digby, A.J. Kimple, J.M. Conley, C.A. Johnston, D. Bosch, M.D. Willard, V.J. Watts, N.A. Lambert, S.R. Ikeda, Q. Du, and D.P. Siderovski, *A point mutation to Galphai selectively blocks GoLoco motif binding: direct evidence for Galpha.GoLoco complexes in mitotic spindle dynamics*. J Biol Chem, 2008. **283**(52): p. 36698-710.

147. Du, Q. and I.G. Macara, *Mammalian Pins is a conformational switch that links NuMA to heterotrimeric G proteins*. Cell, 2004. **119**(4): p. 503-16.

148. Yu, F., Y. Cai, R. Kaushik, X. Yang, and W. Chia, *Distinct roles of Galphai and Gbeta13F subunits of the heterotrimeric G protein complex in the mediation of Drosophila neuroblast asymmetric divisions*. J Cell Biol, 2003. **162**(4): p. 623-33.

149. Schaefer, M., A. Shevchenko, and J.A. Knoblich, *A protein complex containing Inscuteable and the Galpha-binding protein Pins orients asymmetric cell divisions in Drosophila*. Curr Biol, 2000. **10**(7): p. 353-62.

150. Yu, F., X. Morin, Y. Cai, X. Yang, and W. Chia, *Analysis of partner of inscuteable, a novel player of Drosophila asymmetric divisions, reveals two distinct steps in inscuteable apical localization*. Cell, 2000. **100**(4): p. 399-409.

151. Kraut, R., W. Chia, L.Y. Jan, Y.N. Jan, and J.A. Knoblich, *Role of inscuteable in orienting asymmetric cell divisions in Drosophila*. Nature, 1996. **383**(6595): p. 50-5.

152. Parmentier, M.L., D. Woods, S. Greig, P.G. Phan, A. Radovic, P. Bryant, and C.J. O'Kane, *Rapsynoid/partner of inscuteable controls asymmetric division of larval neuroblasts in Drosophila*. J Neurosci, 2000. **20**(14): p. RC84.

153. Schaefer, M., M. Petronczki, D. Dorner, M. Forte, and J.A. Knoblich, *Heterotrimeric G proteins direct two modes of asymmetric cell division in the Drosophila nervous system*. Cell, 2001. **107**(2): p. 183-94.

154. Cho, H., K. Harrison, and J.H. Kehrl, *Regulators of G protein signaling: potential drug targets for controlling cardiovascular and immune function*. Curr Drug Targets Immune Endocr Metabol Disord, 2004. **4**(2): p. 107-18.

155. Liebmann, C., *G protein-coupled receptors and their signaling pathways: classical therapeutical targets susceptible to novel therapeutic concepts*. Curr Pharm Des, 2004. **10**(16): p. 1937-58.

156. Riddle, E.L., R.A. Schwartzman, M. Bond, and P.A. Insel, *Multi-tasking RGS proteins in the heart: the next therapeutic target?* Circ Res, 2005. **96**(4): p. 401-11.

157. Neubig, R. and D. Siderovski, *Regulators of G-protein signalling as new central nervous system drug targets*. Nat Rev Drug Discov, 2002. **1**(3): p. 187-97.

158. Sowa, M.E., W. He, T.G. Wensel, and O. Lichtarge, *A regulator of G protein signaling interaction surface linked to effector specificity*. Proc Natl Acad Sci U S A, 2000. **97**(4): p. 1483-8.

159. Popov, S.G., U.M. Krishna, J.R. Falck, and T.M. Wilkie, *Ca2+/Calmodulin reverses phosphatidylinositol 3,4, 5-trisphosphate-dependent inhibition of regulators of G protein-signaling GTPase-activating protein activity*. J Biol Chem, 2000. **275**(25): p. 18962-8.

160. Ishii, M., A. Inanobe, S. Fujita, Y. Makino, Y. Hosoya, and Y. Kurachi, *Ca(2+) elevation evoked by membrane depolarization regulates G protein cycle via RGS proteins in the heart*. Circ Res, 2001. **89**(11): p. 1045-50.

161. Ishii, M., A. Inanobe, and Y. Kurachi, *PIP3 inhibition of RGS protein and its reversal by Ca2+/calmodulin mediate voltage-dependent control of the G protein cycle in a cardiac K+ channel*. Proc Natl Acad Sci U S A, 2002. **99**(7): p. 4325-30.

162. Ishii, M., S. Fujita, M. Yamada, Y. Hosaka, and Y. Kurachi, *Phosphatidylinositol 3,4,5-trisphosphate and Ca2+/calmodulin competitively bind to the regulators of G-protein-signalling (RGS) domain of RGS4 and reciprocally regulate its action*. Biochem J, 2005. **385**(Pt 1): p. 65-73.

163. Ishii, M. and Y. Kurachi, *Assays of RGS Protein Modulation by Phosphatidylinositides and Calmodulin*. Methods Enzymol, 2004. **389**: p. 105-118.

164. Willard, F.S., A.J. Kimple, C.A. Johnston, and D.P. Siderovski, *A direct fluorescence-based assay for RGS domain GTPase accelerating activity*. Anal Biochem, 2005. **340**(2): p. 341-51.

165. Ross, E.M., *Quantitative assays for GTPase-activating proteins*. Methods Enzymol, 2002. **344**: p. 601-17.

166. Nieuwenhuijsen, B.W., Y. Huang, Y. Wang, F. Ramirez, G. Kalgaonkar, and K.H. Young, *A dual luciferase multiplexed high-throughput screening platform for protein-protein interactions*. J Biomol Screen, 2003. **8**(6): p. 676-84.

167. Wang, Y. and K.H. Young, *Analysis of RGSZ1 protein interaction with Galphai subunits*. Methods Enzymol, 2004. **390**: p. 31-52.

168. Fitzgerald, K., S. Tertyshnikova, L. Moore, L. Bjerke, B. Burley, J. Cao, P. Carroll, R. Choy, S. Doberstein, Y. Dubaquie, Y. Franke, J. Kopczynski, H. Korswagen, S.R. Krystek, N.J. Lodge, R. Plasterk, J. Starrett, T. Stouch, G. Thalody, H. Wayne, A. van der Linden, Y. Zhang, S.G. Walker, M. Cockett, J. Wardwell-Swanson, P. Ross-Macdonald, and R.M. Kindt, *Chemical genetics reveals an RGS/G-protein role in the action of a compound*. PLoS Genet, 2006. **2**(4): p. e57.

169. Mossessova, E., R.A. Corpina, and J. Goldberg, *Crystal structure of ARF1*Sec7 complexed with Brefeldin A and its implications for the guanine nucleotide exchange mechanism*. Mol Cell, 2003. **12**(6): p. 1403-11.

170. Roman, D.L., S. Ota, and R.R. Neubig, *Polyplexed flow cytometry protein interaction assay: a novel high-throughput screening paradigm for RGS protein inhibitors*. J Biomol Screen, 2009. **14**(6): p. 610-9.

171. Roman, D.L., J.N. Talbot, R.A. Roof, R.K. Sunahara, J.R. Traynor, and R.R. Neubig, *Identification of small-molecule inhibitors of RGS4 using a high-throughput flow cytometry protein interaction assay*. Mol Pharmacol, 2007. **71**(1): p. 169-75.

172. Kimple, A.J., F.S. Willard, P.M. Giguere, C.A. Johnston, V. Mocanu, and D.P. Siderovski, *The RGS protein inhibitor CCG-4986 is a covalent modifier of the RGS4 Galpha-interaction face*. Biochim Biophys Acta, 2007. **1774**(9): p. 1213-20.

173. Stokes, G.G., *On the Change of Refrangibility of Light*. Philosophical Transactions of the Royal Society of London, 1852. **142**: p. 463-562.

174. Giepmans, B.N., S.R. Adams, M.H. Ellisman, and R.Y. Tsien, *The fluorescent toolbox for assessing protein location and function*. Science, 2006. **312**(5771): p. 217-24.

175. Hahn, K. and A. Toutchkine, *Live-cell fluorescent biosensors for activated signaling proteins*. Curr Opin Cell Biol, 2002. **14**(2): p. 167-72.

176. Perrin, F., *Polarisation de la lumiËre de fluorescence. Vie moyenne des molÈcules dans l'etat excitÈ*. J. Phys. Radium, 1926. **7**(12): p. 390-401.

177. Akula, N., Y.S. Chen, K. Hennessy, T.G. Schulze, G. Singh, and F.J. McMahon, *Utility and accuracy of template-directed dye-terminator incorporation with fluorescence-polarization detection for genotyping single nucleotide polymorphisms*. Biotechniques, 2002. **32**(5): p. 1072-6, 1078.

178. Bonin, P.D. and L.A. Erickson, *Development of a fluorescence polarization assay for peptidyl-tRNA hydrolase*. Anal Biochem, 2002. **306**(1): p. 8-16.

179. Duan, W., L. Sun, J. Liu, X. Wu, L. Zhang, and M. Yan, *Establishment and application of a high throughput model for Rho kinase inhibitors screening based on fluorescence polarization*. Biol Pharm Bull, 2006. **29**(6): p. 1138-42.

180. Hsu, T.M., X. Chen, S. Duan, R.D. Miller, and P.Y. Kwok, *Universal SNP genotyping assay with fluorescence polarization detection*. Biotechniques, 2001. **31**(3): p. 560, 562, 564-8, passim.

181. Zhang, T.T., Z.T. Huang, Y. Dai, X.P. Chen, P. Zhu, and G.H. Du, *High-throughput fluorescence polarization method for identifying ligands of LOX-1*. Acta Pharmacol Sin, 2006. **27**(4): p. 447-52.

182. Lakowicz, J.R., *Principles of fluorescence spectroscopy*. 2nd ed. 1999, New York: Kluwer Academic/Plenum. xxiii, 698 p.

183. Guo, X.Q., F.N. Castellano, L. Li, and J.R. Lakowicz, *Use of a long-lifetime Re(I) complex in fluorescence polarization immunoassays of high-molecular-weight analytes*. Anal Chem, 1998. **70**(3): p. 632-7.

184. Szmacinski, H., F.N. Castellano, E. Terpetschnig, J.D. Dattelbaum, J.R. Lakowicz, and G.J. Meyer, *Long-lifetime Ru(II) complexes for the measurement of high molecular weight protein hydrodynamics*. Biochim Biophys Acta, 1998. **1383**(1): p. 151-9.

185. Terpetschnig, E., H. Szmacinski, and J.R. Lakowicz, *Fluorescence polarization immunoassay of a high-molecular-weight antigen based on a long-lifetime Ru-ligand complex*. Anal Biochem, 1995. **227**(1): p. 140-7.

186. Resch-Genger, U. and M. Ameloot, *Standardization and quality assurance in fluorescence measurements I : techniques*. 2008, New York: Springer. xvi, 496 p.

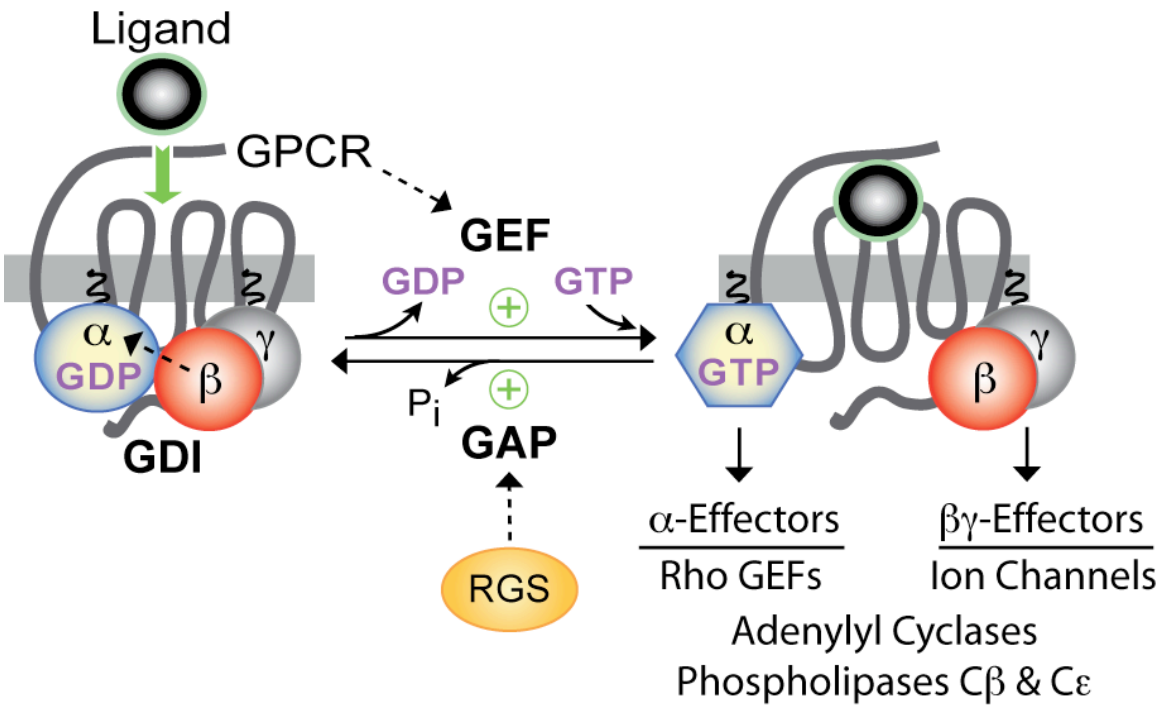

Figure 1.1 – Standard model of guanine nucleotide cycle of G-protein coupled receptors. When the seven-transmembrane receptor is unliganded the heterotrimeric G-protein consists of a GDP-bound Gα subunit associated with the Gβγ heterodimer. The Gβγ serves as a guanine nucleotide dissociation inhibitor (GDI) preventing the release of GDP. Upon binding of an agonist at the receptor, conformation changes result in the GPCR acting as a guanine nucleotide exchange factor (GEF) causing the release of GDP and subsequent binding of GTP. This exchange of bound nucleotide results in the dissociation of Gβγ and both Gα-GTP and Gβγ are free to signal to downstream effectors. Downstream effectors are activated until the GTP is hydrolyzed by the intrinsic GTP hydrolysis activity of the Gα subunit. Upon hydrolysis of GTP, Gα-GDP rebinds Gβγ and the system returns to the inactive state. The rate of GTP hydrolysis can be catalyzed by the "regulators of G-protein signaling" (RGS proteins) which serve as GTPase-accelerating proteins (GAPs).

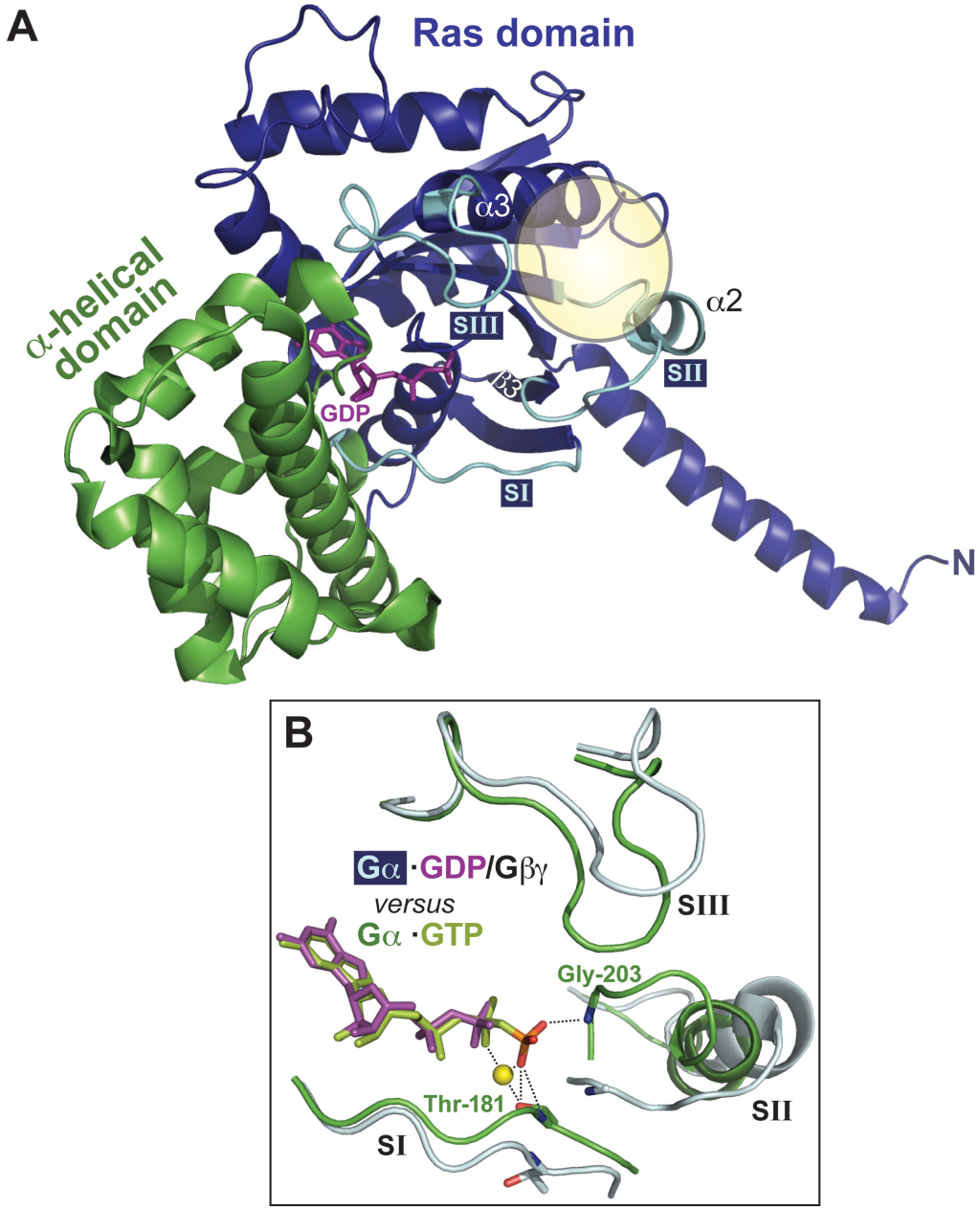

Figure 1.2 Overall structural fold of the heterotrimeric G-protein Gα subunit in its inactive, GDP-bound form (panel A) and details of structural differences between GDP- and GTP-bound states (panel B). **A**, The Gα subunit is composed of a Ras-like domain (*blue*) and an all alpha-helical domain (*green*), between which is found the guanine nucleotide binding pocket (GDP in *purple*). The three conformationally-flexible switch regions (SI, SII, and SIII) are highlighted in *cyan*. Coordinates are from PDB record 1GP2. **B**, The additional (third) phosphate (*orange* and *red*) of bound GTP establishes contacts with residues threonine-181 and glycine-203 of switches I and II, respectively, thereby leading to changes in all three switch regions (*green*) *versus* their conformation in the GDP-bound state (*cyan*). Magnesium ion is highlighted in *yellow*. Coordinates are from PDB records 1GP2 and 1GIA.

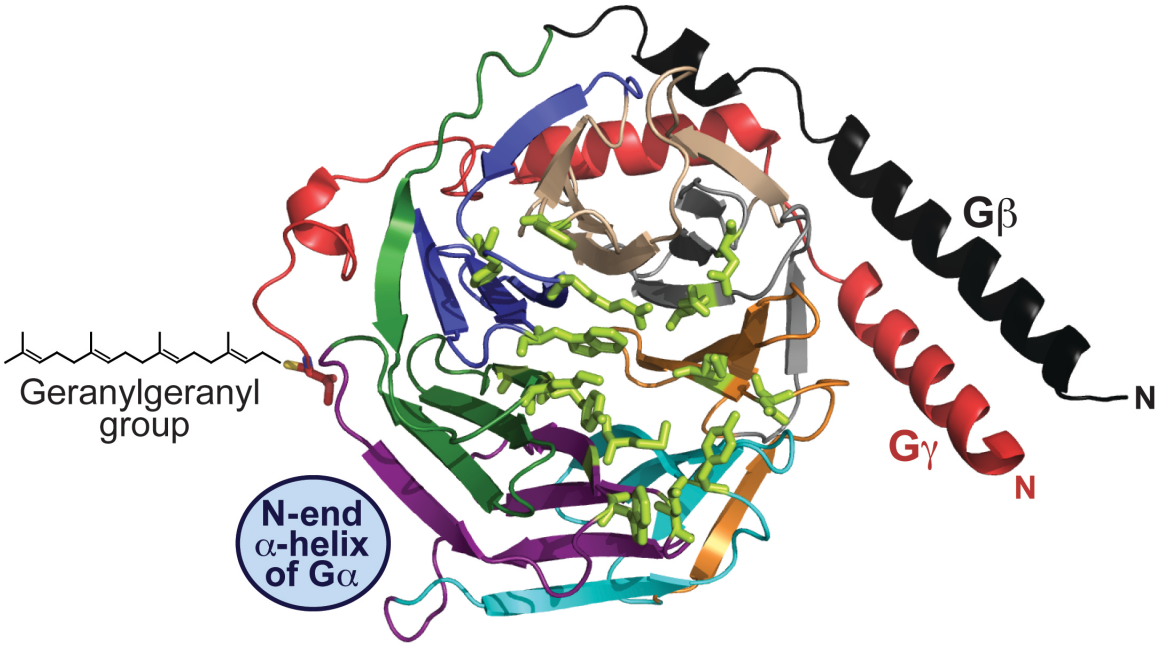

Figure 1.3. Overall structural fold of the Gβγ heterodimer. The Gβγ subunit is colored to highlight the seven WD40 repeats that comprise the beta-propeller (or "torus") fold. The cysteine residue within Gβγ (*red*) that is subjected to post-translational geranylgeranylation is highlighted in sticks configuration. The relative positioning of the N-terminal alpha-helix of the Gβγ subunit (when in the Gα·GDP/Gβγ heterotrimeric complex) is also highlighted. Coordinates are from PDB record 1OMW.

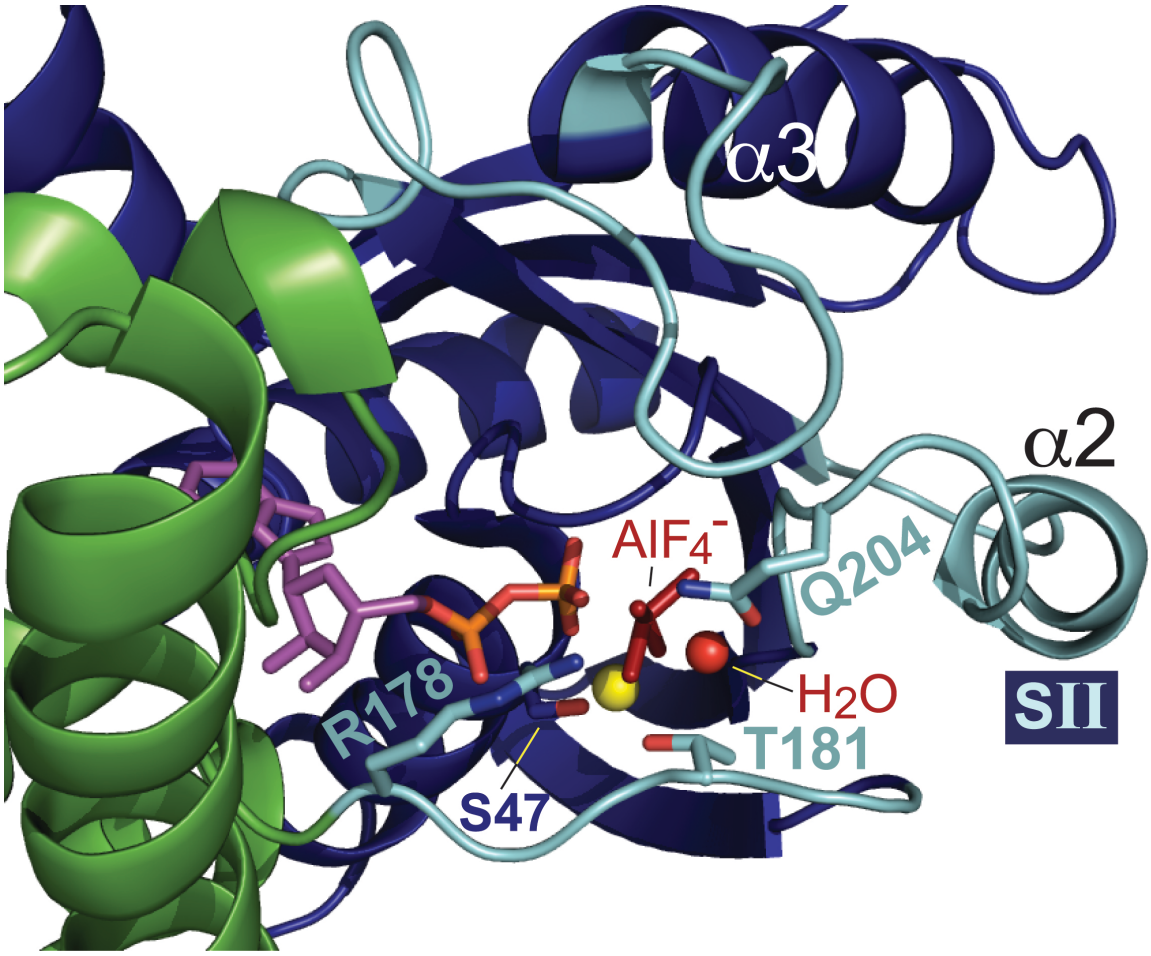

Figure 1.4. Structural basis of GTP hydrolysis. Residues within Gα that are critical to the GTP hydrolysis mechanism include arginine-178 and threonine-181 from switch I and glutamine-204 from switch II (colored as in Figure 1.2 and numbered as in $G\alpha_{i1}$; coordinates are from PDB record 1GFI). Magnesium ion is highlighted in *yellow*. The planar anion aluminum tetrafluoride, which mimics the γ-phosphate leaving group in the hydrolysis reaction, is depicted in *metallic red*.

Figure 1.5 Overall structure of the canonical RGS domain. Structure of RGS8 from the RGS8/Gα_{i3} structure (PDB id 2ODE) as rendered using PyMOL. Nine α-helices (αI-αIX; Roman numerals) form into two subdomains, the first subdomain comprised of αI, αII, αIII, αVIII, and αIX while the remaining helixes are arranged into an anti-parallel four helix bundle.

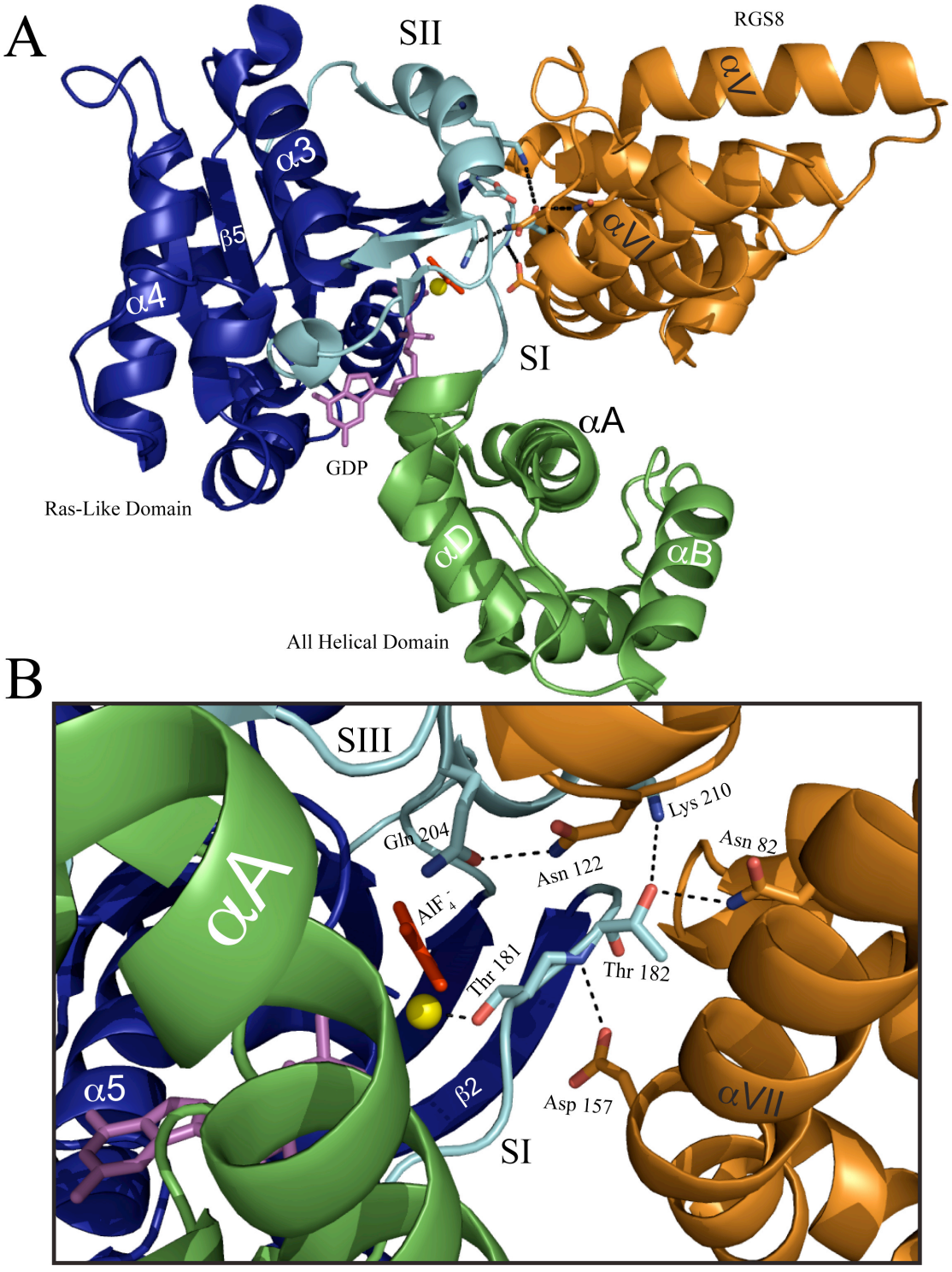

Figure 1.6 RGS proteins stabilize the transition state of Gα subunits. Cartoon representation of the RGS8/$G\alpha_{i3}$ structure (PDB id 2ODE) is rendered using PyMOL. The all-helical subdomain of $G\alpha_{i3}$ is shown in *green*, while the Ras-like nucleotide binding domain in shown in *dark blue*. The three flexible switch regions (SI, SII and SIII) are

highlighted in *cyan*. The guanine nucleotide, AlF_4^-, and Mg^{2+} are highlighted in *magenta*, *red* and *yellow* respectively while RGS8 is illustrated in *orange*. **A** The RGS8/$G\alpha_{i3}$ interface consists primarily of the SI and SII regions. **B** The Asn 122 amide forms a hydrogen bond with Gln 204 of $G\alpha_{i3}$, orienting it to help stabilize the planar leaving group while the Asn 82 of RGS8 forms contacts with side chain carbonyl of Thr 182 allowing the side chain carbonyl to make a contact with Lys 210 of SII, stabilizing SI and SII in their transition state orientations. Additionally Asp 157 of RGS8 stabilizes the backbone amine of Thr 183 allowing the Thr 181 side chain hydroxyl group to stabilize the Mg^{2+} ion.

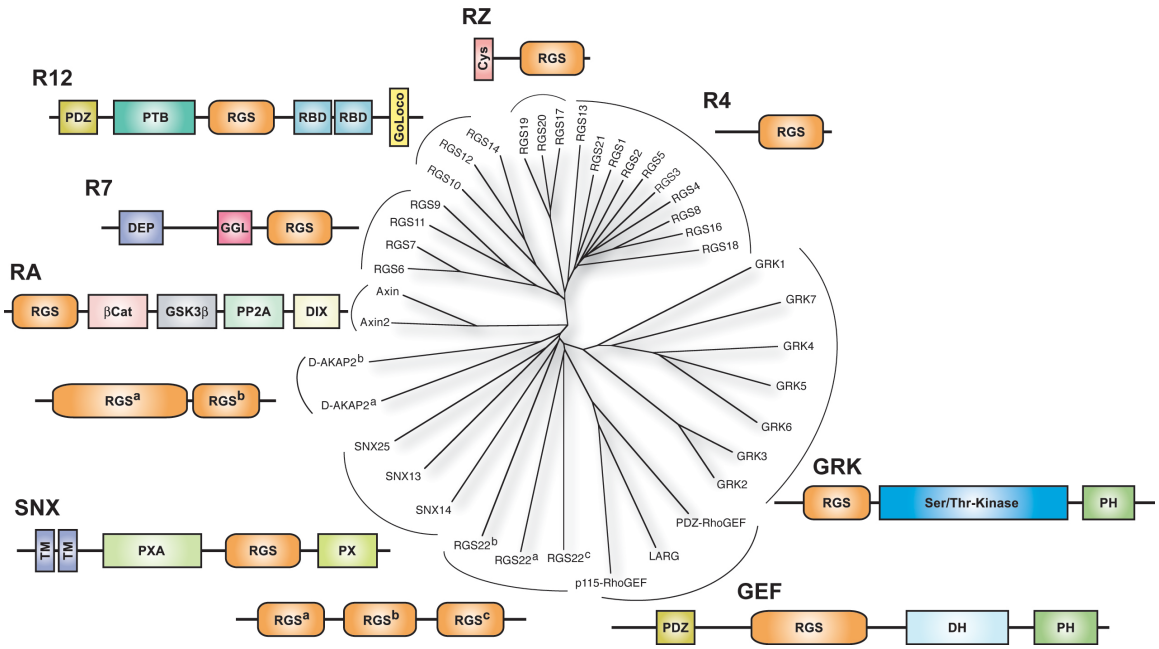

Figure 1.7 Phylogenetic relationship of the 37 RGS containing proteins identified in humans and their domain architecture. An unrooted dendogram was generated using ClustalW and visualized using TreeView. Domain boundaries were predicted using SMART.

Immobilized ligand:Gα subunits

RED= Gα·GDP BLUE= Gα·GDP·AlF_4^-

$G\alpha_{i1}$

Analyte:RGS domains at [1 μM]

$G\alpha_q$

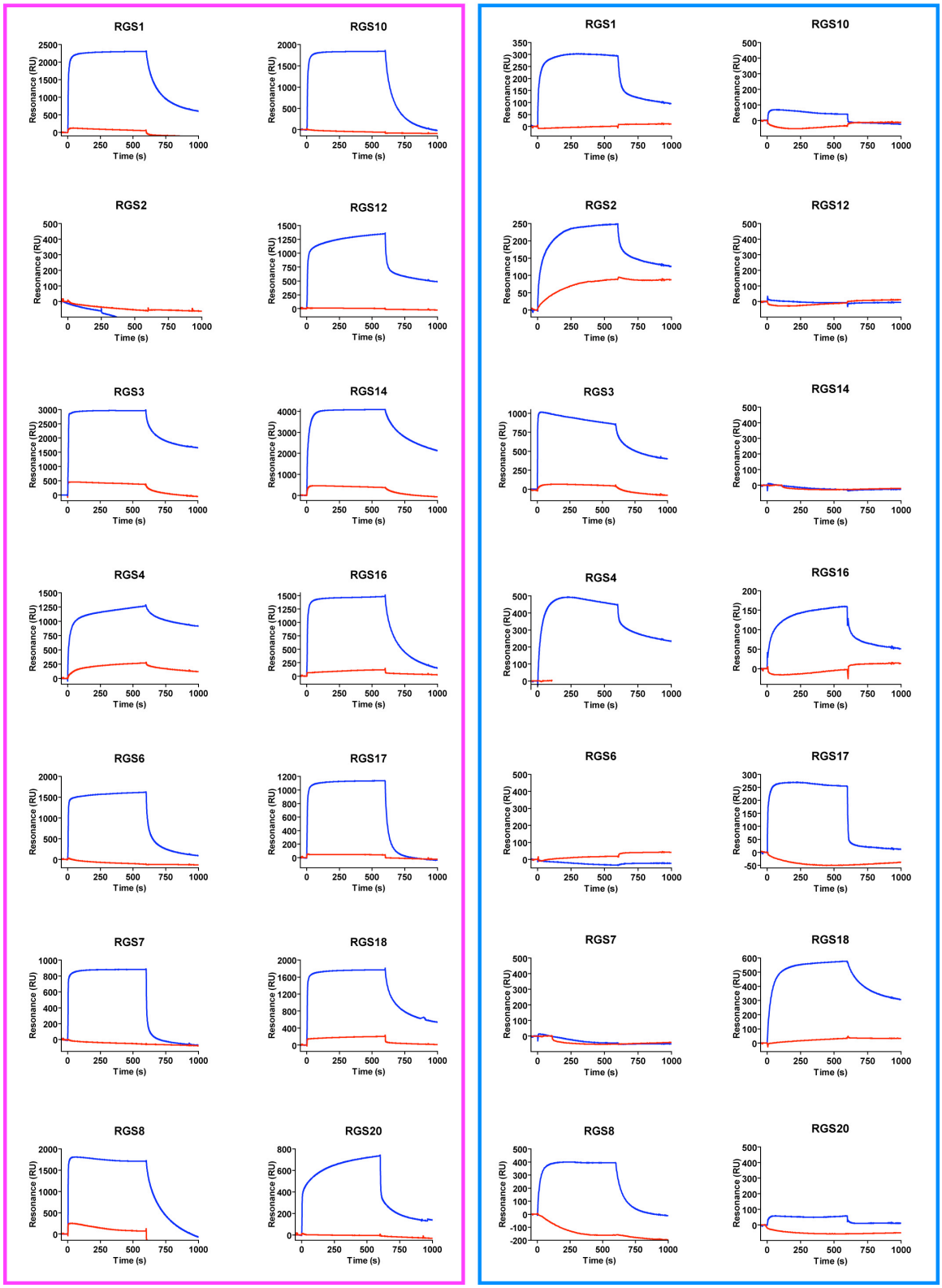

Figure 1.8. Gαi *vs* Gαq selectivity of fourteen RGS proteins as determined by surface plasmon resonance. Surface plasmon resonance (SPR) spectroscopic analyses of the binding of indicated RGS proteins (at 1 μM final concentration) to immobilized $G\alpha_{i1}$-biotin (*left side*; *pink* border) or His6-$G\alpha_q$ (*right side; cyan* border). Proteins were injected over biosensor-immobilized Gα subunits for 600 seconds (injections start at time = 0). Experiments were conducted with Gα subunits both in the inactive, GDP-bound conformation (*red* curves) and in the transition state for nucleotide hydrolysis (GDP·AlF_4^--bound; *blue* curves). All RGS domains bound to Gα in the transition state for GTP hydrolysis (*i.e.*, bound to GDP and aluminum tetrafluoride), consistent with their known biochemistry. Reprinted from Soundarajaran, Kimple, *et al.* 2008 *Proceedings of the National Academy of Sciences USA*, vol. 105, pgs. 6457-6462.

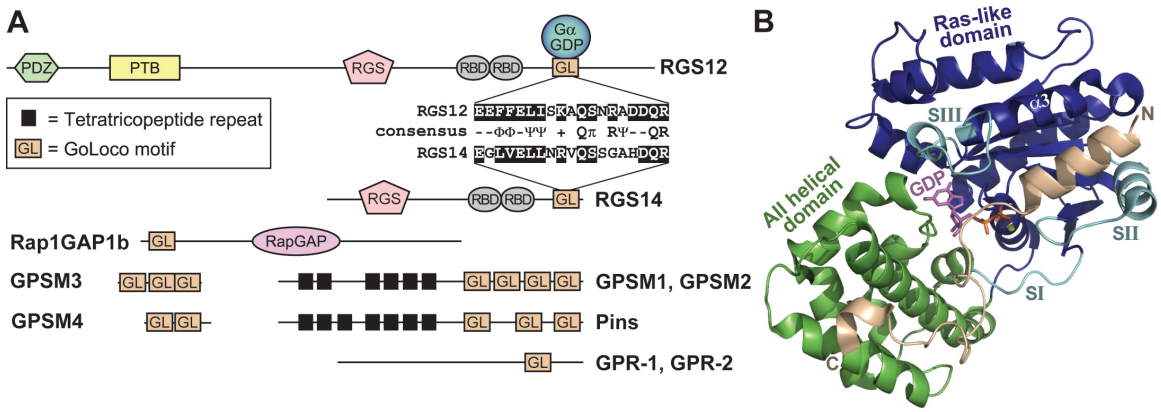

Figure 1.9. The GoLoco motif is a $G\alpha_i$·GDP -interacting polypeptide found singly or in arrays in various proteins. (A) Domain architecture of representative GoLoco motif proteins and a sequence alignment of the conserved core of the RGS12 and RGS14 GoLoco motifs. Domain abbreviations: GPSM, G-protein signaling modulator; PDZ, PSD-95/Discs large/ZO-1 homology; PTB, phosphotyrosine-binding domain; RGS, regulator of G-protein signaling box; RBD, Ras-binding domain; RapGAP, Rap-specific GTPase-activating protein domain. (B) The crystal structure of $G\alpha_{i1}$ (Ras-like domain in *blue*, all α-helical domain in *green*, switch regions in *cyan*) bound to the GoLoco motif of RGS14 (PDB ID 2OM2). The GoLoco motif peptide (*tan*) binds across the Ras-like and all-helical domains of $G\alpha_{i1}$, trapping GDP (*magenta*, with α- and β-phosphates in *orange*) within its binding site. The bound magnesium ion is illustrated in *lime green*. Reprinted from Kimple, *et al.* 2008 *Combinatorial Chemistry & High Throughput Screening*, vol. 11, pgs. 396-409.

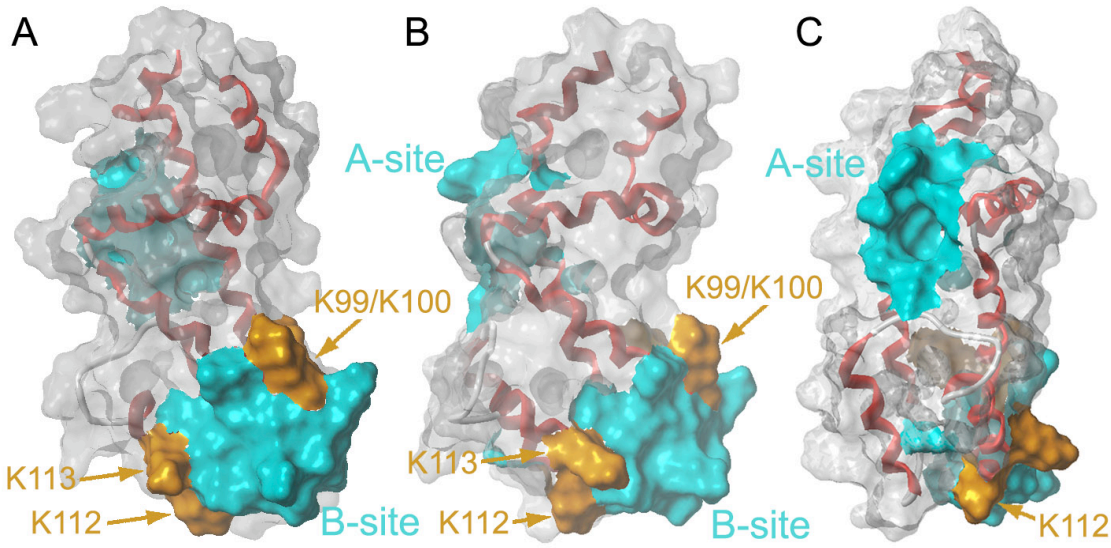

Figure 1.10. Visualization of functional sites within the RGS domain of RGS4. Orange regions depict lysines necessary for PIP_3 binding, while solid cyan areas depict the Gα binding side (A-site) and the PIP_3/Calmodulin binding site. Alpha-helical secondary structure that comprises the conserved RGS domain fold is displayed in red. Rotation about the vertical axis by 90º and 180º are shown in panels B, and C, respectively.

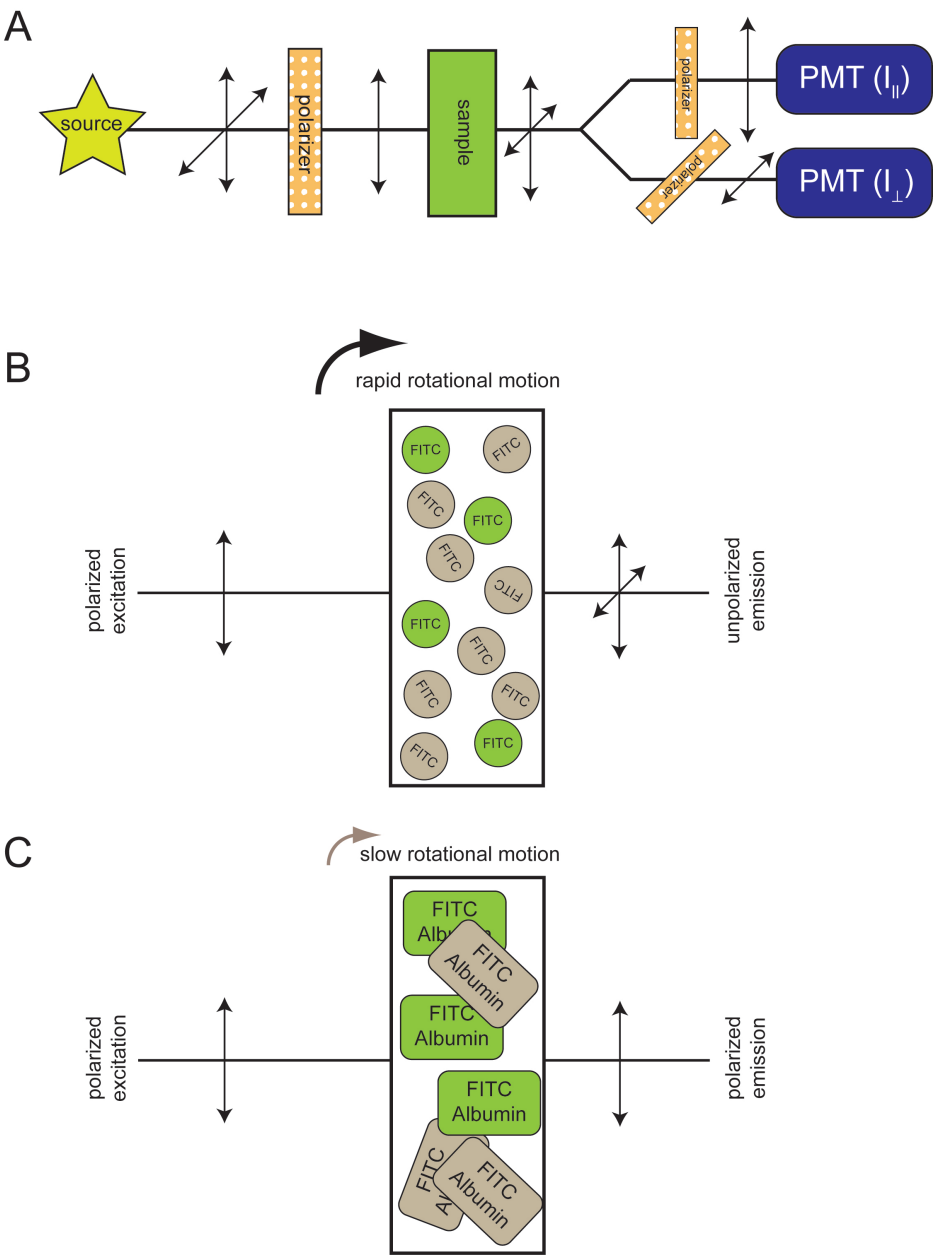

Figure 1.11. Schematic of detection of fluorescence polarization. (A) An appropriate source generates unpolarized light that is then passed through a polarizer. The polarized light enters the sample and excites a subset of the fluorescent molecules that are aligned with the incident excitation. If the sample is rapidly rotating, the incident light is depolarized. The emission is passed through a beam splitter before being passed through a polarizer that is aligned with the excitation plane in either a parallel or a perpendicular fashion. Independent photomultiplier tubes are then use to quantify the amount of emission that reaches each detector. (B) Free fluorescein (FITC) in solution completely depolarizes the excitation emission. (C) Upon conjugation to albumin, fluorescein's rotational correlation is dramatically increased and thus the emitted light remains in the same plane as the light of excitation.

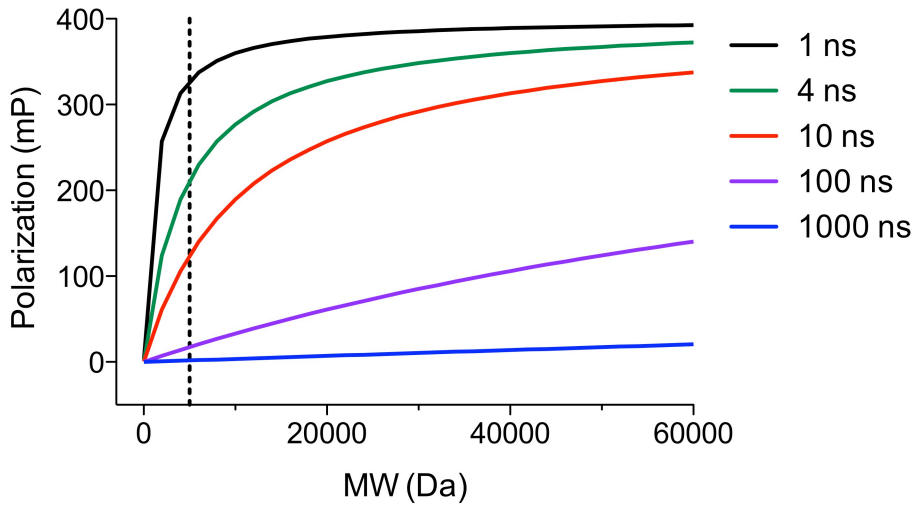

Figure 1.12 Fluorescence polarization depends on the molecular weight of the probe and its fluorescence lifetime. Curves are simulated using equation (3) and equation (4) assuming that $P_0 = 35, \bar{v} + h = 1.9$. The dotted line shows the expected polarization of a molecule of 5,000 Da with the indicated fluorescence lifetimes (color coded in the legend). The green line, representing a fluorescence lifetime of 4 ns, represents Fluorescein, a widely used dye for fluorescence polarization experiments.

CHAPTER 2

STRUCTURAL DETERMINANTS OF G-PROTEIN ALPHA SUBUNIT SELECTIVITY BY REGULATOR OF G-PROTEIN SIGNALING 2 (RGS2)*

Elements of this work referenced in this chapter have been published in:

Kimple, A. J., Soundararajan, M., Hutsell, S. Q., Roos, A. K., Urban, D. J., Setola, V., Temple, B. R., Roth, B. L., Knapp, S., Willard, F. S. and Siderovski, D. P. (2009) Structural determinants of G-protein {alpha} subunit selectivity by regulator of G-protein signaling 2 (RGS2). *J Biol Chem*. 284: 19402-19411.

2.1 ABSTRACT

"Regulator of G-protein Signaling" (RGS) proteins facilitate the termination of G-protein coupled receptor (GPCR) signaling via their ability to increase the intrinsic GTP hydrolysis rate of Gα subunits (known as GTPase-accelerating protein or "GAP" activity). RGS2 is unique in its *in vitro* potency and selectivity as a GAP for $G\alpha_q$ subunits. As many vasoconstrictive hormones signal via Gq-heterotrimer coupled receptors, it is perhaps not surprising that RGS2-deficient mice exhibit constitutive hypertension. However, to date the particular structural features within RGS2 determining its selectivity for $G\alpha_q$ over $G\alpha_{i/o}$ substrates have not been completely characterized. Here, we examine a trio of point mutations to RGS2 that elicit $G\alpha_i$-directed binding and GAP activities without perturbing its association with $G\alpha_q$. Using X-ray crystallography, we determined a model of the triple-mutant RGS2 in complex with a transition state-mimetic form of $G\alpha_i$ at 2.8 Å resolution. Structural comparison with unliganded, wildtype RGS2 and of other RGS domain/Gα complexes highlighted the roles of these residues in wildtype RGS2 that weaken $G\alpha_i$ subunit association. Moreover, these three amino acids are seen to be evolutionarily-conserved among organisms with modern cardiovascular systems, suggesting that RGS2 arose from the R4-subfamily of RGS proteins to have specialized activity as a potent and selective $G\alpha_q$ GAP that modulates cardiovascular function.

2.2 INTRODUCTION

G-protein coupled receptors (GPCRs) form an interface between extracellular and intracellular physiology, as they convert hormonal signals into changes in intracellular

metabolism and ultimately cell phenotype and function [1-3]. GPCRs are coupled to their underlying second messenger systems by heterotrimeric guanine nucleotide binding protein ("G-proteins") composed of three subunits: Gα, Gβ, and Gγ. Four general classes of Gα subunits have been defined based on functional couplings (in the GTP-bound state) to various effector proteins. G_s-subfamily Gα subunits are stimulatory to membrane-bound adenylyl cyclases that generate the second messenger 3'-5'-cyclic adenosine monophosphate (cAMP); conversely, G_i-subfamily Gα subunits are generally inhibitory to adenylyl cyclases [4]. $G_{12/13}$-subfamily Gα subunits activate the small G-protein RhoA through stimulation of the GEF-subfamily of RGS proteins, namely p115-RhoGEF, LARG, and PDZ-RhoGEF [5]. G_q-subfamily Gα subunits are potent activators of phospholipase-Cβ enzymes that generate the second messengers diacylglycerol and inositol triphosphate [6]; more recently, two additional $G\alpha_q$ effector proteins have been described: the receptor kinase GRK2 and the RhoA nucleotide exchange factor p63RhoGEF [7, 8].

The duration of GPCR signaling is controlled by the time Gα remains bound to GTP before its hydrolysis to GDP. RGS proteins are key modulators of GPCR signaling by virtue of their ability to accelerate the intrinsic GTP hydrolysis activity of Gα subunits (reviewed in [9, 10]). RGS2/G0S8, one of the first mammalian RGS proteins identified [11] and member of the R4 subfamily [10], has a critical role in the maintenance of normostatic blood pressure both in mouse models [12, 13] and in humans [14, 15]; additionally, *Rgs2*-deficient mice exhibit impaired aggression and increased anxiety [16, 17], behavioral phenotypes with potential human clinical correlates [18, 19].

While many RGS proteins are promiscuous and thus act on multiple Gα substrates *in vitro* (*e.g.*, ref. [20]), RGS2 exhibits exquisite specificity for $G\alpha_q$ in biochemical binding

assays and single turnover GTPase acceleration assays [20, 21]. Consistent with this *in vitro* selectivity[1], mice deficient in RGS2 uniquely exhibit constitutive hypertension and prolonged responses to vasoconstrictors, as would be expected upon loss of a potent negative regulator of $G\alpha_q$ which mediates signaling from various vasoconstrictive hormones such as angiotensin II, endothelin, thrombin, norepinephrine, and vasopressin [22]. In addition, RGS2-deficient mice respond to sustained pressure overload with an accelerated time-course of maladaptive cardiac remodeling [23] – a pathophysiological response which evokes myocardial hypertrophy known to be critically dependent on $G\alpha_q$ signaling [24, 25].

To gain insight into the structural basis of the unique $G\alpha$ substrate selectivity exhibited by RGS2, a series of point mutants in RGS2 were evaluated that enable this protein to bind and accelerate GTP hydrolysis by $G\alpha_i$; we subsequently delineated the structural determinants of the $G\alpha_i$/mutant RGS2 interaction using X-ray crystallography. Three key positions, first identified by Heximer and colleagues [21] and highlighted in our structural studies as key determinants of RGS2 substrate selection, were also found to be conserved throughout the evolution of the RGS2 protein in a manner suggestive of specialization towards cardiovascular signaling modulation.

2.3 EXPERIMENTAL PROCEDURES

2.3.1 Chemicals and Assay Materials

Unless otherwise noted, all chemicals were the highest grade available from Sigma Aldrich (St. Louis, MO) or Fisher Scientific (Pittsburgh, PA).

2.3.2 Protein Expression and Purification

Using ligation-independent cloning, DNA encoding human RGS2 (Lys71-His209), fused to either hexahistidine alone (His_6) or to His_6-tagged enhanced yellow fluorescent protein (YFP), was hybridized into a Novagen (San Diego, CA) pET vector-based prokaryotic expression construct as previously described [26, 27]. Point mutations corresponding to Cys106-to-serine (C106S), Asn184-to-aspartate (N184D), Arg188-to-glutamate (R188E), and Glu191-to-lysine (E191K) were made using QuikChange site-directed mutagenesis (Stratagene, La Jolla, CA). For expression of hexahistidine- and His_6-YFP-fusion RGS2 constructs, BL21(DE3) *E. coli* were grown to an OD_{600nm} of 0.7-0.8 at 37°C before induction with 0.5 mM of isopropyl-β-D-thiogalactopyranoside. After culturing for 14-16 hours at 20°C, cells were pelleted by centrifugation and frozen at -80°C. Bacterial pellets were then resuspended in N1 buffer (50 mM HEPES pH 8.0, 400 mM NaCl, 30 mM imidazole, 5% (w/v) glycerol) and lysis of bacterial slurry was performed using an Emulsiflex (Avestin; Ottawa, Canada) according to manufacturer's instructions. Cellular lysates were clarified by centrifugation at 100,000 x g for 30 minutes at 4°C. The supernatant was applied to a Ni^{2+} chelating FPLC column (FF HisTrap; GE Healthcare, Piscataway, NJ), washed with 7 column volumes of N1 buffer then 3 column volumes of N1 buffer containing an additional 30 mM imidazole before elution of recombinant RGS2 protein with N1 buffer containing 300 mM imidazole. His_6-tagged RGS2 protein was cleaved with tobacco etch virus (TEV) protease overnight at 4°C and dialyzed into N1 buffer containing 5 mM DTT. To separate residual His_6-RGS2 from untagged, cleaved RGS2, the protein was passed over a second Ni^{2+}-chelating FPLC column. The flow-through was pooled, concentrated to final volume of ~5 ml, and resolved using a calibrated 150 ml size-exclusion column (Sephacryl S200; GE

Healthcare) using S200 buffer (10 mM HEPES pH 8.0, 300 mM NaCl, DTT 5 mM, 5% (w/v) glycerol). Fractions containing monodisperse protein were then pooled and concentrated to approximately 500 μM, as determined by A_{280nm} measurements upon denaturation in 8 M guanidine hydrochloride. Concentration was calculated based on predicted extinction coefficient (http://us.expasy.org/tools/protparam.html). Additional details regarding protein purification for crystallography can be found at http://www.sgc.ox.ac.uk/structures/MM/XX03GNAI3A_2v4z_MM.html. Human RGS16 constructs, C-terminally biotinylated $G\alpha_{i1}$, N-terminally deleted (ΔN30) $G\alpha_{i1}$, CFP-$G\alpha_{i1}$, and $G\alpha_{i3}$ were purified exactly as previously described [20, 28, 29].

2.3.3 Single Turnover GTPase Assays

Single turnover [γ-^{32}P]GTP hydrolysis assays were conducted using recombinant $G\alpha_{i1}$ and various concentrations of RGS proteins as previously described [20]. Briefly, 100 nM $G\alpha_{i1}$ in reaction buffer (50 mM Tris pH 7.5, 0.05% $C_{12}E_{10}$, 1 mM DTT, 10 mM EDTA, 100 mM NaCl, and 5 μg/ml BSA) was incubated for 10 minutes at 30 ^{o}C with 1 x 10^6 cpm (2 nM) of [γ-^{32}P]GTP (specific activity of 6500 dpm/Ci). The reaction was then chilled on ice for 5 minutes prior to the addition of 10 mM $MgCl_2$ and 100 μM unlabeled GTPγS (final concentration) with or without added RGS protein. Reactions were kept on ice and 100 μl aliquots were taken at indicated time points, quenched in 900 μl of charcoal slurry, and centrifuged before 600 μl aliquots of supernatant were counted via liquid scintillation.

2.3.4 Surface Plasmon Resonance

Optical detection of protein-protein interactions by surface plasmon resonance (SPR) was performed using a Biacore 3000 (GE Healthcare; Piscataway, NJ) exactly as previously described [20, 29, 30].

2.3.5 Förster resonance energy transfer (FRET)-based Binding Assays

Förster resonance energy transfer was used to measure binding between $G\alpha_{i1}$ and triple point-mutant RGS2 (C106S+N184D+E191K) as previously described [26, 28]. In brief, FRET between recombinant $G\alpha_{i1}$-CFP and YFP-RGS2(C106S+N184D+E191K) proteins was measured using a SpectraMax Gemini fluorescence reader (Molecular Devices; Sunnyvale, CA) using an excitation wavelength of 433 nm (455 nm cutoff) and emission scans from 470-535 nm at 2 nm intervals.

2.3.6 Structure Determination

Purified Gα and RGS2(C106S+N184D+E191K) proteins were mixed at a molar ratio of 1:1.5 and incubated at 4°C for 20 minutes. The sample was passed through an S200 gel filtration column pre-equilibrated with 25 mM Hepes pH 7.5, 150 mM NaCl, 5 % glycerol, 2 mM DTT, 100 μM $AlCl_3$, 20 mM NaF and 100 μM GDP. Protein fractions that eluted as a complex were identified using SDS-PAGE and the fractions were pooled and concentrated to 23 mg/ml prior to crystallization condition screens using 150 nl drop volume with an TTP Labtech Mosquito nanoliter liquid-handling system. The crystal of the RGS2(C106S+N184D+E191K) / $G\alpha_{i3}$ complex used for data collection was crystallized by vapour diffusion in sitting drops of 400 nL protein and 200 nL reservoir solution containing 0.1 M Hepes pH 7.5 and 2 M ammonium sulphate (TTP Labtech Mosquito).

After cryoprotection in a solution of 2 M ammonium sulphate, 0.1 M Hepes pH 7.5 and 20% (w/v) D-glucose, crystals were flash cooled in liquid nitrogen. A complete data set was collected at 100 K on a Rigaku/MSC FR-E rotating anode x-ray generator equipped with an R-AXIS HTC image plate detector. Diffraction images were evaluated with MOSFLM [31], and data were scaled using SCALA [32]. The crystal belonged to the space group $P3_221$ with unit cell dimensions a = 114.54 Å, b = 114.54 Å and c = 99.33 Å. A molecular replacement solution was found in this space group using PHASER [33] with the RGS10/Gα_{i3} complex (PDB id 2IHB) as the search model. The RGS2 coordinates from PDB id 2AF0 were superimposed onto the RGS10 coordinates of the RGS10/Gα_{i3} positioned complex and rigid body refinement into the electron density was performed using REFMAC5 [34]. Difference density in the GDP binding site was modeled using the higher resolution structure of Gα_{i3} in the RGS8/Gα_{i3} complex (PDB id 2ODE) with one molecule of GDP, a tetrafluoroaluminate ion, and a magnesium ion coordinated by two additional water molecules. Several rounds of manual rebuilding in COOT [35] and restrained refinement with REFMAC5 [34], using Translation/Libration/Screw (TLS) groups calculated with TLSMD [36], resulted in the final structural model described in Table 2.1. Coordinates of the RGS2 (C106S+N184D+E191K)/Gα_{i3} complex were deposited in the Protein Data Bank with the entry code of 2V4Z.

2.3.7 Cellular cAMP Signaling Assays

HEK293T cells were transfected using Lipofectamine 2000 (Invitrogen) in 6-well dishes with 4 μg of total DNA including pGloSensor™-20F cAMP biosensor plasmid (Promega Corp., Madison WI), dopamine D2 receptor (D2R; www.cdna.org), and either empty vector,

HA-RGS2(wt) or HA-RGS2(C106S+N184D+E191K). The RGS2 expression vectors encoded solely the RGS domain (aa Lys71-His209; with an N-terminal HA-epitope tag) to avoid the influence of non-RGS-domain regions on adenylyl cyclase function (*e.g.*, ref. [37]). Twenty-four hours post–transfection, cells were re-plated on poly-D-lysine-treated, clear–bottom, white 96-well plates at a density of 60,000 cells/well. Forty-eight hours post–transfection, culture medium was aspirated and cells were washed once with assay medium (DMEM with 10% FBS (without phenol), 15 mM HEPES pH 7.4) before being incubated for 2 hours with 40 μl/well of equilibration medium (assay medium with 4% GloSensor™ substrate). After two hours, 6.6 μl of 6x final concentration quinpirole (diluted in 10 μM forskolin-containing assay medium) was added to each well and allowed to incubate for 10 minutes before GloSensor emission was read on a MicroBeta Plate Counter (PerkinElmer). Before plotting, luminescence counts were normalized to 100% maximal response for each condition to account for variability in GloSensor expression, transfection efficiency, and the exact number of cells per well.

2.4 RESULTS AND DISCUSSION

2.4.1 Evaluating point mutations to RGS2 that facilitate interaction with $G\alpha_{i1}$

RGS2 is the only member of the R4 subfamily known to bind specifically to $G\alpha_q$ and not to $G\alpha_{i/o}$ heterotrimeric G-protein subunits *in vitro* [20, 21]. Three amino-acids within RGS2 were identified by Heximer and colleagues as potential selectivity determinants in studies of $G\alpha_o$-directed GAP activity by RGS domain chimera derived from RGS2 and RGS4 sequences [21]: namely, cysteine-106, asparagine-184, and glutamate-191. In the present study, we mutated these three amino acids to the highly-conserved corresponding amino

acids in R4 subfamily members (C106 to serine, N184 to aspartate, and E191 to lysine; Figure 2.1) to identify their respective contributions to Gα substrate specificity.

RGS2 proteins containing these point mutations, either singly, in tandem, or all three together, were expressed in *E. coli* and purified to homogeneity (Figure 2.2). Surface plasmon resonance (SPR) spectroscopy was used (*e.g.*, Figure 2.3) to assess if any individual mutation, or combination of point mutations, was capable of changing the selectivity of RGS2. All mutants retained wild type binding towards $G\alpha_q$ (*e.g.*, Figure 2.3B). Single mutations to RGS2 (C106S, N184D, or E191K) did not enhance binding to $G\alpha_{i1}$ and only minimal enhancements to binding were observed with the C106S+N184D, C106S+N191D, and E191K+N184D double mutants (*e.g.*, Figure 2.3A); in contrast, the triple mutant RGS2 exhibited a dramatic increase in $G\alpha_{i1}$ binding *vs* wild type RGS2. Although the magnitude of binding of the RGS2 double mutants was significantly less than that observed with the triple mutant, binding isotherms were nonetheless generated for all double mutants along with the triple mutant by injecting increasing concentrations of RGS2 protein over the $G\alpha_{i1}$·GDP·AlF_4^- surface. Using equilibrium binding analyses (Figure 2.4), dissociation constants (K_D values) for the RGS2/$G\alpha_{i1}$·GDP·AlF_4^- interaction were estimated to be ≥5.3 μM, ≥8.6 μM, and ≥21.1 μM, for C106S+N184D, E191K+N184D, and C106S+E191K, respectively, while the K_D value was determined to be 1.25 μM for the RGS2(C106S+N184D+E191K) triple mutant. Dissociation constants derived for the RGS2 double mutants are likely underestimated given an inability to attain saturating concentrations of these particular RGS2 analytes and thereby attain maximal binding (B_{max}).

To determine if the enhanced affinity of the RGS2 triple mutant was the result of improvements to a canonical RGS domain/Gα interaction interface, a highly-conserved,

surface-exposed arginine within this canonical interface (Arg188 in the αVIII helix; Figure 2.1) was mutated to glutamic acid. As has been shown for other RGS proteins [3], this single charge-reversal point mutation (R188E) on the Gα-binding surface of the RGS2 triple mutant abolished binding to $G\alpha_{i1}$·GDP·AlF_4^- (Figure 2.4B, bottom panel).

To quantify any difference in the ability of the RGS2(C106S+N184D+E191K) triple mutant to bind $G\alpha_q$, increasing concentrations of wildtype RGS2 and RGS2 triple mutant proteins were separately injected over an immobilized $G\alpha_q$·GDP·AlF_4^- surface (Figure 2.5). Dissociation constants were determined to be 55 nM (95% confidence interval [C.I.] of 23 - 87 nM) and 17 nM (95% C.I. 9 - 27 nM) for wildtype RGS2- and RGS2(C106S+N184D+E191K)-bound $G\alpha_q$, respectively.

To confirm these SPR-derived results with an orthogonal technique of assessing the RGS domain/Gα interaction, FRET measurements were performed using a YFP-RGS2 (C106S+N184D+E191K) / $G\alpha_{i1}$-CFP pair, similar to the RGS4/$G\alpha_{i1}$ interaction FRET assay we have previously described [28]. In the presence of GDP, aluminum tetrafluoride, and Mg^{2+} ("AMF"), binding between RGS protein and Gα subunit is observed as an increase in YFP emission and decrease in CFP emission; in the presence of GDP alone, no binding is observed as expected [28, 38] and so the ratio of YFP-to-CFP emission remains low. The relative affinities of wildtype RGS2, RGS16, and RGS2 triple mutant were assessed by using this FRET binding assay in a competitive manner: unlabeled RGS protein was added in increasing amounts to a fixed concentration of YFP-RGS2(C106S+N184D+E191K) and $G\alpha_{i1}$-CFP proteins. As expected, only unlabeled RGS2(C106S+N184D+E191K) and RGS16 proteins were able to inhibit the binding of the RGS2(C106S+N184D+E191K)/$G\alpha_{i1}$ FRET pair (Figure 2.6), with observed IC_{50} values of 526 nM (95% C.I. 236-1171 nM) and 115 nM

(78-168 nM), respectively. At no concentration tested was wildtype RGS2 able to inhibit binding of the RGS2(C106S+N184D+E191K)/$G\alpha_{i1}$ FRET pair (Figure 2.6B), consistent with the lack of affinity between wildtype RGS2 and $G\alpha_i$ subunits seen in our present SPR analyses and previously published studies [20, 21].

2.4.2 Determinants of RGS2 GAP activity on $G\alpha_{i1}$ *in vitro*

Using SPR and FRET, we demonstrated that all three point mutations were required to facilitate high affinity binding of RGS2 to $G\alpha_{i1}$. To determine if this enhanced binding affected the ability of RGS2 to accelerate GTP hydrolysis by $G\alpha_{i1}$, we performed single turnover GTPase assays with both wildtype and triple mutant RGS2 proteins (Figure 2.7). At no concentration tested was wildtype RGS2 capable of increasing GTP hydrolysis over the intrinsic GTP hydrolysis rate of $G\alpha_{i1}$ (Figure 2.7A). In contrast, a substoichiometric amount of RGS16 (a known $G\alpha_{i1}$ GAP; ref. [39]) was able to accelerate $G\alpha_{i1}$ GTPase activity; complete hydrolysis of bound GTP was observed in less than 15 seconds at 0°C. Unlike wildtype RGS2, the RGS2 (C106S+N184D+E191K) triple mutant was able to increase the rate of $G\alpha_{i1}$ GTP hydrolysis in a dose-dependent manner (Figure 2.7B); however, adding the R188E mutation to the triple mutant resulted in a complete loss in GAP activity, consistent with the loss of $G\alpha_{i1}$ binding observed in SPR and FRET assays. To further confirm that the mechanism of action of the RGS2(C106S+N184D+E191K) triple mutant in increasing GTP hydrolysis by $G\alpha_{i1}$ was related to a canonical RGS domain/$G\alpha$ interaction and not the inadvertant addition of a contaminating GTPase, we assessed the effects of both RGS2(C106S+N184D+E191K) and RGS16 proteins on an RGS-insensitive $G\alpha_{i1}$ point mutant: specifically, G183S in the $G\alpha$ switch I region [40]. Neither RGS2

(C106S+N184D+E191K) nor RGS16 proteins were able to increase the intrinsic rate of GTP hydrolysis exhibited by this RGS-insensitive $G\alpha_{i1}$ (Figure 2.7C,D).

2.4.3 Determinants of RGS2 activity on G_i-coupled GPCR signaling in cells

To validate in a cellular context the change in Gα specificity exhibited *in vitro* by the RGS2(C106S+N184D+E191K) triple mutant, we used an intracellular cAMP biosensor to measure G_i-heterotrimer-mediated inhibition of forskolin-stimulated cAMP production in HEK293T expressing the G_i-coupled D2 dopamine receptor along with either wildtype RGS2 or the RGS2(C106S+N184D+E191K) mutant. Upon treatment of transfected cells with forskolin, a robust increase in luminescence was observed from the cAMP sensor, reflecting direct activation of adenylyl cyclase by forskolin [4]; upon administration of the dopamine D2/D3-receptor selective agonist, quinpirole, dose-dependent inhibition of this cAMP production was observed. Wildtype RGS2 had no effect on the IC_{50} of quinpirole (Figure 2.8). However, cellular expression of the RGS2(C106S+N184D+E191K) triple mutant resulted in a significantly higher IC_{50} for quinpirole (762 nM *versus* 18 nM for empty vector; Figure 2.8), indicating that the gain of $G\alpha_i$-directed activity is readily apparent in a cellular context as well as *in vitro* for the RGS2 triple mutant.

2.4.4 Structural determinants of RGS2 interaction with Gα subunits

To determine the structural basis for the Gα selectivity of RGS2, we used X-ray crystallography to obtain a structural model of the RGS2 triple mutant bound to a $G\alpha_i$ subunit. A diffraction pattern data set was collected on a single crystal containing a complex between the RGS2(C106S+N184D+E191K) triple mutant and $G\alpha_{i3}{\cdot}GDP{\cdot}AlF_4^-$ and was refined to 2.8 Å resolution (Table 2.1). The resultant structural model revealed canonical

RGS domain/Gα interactions [20, 41] – specifically, contacts between the flexible switch regions of $G\alpha_{i3}$ and the nine alpha-helical bundle formed by the RGS2 triple mutant (Figure 2.9).

One of the three mutation sites within the RGS2 triple mutant, aspartate-184, is observed to form a double salt bridge (Figure 2.10A and Figure 2.11) with the neighboring arginine-188 – the latter being an αVIII residue completely conserved among all other R4-subfamily RGS domains (Figure 2.1). Asparagine-184 of wildtype RGS2, located between helix αVII and αVIII, is an aspartic acid in all other R4-subfamily RGS domains (Figure 2.1). The additional terminal oxygen present in the aspartate side-chain (and missing in asparagine) normally allows two salt bridges to be formed (Figure 2.10A) with the conserved αVIII helix arginine residue (*e.g.*, Arg-170 of RGS16, Arg-188 of RGS2). These salt bridges are not consistently observed in all unliganded RGS domain structures [20]; however, this double salt bridge is present in all R4-subfamily RGS domains complexed with $G\alpha_{i/o}$ subunits (Table 2.2), suggesting that their formation is important for making the RGS domain competent to bind $G\alpha_{i/o}$ subunits. The importance of this Arg-Asn side-chain interaction is supported by the loss of $G\alpha_i$ binding and $G\alpha_i$-directed GAP activity when this αVIII helix arginine is mutated to glutamate (Figures 2.4 & 2.7). The significance of this intramolecular interaction is further supported by observations that mutating the analogous αVIII helix arginine in RGS4 (Arg-167) and RGS12 (Arg-821) results in loss of $G\alpha_{i/o}$ binding and $G\alpha_{i/o}$-directed GAP activity [3, 42, 43]. While Arg-188 of RGS2 does not make any critical contacts with $G\alpha_{i3}$ *per se*, it has a critical role in orienting Asp-184 (Figure 2.10B) to form a conserved hydrogen bond with the main chain amide of a threonine residue in the Gα switch I region (Thr-182 of $G\alpha_i$ [20, 41]; Thr-183 of $G\alpha_o$ [44]). In the structure of wildtype,

uncomplexed RGS2 (PDB id 2AF0; ref. [20]), asparagine at this position (Asn-184) forms only a single hydrogen bond with terminal amine of Arg-188 and, rotated in this manner, the side-chain cannot at the same time form a hydrogen bond the the Thr-182 backbone (Figure 2.10A and Table 2.2).

The aspartate substitution at position Asn-184 is critical to allow binding of RGS2 to $G\alpha_i$; however, this single substitution alone is not sufficient to engender robust $G\alpha_i$ binding (Figure 2.3). Ser-106 is completely conserved among all R4-subfamily RGS domains except RGS2, in which this position is a cysteine residue (Figure 2.1). Mutating Cys-106 to serine was also necessary to obtain high affinity binding to $G\alpha_i$ subunits (Figures 2.3 & 2.4); while the Ser-106 side chain was not observed in the structural model to make any critical contacts with $G\alpha_{i3}$, this residue is tightly packed amongst other residues (Figure 2.10B). The structure of the RGS2(C106S+N184D+E191K)/$G\alpha_{i3}$ complex reveals that the β-carbon of Ser-106 is closely juxtaposed with the backbone carbonyl and γ-hydroxyl of Thr-182 within switch I of $G\alpha_{i3}$; additionally, the α-carbon of Ser-106 is 3.8 Å from the terminal amine of Lys-210 within switch II of $G\alpha_{i3}$. In conjunction with the SPR binding data, the observed tight packing of Ser-106 within the RGS2(C106S+N184D+E191K)/$G\alpha_{i3}$ complex suggests that the Cys-106 residue of wildtype RGS2 prevents high affinity binding to $G\alpha_i$ subunits by steric blockade of interactions with switch I and switch II of the Gα subunit.

While amino-acid positions 106 and 184 are completely conserved among all R4-subfamily RGS domains except RGS2, the specific amino acid at position 191 is conserved only in its basic character, being either a lysine or an arginine in all R4-subfamily RGS domains (Figure 2.1). In wildtype RGS2, this position is instead an acidic residue (glutamate-191). In the structural data derived from the RGS2(C106S+N184D+E191K)/$G\alpha_{i3}$ complex,

electron density was present only for the α-, β-, and γ-carbons of the mutated position Lys-191; however, the final ordered carbon atom was found to be only 5.1 Å from the hydroxyl oxygen of Glu-65 in the αA helix of the $G\alpha_{i3}$ all-helical domain. Electron density was present to fit the Cα, Cβ, Cγ, and Cδ atoms of the Lys-191 residue (Figure 2.11). The Cε and terminal amine were modeled by superimposing a Lys over those parts of the carbon atom-chain that could be placed with electron density, revealing that this basic side-chain would be less than 3.0 Å from the hydroxyl oxygen of $G\alpha_{i3}$ Glu-65 and thus within hydrogen bonding distance. It is possible that the high salt concentration necessary for crystallization screened the electrostatic contribution of this interaction away, resulting in a partially disordered side chain. In wildtype RGS2, this salt bridge would be lacking and this position instead would create electrostatic repulsion between RGS2 Glu-191 and the all-helical domain of $G\alpha_{i3}$. The importance of all-helical domain contacts to RGS protein selectivity for Gα substrates has been previously speculated for the retinal-specific proteins RGS9-1 and Gα-transducin [45]; our present finding with RGS2 provides one of the first structural insights into these interactions. These RGS domain/all-helical domain interactions, while typically underappreciated when considering the structural determinants of the RGS protein/Gα interaction interface (*e.g.*, ref. [41]; *cf.* ref. [20]), may provide a unique point of interdiction to exploit with selective RGS protein inhibitors.

2.4.5 Unique determinants of RGS2 $G\alpha_q$ selectivity are conserved among species with cardiovascular systems

Current knowledge of Gα selectivity suggests that R4-subfamily members, as well as proteins from the more ancestral RZ-subfamily (*e.g.*, RGS17, -19, -20), can act as GAPs for both $G\alpha_i$ and $G\alpha_q$ subunits [20, 46], with the R4-protein RGS2 particularly attuned to $G\alpha_q$

over $G\alpha_i$. Given its unique $G\alpha$ selectivity and its specialized role in cardiovascular signal transduction, RGS2 is likely to have arisen from the R4-subfamily in response to the development of cardiovascular structures and function.

In evolutionary terms, $G\alpha_q$ emerged as the harbinger of a distinct and recognizable $G\alpha$ subfamily in fungi, and $G\alpha_q$ subunits are present in all metazoans including sponges [47, 48]. While RZ-subfamily RGS proteins are represented within the genomes of nematodes and arthropods [49], a distinct R4-subfamily does not appear until the evolution of urochordates. The genome of the urochordate *C. intestinalis* (sea squirt) encodes at least two RGS proteins (Figure 2.12), an ortholog of the ancestral RZ-subfamily progenitor found in nematodes and arthropods, as well as a newly-divergent R4-subfamily member (but not an RGS2 ortholog *per se*). With specialized tissues such as a notochord, digestive tract, single chamber heart, and gonads, *C. intestinalis* is commonly considered an excellent modern representative of the precursor to higher vertebrates [50, 51]. Agnatha (jawless fish) such as the sea lamprey *Petromyzon marinus* are considered the most primitive extant members of early vertebrates [52] and represent the first vertebrate to exhibit cardiac innervation [53]. While the *P. marinus* cardiovascular system is more advanced than the open system of *C. intestinalis*, it is still considered primitive in that it lacks an elastin-reinforced vasculature [54], coronary circulation, and a pericardial-contained fourth chamber (conus or bulbus arteriosus) to dampen systolic oscillations in blood pressure [53]. Similar to *C. intestinalis,* the genome of *P. marinus* encodes at least two RGS proteins, the ancestral RZ member and a single R4 member (Figure 2.12); however, no RGS2-like protein has yet been identified in this species.

As chordates evolved into the Gnathostomata (jawed vertebrates), the cardiovascular system rapidly developed coronary vessels, inhibitory vagal innervation, excitatory adrenergic innervation, and responses to prostaglandins, nitric oxide, and endothelin [55]. This advance is marked in *D. rerio* by the addition of multiple R4 proteins, specifically including a $G\alpha_q$-specific RGS2 protein (Figure 2.12). This unique member of the R4-subfamily, with cysteine, asparagine, and aspartate at the three key specificity positions, is highly conserved in the extant representatives of all subsequent evolutionary steps: amphibians (*e.g.*, *X. laevis* and *X. tropicalis*), avians (*e.g.*, *G. gallus*) and mammals (Figure 2.12); the three defining residues are seen to be unique amongst all R4-subfamily members within a given species (*e.g.*, human R4 paralogs aligned in Figure 2.1). Only amphibians (*X. laevis* and *X. tropicalis*) do not contain all three RGS2-defining amino acids (Figure 2.12): while the RGS2 signature residue asparagine is present at position 184, serine (not cysteine) is present at position 106 and a neutral glutamine (not glutamate) is present at position 191. (Note that the latter glutamine is not seen in RGS2, RGS4, nor RGS20 paralogs). Even though the conservation is not absolute in the amphibians, we have shown that asparagine in position 184 is sufficient on its own to significantly reduce $G\alpha_i$ affinity (*i.e.*, ~20-fold; compare K_D of >21 μM for the C106S/E191K RGS2 double mutant *vs* K_D of 1.25 μM for the C106S/N184D/E191K triple mutant in Figure 2.4). In conclusion, the conservation of these three key residue positions suggests that RGS2 has indeed evolved from the R4-subfamily to be a specialized $G\alpha_q$ GAP for the modern cardiovascular system by acquiring particular residues at one or more of three key positions that have been highlighted in our mutagenesis/crystallography studies.

2.5 REFERENCES

1. Pierce, K.L., R.T. Premont, and R.J. Lefkowitz, *Seven-transmembrane receptors.* Nat Rev Mol Cell Biol, 2002. **3**(9): p. 639-50.

2. Offermanns, S., *G-proteins as transducers in transmembrane signalling.* Prog Biophys Mol Biol, 2003. **83**(2): p. 101-30.

3. McCudden, C.R., M.D. Hains, R.J. Kimple, D.P. Siderovski, and F.S. Willard, *G-protein signaling: back to the future.* Cell Mol Life Sci, 2005. **62**(5): p. 551-77.

4. Sunahara, R.K. and R. Taussig, *Isoforms of mammalian adenylyl cyclase: multiplicities of signaling.* Mol Interv, 2002. **2**(3): p. 168-84.

5. Fukuhara, S., H. Chikumi, and J.S. Gutkind, *RGS-containing RhoGEFs: the missing link between transforming G proteins and Rho?* Oncogene, 2001. **20**(13): p. 1661-8.

6. Rhee, S.G., *Regulation of phosphoinositide-specific phospholipase C.* Annu Rev Biochem, 2001. **70**: p. 281-312.

7. Lutz, S., A. Shankaranarayanan, C. Coco, M. Ridilla, M.R. Nance, C. Vettel, D. Baltus, C.R. Evelyn, R.R. Neubig, T. Wieland, and J.J. Tesmer, *Structure of Galphaq-p63RhoGEF-RhoA complex reveals a pathway for the activation of RhoA by GPCRs.* Science, 2007. **318**(5858): p. 1923-7.

8. Tesmer, V.M., T. Kawano, A. Shankaranarayanan, T. Kozasa, and J.J. Tesmer, *Snapshot of activated G proteins at the membrane: the Galphaq-GRK2-Gbetagamma complex.* Science, 2005. **310**(5754): p. 1686-90.

9. Hollinger, S. and J.R. Hepler, *Cellular regulation of RGS proteins: modulators and integrators of G protein signaling.* Pharmacol Rev, 2002. **54**(3): p. 527-59.

10. Willard, M.D., F.S. Willard, and D.P. Siderovski, *The superfamily of 'regulator of G-protein signaling' (RGS) proteins*, in *Handbook of Cell Signaling*, R. Bradshaw and E. Dennis, Editors. 2008, Elsevier: San Diego.

11. Siderovski, D.P., A. Hessel, S. Chung, T.W. Mak, and M. Tyers, *A new family of regulators of G-protein-coupled receptors?* Curr Biol, 1996. **6**(2): p. 211-2.

12. Heximer, S.P., R.H. Knutsen, X. Sun, K.M. Kaltenbronn, M.H. Rhee, N. Peng, A. Oliveira-dos-Santos, J.M. Penninger, A.J. Muslin, T.H. Steinberg, J.M. Wyss, R.P. Mecham, and K.J. Blumer, *Hypertension and prolonged vasoconstrictor signaling in RGS2-deficient mice.* J Clin Invest, 2003. **111**(4): p. 445-52.

13. Tang, K.M., G.R. Wang, P. Lu, R.H. Karas, M. Aronovitz, S.P. Heximer, K.M. Kaltenbronn, K.J. Blumer, D.P. Siderovski, Y. Zhu, and M.E. Mendelsohn, *Regulator of*

G-protein signaling-2 mediates vascular smooth muscle relaxation and blood pressure. Nat Med, 2003. **9**(12): p. 1506-12.

14. Gu, S., S. Tirgari, and S.P. Heximer, *The RGS2 gene product from a candidate hypertension allele shows decreased plasma membrane association and inhibition of Gq.* Mol Pharmacol, 2008. **73**(4): p. 1037-43.

15. Semplicini, A., L. Lenzini, M. Sartori, I. Papparella, L.A. Calo, E. Pagnin, G. Strapazzon, C. Benna, R. Costa, A. Avogaro, G. Ceolotto, and A.C. Pessina, *Reduced expression of regulator of G-protein signaling 2 (RGS2) in hypertensive patients increases calcium mobilization and ERK1/2 phosphorylation induced by angiotensin II.* J Hypertens, 2006. **24**(6): p. 1115-24.

16. Oliveira-Dos-Santos, A.J., G. Matsumoto, B.E. Snow, D. Bai, F.P. Houston, I.Q. Whishaw, S. Mariathasan, T. Sasaki, A. Wakeham, P.S. Ohashi, J.C. Roder, C.A. Barnes, D.P. Siderovski, and J.M. Penninger, *Regulation of T cell activation, anxiety, and male aggression by RGS2.* Proc Natl Acad Sci U S A, 2000. **97**(22): p. 12272-7.

17. Yalcin, B., S.A. Willis-Owen, J. Fullerton, A. Meesaq, R.M. Deacon, J.N. Rawlins, R.R. Copley, A.P. Morris, J. Flint, and R. Mott, *Genetic dissection of a behavioral quantitative trait locus shows that Rgs2 modulates anxiety in mice.* Nat Genet, 2004. **36**(11): p. 1197-202.

18. Cui, H., N. Nishiguchi, E. Ivleva, M. Yanagi, M. Fukutake, H. Nushida, Y. Ueno, N. Kitamura, K. Maeda, and O. Shirakawa, *Association of RGS2 gene polymorphisms with suicide and increased RGS2 immunoreactivity in the postmortem brain of suicide victims.* Neuropsychopharmacology, 2008. **33**(7): p. 1537-44.

19. Smoller, J.W., M.P. Paulus, J.A. Fagerness, S. Purcell, L.H. Yamaki, D. Hirshfeld-Becker, J. Biederman, J.F. Rosenbaum, J. Gelernter, and M.B. Stein, *Influence of RGS2 on anxiety-related temperament, personality, and brain function.* Arch Gen Psychiatry, 2008. **65**(3): p. 298-308.

20. Soundararajan, M., F.S. Willard, A.J. Kimple, A.P. Turnbull, L.J. Ball, G.A. Schoch, C. Gileadi, O.Y. Fedorov, E.F. Dowler, V.A. Higman, S.Q. Hutsell, M. Sundstrom, D.A. Doyle, and D.P. Siderovski, *Structural diversity in the RGS domain and its interaction with heterotrimeric G protein alpha-subunits.* Proc Natl Acad Sci U S A, 2008. **105**(17): p. 6457-62.

21. Heximer, S.P., S.P. Srinivasa, L.S. Bernstein, J.L. Bernard, M.E. Linder, J.R. Hepler, and K.J. Blumer, *G protein selectivity is a determinant of RGS2 function.* J Biol Chem, 1999. **274**(48): p. 34253-9.

22. Keys, J.R., E.A. Greene, W.J. Koch, and A.D. Eckhart, *Gq-coupled receptor agonists mediate cardiac hypertrophy via the vasculature.* Hypertension, 2002. **40**(5): p. 660-6.

23. Takimoto, E., N. Koitabashi, S. Hsu, E.A. Ketner, M. Zhang, T. Nagayama, D. Bedja, K.L. Gabrielson, R. Blanton, D.P. Siderovski, M.E. Mendelsohn, and D.A. Kass,

Regulator of G protein signaling 2 mediates cardiac compensation to pressure overload and antihypertrophic effects of PDE5 inhibition in mice. J Clin Invest, 2009. 119(2): p 408-20

24. Akhter, S.A., L.M. Luttrell, H.A. Rockman, G. Iaccarino, R.J. Lefkowitz, and W.J. Koch, *Targeting the receptor-Gq interface to inhibit in vivo pressure overload myocardial hypertrophy.* Science, 1998. **280**(5363): p. 574-7.

25. Wettschureck, N., H. Rutten, A. Zywietz, D. Gehring, T.M. Wilkie, J. Chen, K.R. Chien, and S. Offermanns, *Absence of pressure overload induced myocardial hypertrophy after conditional inactivation of Galphaq/Galpha11 in cardiomyocytes.* Nat Med, 2001. **7**(11): p. 1236-40.

26. Kimple, A.J., F.S. Willard, P.M. Giguere, C.A. Johnston, V. Mocanu, and D.P. Siderovski, *The RGS protein inhibitor CCG-4986 is a covalent modifier of the RGS4 Galpha-interaction face.* Biochim Biophys Acta, 2007. **1774**(9): p. 1213-20.

27. Stols, L., M. Zhou, W.H. Eschenfeldt, C.S. Millard, J. Abdullah, F.R. Collart, Y. Kim, and M.I. Donnelly, *New vectors for co-expression of proteins: structure of Bacillus subtilis ScoAB obtained by high-throughput protocols.* Protein Expr Purif, 2007. **53**(2): p. 396-403.

28. Willard, F.S., R.J. Kimple, A.J. Kimple, C.A. Johnston, and D.P. Siderovski, *Fluorescence-based assays for RGS box function.* Methods Enzymol, 2004. **389**: p. 56-71.

29. Willard, F.S., A.B. Low, C.R. McCudden, and D.P. Siderovski, *Differential G-alpha interaction capacities of the GoLoco motifs in Rap GTPase activating proteins.* Cell Signal, 2007. **19**(2): p. 428-38.

30. Willard, F.S. and D.P. Siderovski, *Covalent immobilization of histidine-tagged proteins for surface plasmon resonance.* Anal Biochem, 2006. **353**(1): p. 147-9.

31. Leslie, A.G., *Integration of macromolecular diffraction data.* Acta Crystallogr D Biol Crystallogr, 1999. **55**(Pt 10): p. 1696-702.

32. Evans, P.R., in *Proceedings of the CCP4 Study Weekend on Data Collection and Processing*, L. Sawyer, N. Issacs, and S. Burley, Editors. 1993, Science and Engineering Research Council/Daresbury Laboratory: Warrington, England. p. 114-122.

33. Storoni, L.C., A.J. McCoy, and R.J. Read, *Likelihood-enhanced fast rotation functions.* Acta Crystallogr D Biol Crystallogr, 2004. **60**(Pt 3): p. 432-8.

34. Murshudov, G.N., A.A. Vagin, and E.J. Dodson, *Refinement of macromolecular structures by the maximum-likelihood method.* Acta Crystallogr D Biol Crystallogr, 1997. **53**(Pt 3): p. 240-55.

35. Emsley, P. and K. Cowtan, *Coot: model-building tools for molecular graphics.* Acta Crystallogr D Biol Crystallogr, 2004. **60**(Pt 12 Pt 1): p. 2126-32.

36. Painter, J. and E.A. Merritt, *Optimal description of a protein structure in terms of multiple groups undergoing TLS motion.* Acta Crystallogr D Biol Crystallogr, 2006. **62**(Pt 4): p. 439-50.

37. Sinnarajah, S., C.W. Dessauer, D. Srikumar, J. Chen, J. Yuen, S. Yilma, J.C. Dennis, E.E. Morrison, V. Vodyanoy, and J.H. Kehrl, *RGS2 regulates signal transduction in olfactory neurons by attenuating activation of adenylyl cyclase III.* Nature, 2001. **409**(6823): p. 1051-5.

38. Popov, S., K. Yu, T. Kozasa, and T.M. Wilkie, *The regulators of G protein signaling (RGS) domains of RGS4, RGS10, and GAIP retain GTPase activating protein activity in vitro.* Proc Natl Acad Sci U S A, 1997. **94**(14): p. 7216-20.

39. Wieland, T., N. Bahtijari, X.B. Zhou, C. Kleuss, and M.I. Simon, *Polarity exchange at the interface of regulators of G protein signaling with G protein alpha-subunits.* J Biol Chem, 2000. **275**(37): p. 28500-6.

40. Ingi, T., A.M. Krumins, P. Chidiac, G.M. Brothers, S. Chung, B.E. Snow, C.A. Barnes, A.A. Lanahan, D.P. Siderovski, E.M. Ross, A.G. Gilman, and P.F. Worley, *Dynamic regulation of RGS2 suggests a novel mechanism in G-protein signaling and neuronal plasticity.* J Neurosci, 1998. **18**(18): p. 7178-88.

41. Tesmer, J.J., D.M. Berman, A.G. Gilman, and S.R. Sprang, *Structure of RGS4 bound to AlF4--activated G(i alpha1): stabilization of the transition state for GTP hydrolysis.* Cell, 1997. **89**(2): p. 251-61.

42. Druey, K.M. and J.H. Kehrl, *Inhibition of regulator of G protein signaling function by two mutant RGS4 proteins.* Proc Natl Acad Sci U S A, 1997. **94**(24): p. 12851-6.

43. Srinivasa, S.P., N. Watson, M.C. Overton, and K.J. Blumer, *Mechanism of RGS4, a GTPase-activating protein for G protein alpha subunits.* J Biol Chem, 1998. **273**(3): p. 1529-33.

44. Slep, K.C., M.A. Kercher, T. Wieland, C.K. Chen, M.I. Simon, and P.B. Sigler, *Molecular architecture of Galphao and the structural basis for RGS16-mediated deactivation.* Proc Natl Acad Sci U S A, 2008. **105**(17): p. 6243-8.

45. Skiba, N.P., C.S. Yang, T. Huang, H. Bae, and H.E. Hamm, *The alpha-helical domain of Galphat determines specific interaction with regulator of G protein signaling 9.* J Biol Chem, 1999. **274**(13): p. 8770-8.

46. Hepler, J.R., D.M. Berman, A.G. Gilman, and T. Kozasa, *RGS4 and GAIP are GTPase-activating proteins for Gq alpha and block activation of phospholipase C beta by gamma-thio-GTP-Gq alpha.* Proc Natl Acad Sci U S A, 1997. **94**(2): p. 428-32.

47. Seack, J., M. Kruse, and W.E. Muller, *Evolutionary analysis of G-proteins in early metazoans: cloning of alpha- and beta-subunits from the sponge Geodia cydonium.* Biochim Biophys Acta, 1998. **1401**(1): p. 93-103.

48. Suga, H., M. Koyanagi, D. Hoshiyama, K. Ono, N. Iwabe, K. Kuma, and T. Miyata, *Extensive gene duplication in the early evolution of animals before the parazoan-eumetazoan split demonstrated by G proteins and protein tyrosine kinases from sponge and hydra.* J Mol Evol, 1999. **48**(6): p. 646-53.

49. Sierra, D.A., D.J. Gilbert, D. Householder, N.V. Grishin, K. Yu, P. Ukidwe, S.A. Barker, W. He, T.G. Wensel, G. Otero, G. Brown, N.G. Copeland, N.A. Jenkins, and T.M. Wilkie, *Evolution of the regulators of G-protein signaling multigene family in mouse and human.* Genomics, 2002. **79**(2): p. 177-85.

50. Chiba, S., A. Sasaki, A. Nakayama, K. Takamura, and N. Satoh, *Development of Ciona intestinalis juveniles (through 2nd ascidian stage).* Zoolog Sci, 2004. **21**(3): p. 285-98.

51. Davidson, B., *Ciona intestinalis as a model for cardiac development.* Semin Cell Dev Biol, 2007. **18**(1): p. 16-26.

52. Pancer, Z., W.E. Mayer, J. Klein, and M.D. Cooper, *Prototypic T cell receptor and CD4-like coreceptor are expressed by lymphocytes in the agnathan sea lamprey.* Proc Natl Acad Sci U S A, 2004. **101**(36): p. 13273-8.

53. McKenzie, D.J., A.P. Farrell, and C.J. Brauner, *Primitive fishes*. Fish physiology, v. 26. 2007, Amsterdam; Boston: Academic Press.

54. Davison, I.G., G.M. Wright, and M.E. DeMont, *The structure and physical properties of invertebrate and primitive vertebrate arteries.* J Exp Biol, 1995. **198**(Pt 10): p. 2185-96.

55. Evans, D.H. and J.B. Claiborne, *The physiology of fishes*. 2006, Boca Raton, FL: CRC, Taylor & Francis.

56. Cladman, W. and P. Chidiac, *Characterization and comparison of RGS2 and RGS4 as GTPase-activating proteins for m2 muscarinic receptor-stimulated G(i).* Mol Pharmacol, 2002. **62**(3): p. 654-9.

57. Hains, M.D., D.P. Siderovski, and T.K. Harden, *Application of RGS box proteins to evaluate G-protein selectivity in receptor-promoted signaling.* Methods Enzymol, 2004. **389**: p. 71-88.

58. Heximer, S.P. and K.J. Blumer, *RGS proteins: Swiss army knives in seven-transmembrane domain receptor signaling networks.* Sci STKE, 2007. **2007**(370): p. pe2.

2.6 FOOTNOTES

* Coordinates for the triple point-mutant RGS2/$G\alpha_{i3}$·GDP·AlF_4^- complex are available in the Protein Data Bank (id 2V4Z). This work was supported by funding from the U.S. National Institutes of Health (R01 GM082892 to D.P.S., T32 GM008570 to S.Q.H., T32 GM008719 and F30 MH074266 to A.J.K.), and the American Heart Association Mid-Atlantic Affiliate (0815239E to D.J.U.). The Structural Genomics Consortium is a registered charity (number 1097737) that receives funds from the Canadian Institutes for Health Research, the Canadian Foundation for Innovation, Genome Canada through the Ontario Genomics Institute, GlaxoSmithKline, Karolinska Institutet, the Knut and Alice Wallenberg Foundation, the Ontario Innovation Trust, the Ontario Ministry for Research and Innovation, Merck & Co., Inc., the Novartis Research Foundation, the Swedish Agency for Innovation Systems, the Swedish Foundation for Strategic Research and the Wellcome Trust. Current address for F.S.W.: Lilly Research Laboratories, Eli Lilly and Company, Indianapolis, IN 46285.

[1] Independent reports (*e.g.*, refs. [40, 56, 57]) have demonstrated that, in membrane-reconstitution systems containing GPCRs and G-protein heterotrimers, RGS2 can affect the agonist-dependent GTPase activity of G_i-coupled signaling systems. The basis for this discrepancy between RGS2 selectivity for $G\alpha_q$ in binary, solution-based assays and apparent RGS2 activity on $G\alpha_i$ in reconstituted systems has not yet been resolved, but it is important to note that RGS2 (like other RGS proteins) is known to interact with other components of GPCR signal transduction beyond $G\alpha$ subunits [58], including isoforms of the $G\alpha_i$ effector target, adenylyl cyclase [37].

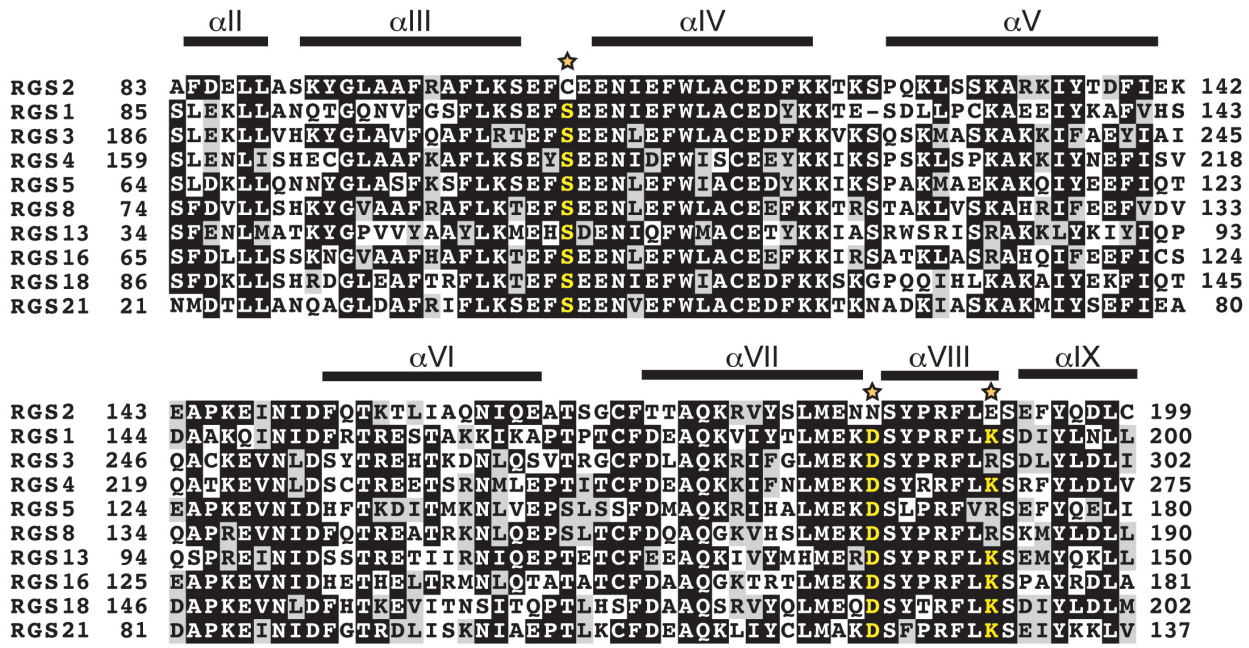

Figure 2.1 - Multiple sequence alignment of the conserved core of R4-subfamily RGS domains. Sequence alignment of the indicated *Homo sapiens* RGS protein RGS domains was made using ClustalW (http://www.ebi.ac.uk/Tools/clustalw/index.html) and BoxShade Server http://www.ch.embnet.org/software/BOX_form.html). Regions of secondary structure, as denoted above the sequence of RGS2, are based on the X-ray crystallographic structure of unliganded wildtype RGS2 (PDB id 2AF0). Open stars highlight the three amino acid positions described in this study.

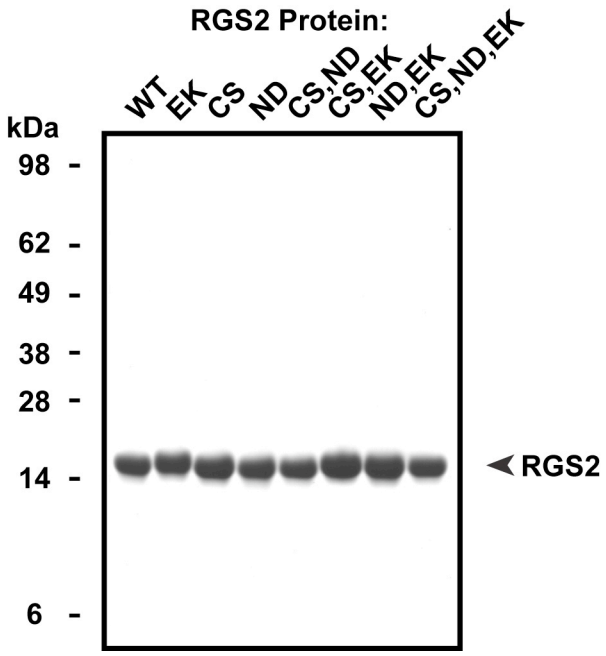

Figure 2.2 - Equivalent purification of wild-type and point-mutant RGS2 proteins used in biochemical analyses is highlighted by Coomassie blue staining of SDS-PAGE resolved proteins. Abbreviations: WT, wild-type sequence; EK, glutamate-191 to lysine; CS, cysteine-106 to serine; ND, asparagine-184 to aspartate.

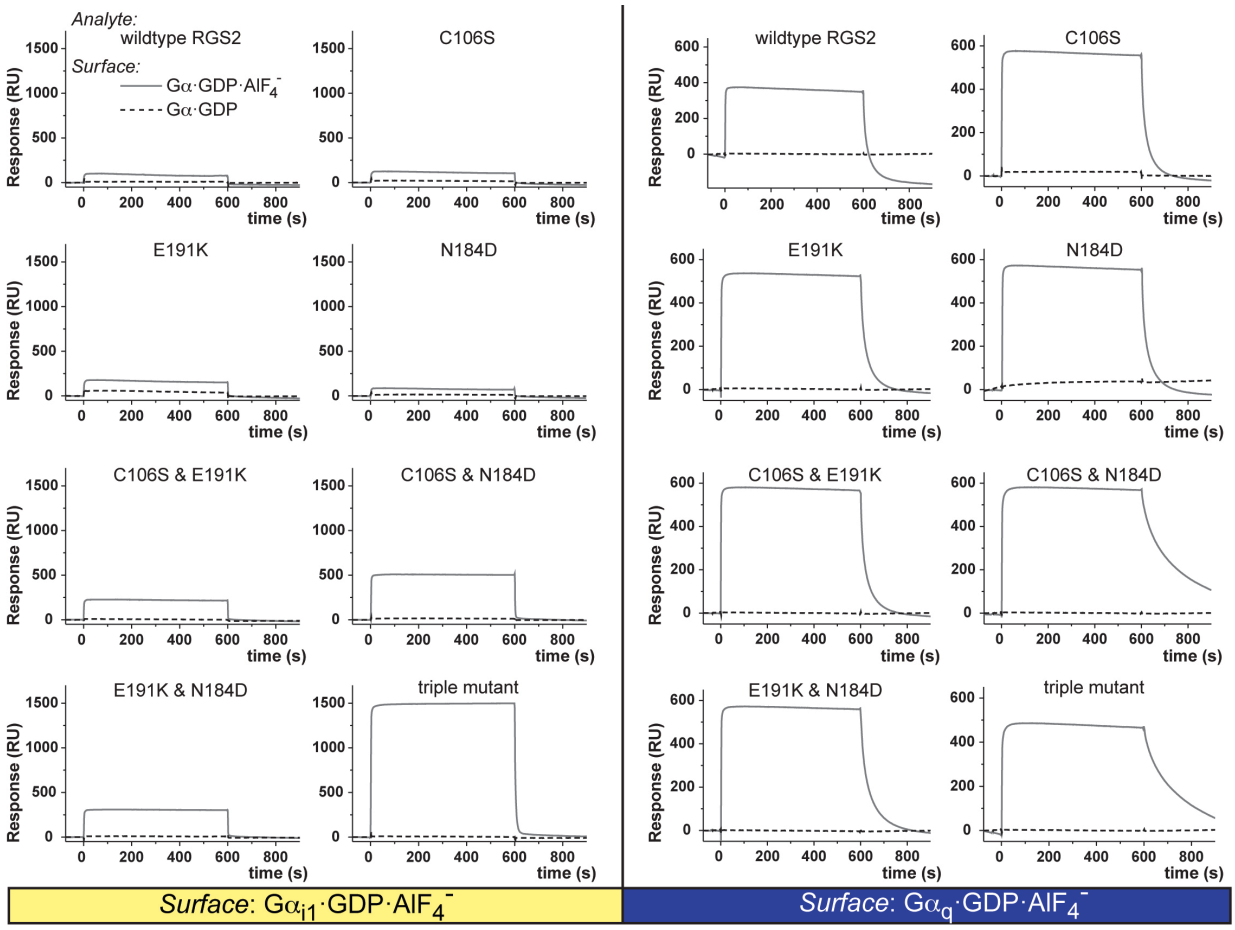

Figure 2.3. $G\alpha_{i1}$ and $G\alpha_q$ selectivity of wildtype RGS2 versus RGS2 point mutants profiled by surface plasmon resonance (SPR). $G\alpha_{i1}$-biotin (*left*) or His_6-$G\alpha_q$ (*right*) was immobilized on sensor surfaces for binding analyses of indicated RGS2 protein analytes (3 μM final concentration). Analyte injections were performed at a flow rate of 20 μl/min for 600 seconds (start time = 0 s) over surfaces of Gα subunits in the inactive state (GDP-bound; dashed lines) or in the transition-state for GTP hydrolysis (*i.e.*, GDP·AlF_4^--bound; solid lines). Legend in panel A also applies to sensorgrams of panel B.

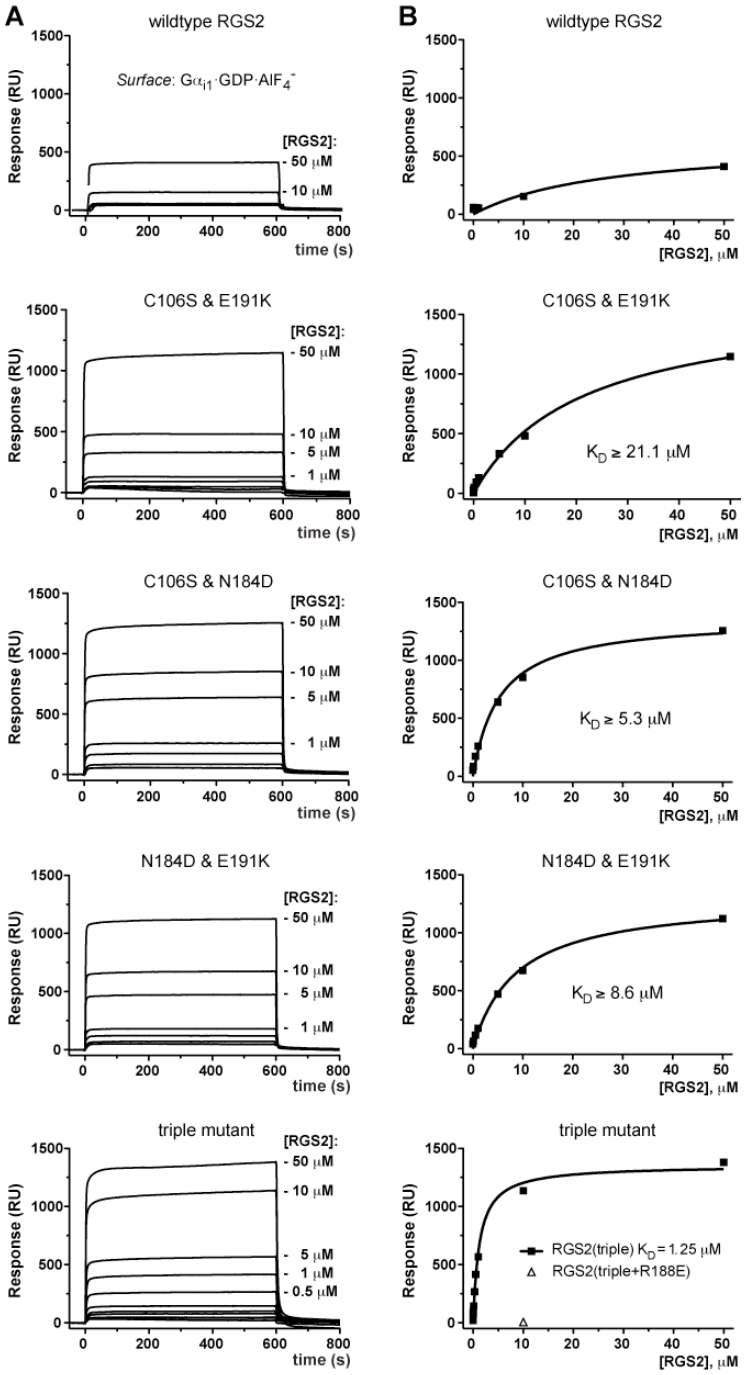

Figure 2.4. Quantitation of RGS2 binding to $G\alpha_{i1}$. SPR was performed as described in Figure 2.3, with the concentration of the RGS2 analyte titrated from 1 nM to 50 μM. Sensorgrams were subsequently used in equilibrium saturation binding analyses to determine RGS2/$G\alpha_{i1}$ interaction binding affinities. Dissociation constants (K_D values) were estimated to be ≥21.1 (95% confidence interval [C.I.] 11.6 - 30.7) μM, ≥5.3 (95% C.I. 3.1 - 7.5) μM, and ≥8.6 (95% C.I. 5.4 - 11.9) μM for the double mutants RGS2(C106S+E191K), RGS2(C106S+N184D), RGS2(N184D+E191K), respectively, and determined to be 1.25 (95% C.I. 1.0 - 1.6) μM for the triple mutant RGS2(C106S+N184D+E191K). A K_D value for the wildtype RGS2/$G\alpha_{i1}$ interaction could not be estimated because saturation was not obtained at concentrations tested.

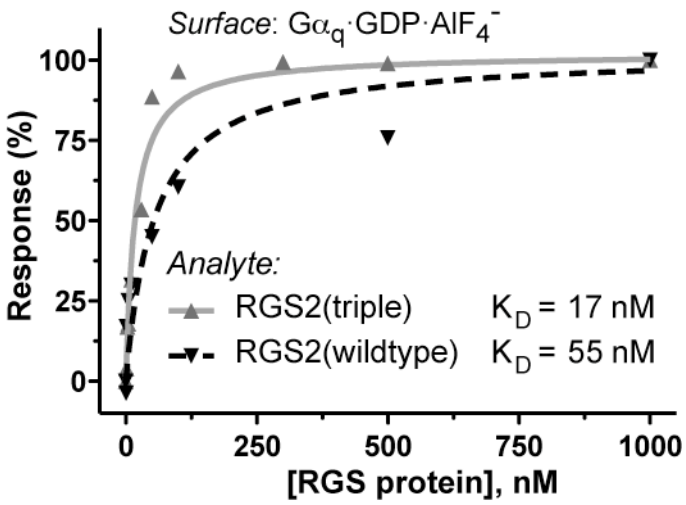

Figure 2.5. Quantification of RGS2 binding to $G\alpha_q$. SPR was performed as described in Figure 2.3, using an immobilized His_6-$G\alpha_q$·GDP·AlF_4^- surface and RGS2 analyte concentrations from 0.5 - 1000 nM. Using equilibrium saturation binding analyses, RGS2/$G\alpha_q$ dissociation constants were determined to be 55 nM (95% C.I. 23.4 – 86.9 nM) for wildtype RGS2 and 17 nM (95% C.I. 8.7 - 27.0 nM) for the RGS2(C106S+N184D+E191K) triple mutant.

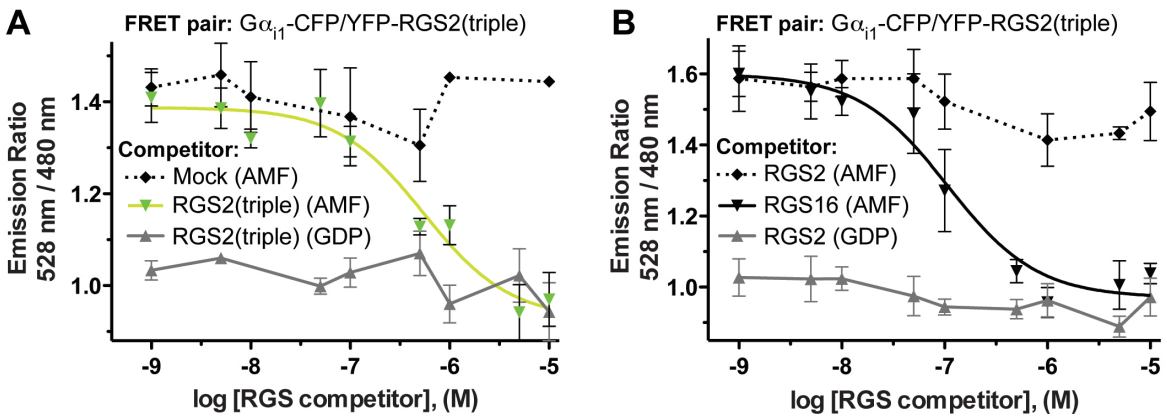

Figure 2.6. Competition FRET Assays of the Gα$_{i1}$-CFP/YFP-RGS2(triple) interaction. (**A**) The fusion proteins YFP-RGS2(C106S+N184D+E191K) and Gα$_{i1}$-CFP interact in the presence of GDP and $AlF_4^-{\cdot}Mg^{2+}$ ("AMF") but not in the presence of GDP alone. This interaction can be inhibited by the addition of unlabeled RGS2(C106S+N184D+E191K) "triple" mutant protein (IC_{50} value of 526 nM; 95% C.I. 236-1171 nM), but not by the addition of buffer alone. (**B**) The addition of unlabeled wildtype RGS2 to the Gα$_{i1}$-CFP/YFP-RGS2(triple mutant) FRET pair does not result in a decrease in FRET; however, the addition of RGS16 (known to have affinity for Gα$_{i1}$; ref. (20)) competitively inhibits binding (IC_{50} value of 115 nM; 95% C.I. 78-168 nM).

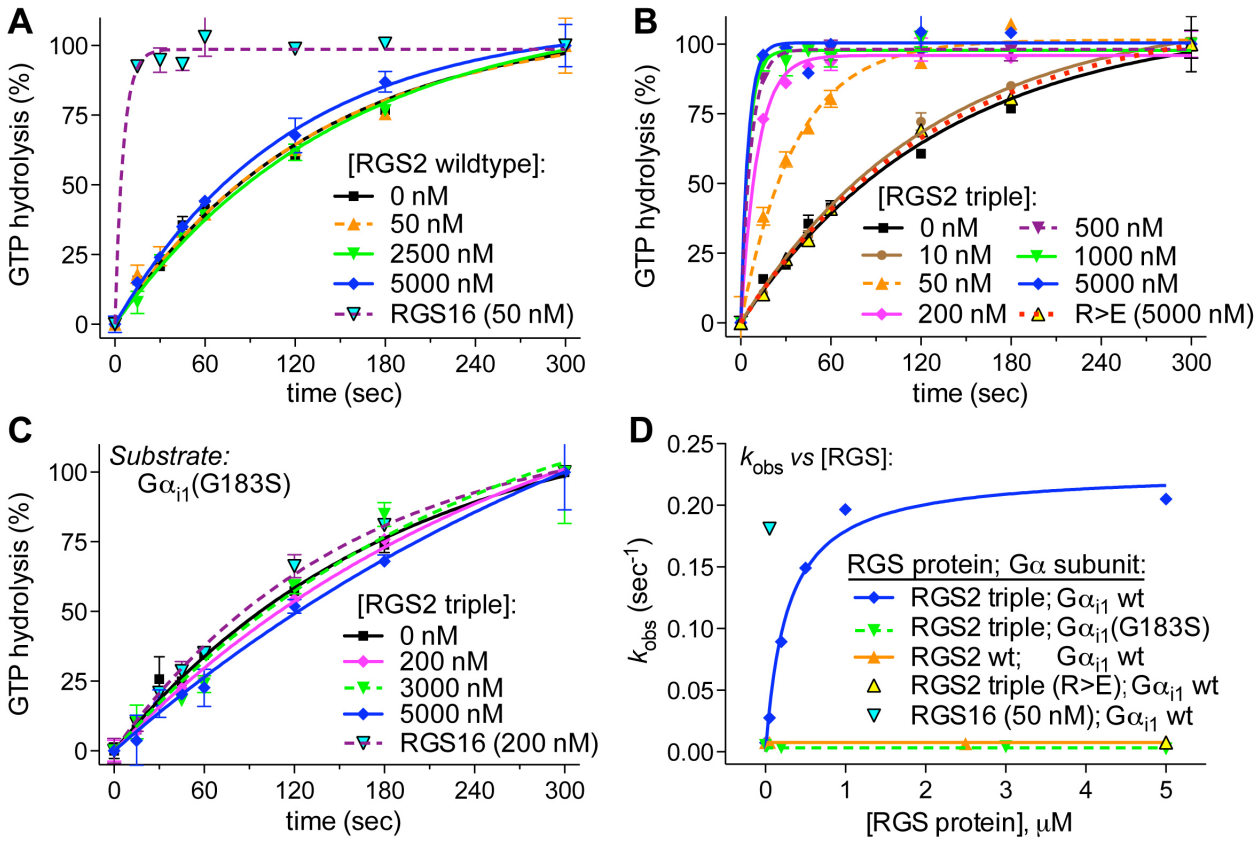

Figure 2.7. The triple mutant RGS2(C106S+N184D+E191K), but not wildtype RGS2, accelerates the GTP hydrolysis rate of $G\alpha_{i1}$. (**A**) Increasing concentrations of wildtype RGS2 (as indicated) are unable to accelerate the GTP hydrolysis of 200 nM $G\alpha_{i1}$. Intrinsic GTP hydrolysis by isolated $G\alpha_{i1}$ (k_{obs}) was measured at 0.0075 sec^{-1} (95% C.I. 0.0055-0.010 sec^{-1}), while k_{obs} values of 0.0076 (0.0055-0.0097) sec^{-1}, 0.0066 (0.0054-0.0078) sec^{-1} and 0.0086 (0.0069-0.010) sec^{-1} were observed upon the addition of 50 nM, 2500 nM, or 5000 nM wildtype RGS2, respectively. RGS16 is a potent GAP for $G\alpha_i$ subunits (*e.g.*, ref. (20)) and, at substoichiometic concentrations (50 nM), was found to accelerate GTP hydrolysis by $G\alpha_{i1}$: k_{obs} of at least 0.18 sec^{-1} (an underestimate as the measurement is limited by sampling-time constraints). (**B**) The triple mutant RGS2(C106S+N184D+E191K) was observed to accelerate GTP hydrolysis by 200 nM $G\alpha_{i1}$ in a dose-dependent manner: k_{obs} values of 0.0075 (0.0055-0.0095) sec^{-1}, 0.0079 (0.0068-0.0089) sec^{-1}, and 0.028 sec^{-1} (0.023-0.032 sec^{-1}) were observed upon the addition of 0 nM, 10 nM, and 50 nM of RGS2(triple) protein, respectively. Higher concentrations of RGS2(triple) protein (200 nM, 500 nM, 1000 nM, and 5000 nM) led to GTPase rates of at least 0.1 - 0.2 sec^{-1} (again underestimated due to sampling-time constraints). The triple mutant also containing a fourth, loss-of-function point mutation (namely, RGS2(C106S+N184D+E191K;R188E)) was unable to accelerate GTP hydrolysis by $G\alpha_{i1}$: k_{obs} value of 0.0076 (0.0066-0.0086) sec^{-1}. (**C**) The single point mutation to $G\alpha_{i1}$ (glycine-183-to-serine, "G183S"; ref. (41)) renders $G\alpha_{i1}$ insensitive to the GAP activity of RGS proteins. The

intrinsic hydrolysis rate of the $G\alpha_{i1}$(G183S) mutant was determined to be 0.0053 (0.0037-0.0069) sec^{-1}. Upon addition of 200 nM, 3000 nM, or 5000 nM of the RGS2(C106S+N184D+E191K) triple mutant, the k_{obs} was found to be 0.0036 (0.0026-0.0046) sec^{-1}, 0.0042 (0.0060-0.0078) sec^{-1} and 0.0025 (0.00017-0.0048) sec^{-1}, respectively; the k_{obs} for GTP hydrolysis after addition of 200 nM RGS16 was observed to be 0.0064 (0.0052-0.0076) sec^{-1}. (**D**) The k_{obs} values are plotted *versus* concentration of RGS protein to demonstrate the dose-dependent increase in GAP activity upon the addition of RGS2(C106S+N184D+E191K) protein to wildtype $G\alpha_{i1}$, but not the RGS-insensitive $G\alpha_{i1}$(G183S) mutant.

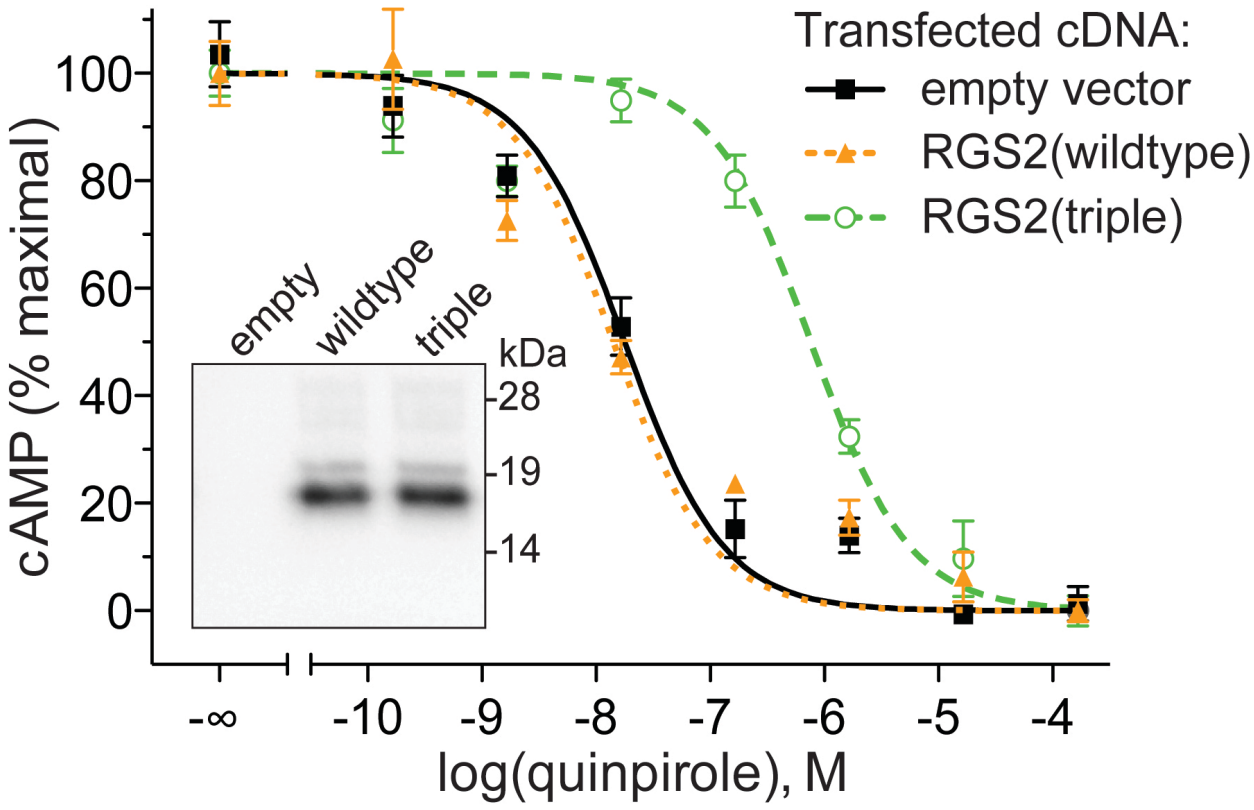

Figure 2.8. The triple mutant RGS2(C106S+N184D+E191K), but not wildtype RGS2, inhibits dopamine D2-receptor influence on forskolin-stimulated cAMP production. HEK293T cells were transiently co-transfected with expression vectors for the GloSensor™ cAMP biosensor and the G_i-coupled dopamine D2-receptor with either empty vector, wildtype RGS2, or the RGS2(triple) mutant. Inhibition of forskolin-stimulated cAMP production was determined after activation of the D2 receptor with various concentrations of quinpirole as indicated. The IC_{50} (95% C.I.) for quinpirole was determined to be 18 (12 – 26) nM, 14 (9 - 22) nM, and 762 (498 - 1170) nM in the presence of empty vector, wildtype RGS2, and the triple mutant, respectively. ***Inset***, Post-transfection cell lysates were immunoblotted with anti-HA epitope tag antibody to confirm the equivalent overexpression of HA-RGS2 and HA-RGS2(C106S+N184D+E191K) proteins.

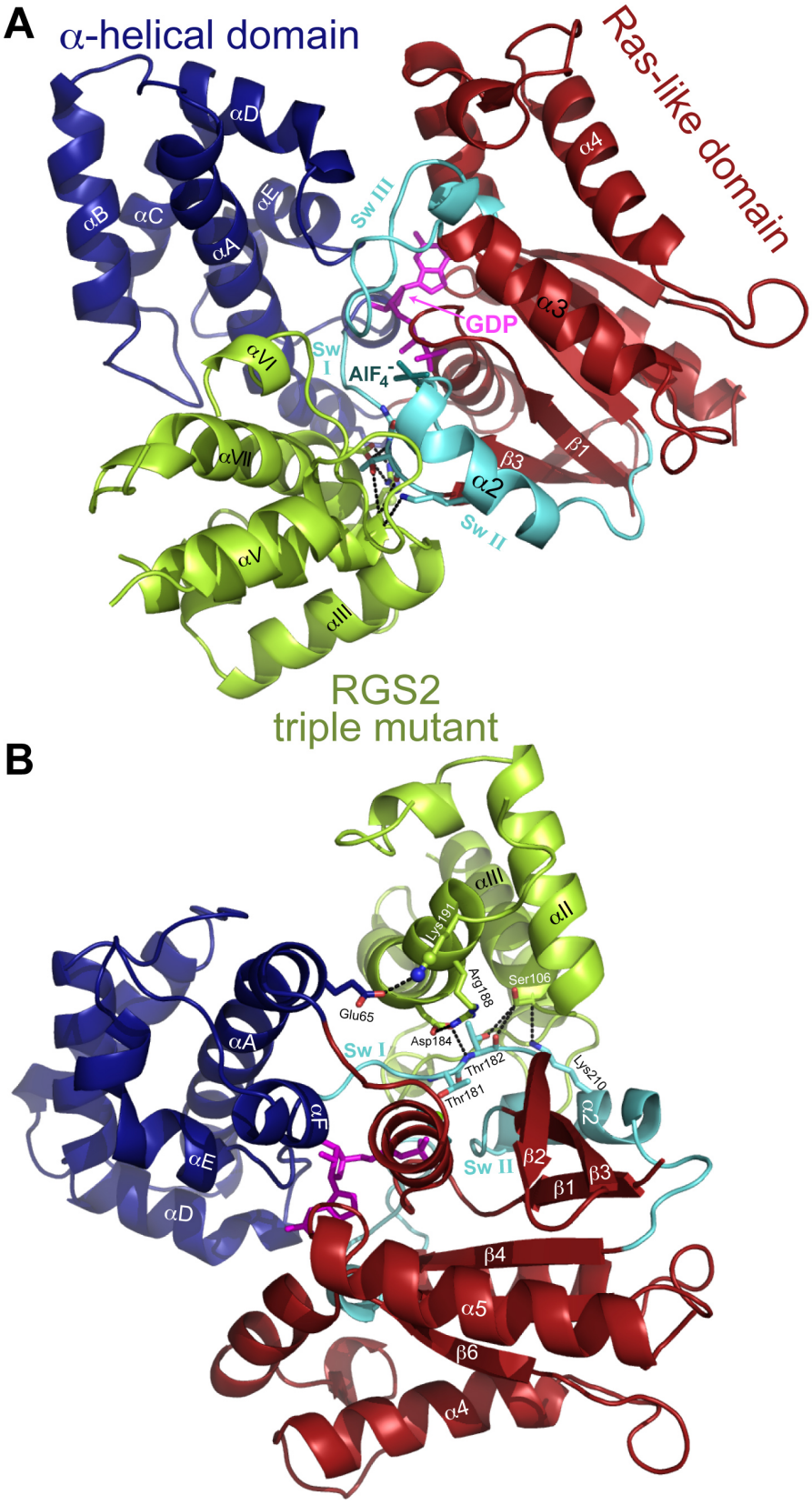
A
α-helical domain
Ras-like domain
αD
αB
αC
αA
αE
Sw III
α4
α3
GDP
Sw I
αVI
AlF4-
αVII
β3
β1
α2
Sw II
αV
αIII
RGS2
triple mutant
B
αIII
αII
Lys191
Arg188
Ser106
Glu65
Asp184
Thr182
Lys210
Thr181
αA
Sw I
αF
α2
Sw II
β2
β3
β1
αE
αD
β4
α5
β6
α4

Figure 2.9. Overall structural features of the RGS2(C106S+N184D+E191K)/$G\alpha_{i3}$·GDP·AlF_4^- complex. (A) The tertiary structure of $G\alpha_{i3}$ is composed of a Ras-like domain (*red*) and an all α-helical domain (*blue*) and is present in a transition-state mimetic form bound to a molecule of GDP (*magenta*) and tetrafluoroaluminate (AlF_4^-) ion (*gray/blue sticks*). The three critical switch regions of Gα (numbered Sw I to Sw III) are colored *cyan*. All three switch regions are engaged by the RGS2 RGS domain (*yellow-green*). Panel (**B**) represents the same structural model as in panel (**A**), but rotated to highlight contacts made by residues serine-106, aspartate-184, and lysine-191 of the RGS2(C106S+N184D+E191K) triple mutant. This same orientation of the complex is presented in the zoomed-in view in Figure 2.9B.

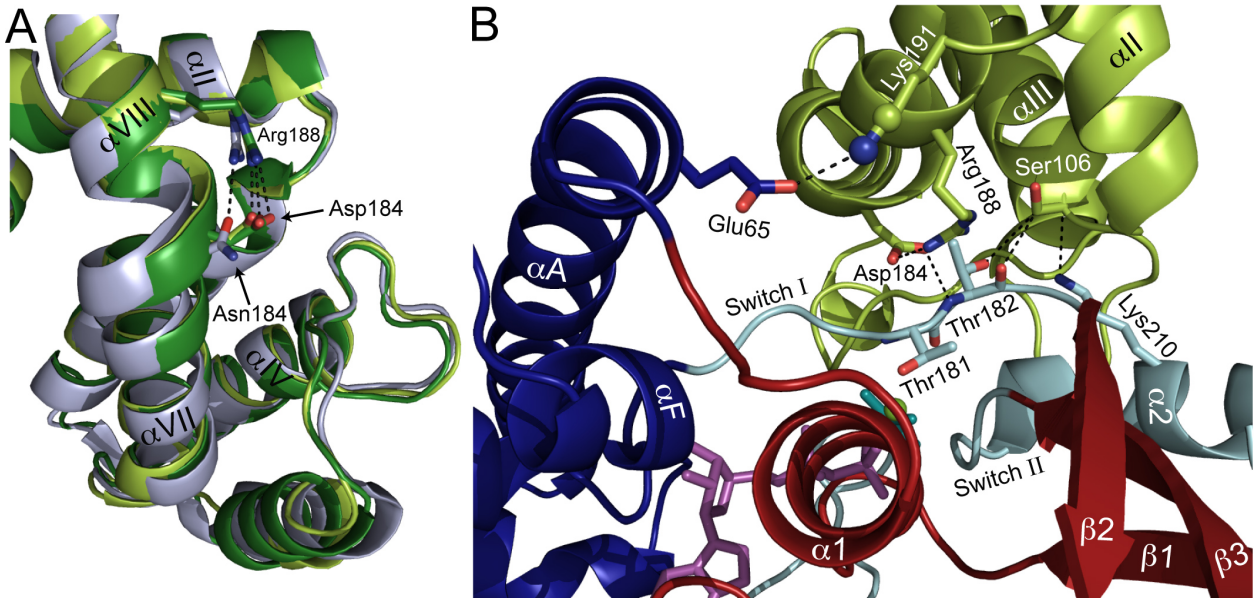

Figure 2.10. Particular Gα selectivity determinants inferred from the structural model of the triple mutant RGS2(C106S+N184D+E191K) bound to $G\alpha_{i3}$.

(**A**) Illustration of the αVII-αVIII region of the RGS domain to highlight the intramolecular interaction between the highly conserved αVIII helix arginine (Arg-188 of RGS2) and position 184 (asparagine in wildtype RGS2 and aspartate in the triple mutant). RGS2(C106S+N184D+E191K) triple mutant (*yellow-green*; PDB id 2V4Z), unliganded wildtype RGS2 (*grey*; PDB id 2AF0), and the $G\alpha_{i1}$-bound RGS16 (*dark green*; PDB id 2IK8) were aligned by sequence and then structure (Cα atoms) using the Align command with default align settings of MacPyMOL (DeLano Scientific, Palo Alto, CA), resulting in RMSDs of 0.92 Å and 0.80 Å, respectively. The conserved Arg-188 makes salt bridges with the terminal oxygens of the Asp-184 side-chain in the RGS2(C106S+N184D+E191K) mutant and the analogous asparate side-chain in RGS16; however, only one contact can be made between Arg-188 and the Asn-184 side-chain of wildtype RGS2. Loss of the second salt bridge creates a torsion in the wildtype RGS2 Asp-184 residue, resulting of the loss of the stabilizing hydrogen bond to Thr-182 in switch I of the Gα subunit. (**B**) Critical contacts between the three mutated positions of RGS2(C106S+N184D+E191K) (*yellow-green*) and its Gα binding partner (Ras-like domain in *red*; all-helical domain in *blue*; switch regions in *cyan*; bound GDP in *magenta*). The modeled terminal atoms of the Lys-191 side-chain (*spheres*) within RGS2(C106S+N184D+E191K) are in close enough proximity to make a hydrogen bond with Glu-65 of the Gα all-helical domain. Asp-184 makes two hydrogen bonds with Arg-188 and an additional bond with the backbone amine of the peptide bond connecting Thr-181 and Thr-182, both located within switch I of Gα. Ser-106 of the RGS2 triple mutant is tightly packed with the backbone carbonyl and γ-hydroxyl of Gα Thr-182, both being less than 3.9 Å from β-carbon of Ser-106. Additionally, the Gα switch II residue Lys-210 is 3.8 Å from the Ser-106 α-carbon.

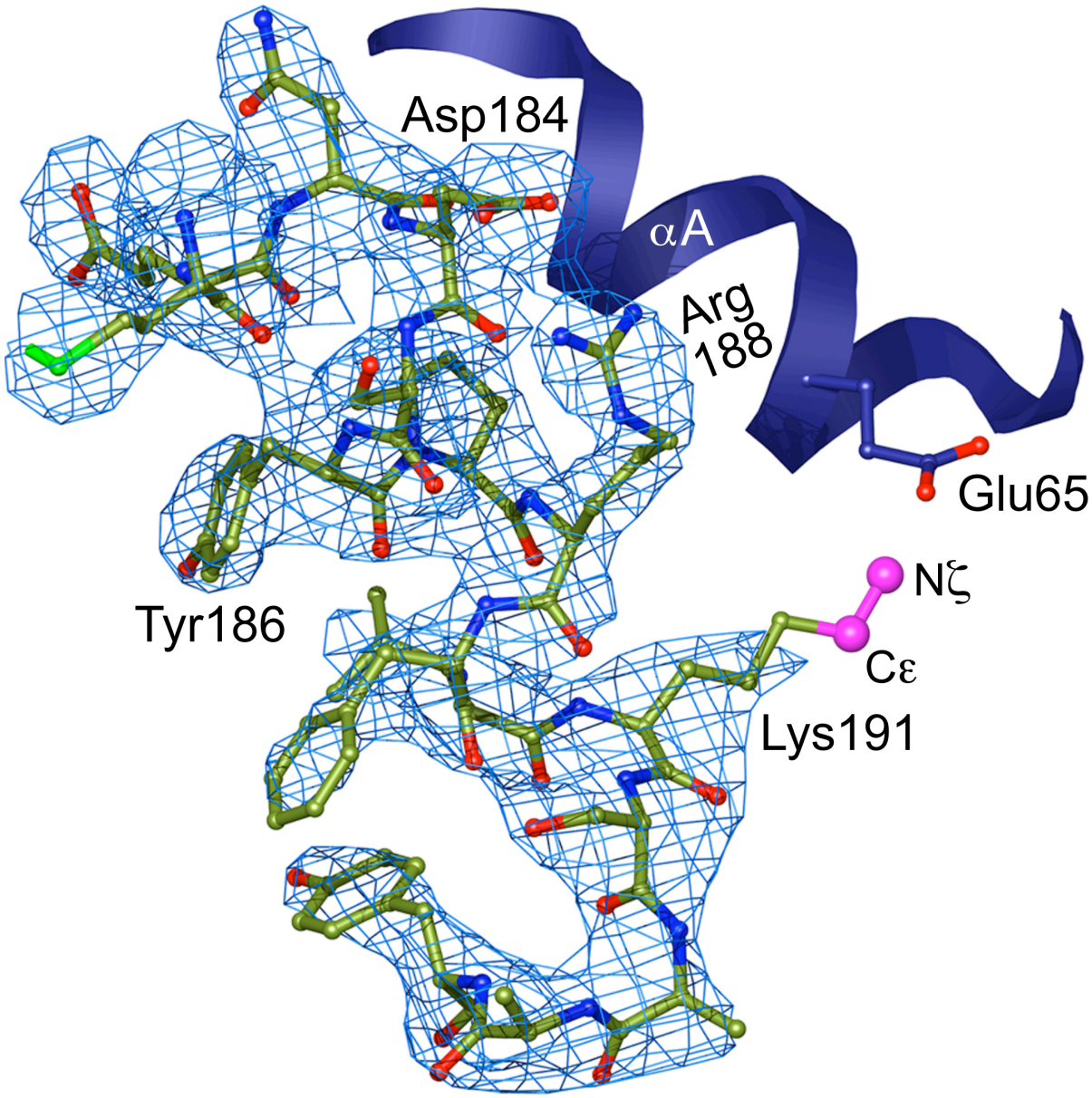

Figure 2.11. Electron density representation of the RGS2(C106S+N184D+E191K)/Gα_{i3}·GDP·AlF_4^- highlighting RGS2 residues Asp184, Arg188, and Lys191. The final refined $2|F_o|-|F_c|$ electron density map contoured at 1 sigma (0.2 $e^-/Å^3$) is shown in blue mesh over the αVIII helix of RGS2(C106S+N184D+E191K). The residues of the deposited structure (PDB id 2V4Z) are seen in a ball and stick representation with carbon atoms in *yellow-green*. The two modeled atoms of Lys191 are depicted as larger spheres (*magenta*). The density in the figure is a representative portion of the map of the B molecule and, apart from Lys191, also shows the salt bridge interaction of Asp184 and Arg188. The placement of the αA helix with Glu65 of the Gα_{i3} binding partner is included to emphasize the possible hydrogen bond to Lys191.

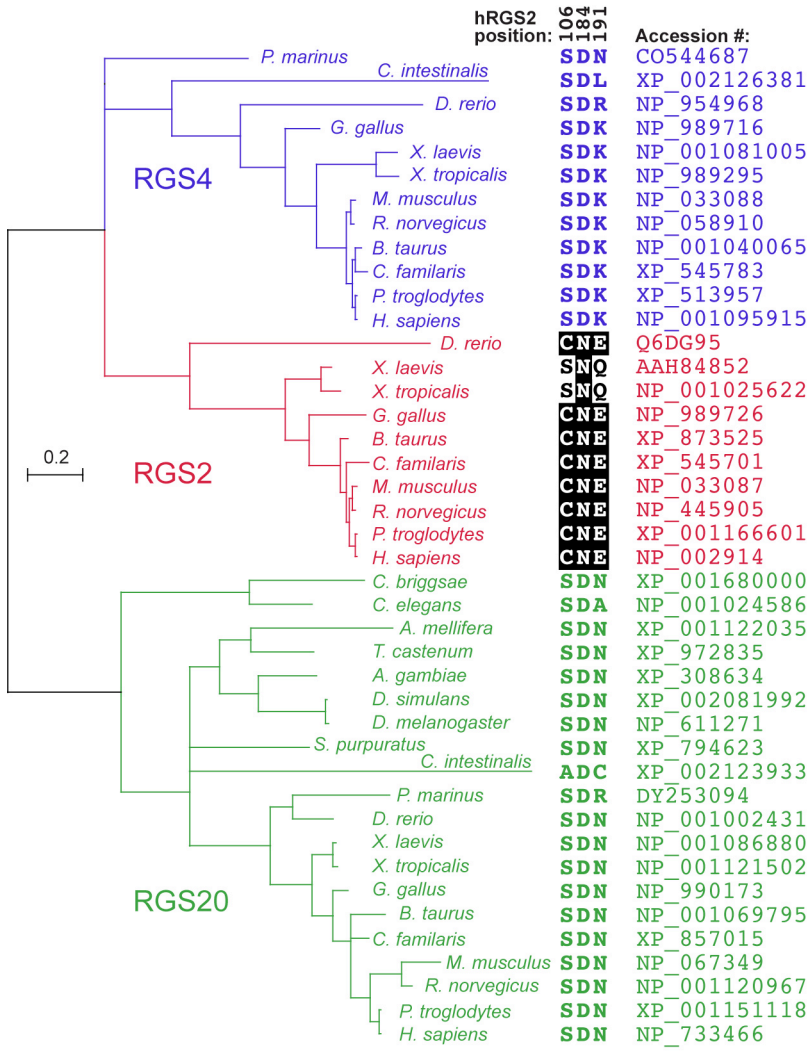

Figure 2.12. Emergence of the specialized R4-subfamily member RGS2 and evolutionary conservation of its three $G\alpha_q$-selectivity residues. Full-length, protein open-reading frame sequences for RGS2, RGS4, and RGS20 orthologs were obtained from the genomes of indicated multi-cellular organisms and aligned using T-Coffee v1.37 (61). Sequence alignments were manually adjusted using SEAVIEW v3.2 (ref. (62)) prior to the generation of a Markov-chain Monte Carlo-based phylogeny using MrBayes v3.1.2 (refs. (63,64)); dendrogram was visualized using Njplot v2.3 (ref. (65)).

Table 2.1: Data collection and refinement statistics for the RGS2(C106S+N184D+E191K)/Gα_{i3}·GDP·AlF_4^- complex (PDB id 2V4Z).

Data collection (highest resolution shell)	
Space group	$P3_221$
Number of protomers in asymmetric unit	1
Unit cell dimensions:	
a, b, c (Å)	114.54, 114.54, 99.33
α, β, γ (degrees)	90, 90, 120
Wavelength (Å)	1.54
Resolution (Å)	35.09-2.8 (2.95-2.8)
Total observations	136716 (19702)
Unique observations	18916 (2722)
R_{meas} [a]	0.128 (0.931)
$\langle I/\sigma(I)\rangle$	16.2 (2.3)
Completeness (%)	99.9 (100.0)
Redundancy	7.2 (7.2)
Wilson B value ($Å^2$)	67.5
Solvent content (%)	64.6 (V_M = 3.47) [b]
Refinement	
Resolution (Å)	33.4-2.8
Reflections (working/test)	17941/956
R_{work}/R_{free} (%) [c]	20.7/25.4
Non-hydrogen atoms/Average B-factor ($Å^2$) [d]	
Protein - Gα_{i3}	2513/53.8
- RGS2	883/90.4
Ligand - GDP, AlF_4^-, Mg^{2+}	34/35.2
Water	18/38.8
R.m.s. deviations:	
Bond lengths (Å) [e]	0.007
Angles (°)	0.97
Ramachandran plot (%):	
Most-favored regions	96.8
Allowed regions	3.0
Disallowed regions	0.2

[a] Multiplicity weighted merging R-factor, $R_{meas} = \Sigma_h (n_h / (n_h - 1))^{1/2} \Sigma_i | I_{h,i} - \langle I_h \rangle | / \Sigma_h \Sigma_i | I_{h,i} |$, where $\langle I_h \rangle$ is the mean intensity for reflection *h* and n_h is its multiplicity (ref . (1));
[b] V_M is defined as the density of the protein in the crystal in $Å^3$ per Da (ref. (2)) ;
[c] $\Sigma | F_P - F_{P(calc)} | / \Sigma F_P$, where F_P and $F_{P(calc)}$ are the observed and calculated structure factor amplitudes, respectively. R_{free} is calculated similarly using test set reflections never used during refinement;
[d] Average B-factors include TLS contributions;
[e] Using the parameters of Engh & Huber (3).

References for Collection & Refinement Information:

1. Diederichs, K., and Karplus, P. A. (1997) Nat Struct Biol 4, 269-275
2. Matthews, B. W. (1968) J Mol Biol 33, 491-497
3. Engh, R. A., and Huber, R. (1991) Acta Crystallographica Section A 47, 392-400

Table 2.2: Atomic distances (in Å) between side-chain nitrogens of conserved αVIII arginine within R4-family RGS domains and neighboring aspartate/asparagine at junction of helices αVII and αVIII.

RGS domain	PDB id	Residue (side-chain atoms)	Side-chain atom of αVIII arginine	
			NH1	NH2
RGS2(wildtype)	2AF0	Asn-184 (OD1, ND2)	3.2	5.9
RGS1	2BV1	Asp-172 (OD1, OD2)	2.8	3.4
RGS8	2IHD	Asp-157 (OD1, OD2)	5.0	5.7
RGS16	2BT2	Asp-166 (OD1, OD2)	2.5	6.0
RGS16	3C7L	Asp-165 (OD2, OD1)	5.1	3.2
RGS/G$\alpha_{i/o}$ complex				
RGS2(triple)/Gα_{i3}	2V4Z	Asp-184 (OD2, OD1)	2.7	3.0
RGS1/Gα_{i1}	2GTP	Asp-172 (OD1, OD2)	3.0	3.0
RGS4/Gα_{i1}	1AGR	Asp-161 (OD1, OD2)	2.7	3.2
RGS8/Gα_{i3}	2ODE	Asp-157 (OD1, OD2)	2.9	3.0
RGS16/Gα_{i1}	2IK8	Asp-166 (OD2, OD1)	3.0	3.1
RGS16/Gα_{o}	3C7K	Asp-165 (OD1, OD2)	3.7	2.8

CHAPTER 3

THE RGS PROTEIN INHIBITOR CCG-4986 IS A COVALENT MODIFIER OF THE RGS4 Gα-INTERACTION FACE

Elements of this work referenced in this chapter have been published in:

Kimple, A. J., Willard, F. S., Giguere, P. M., Johnston, C. A., Mocanu, V. and Siderovski, D. P. (2007) The RGS protein inhibitor CCG-4986 is a covalent modifier of the RGS4 Galpha-interaction face. *Biochim Biophys Acta*. 1774: 1213-1220.

3.1 ABSTRACT

Regulator of G-protein signaling (RGS) proteins accelerate GTP hydrolysis by heterotrimeric G-protein alpha subunits and are thus crucial to the timing of G protein-coupled receptor (GPCR) signal transduction. Small molecule inhibition of RGS proteins is an attractive therapeutic approach to diseases that involve dysregulated GPCR signaling. Methyl-N-[(4-chlorophenyl)sulfonyl]-4-nitrobenzenesulfinimidoate (CCG-4986) was recently reported as a selective RGS4 inhibitor, but with an unknown mechanism of action [1]. Here, we describe the mechanism of action of CCG-4986 as covalent modification of RGS4. Mutant RGS4 proteins devoid of surface-exposed cysteine residues were characterized as to their sensitivity to CCG-4986 inhibition using surface plasmon resonance and Förster resonance energy transfer (FRET) assays of Gα binding as well as single-turnover GTP hydrolysis assays of RGS4 GAP activity. From these analyses, we identified cysteine-132 within RGS4 as required for the inhibitory activity of CCG-4986. Mass spectrometry analysis identified a 153 dalton fragment of CCG-4986 as being covalently attached to the surface-exposed cysteines of the RGS4 RGS domain. We therefore conclude that the mechanism of action of the RGS protein inhibitor CCG-4986 is via covalent modification of Cys-132 of RGS4, likely causing steric hinderance with the all-helical domain of the Gα substrate.

3.2 INTRODUCTION

The single largest class of pharmaceuticals currently prescribed are those that target G protein-coupled receptor (GPCR) signaling pathways [2]. Recently, members of the "regulator of G-protein signaling" (RGS) protein superfamily have emerged as critical endogenous modulators of GPCR signal transduction (reviewed in [3, 4]). Via their conserved RGS domain that confers "GTPase-accelerating protein" (GAP) activity, RGS proteins deactivate heterotrimeric G-protein α subunits and thereby attenuate GPCR signal transduction [5, 6]. We and others have speculated that small molecule RGS protein modulators should have clinical utility in potentiating or inhibiting the actions of endogenous GPCR agonists (*e.g.*, refs. [7, 8]); combining existing GPCR agonists with specific RGS domain inhibitors should potentiate cellular responses and could also markedly increase specificity of action of existing drugs. In particular, the diversity of RGS proteins with highly localized and dynamically regulated distributions in the human brain makes them attractive targets for pharmacotherapy of central nervous system disorders such as Parkinson's disease and opiate addiction (reviewed in [9, 10]).

Despite their obvious potential as vanguards of a novel pharmacotherapeutic strategy, few reports currently exist of small molecule inhibitors of RGS protein action. Two groups have recently described identifying inhibitors of the RGS protein/Gα interaction (BMS-195270, CCG-4986), but the specific biochemical mechanism of action for each compound remained unresolved in these initial studies [1, 11]. Roman *et al*. identified CCG-4986 in a flow-cytometric protein interaction assay as an inhibitor of RGS4 binding to the G-protein subunit $G\alpha_o$ [1]. CCG-4986 inhibits the GAP activity of RGS4 in single-turnover GTP hydrolysis and inactivates the action of recombinant RGS4 protein in inhibiting μ-opioid

receptor signaling by permeabilized C6 glioma cells; in contrast, Gα binding and inhibition of μ-opioid receptor signaling by a related R4-subfamily RGS protein (RGS8) is unperturbed by the actions of CCG-4986 [1]. Here, we describe biochemical, biophysical, and mass spectrometric analyses of the interaction between CCG-4986 and RGS4, which support the conclusion that this small molecule RGS inhibitor is a reactive modifier of a solvent-exposed cysteine present in RGS4 and not RGS8, thereby explaining its *in vitro* RGS protein specificity.

3.3. MATERIALS

3.3.1 Chemicals

Methyl-N-[(4-chlorophenyl)sulfonyl]-4-nitrobenzenesulfinimidoate (CCG-4986; MW 374.82) was purchased from ChemBridge (San Diego, CA); identity and purity of CCG-4986 was confirmed by electrospray mass spectrometry (ESI-MS) conducted at the UNC-Duke Michael Hooker Proteomics Core Facility. Unless otherwise noted, all reagents used were the highest grade available from Sigma Aldrich (St. Louis, MO) or Fisher Scientific (Pittsburgh, PA).

4.3.2 Protein expression and purification

Wildtype human RGS4 (amino acids 29-198; cloned as a hexahistidine-tagged fusion in pSGC-LIC) was obtained from the Structural Genomics Consortium (Oxford, UK); point mutations were made using QuikChange site directed mutagenesis (Stratagene, La Jolla, CA). DNA encoding amino acids 50-177 of wildtype human RGS4, and cysteine point mutants thereof, were also subcloned into a Novagen (San Diego, CA) pET vector-based prokaryotic expression construct ("pET-YFP-LIC-C") using PCR and ligation-independent

cloning [12]. The resultant constructs encoded RGS4 as C-terminal fusions to enhanced yellow fluorescent protein (hereafter described as YFP; Clontech, Mountain View, CA) with an intervening 12 amino acid linker sequence (TSRGRMYTQSNA).

For expression of both hexahistidine-tagged and YFP-tagged RGS4 proteins, BL21(DE3) *E. coli* were grown to an OD_{600nm} of 0.7-0.8 at 37°C before induction with 0.5 mM isopropyl-β-D-thiogalactopyranoside. After culture for 14-16 hours at 20°C, cells were pelleted by centrifugation and frozen at -80°C. Prior to purification, bacterial cell pellets were resuspended in N1 buffer (50 mM HEPES pH 8.0, 300 mM NaCl, 30 mM imidazole, 2.5% (w/v) glycerol). Bacteria were lysed at 10,000 kPa using pressure homogenization with an Emulsiflex (Avestin; Ottawa, Canada). Cellular lysates were centrifuged at 100,000 x g for 30 minutes at 4°C. The supernatant was applied to a nickel-nitrilotriacetic acid resin FPLC column (FF HisTrap; GE Healthcare, Piscataway, NJ), washed with 7 column volumes of N1 then 3 column volumes of 30 mM imidazole before elution of RGS4 proteins with 300 mM imidazole. Eluted protein was cleaved with tobacco etch virus (TEV) protease overnight at 4°C and dialyzed into low imidazole buffer (N1 plus 5 mM DTT) before being passed over a second HisTrap column to separate residual His_6-RGS4 from untagged, cleaved RGS4. The column flow-through was pooled and resolved using a calibrated 150 ml size exclusion column (Sephacryl S200; GE Healthcare) with S200 buffer (50 mM Tris pH 8.0, 250 mM NaCl, DTT 5 mM, 2.5% (w/v) glycerol). Protein was then concentrated to approximately 1 mM, as determined by A_{280nm} measurements upon denaturation in 8 M guanidine hydrochloride. Concentration was calculated based on predicted extinction coefficient (http://us.expasy.org/tools/protparam.html). RGS4 was prepared for MS analysis using S200 buffer without glycerol ("MS Buffer"). Human RGS8 and RGS16 constructs were also

provided by the Structural Genomic Consortium and purified as described (RGS8: http://www.sgc.ox.ac.uk/structures/MM/RGS8A_2ihd_MM.html, RGS16: http://www.sgc.ox.ac.uk/structures/MM/RGS16A_2bt2_MM.html). C-terminally biotinylated $G\alpha_{i1}$ and $G\alpha_{i1}$-CFP fusion proteins were prepared as described previously [13, 14]. His_6-$G\alpha_{oA}$ was purifed as described [15].

4.3.3 Fluorescent and radiolabelled nucleotide single-turnover GTPase assays

BODIPYFL-GTP (Invitrogen; Carlsbad, CA) hydrolysis was measured and quantified using single nucleotide binding-and-turnover assays as previously described [15]. Single turnover [γ-^{32}P]GTP hydrolysis assays were conducted using 100 nM $G\alpha_{i1}$, 200 nM RGS4 protein, and 2 μM CCG-4986 as previously described [16]. Briefly, 100 nM $G\alpha_{i1}$ was incubated for 10 minutes at 30^{o}C with 1 x 10^6 cpm of [γ-^{32}P]GTP (specific activity of 6500 dpm/Ci) in the absence of free magnesium. Reaction was then chilled on ice for 1 minute prior to the addition of 10 mM $MgCl_2$ (final concentration) with or without added RGS protein (200 nM final) in the presence or absence of 10-fold molar excess CCG-4986. Reactions were kept on ice and 100 ml aliquots were taken at 30 second intervals, quenched in 900 μl of charcoal slurry, centrifuged, and 600 μl aliquots of supernatant counted via liquid scintillation as described [16].

4.3.4 Surface plasmon resonance-based binding assays

Optical detection of surface plasmon resonance (SPR) was performed using a Biacore 3000 (Biacore Inc., Piscataway, NJ). Biotinylated $G\alpha_{i1}$ was immobilized on streptavidin sensor

chips (Biacore) to densities of ~6000 RU as previously described [14]. In pilot studies, CCG-4986 was observed to react with, and thereby irreversibly modify, the biosensor surface, preventing us from obtaining high-quality protein/protein interaction data in its presence (data not shown). To obviate this problem, we removed excess CCG-4986 from RGS protein samples using rapid gel filtration. Specifically, all proteins samples were first incubated for 3 minutes at room temperature in a 50 μl volume containing 30 μM RGS protein with a 10-fold molar excess of CCG-4986 (or DMSO equivalent) in the absence or presence of 10 mM DTT. RGS protein was then separated from unbound compound and other low-molecular weight reagents by Sephadex G-25 chromatography (Illustra™ MicroSpin™ G-25 Column; GE Healthcare) via centrifugation for 1 minute at 735 x g. The flow through was then diluted in 250 μl of BIA running buffer (10 mM HEPES pH 7.4, 150 mM NaCl, 0.05% NP40, 100 μM GDP, 5 μM EDTA, 10 mM $MgCl_2$, 10 mM NaF, 30 μM $AlCl_3$) for injection across biosensor surfaces. Binding curves for wildtype RGS proteins and cysteine point-mutants of RGS4 were obtained at 20°C using 200 μl injections (using the KINJECT command) with a 200 second dissociation phase at 20 μl/min. Non-specific binding to a denatured $G\alpha_{i1}$-biotin surface was subtracted from each curve (BIAevaluation software v3.0; Biacore).

4.3.5 Förster resonance energy transfer (FRET)-based binding assays

Förster resonance energy transfer was used to measure binding interactions between $G\alpha_{i1}$ and RGS4 as previously described [13]. Briefly, FRET between $G\alpha_{i1}$-CFP and YFP-RGS4 fusion proteins was measured using a SpectraMax Gemini 96-well plate fluorescence reader (Molecular Devices; Sunnyvale, CA); association of $G\alpha_{i1}$-CFP and YFP-RGS4 induced by the addition of aluminum tetrafluoride results in non-photonic energy transfer and a

subsequent increase in emission at 528 nm relative to the emission at 480 nm. All runs were conducted with excitation wavelength of 433 nm, a 455 nm cutoff filter, and emission scans from 474 nm to 532 nm at 2 nm intervals. FRET was calculated as the ratio of emission at 528 nm / 480 nm. Binding assays were initiated by the addition of $G\alpha_{i1}$-CFP and fluorescence was measured within 2 minutes, given that reactions containing CCG-4986 did not appear to be stable over long time periods.

4.3.6 Mass spectrometry

Sample Preparation: 39 nmol of RGS4 proteins were incubated in MS Buffer with a 15-fold molar excess of CCG-4986 (30 mM in DMSO) for 5 minutes at room temperature and then filtered on a 5 ml sephadex G-25 column (HiTrap Desalting Column; GE Healthcare) in order to remove DMSO and excess CCG-4896**.**

Sample Analysis: Prior to mass spectrometric analyses, RGS4 protein samples were applied to C4 ZipTip columns (Millipore, Billerica, MA) and eluted using 50% acetonitrile/2% acetic acid. For intact molecular weight determination, 1 μl of each sample was analyzed by electrospray ionization mass spectrometry (ESI-MS) on an ABI QSTAR-Pulsar QTOF mass spectrometer fitted with a nanoelectrospray source (Proxeon Biosistems A/S, Odense, Denmark). To determine the labeled sites of RGS4, tryptic digestions of untreated and CCG-4986-treated RGS4 were performed. Digested samples were then applied to C18 ZipTips and eluted with 50% acetonitrile/0.1% trifluoroacetic acid. 0.5 μl of each sample was mixed with 0.5 μl matrix (a saturated solution of a–cyano-4-hydroxycinnamic acid in 50% acetonitrile/0.1% trifluoroacetic acid) and analyzed by matrix-assisted laser desorption/ionization mass spectrometry (MALDI-MS and MALDI-MS/MS fragmentation)

on a Bruker Ultraflex I mass spectrometer (Bruker Daltonics, Billerica, MA, USA). All mass spectrometric data were gathered at the UNC-Duke Michael Hooker Proteomics Center (Chapel Hill, NC).

4.3.7 Molecular modeling

Model building using the RGS4/Gα_{i1} complex coordinates (PDB id 1AGR; ref. [17]) was performed in the program O [18]. Structural images were made with PyMol (DeLano Scientific, South San Francisco, CA).

4.4. RESULTS AND DISCUSSION

4.4.1 CCG-4986 is a cysteine-dependent RGS4 inhibitor

In a desire to establish the structural determinants of CCG-4986 function as an RGS protein inhibitor, we initiated crystallization trials towards obtaining a high-resolution structure of a RGS4/CCG-4986 complex by x-ray diffraction. However, we found that admixture of CCG-4986 with purified RGS4 protein solutions containing reducing agents (*e.g.*, dithiothreitol [DTT]) led to an immediate generation of a bright yellow substance (data not shown); this proved problematic to continued crystallization trials, as the purification of RGS4 in the absence of reducing agent resulted in a heterogenous mixture of monomer and dimers (data not shown). This bright yellow color reaction was reproduced by exposing CCG-4986 to DTT only. As CCG-4986 contains two sulfur atoms, we hypothesized that its mechanism of action could be one of thiol reactivity and, hence, covalent modification of cysteine residue(s) in RGS4.

To highlight solvent-exposed residues within RGS4, a multiple sequence alignment of RGS domains was created in combination with the GETAREA 1.1 algorithm for calculating accessible surface area [19] as applied to the NMR structural coordinates of uncomplexed RGS4 (PDB id 1EZT; ref. [20]). This alignment revealed two solvent-exposed cysteines present within the RGS domain of RGS4 (Cys-71 and Cys-132, Figure 3.1A). These two cysteines within RGS4 are not conserved among other R4-subfamily RGS proteins; for example, the corresponding residues in RGS8 are Tyr-65 and Gln-126 and in RGS16 are Asn-74 and Glu-135 (Figure 3.1A). To determine if the inhibitory activity of CCG-4986 was dependent on the Cys-71 and/or Cys-132 residues unique to RGS4, mutant RGS4 proteins were purified bearing Cys-71-to-Asn and/or Cys-132-to-Glu point mutations (Figure 3.1B) and subjected to biochemical analyses of RGS protein function.

Assays of RGS4 GAP activity were initially performed using the fluorescent nucleotide analog BODIPYFL-GTP [15]. Wildtype RGS4 stimulated the intrinsic GTPase activity of $G\alpha_{oA}$ in a dose-dependent manner (Figure 3.2A). GAP activity was substantially diminished by preincubation of wildtype RGS4 with 30 mM CCG-4986 (Figure 3.2A). The double point-mutant RGS4(C71N/C132E) also had potent GAP activity toward $G\alpha_{oA}$, but this activity was not inhibited by preincubation with 30 mM CCG-4986 (Figure 3.2B), thus demonstrating the requirement of a cysteine residue in RGS4 for CCG-4986 bioactivity.

Surface plasmon resonance (SPR) was used to measure the ability of wildtype and mutant RGS4 proteins to bind immobilized $G\alpha_{i1}$ in its GDP/aluminum tetrafluoride-bound transition state (the $G\alpha$ nucleotide state bound most avidly by RGS proteins; ref. [21]). Addition of a 10-fold molar excess of CCG-4986 completely abolished wildtype RGS4 binding to $G\alpha_{i1}\cdot GDP\cdot AlF_4^-$ (Figure 3.3A), but had no significant effect on $G\alpha_{i1}$ binding by

RGS8 and RGS16 proteins (Figure 3.3B-C). Preincubation of CCG-4986 with DTT blocked its inhibitory action on the RGS4/$G\alpha_{i1}$ interaction (Figure 3.3A). Mutation of the two solvent-exposed cysteines of RGS4 also resulted in a dramatic reduction in the inhibitory effect of CCG-4986 on the RGS4/$G\alpha_{i1}$ interaction (Figure 3.3D). To determine the individual roles of Cys-71 and Cys-132 in CCG-4986 activity, the single point-mutants of RGS4 were also profiled for $G\alpha_{i1}$ binding using SPR. The Cys-71-to-Asn mutant remained sensitive to inhibition by CCG-4986; as with wildtype RGS4, this inhibitory effect was lost upon treatment of CCG-4986 with DTT (Figure 3.3E). In contrast, $G\alpha_{i1}$ binding by the Cys-132-to-Glu mutant of RGS4 was unaffected by CCG-4986 (Figure 3.3F). These results suggest that Cys-132 is required for CCG-4986-mediated inhibition of $G\alpha_{i1}$ binding by RGS4.

To confirm these SPR findings, we used an independent experimental approach of *in vitro* FRET between CFP- and YFP-labeled fusion proteins to quantify RGS4/$G\alpha_{i1}$ binding in the presence of CCG-4986. We previously reported [13] that, upon interaction between YFP-RGS4 and $G\alpha_{i1}$-CFP (the latter in its GDP/aluminum tetrafluoride-bound transition state), excitation of CFP at 433 nm results in an increase in acceptor (YFP) emission at 528 nm and a corresponding decrease in donor (CFP) emission at 480 nm. The ratio of emissions at 528 nm and 480 nm can thus be used to quantify binding between RGS4 and $G\alpha_{i1}$. We observed a concentration-dependent reduction in FRET between YFP-RGS4 and transition-state $G\alpha_{i1}$-CFP upon the addition of CCG-4986 (Figure 3.4A). Similarly, addition of CCG-4986 to YFP-RGS4(C71N) reduced observed FRET (Figure 3.4B), while the addition of solvent alone (DMSO) had no inhibitory effect on FRET from either protein pairing (Figure 3.4A,B). In contrast, no reduction in FRET was seen upon addition of CCG-4986 to YFP-RGS4(C132E) or YFP-RGS4(C71N, C132E) proteins (Figure 3.4C,D). To confirm that the

interaction between transition state $G\alpha_{i1}$-CFP and YFP-RGS4 was reversible, unlabeled RGS4 was used as a positive control for inhibition (Figure 3.4C,D).

Our BODIPYFL-GTP hydrolysis, SPR, and FRET data all confirmed previously published findings describing CCG-4986 as a selective inhibitor of the RGS4/Gα binding interaction and of RGS4 GAP activity on $G\alpha_o$ [1]; our analysis of cysteine point-mutants of RGS4 further demonstrated that Cys-132 is necessary for the inhibitory activity of CCG-4986. To confirm that CCG-4986 inhibition of RGS4-mediated GAP activity required the Cys-132 residue within RGS4, we repeated *in vitro* GAP assays using radiolabeled GTP as previously described [16]. Calculated initial rates of [γ-^{32}P]GTP hydrolysis from these single-turnover assays were as follows:

Gα alone, 0.011 s^{-1}; Gα + RGS4(wildtype), 0.21 s^{-1}; Gα + RGS4(wildtype) + CCG-4986, 0.074 s^{-1}; Gα + RGS4(C132E), 0.044 s^{-1}; Gα + RGS4(C132E) + CCG-4986, 0.036 s^{-1}. The Cys-132-to-Glu mutation reduced the GAP activity of RGS4 (4-fold increase in initial GTP hydrolysis rate *vs* 19-fold for wildtype RGS4); however, this mutant RGS protein was clearly still active as an accelerator of Gα GTP hydrolysis and not significantly inhibited by preincubation with a 10-fold molar excess CCG-4986 (18% reduction in GAP activity *vs* 65% reduction of wildtype RGS4 GAP activity). These results again highlight the requirement of the Cys-132 residue in RGS4 to CCG-4986 inhibitory activity.

4.4.2 CCG-4986 covalently modifies RGS4 cysteine residues

To unambiguously determine if CCG-4986 is a covalent modifier of RGS4, intact molecular weight determinations of unreacted and CCG-4986-treated RGS4 protein samples were performed by nano-ESI-MS. Compared to unreacted RGS4 protein (Figure 3.5A), CCG-

4986-treated RGS4 protein revealed three prominent forms (Figure 3.5B), with molecular weights that correspond to wildtype RGS4 (19,743 Da), RGS4 plus one 153 Da substituent (19,896 Da), and RGS4 plus two 153 Da substituents (20,050 Da). To identify specific reaction sites, tryptic digestion of unreacted and CCG-4986-treated RGS4 protein samples was performed, followed by MALDI-MS detection of tryptic peptide fragments. Two tryptic peptides, T13 (amino acids 59-WAESLENLISHE<u>C</u>GLAAFK-77) and T23 (amino acids 126-EVNLDS<u>C</u>TR-134), that contain Cys-71 and Cys-132, respectively, were found to have an increased mass of 153 Da in the CCG-4986 treated sample (data not shown). MS/MS data from peptide fragmentation confirmed that the molecular mass modification reaction arising from CCG-4986 treatment occurred specifically on Cys-71 and Cys-132 residues (data not shown). While such MS/MS analysis does not define the structure of the attached moiety, it most likely represents a fragment of CCG-4986 covalently bonded to a cysteine via a disulfide bond (Figure 3.5C). We hypothesize that the attached fragment is a 4-nitrobenzenethiol radical (MW 154.17) derived from breakdown of CCG-4986. Formation of a disulfide bond by this reacting fragment of CCG-4986 would result in the loss of a hydrogen atom from the thiol of cysteine (1.0 Da) and account for the observed 153 Da moiety observed as a covalent substituent on Cys-71 and Cys-132 residues.

4.4.3 Structural basis of RGS4 inhibition by CCG-4986

From the atomic resolution structure of the RGS4/Gα_{i1} complex [17], it is apparent that covalent addition of a 153 Da 4-nitrobenzenethiol moiety to the Cys-132 residue of RGS4 would cause significant steric hindrance to the binding of Gα. Specifically, the addition of a CCG-4986 fragment is predicted to result in van der Waals collisions with Arg-86 and Arg-

90 residues of the all-helical domain of $G\alpha_{i1}$ (Figure 3.6). Hence, from the biochemical and mass spectrometry data presented above, our conclusion is that the most likely mechanism for the inhibitory properties of CCG-4986 is non-specific modification of surface-exposed cysteine residues in RGS4 causing a steric inhibition of the RGS4/$G\alpha_{i1}$ interaction. While reactive inhibitors have made widely successful drugs (*e.g.*, aspirin, clopidogrel; refs. [22, 23]), the lack of selectivity of CCG-4986 for cysteines on RGS4 suggests that CCG-4986 will react with surface-exposed cysteines in a myriad of proteins beyond its intended RGS protein target. Furthermore, although Roman and colleagues have speculated that the lack of CCG-4986 activity on intact RGS4-transfected cells is a result of poor membrane permeability [1], it is more likely that the requirement for cell membrane permeabilization to observe the effects of CCG-4986 reflects sensitivity to a reducing environment such as that found inside intact cells. These predictions as to the labile and reactive nature of CCG-4986 bode ill for its further development as a lead chemical entity for RGS protein-directed pharmacotherapy.

4.5 ACKNOWLEDGEMENTS

We thank Drs. Declan Doyle and Meera Soundararajan (SGC Oxford) for RGS protein expression vectors, and Dr. Dmitriy Gremyachinskiy (UNC) for his chemistry advice. A.J.K. gratefully acknowledges prior support of the UNC MD/PhD program (T32 GM008719) and current predoctoral support from National Institute of Mental Health (F30 MH074266). C.A.J. and D.P.S. were supported by National Institutes of Health grants F32 GM076944 and R03 NS053754, respectively.

4.6 REFERENCES

1. Roman, D.L., J.N. Talbot, R.A. Roof, R.K. Sunahara, J.R. Traynor, and R.R. Neubig, *Identification of small-molecule inhibitors of RGS4 using a high-throughput flow cytometry protein interaction assay.* Mol Pharmacol, 2007. **71**(1): p. 169-75.

2. Overington, J.P., B. Al-Lazikani, and A.L. Hopkins, *How many drug targets are there?* Nat Rev Drug Discov, 2006. **5**(12): p. 993-6.

3. Ross, E.M. and T.M. Wilkie, *GTPase-activating proteins for heterotrimeric G proteins: regulators of G protein signaling (RGS) and RGS-like proteins.* Annu Rev Biochem, 2000. **69**: p. 795-827.

4. Siderovski, D.P. and F.S. Willard, *The GAPs, GEFs, and GDIs of heterotrimeric G-protein alpha subunits.* Int J Biol Sci, 2005. **1**(2): p. 51-66.

5. Berman, D.M., T.M. Wilkie, and A.G. Gilman, *GAIP and RGS4 are GTPase-activating proteins for the Gi subfamily of G protein alpha subunits.* Cell, 1996. **86**(3): p. 445-52.

6. Siderovski, D.P., A. Hessel, S. Chung, T.W. Mak, and M. Tyers, *A new family of regulators of G-protein-coupled receptors.* Curr Biol, 1996. **6**(2): p. 211-2.

7. Chasse, S.A. and H.G. Dohlman, *RGS proteins: G protein-coupled receptors meet their match.* Assay Drug Dev Technol, 2003. **1**(2): p. 357-64.

8. Neubig, R.R. and D.P. Siderovski, *Regulators of G-protein signalling as new central nervous system drug targets.* Nat Rev Drug Discov, 2002. **1**(3): p. 187-97.

9. Jones, M.B., D.P. Siderovski, and S.B. Hooks, *The Gbetagamma dimer as a novel source of selectivity in G-protein signaling: GGL-ing at convention.* Mol Interv, 2004. **4**(4): p. 200-214.

10. Traynor, J.R. and R.R. Neubig, *Regulators of G protein signaling & drugs of abuse.* Mol Interv, 2005. **5**(1): p. 30-41.

11. Fitzgerald, K., S. Tertyshnikova, L. Moore, L. Bjerke, B. Burley, J. Cao, P. Carroll, R. Choy, S. Doberstein, Y. Dubaquie, Y. Franke, J. Kopczynski, H. Korswagen, S.R. Krystek, N.J. Lodge, R. Plasterk, J. Starrett, T. Stouch, G. Thalody, H. Wayne, A. van der Linden, Y. Zhang, S.G. Walker, M. Cockett, J. Wardwell-Swanson, P. Ross-Macdonald, and R.M. Kindt, *Chemical genetics reveals an RGS/G-protein role in the action of a compound.* PLoS Genet, 2006. **2**(4): p. e57.

12. Stols, L., M. Gu, L. Dieckman, R. Raffen, F.R. Collart, and M.I. Donnelly, *A new vector for high-throughput, ligation-independent cloning encoding a tobacco etch virus protease cleavage site.* Protein Expr Purif, 2002. **25**(1): p. 8-15.

13. Willard, F.S., R.J. Kimple, A.J. Kimple, C.A. Johnston, and D.P. Siderovski, *Fluorescence-based assays for RGS box function.* Methods Enzymol, 2004. **389**: p. 56-71.

14. Willard, F.S., A.B. Low, C.R. McCudden, and D.P. Siderovski, *Differential G-alpha interaction capacities of the GoLoco motifs in Rap GTPase activating proteins.* Cell Signal, 2007. **19**(2): p. 428-38.

15. Willard, F.S., A.J. Kimple, C.A. Johnston, and D.P. Siderovski, *A direct fluorescence-based assay for RGS domain GTPase accelerating activity.* Anal Biochem, 2005. **340**(2): p. 341-51.

16. Afshar, K., F.S. Willard, K. Colombo, C.A. Johnston, C.R. McCudden, D.P. Siderovski, and P. Gonczy, *RIC-8 is required for GPR-1/2-dependent Galpha function during asymmetric division of C. elegans embryos.* Cell, 2004. **119**(2): p. 219-30.

17. Tesmer, J.J., D.M. Berman, A.G. Gilman, and S.R. Sprang, *Structure of RGS4 bound to AlF4--activated G(i alpha1): stabilization of the transition state for GTP hydrolysis.* Cell, 1997. **89**(2): p. 251-61.

18. Jones, T.A., J.Y. Zou, S.W. Cowan, and Kjeldgaard, *Improved methods for building protein models in electron density maps and the location of errors in these models.* Acta Crystallogr A, 1991. **47 (Pt 2)**: p. 110-9.

19. Fraczkiewicz, R. and W. Braun, *Exact and efficient analytical calculation of the accessible surface areas and their gradients for macromolecules.* J. Comput. Chem., 1998. **19**(3): p. 319-333.

20. Moy, F.J., P.K. Chanda, M.I. Cockett, W. Edris, P.G. Jones, K. Mason, S. Semus, and R. Powers, *NMR structure of free RGS4 reveals an induced conformational change upon binding Galpha.* Biochemistry, 2000. **39**(24): p. 7063-73.

21. Berman, D.M., T. Kozasa, and A.G. Gilman, *The GTPase-activating protein RGS4 stabilizes the transition state for nucleotide hydrolysis.* J Biol Chem, 1996. **271**(44): p. 27209-12.

22. Patrono, C., *Aspirin and human platelets: from clinical trials to acetylation of cyclooxygenase and back.* Trends Pharmacol Sci, 1989. **10**(11): p. 453-8.

23. Savi, P. and J.M. Herbert, *Clopidogrel and ticlopidine: P2Y12 adenosine diphosphate-receptor antagonists for the prevention of atherothrombosis.* Semin Thromb Hemost, 2005. **31**(2): p. 174-83.

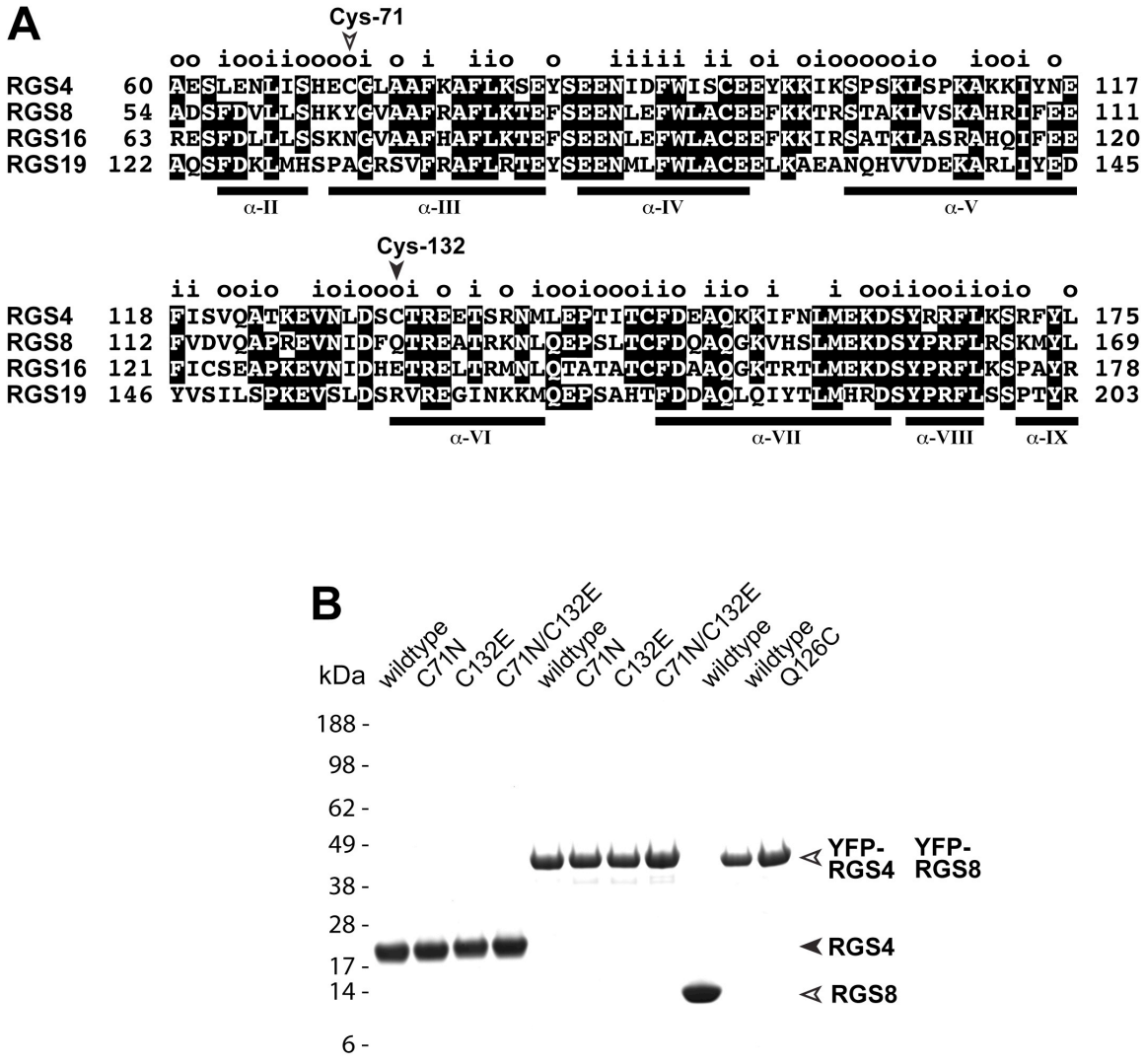

Figure 3.1. Multiple sequence alignment of human R4-subfamily RGS proteins RGS4, -8, -16, and the RZ-subfamily member RGS19. (A) Solvent-accessible residues within RGS4 are demarcated by "o" (outside), while internal residues are noted by "i" (inside) and partially solvent-exposed residues are unlabeled, as predicted by the GETAREA 1.1 algorithm [19] using a solvent probe of 1.40 Å as applied to the high-resolution structure of free RGS4 [20]. Position of Cys-71 and Cys-132, found uniquely within RGS4, are indicated by arrowheads. Alpha-helices observed within the NMR structures of RGS4 and RGS19 [20, 24] are numbered in Roman numerals. (B) Equivalent purification of wildtype and cysteine point-mutant RGS4 proteins for biochemical and mass spectrometry analyses is highlighted by coomassie blue staining of SDS-PAGE resolved proteins.

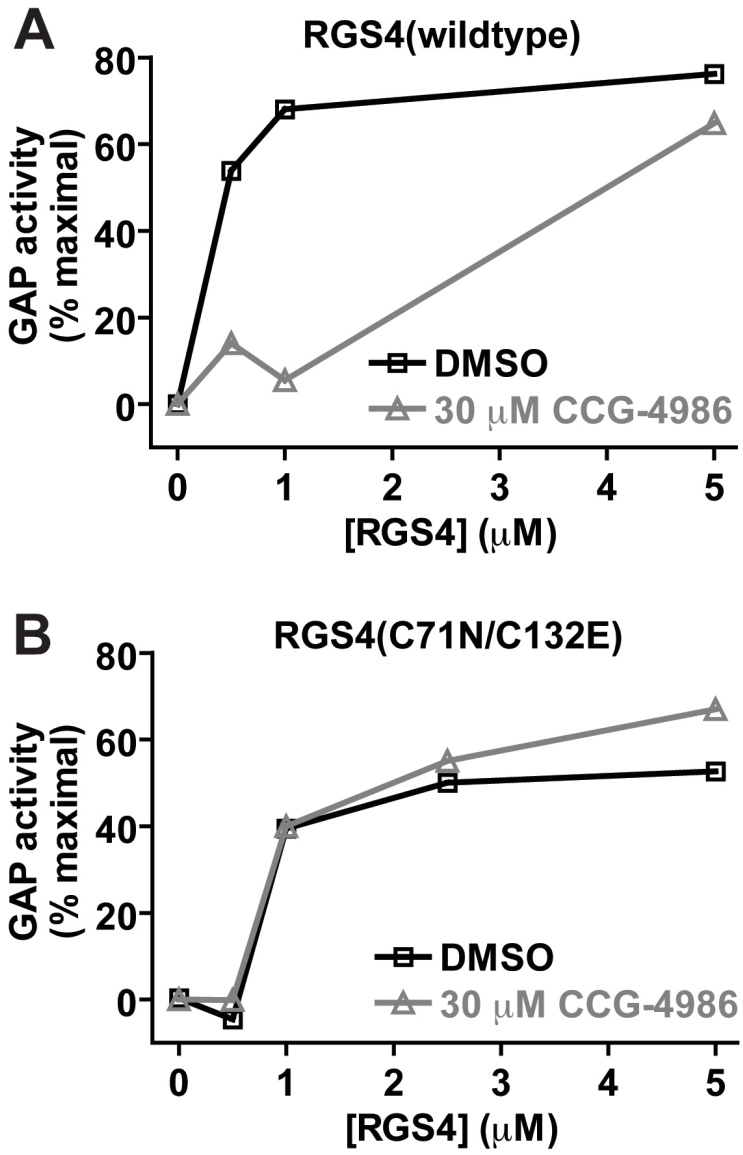

Figure 3.2. In vitro assays of RGS4 GAP activity. Single nucleotide binding-and-hydrolysis assays were conducted to measure acceleration of $G\alpha_{oA}$ GTP hydrolysis rate by (A) wildtype and (B) cysteine-substituted (C71N/C132E) forms of RGS4. The fluorescence of 50 nM BODIPYFL-GTP was measured at 20 °C in 1 ml of buffer containing various concentrations of RGS4 protein (0 to 5 mM) previously incubated for 2 minutes with 30 mM CCG-4986 or DMSO vehicle only. Fluorescence measurements were initiated and, at 60 seconds, $G\alpha_{oA}$ (100 nM) was added to cuvettes. Normalized GAP activity was then calculated as described [15] and plotted on the ordinate *versus* RGS4 concentration on the abscissa.

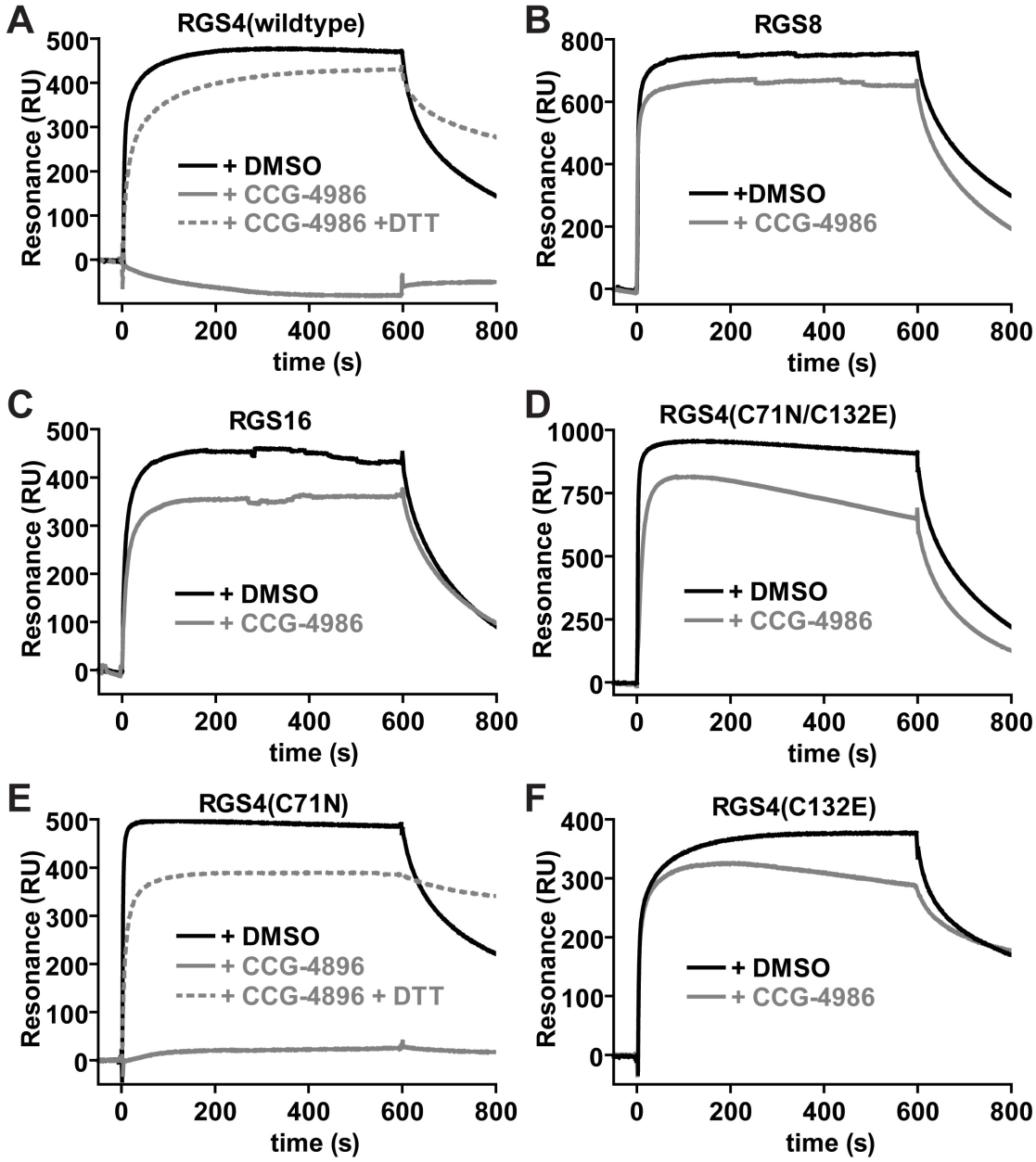

Figure 3.3. Surface plasmon resonance-based Gα-binding assays analyzing the inhibitory properties of CCG-4986 on wildtype RGS4 (A), RGS8 (B), RGS16 (C), and indicated cysteine mutants of RGS4 (panels D-F). 6000 resonance units (RU) of biotin-$G\alpha_{i1}$ protein was immobilized on a streptavidin biosensor surface. A 200 µl aliquot of 5 µM RGS protein, previously incubated with either DMSO vehicle (*black*), CCG-4986 (*gray*), or DTT-reduced CCG-4986 (*dotted gray*), was injected at 20 µl/min (0 to 600 seconds) with a follow-up 200 seconds of dissociation time in running buffer only (600 to 800 seconds).

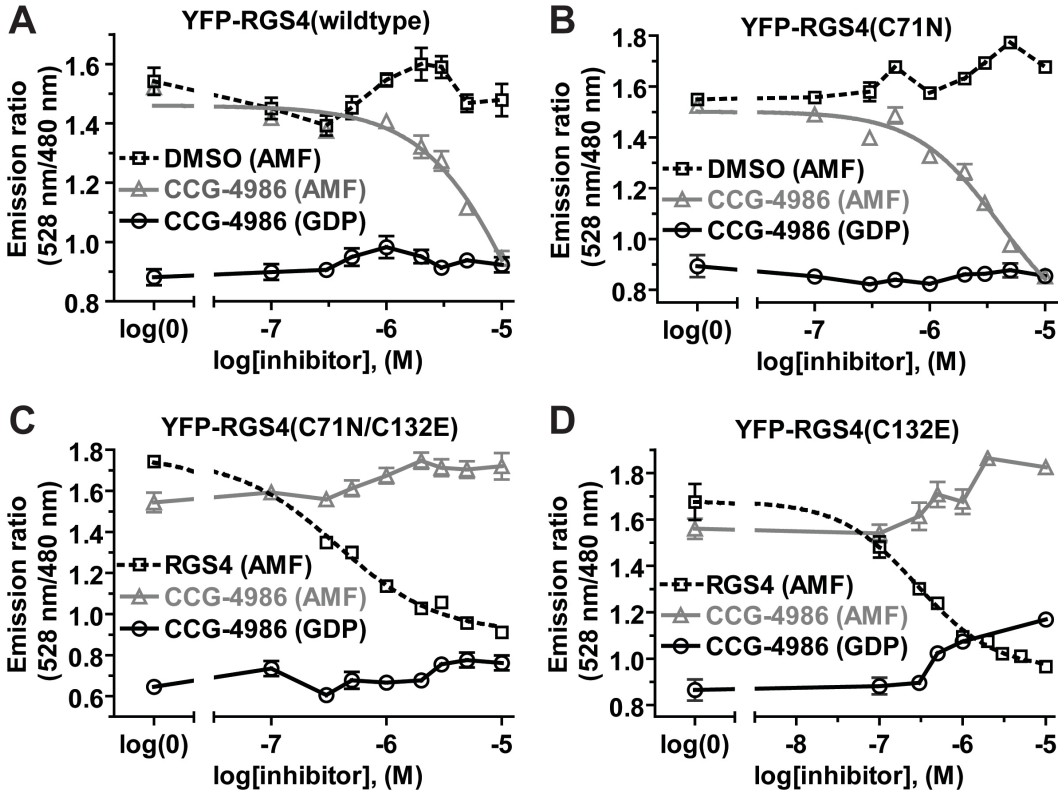

Figure 3.4. Competition FRET assays of the $G\alpha_{i1}$-CFP /YFP-RGS4 interaction. (A) Addition of increasing concentrations of CCG-4986 inhibitor to 200 nM $G\alpha_{i1}$-CFP and 280 nM YFP-RGS4, in buffer containing aluminum tetrafluoride (AMF), decreased the 528 nm/ 480 nm emission ratio, indicating a decrease in the RGS4/$G\alpha_{i1}$ interaction. Neither mock treatment with DMSO vehicle alone nor addition of CCG-4986 in GDP-containing buffer (*i.e.*, lacking aluminum tetrafluoride) resulted in a significant change in the FRET ratio, indicating that competition is caused specifically by CCG-4986. While a covalent reaction cannot be characterized by traditional pharmacological analysis (*i.e.*, IC_{50} or K_i calculations), the signal was seen to be reduced by 50% at 18 μM CCG-4986. (B) Analogous to wildtype YFP-RGS4, the YFP-RGS4(C71N) mutant displayed a dose-dependent decrease in the emission ratio, indicating the ability of CCG-4986 to act as an inhibitor of its association with $G\alpha_{i1}$-CFP. 50% inhibition was achieved at 4 μM CCG-4986. No inhibitory effect was seen as the result of DMSO treatment alone. (C) Increasing amounts of CCG-4986 had no inhibitory effects on the interaction between the C71N/C132E double mutant of YFP-RGS4 (560 nM) and 400 nM $G\alpha_{i1}$-CFP in its aluminum tetrafluoride-loaded form. Unlabeled RGS4, added as a positive control for competitive inhibition of YFP-RGS4 binding, was able to decrease the emission ratio as expected (IC_{50} value of 375 nM; 95% confidence interval of 300-470 nM). (D) As with the double mutant, the inhibitory effects of CCG-4986 were abolished upon mutating solely the cysteine-132 of YFP-RGS4. To confirm that this single cysteine mutation did not alter the sensitivity of the assay to detect inhibition, unlabeled RGS4 was used as a competitor and found to have an IC_{50} of 284 nM (95% C.I. of 200-410 nM). All samples in all panels were performed in triplicate, with error bars representing the mean ± SEM.

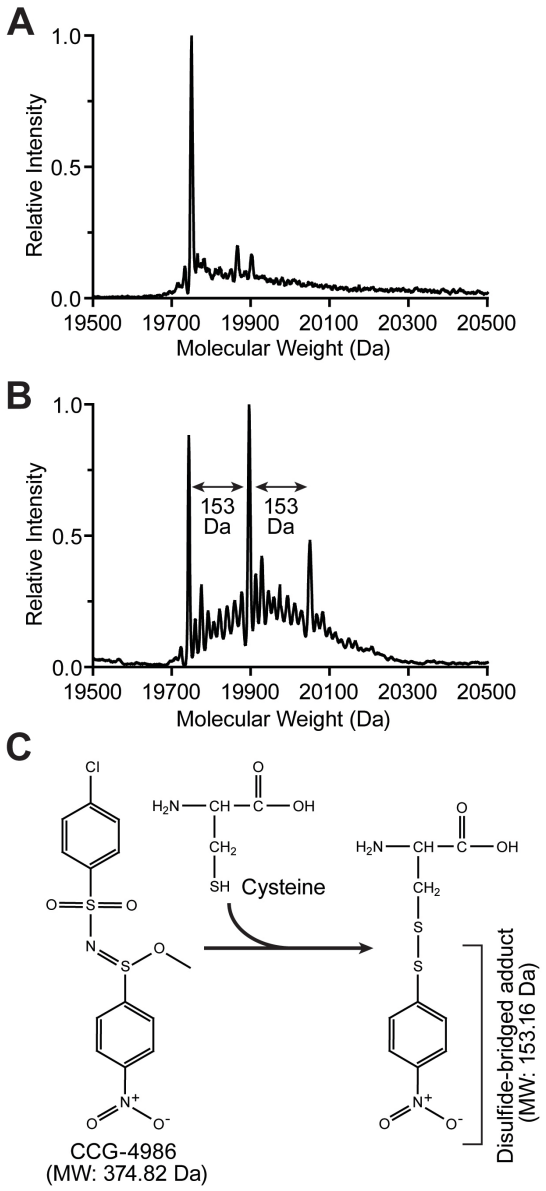

Figure 3.5. Intact molecular weight determination of unreacted and CCG-4986 treated RGS4. (A) Untreated RGS4 was found to exist in a single dominant form corresponding to its predicted molecular weight. (B) RGS4 preincubated with CCG-4986 was found in to consist of three major forms. The three peaks obtained by nano-ESI-MS correspond to the molecular weight of RGS4 (19,743 Da), RGS4 + 153 Da (19,896 Da), and RGS4 + 2x(153 Da) (20,050 Da). (C) CCG-4986 (methyl-N-[(4-chlorophenyl)sulfonyl]-4-nitrobenzenesulfinimidoate) has two sulfur atoms that potentially could react with thiol groups of solvent-exposed cysteine residues. Based on the mass spectrometry data from CCG-4986-treated RGS4, we propose that the 4-nitrobenzenethiol group is covalently attached to the two surface-exposed cysteines Cys-71 and Cys-132 in RGS4. The mass of the disulfide-bonded adduct derived from CCG-4986 would correspond precisely with the MS peaks at 19,896 Da (RGS4 + one 4-nitrobenzenethiol group) and 20,050 Da (RGS4 + two 4-nitrobenzenethiol groups).

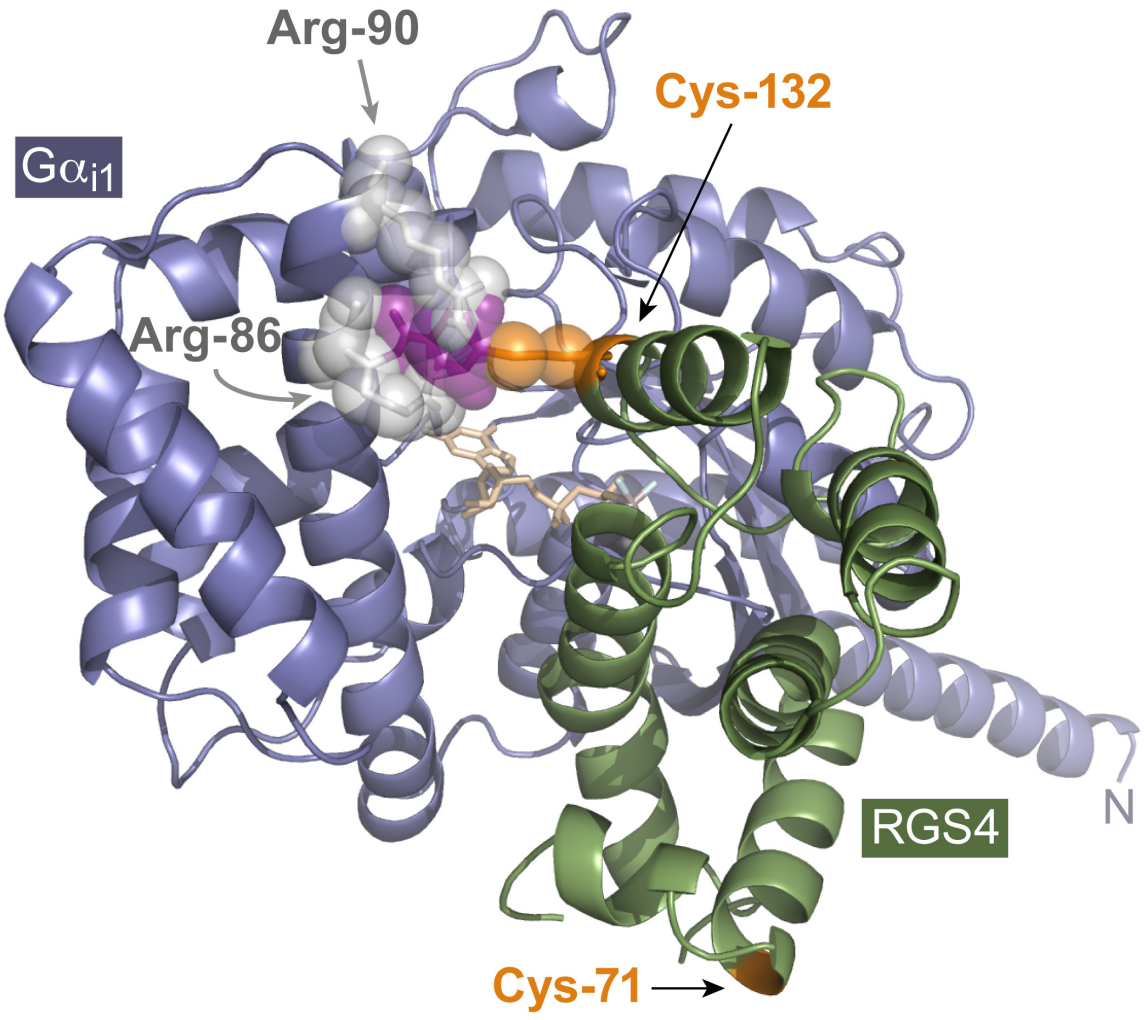

Figure 3.6. Proposed model for RGS4 inhibition by CCG-4986. The presence of the cysteine-132 residue of RGS4 is clearly necessary for the inhibitory action of CCG-4986. While cysteine-132 is not critical for the RGS4/Gα interaction *per se* (*i.e.*, its conversion to glutamate does not eliminate GAP activity [Fig. 2] nor Gα association [Figs. 3 & 4]), the known high-resolution structure of the RGS4/$G\alpha_{i1}$ complex [17] suggests that a small moiety (*purple*) covalently coupled to Cys-132 (*orange*) would result in steric hindrance with the Arg-86 and Arg-90 (*light gray*) of the all-helical domain of $G\alpha_{i1}$ (*steel blue*). The Cα ribbon trace of RGS4 is illustrated in *green*; GDP bound within the G-protein is colored in *wheat*, with the aluminum tetrafluoride ion in *light blue* and *gray*.

CHAPTER 4

A HIGH-THROUGHPUT FLUORESCENCE POLARIZATION ASSAY FOR INHIBITORS OF THE GoLoco MOTIF / G-alpha INTERACTION

Elements of this work referenced in this chapter have been published in:

Kimple, A. J., Yasgar, A., Hughes, M., Jadhav, A., Willard, F. S., Muller, R. E., Austin, C. P., Inglese, J., Ibeanu, G. C., Siderovski, D. P. and Simeonov, A. (2008) A High Throughput Fluorescence Polarization Assay for Inhibitors of the GoLoco Motif/G-alpha Interaction. *Comb Chem High Throughput Screen*. 11: 396-409.

4.1 ABSTRACT

The GoLoco motif is a short Gα-binding polypeptide sequence. It is often found in proteins that regulate cell-surface receptor signaling, such as RGS12, as well as in proteins that regulate mitotic spindle orientation and force generation during cell division, such as GPSM2/LGN. Here, we describe a high-throughput fluorescence polarization (FP) assay using fluorophore-labeled GoLoco motif peptides for identifying inhibitors of the GoLoco motif interaction with the G-protein alpha subunit $G\alpha_{i1}$. The assay exhibits considerable stability over time and is tolerant to DMSO up to 5%. The Z′-factors for robustness of the GPSM2 and RGS12 GoLoco motif assays in a 96-well plate format were determined to be 0.81 and 0.84, respectively; the latter assay was run in a 384-well plate format and produced a Z′-factor of 0.80. To determine the screening factor window (Z-factor) of the RGS12 GoLoco motif screen using a small molecule library, the NCI Diversity Set was screened. The Z-factor was determined to be 0.66, suggesting that this FP assay would perform well when developed for 1,536-well format and scaled up to larger libraries. We then miniaturized to a 4 μL final volume a pair of FP assays utilizing fluorescein- (green) and rhodamine- (red) labeled RGS12 GoLoco motif peptides. In a fully-automated run, the Sigma-Aldrich LOPAC^{1280} collection was screened three times with every library compound being tested over a range of concentrations following the quantitative high-throughput screening (qHTS) paradigm; excellent assay performance was noted with average Z-factors of 0.84 and 0.66 for the green- and red-label assays, respectively.

4.2 INTRODUCTION

Many extracellular signals, including hormones, neurotransmitters, growth factors, and sensory stimuli relay information intracellularly by activation of plasma membrane-bound receptors. The largest class of such receptors is the superfamily of seven transmembrane-domain G protein-coupled receptors (GPCRs), so named because these cell-surface proteins were originally found to couple extracellular stimuli into intracellular changes via activation of G-protein heterotrimers (Gαβγ) [1]. GPCRs represent a major therapeutic target giving rise to the largest single fraction of the prescription drug market with annual sales of several billion dollars [2]; however, opportunities to develop therapeutics that target the intracellular regulatory machinery controlling the kinetics and duration of GPCR signal transduction have been relatively ignored by comparison.

A diverse family of Gα-interacting proteins has been shown to share a common GoLoco ("$G\alpha_{i/o}$-Loco" interaction) motif (Figure 4.1) (reviewed in [3, 4]). GoLoco motif-containing proteins generally bind to GDP-bound Gα subunits of the Gi (adenylyl-cyclase inhibitory) class and act as GDP dissociation inhibitors (GDIs), slowing the spontaneous exchange of GDP for GTP and preventing re-association with Gβγ subunits [5-13]. Determination of the crystallographic structure of $G\alpha_{i1}$·GDP in complex with the GoLoco motif of RGS14 [14] revealed critical determinants of Gα subunit specificity and GDI activity. The N-terminal alpha-helix of the GoLoco motif peptide binds between switch II and the α3 helix of the $G\alpha_{i1}$ Ras-like domain (Figure 4.1B), grossly deforming the normal site of Gβγ interaction [7]. The aspartate-glutamine-arginine triad, which defines the final residues of the highly-conserved 19 amino-acid GoLoco motif signature (Figure 4.1A),

orients the arginine residue into the guanine nucleotide-binding pocket of Gα, allowing contacts to be made between its basic δ-guanido group and the α- and β-phosphates of GDP [7]. Mutation of this single arginine residue within the Asp-Gln-Arg triad causes a loss of GDI activity [7, 8, 11].

A well-characterized physiological function of GoLoco motif proteins is in the regulation of asymmetric cell division in worm, fruit fly, and mammalian development (reviewed in [15, 16]). For example, GPSM2 (a quadruple GoLoco motif-containing protein, previously known as LGN) binds to nuclear mitotic apparatus protein (NuMA) and regulates mitotic spindle assembly; altering endogenous cellular levels of GPSM2, either via overexpression or RNA interference-mediated knockdown, leads to aberrant chromosomal segregation during mitosis [17]. Similar functions have also been ascribed to Drosophila and *C. elegans* homologs of GPSM2 (Pins and GPR-1/-2, respectively; refs. [18-22]).

Evidence is also emerging that GoLoco motif-containing proteins act as critical components of cell-surface receptor-mediated signal transduction pathways. GPSM2 over-expression has been found to affect both basal and GPCR-activated potassium currents from GIRK channels [23], the latter effect similar to what we previously observed via cellular microinjection of GoLoco motif peptides [24]. We have recently shown RGS12 to be a receptor-selective scaffold for components of the mitogen-activated protein kinase (MAPK) cascade [13]. RNA interference-mediated knockdown of RGS12 protein levels in primary mouse dorsal root ganglion neurons blunts nerve growth factor-stimulated axonogenesis [13]. Mutating the arginine residue within the Asp-Gln-Arg triad of the RGS12 GoLoco motif leads to a mislocalization of RGS12 to the nucleus, away from its normally punctate endosomal pattern of expression [25]. This latter finding suggests that small molecule

inhibition of the GoLoco motif/$G\alpha_i$ interaction could serve to abrogate the normal signaling regulatory properties of GoLoco motif proteins, not only for RGS12 in the context of inhibiting sustained MAPK signal output, but also for GPSM2 and homologs in the context of dysregulating cell division processes in cancerous states of unchecked cellular proliferation [14, 26].

In this article, we describe the development of high-throughput screening (HTS) assays based on fluorescence polarization (FP) for the identification of small molecule inhibitors of the GoLoco motif/Gα protein interaction (Figure 4.2). FP is often used to detect the binding of fluorescently-labeled small ligands to larger binding partners (*e.g.*, refs. [27-32]). FP is based on the physical principle that fluorescein and other fluorophores are only excited by incident light that is polarized parallel to their axis. If this fluorophore is stationary or only slowly rotating, subsequent emission remains polarized along the same axis. Conversely, if polarized light excites a fluorophore rapidly tumbling in solution (Figure 2A), the resulting emission is depolarized by the rapid rotational diffusion that occurs during the lifetime of the excited state (~4 ns for fluorescein, ref. [33]). This depolarization is quantified as fluorescence anisotropy (FA) or fluorescence polarization (FP) by measuring the intensity of the emission perpendicular ($I_\perp$) and parallel ($I_\parallel$) to the plane of excitation (Equation (4.1); for a more comprehensive explanation of FA and FP, we refer the reader to ref. [33]). FA and FP are not equal but can be interconverted using equation (4.2). FP is a unitless ratio; however, it is often expressed as "milliP" (mP).

$$(4.1)\quad FA = \frac{I_\parallel - I_\perp}{I_\parallel + 2I_\perp} \qquad FP = \frac{I_\parallel - I_\perp}{I_\parallel + I_\perp}$$

$$(4.2)\ FA = \frac{2(FP)}{3 - FP}$$

Because the depolarization of fluorophore-emitted light is directly related to the rotational motion of the fluorophore-labeled molecule, and thus inversely related to its total molecular weight (MW), FA and FP are theoretically limited to measuring the binding of a lower MW ligand to a higher MW substrate (*e.g.*, Figure 4.2B). While in theory this technique can be used to measure binding of any fluorescently-labeled ligand to a substrate as long as the MW_{ligand} is much less than $MW_{substrate}$, in practice these assays are limited to ligands that have a MW of less than 5,000 Da. This limitation arises because of the short half-life (~4 ns) of the excited state of fluorescein isothiocyanate (FITC) [33], the most readily used dye in fluorescence polarization assays. (Rhodamine-based dyes have an even shorter half-life in the excited state; ref. [33]). While other dyes with longer lifetimes can be used to measure binding between larger molecules [34-36], their use has not been widespread.

Fluorescence polarization assays have been developed to detect various biological events such as phosphorylation, proteolytic cleavage, single nucleotide polymorphism detection, cAMP production, protein-protein interactions, and protein-DNA interactions [17, 28, 29, 31, 32, 37-40]. This article focuses on our development and validation of a ligand displacement assay to screen for inhibitors of RGS12/$G\alpha_{i1}$ and GPSM2/$G\alpha_{i1}$ interactions (Figure 4.2C).

4.3 MATERIALS AND METHODS

4.3.1 Chemicals and Assay Material

Unless otherwise noted, all chemicals used were the highest grade available from Sigma Aldrich (St. Louis, MO) or Fisher Scientific (Pittsburgh, PA). Tris-HCl used in the 1,536-well plate format assay was procured from Invitrogen. 96-well black bottom plates were obtained from Costar (Corning, NY). The LOPAC^{1280} library of known bioactives (1280 compounds from Sigma-Aldrich; arrayed for screening as 8 concentrations at 5 μL each in 1,536-well Greiner polypropylene compound plates) was received as DMSO solutions at initial concentration of 10 mM. Plate-to-plate (vertical) dilutions in 384-well format and 384-to-1,536 compressions were performed on an Evolution P^3 dispense system equipped with 384-tip pipetting head and two RapidStak units (Perkin-Elmer; Wellesley, MA). Additional details on the preparation of the compound library for quantitative high-throughput screening (qHTS) are provided elsewhere [41, 42].

4.3.2 Protein Expression and Purification

Expression and purification of human His_6-$G\alpha_{i1}$ from the expression plasmid pProEXHTb-h$G\alpha_{i1}$ was performed essentially as previously described [14]. Briefly, BL21 (DE3) *E. coli* (Novagen; San Diego, CA) were grown to an $OD_{600\,nm}$ of 0.6-0.8 at 37°C before induction with 0.5 mM isopropyl-β-D-thiogalactopyranoside. After culture for 14-16 hours at 20°C, cells were pelleted by centrifugation and frozen at -80°C. Prior to purification, bacterial cell pellets were resuspended in N1 buffer (50 mM Tris pH 8.0, 300 mM NaCl, 10 mM $MgCl_2$, 10 mM NaF, 30 μM $AlCl_3$, 50 μM GDP, 30 mM imidazole, 5% (w/v) glycerol). Bacteria

were lysed at 10 MPa using an Emulsiflex pressure homogenizer (Avestin; Ottawa, Canada). Cellular lysates were centrifuged at 100,000 x g for 30 minutes at 4°C. The supernatant was applied to a nickel-nitrilotriacetic acid resin FPLC column (FF HisTrap; GE Healthcare), washed with 7 column volumes of N1 buffer then 3 column volumes of N1 buffer containing an additional 30 mM of imidazole before eluting with N1 buffer containing an additional 300 mM of imidazole. Eluted protein was incubated with tobacco etch virus (TEV) protease and dialyzed into low imidazole buffer (N1 buffer with 5 mM DTT) overnight at 4°C (to cleave the N-terminal hexahistidine tag) before being passed over a second HisTrap column to separate the untagged $G\alpha_{i1}$ from contaminants and cleavage products. The column flow-through was pooled and resolved using a calibrated 150 ml size exclusion column (Sephacryl S200, GE Healthcare) with S200 buffer (50 mM Tris pH 7.5, 150 mM NaCl, 10 μM GDP, 5% (w/v) glycerol). Protein was then concentrated to approximately 1 mM, as determined by $A_{280\,nm}$ measurements upon denaturation in guanidine hydrochloride. Concentration was calculated based on the predicted extinction coefficient obtained using the ProtParam webtool [43]. His_6-$G\alpha_{oA}$ was purified using similar chromatographic methods as previously described [44].

4.3.3 Peptide Synthesis

Unless otherwise denoted, peptides were synthesized by Fmoc-group protection, purified via HPLC, and confirmed using mass spectrometry by the Tufts University Core Facility (Medford, MA). Peptide sequences were as follows:

FITC-RGS12:

FITC-β-alanine-DEAEEFFELISKAQSNRADDQRGLLRKEDLVLPEFLR-amide;

FITC-GPSM2(GL2):

FITC-β-alanine-NTDEFLDLLASSQSRRLDDQRASFSNLPGLRLTQNSQS-amide;

GPSM1 GoLoco consensus:

TMGEEDFFDLLAKSQSKRMDDQRVDLAG-amide;

GPR-1(GoLoco wildtype)

EPVDMMDLIFSMSSRMDDQRTELPAARFIPPRPVSSASK-amide;

GPR-1(GoLoco R>F):

EPVDMMDLIFSMSSRMDDQFTELPAARFIPPRPVSSASK-amide.

The 5-carboxytetramethylrhodamine (TAMRA)-labeled peptide (TAMRA-DEAEEFFELISKAQSNRADDQRGLLRKEDLVLPEFLR-amide) was synthesized and HPLC-purified by Invitrogen (Carlsbad, CA).

4.3.4 Fluorescence Polarization Measurements in 96-well and 384-well Plate Formats

Polarization measurements during assay pilot trials were conducted using a PHERAstar microplate reader (BMG Labtech; Offenburg, Germany) with the fluorescence polarization module. Excitation wavelength was 485 ± 6 nm and emission was detected at 520 ± 15 nm. For each independent experiment, the gain of the parallel and perpendicular channel was calibrated so that 5 nM of FITC-RGS12 peptide had a polarization value of ~35 mP. The

final volume of each 96-well plate well was brought to 180 µl with PheraBuffer (10 mM Tris pH 7.5, 150 mM NaCl, 10 mM $MgCl_2$, 100 µM GDP, and 0.05% (v/v) NP40); the final volume per well in the 384-well plate format was 50 µL. For nucleotide selectivity studies, PheraBuffer was alternatively supplemented with aluminum tetrafluoride (*i.e.*, addition of 10 µM NaF and 30 µM $AlCl_3$). Data analysis for these assay pilot trials was conducted using PHERAstar software V1.60 (BMG LABTECH, Germany), as well as Excel version X for Macintosh (Microsoft, Seattle, Washington) and GraphPad Prism v4.0 (San Diego, CA). All dissociation constant (K_D) values were determined with non-linear regression and fitting to Equation 4.3, in which *FP* is the fluorescence polarization (measured in mP), [Gα] is the concentration of $G\alpha_{i1}$, B_{max} is the maximum polarization, and FP_{zero} is a correction factor to account for the polarization of unbound peptide (~35 mP).

$$(4.3)\quad FP = \frac{B_{\max}[G\alpha]}{K_D + [G\alpha]} + FP_{zero}$$

4.3.5 Surface Plasmon Resonance (SPR) Binding Assay

As a secondary screen for compounds that demonstrated at least partial concentration-dependent responses in the primary FP screen, optical detection of surface plasmon resonance (SPR) was performed using a Biacore 3000 (GE Healthcare; Piscataway, NJ). Surfaces of carboxymethylated dextran (CM5) biosensors (GE Healthcare) were covalently derivatized with anti-GST antibody as previously described [4, 44]. A GST fusion protein containing the minimal GoLoco motif of RGS12 [25] and GST protein alone (the latter as a

negative control) were separately loaded onto anti-GST antibody surfaces to levels of ~900 resonance units (RUs) before 200 mL of 40 nM $G\alpha_{i1}$·GDP protein (preincubated in either test compound or DMSO vehicle only) was injected over all flow cells using the KINJECT command at a flow-rate of 40 μL/minute with a dissociation phase of 2000 seconds. The biosensor surface was then stripped with a 40 μL injection of 10 mM Glycine pH 2.2 before being reloaded with GST-RGS12 fusion protein or GST alone for subsequent $G\alpha_{i1}$·GDP injections. Non-specific binding to the GST alone surface was subtracted from each sensorgram curve using BIAevaluation software v.3.0 (Biacore). Percent inhibition of binding was calculated as the maximal RUs of specific binding observed (just before the dissociation phase) from a compound-treated $G\alpha_{i1}$·GDP injection compared to a paired DMSO control-treated $G\alpha_{i1}$·GDP injection.

4.3.6 qHTS Validation in 1,536-well Plate Format

Control plate set-up. Titration of the unlabeled control peptide was delivered via pin transfer [45] of 23 nL of solution per well from a separate source plate into column 2 of each assay plate. The starting concentration of the control peptide was 10 mM and 20 mM for the FITC (green) and TAMRA (red) assay, respectively, followed by two-fold dilution points in duplicate, for a total of sixteen concentrations, resulting in final assay concentration range from 57.2 μM to 1.74 nM, and 114 μM to 3.49 nM, for the green and red assay, respectively.

Pre-screen assay miniaturization and optimization. Titration samples containing a constant amount of fluorophore-labeled peptide and variable concentrations of $G\alpha_{i1}$ protein were

prepared in 384-well plates and transferred into 1,536-well black solid bottom plates by the use of CyBiWell 384-tip pipeting system (CyBio Boston, MA). For the subsequent 1,536-well-based experiments, a Flying Reagent Dispenser (FRD, Aurora Discovery, presently Beckman-Coulter) [46] was used to dispense reagents into the assay plates.

qHTS protocol. Four μL of reagents (10 nM FITC- or 15 nM TAMRA-labeled peptide in columns 3 and 4 as negative control; a mixture of 10 nM FITC- or 15 nM TAMRA-labeled peptide with $G\alpha_{i1}$ [50 nM in the green assay and 25 nM in the red assay, respectively] in columns 1, 2, 5 – 48) were dispensed into 1,536-well Greiner black assay plates. Compounds and control peptide (23 nL) were transferred via Kalypsys pintool equipped with a 1,536-pin array (10 nL slotted pins, V&P Scientific, San Diego, CA) [45]. The plate was incubated for 10 min at room temperature, and then read on a ViewLux high-throughput CCD imager (Perkin-Elmer, Wellesley, MA) using FITC polarization filter sets (excitation 480 nm, emission 540 nm) for the green assay and BODIPY sets (excitation 525 nm, emission 598 nm) for the red assay, respectively. During reagent dispensing, reagent bottles were kept submerged in a 4 °C recirculating chiller bath and all liquid lines were covered with aluminum foil to minimize probe and protein degradation. All screening operations were performed on a fully integrated robotic system (Kalypsys, San Diego, CA) containing one RX-130 and two RX-90 anthropomorphic robotic arms (Staubli, Duncan, SC). Library plates were screened starting from the lowest and proceeding to the highest concentration. Vehicle-only plates, with DMSO being pin-transferred to the entire column 5 – 48 compound area, were included at the beginning, middle, and the end of the validation run in order to record any systematic shifts in assay signal.

Analysis of qHTS data. Screening data were corrected and normalized, and concentration-effect relationships derived by using NCGC in-house developed algorithms. Percent activity was computed after normalization using the median values of the uninhibited, or neutral, control (32 wells located in column 1) and the free-probe, or 100% inhibited, control (64 wells, entire columns 3 and 4), respectively. An in-house database was used to track sample concentrations across plates, while ActivityBase (ID Business Solutions Ltd, Guildford, UK) was used for compound and plate registrations. A four-parameter Hill equation [47] was fitted to the concentration-response data by minimizing the residual error between the modeled and observed responses.

4.4 RESULTS

4.4.1 Detection of Gα/GoLoco motif interactions using fluorescence polarization.

We previously described the use of a fluorescein isothiocyanate-labeled RGS12 GoLoco motif peptide (FITC-RGS12) as a probe to measure Gα/GoLoco motif interactions using FP [48]. Our aim in this present study was to validate this FP assay, and develop a corresponding $G\alpha_{i1}$/GPSM2 interaction assay, as robust techniques for high-throughput screening for small molecule inhibitors of the Gα/GoLoco motif interaction. To establish an assay for $G\alpha_{i1}$ binding to a GoLoco motif from GPSM2 (Figure 4.3), we first incubated increasing concentrations of $G\alpha_{i1}$ protein (up to 10 μM) with constant amounts (either 0.1, 1.0, or 10 nM) of FITC-GPSM2(GL2) peptide encoding the second GoLoco motif of GPSM2. We observed robust interaction of $G\alpha_{i1}$ with FITC-GPSM2(GL2), whereby addition of saturating

amounts of $G\alpha_{i1}$ caused an increase in FP from ~35 mP to ~160 mP (Figure 4.3A). Saturation binding isotherms illustrated that signal strength was optimal at FITC-GPSM2(GL2) probe concentrations of 1 nM and above (Figure 4.3A). Non-linear regression was used to fit the binding isotherms from experiments using two different probe concentrations to Equation 4.3, yielding dissociation constants (K_D) of 34 nM (using 1.0 nM probe) and 38 nM (using 10 nM FITC-GPSM2(GL2) probe). Saturation binding isotherms of FITC-RGS12 binding to $G\alpha_{i1}$ were also generated (Figure 4.4). FITC-RGS12 levels were held constant at 0.01, 0.1, 1, or 10 nM while the concentration of $G\alpha_{i1}$ was increased up to 3 μM. While binding was observable with sub-nanomolar concentrations of FITC-RGS12 probe, maximal polarization (~200 mP) was observed at FITC-RGS12 concentrations ≥1 nM (Figure 4.4A); however, at probe concentrations below 5 nM, increased noise was observed upon the addition of DMSO (data not shown). The binding affinity for the FITC-RGS12 to $G\alpha_{i1}$ was 3.8 nM (using 1 nM FITC-RGS12 probe).

To verify that these FP assays truly detect binding of the FITC-GPSM2(GL2) and FITC-RGS12 probes to their intended target of $G\alpha_{i1}$·GDP (consistent with the known biochemistry of GoLoco motif/Gα interactions [16]), we tested the nucleotide dependence of the interaction. Saturation binding isotherms were generated at a constant concentration of 1 nM of FITC-GPSM2(GL2) probe with increasing concentrations of $G\alpha_{i1}$ in either PheraBuffer or PheraBuffer with aluminum tetrafluoride (AlF_4^-, which binds Gα to create a transition state-mimetic form). As expected, upon the addition of AlF_4^-, there was a dramatic decrease in observed binding affinity. FITC-GPSM2(GL2) probe bound three orders of magnitude more avidly to $G\alpha_{i1}$·GDP than to $G\alpha_{i1}$·GDP·AlF_4^- (K_D of 35 nM *versus* 15 μM,

respectively; Figure 4.3B). Binding of FITC-RGS12 probe demonstrated a similar preference for $G\alpha_{i1}$·GDP (K_D of 4.3 nM versus 1.6 μM for $G\alpha_{i1}$·GDP·AlF_4^-; Figure 4.4B).

While GoLoco motifs were originally described as $G\alpha_{i/o}$-binding peptides [3], subsequent biochemical characterization has demonstrated preferential binding to the $G\alpha_i$ subfamily ($G\alpha_{i1}$, $G\alpha_{i2}$, $G\alpha_{i3}$) and not to $G\alpha_o$ (*e.g.*, refs. [6, 9]). To assess Gα subunit specificity, the binding of FITC-GPSM2(GL2) and FITC-RGS12 probes to $G\alpha_{i1}$·GDP and $G\alpha_o$·GDP proteins was compared. Both GoLoco motif probes exhibited significantly higher binding affinities for $G\alpha_{i1}$·GDP than for $G\alpha_o$·GDP. The K_D for the FITC-GPSM2(GL2)/$G\alpha_o$·GDP interaction was determined to be 3 μM, nearly two orders of magnitude higher than the affinity of the FITC-GPSM2(GL2)/$G\alpha_{i1}$·GDP interaction (Figure 4.3B). Similarly, the binding affinity of FITC-RGS12 for $G\alpha_o$·GDP was observed to be 70 μM versus 4.3 nM for $G\alpha_{i1}$·GDP (Figure 4.4B).

To further validate this GoLoco motif/$G\alpha_{i1}$ interaction assay for use in HTS, we characterized time dependence and dimethylsulfoxide (DMSO) tolerance of the assay. To assess the stability of the assay over extended periods of time, we measured saturation binding isotherms using 96-well plates containing FITC-GPSM2(GL2) or FITC-RGS12 probes (and increasing concentration of $G\alpha_{i1}$) that were rescanned at several hour time intervals. The K_D of the FITC-GPSM2(GL2)/$G\alpha_{i1}$ interaction was consistent over the first 25 hours of repeated measurements and increased marginally only at 48 hours (Figure 4.3C). Similar long-term stability was also observed for FITC-RGS12/$G\alpha_{i1}$ interaction (Figure 4.4C). Additional tests were made to establish the sensitivity of the assay to the standard HTS compound solvent DMSO; the FP assay using either FITC-GPSM2(GL2) or FITC-

RGS12 probe demonstrated remarkable tolerance up to at least 5% (v/v) DMSO (Figures 4.3D, 4.4D).

4.4.2 Competitive Binding Studies

To confirm that the FITC-GPSM2(GL2) and FITC-RGS12 probes bound in a reversible manner, unlabeled GoLoco motif peptides were used as "cold competitors" (Figure 4.5). For these competition binding assays, the concentrations of the FITC-labeled probe and $G\alpha_{i1}$ were chosen so that the polarization signal was at ~80% of the maximal response [49]. Addition of unlabeled competitor peptide, derived from GPSM1 GoLoco motifs [5], to a mixture of 5 nM FITC-RGS12 probe and 30 nM $G\alpha_{i1}$ resulted in a dose-dependent decrease in polarization (Figure 4.5A) with an IC_{50} of 1 μM. In separate tests using 1 nM FITC-GPSM2(GL2) probe and 600 nM $G\alpha_{i1}$, the IC_{50} for the unlabeled GoLoco motif competitor (based on GPR-1; [19]) was determined to be 177 nM (Figure 4.5B). To rule out the possibility of the apparent competition being an artifact of high peptide concentrations, we also titrated in a GoLoco motif peptide with the critical arginine of the Asp-Gln-Arg triad mutated to phenylalanine ("GoLoco R>F"; Figure 4.5B). As expected, this mutant peptide had no inhibitory effect at the same or higher concentrations.

4.4.3 Estimation of Screening Window

The next step in validation of this FP-based HTS assay was determining its screening window. An initial screening window can be crudely estimated by measuring many samples that only contain positive or negative controls for inhibition of the probe/Gα interaction [50,

51]. The mean and standard deviation of these controls were used to determine a Z′-factor for the assay using Equation (4.4), where σ is the standard deviation of the positive or negative control for inhibition and μ is the mean of the positive or negative control FP measurement [51]. Unlike other methods for quantifying the quality of an assay, the Z′-factor accounts for both the dynamic range (denominator) of the assay as well as the variation from well-to-well (numerator). The Z′-factor for the FP assay using 5 nM FITC-RGS12 probe, 30 nM $G\alpha_{i1}$, and 30 μM unlabeled GoLoco motif competitor peptide was calculated to be 0.84. This value was obtained by running one 96-well plate of positive controls and one 96-well plate of negative controls at 175 μl final volume and 1% (v/v) DMSO. Reduction in well volume below 175 μl was found to increase the standard deviation of both positive and negative controls (data not shown). Performing the same analysis with the FITC-GPSM2(GL2) probe resulted in a Z′-factor of 0.81. To assess the scalability of this FP assay to higher density plates, the same replicates of positive and negative controls for inhibition were also run with the FITC-RGS12 probe using 384 well plates. The Z′-factor was found to be 0.80 using a final volume of 50 μl.

$$(4.4)\quad Z' = 1 - \frac{3\sigma_+ + 3\sigma_-}{|\mu_- - \mu_+|}$$

4.4.4 Initial Small Molecule Screen in 96-well Plate Format

While computing a Z′-factor is useful in assay development, screening window data from an actual compound library screen is more informative [50]. Towards this goal, we first

obtained the National Cancer Institute (NCI) Developmental Therapeutics Program's Diversity Set (http://dtp.nci.nih.gov/branches/dscb/diversity_explanation.html) and screened 1976 compounds from this collection at 100 μM final concentration (Figure 4.6). Raw fluorescence polarization data was first normalized to the mean polarization signal from negative controls (1% (v/v) DMSO only; set to 100% binding signal) and from positive controls for inhibition (30 μM GPSM1 competitor peptide; set to 0% binding signal) (Figure 4.6A). A total of 286 compounds were excluded based on non-specific effects on the fluorescence polarization and total fluorescence intensity readouts. First, compounds were excluded if the obtained polarization value was 5 standard deviations higher than the negative control or 5 standard deviations lower than the positive control for inhibition ("Polarization filter", Figure 4.6B). Next, compounds were excluded if the raw fluorescence intensity value was 6 standard deviations higher than the negative control or 6 standard deviations lower than the positive control for inhibition ("Intensity filter", Figure 4.6C). The screening window Z-factor from normalized data for the remaining 1690 compounds was 0.66, with a hit-rate of 0.3% (6 out of 1976 compounds tested; 'hit' defined as >75% inhibition) (Figure 4.6C). A parallel screening of the Diversity Set at 50 μM final compound concentration gave a screening window Z-factor of 0.69 with a hit rate of 0.48 % (data not shown).

4.4.5 Screening in the 384-well plate format and hit validation by SPR

To examine the performance of the FP assay against a larger compound collection, we used the 384-well plate formatted assay in a screen of a 33,600-compound subset of the Biogen

Idec 350,000 compound library. Thirty-two compounds were identified as inhibiting the assay by at least 30% (~1% hit rate); most of the hits were found in four clusters (Figure 4.7A), reflecting the grouping of compounds sharing similar chemistry on the same plates which is inherent to the design of the library subset derived from the original 350,000 compound library. Subsequent re-testing of each hit revealed 17 compounds exhibiting at least partial concentration-dependent inhibition of the primary FP assay. To validate these hits as inhibitors of the protein/peptide interaction, a secondary assay was performed based on optical detection of changes in surface plasmon resonance (*e.g.*, Figure 4.7B,C) upon binding $G\alpha_{i1}$ to immobilized GST-RGS12(GoLoco motif) fusion protein [25]. One of the hits from the primary FP assay was also found to inhibit the secondary SPR assay in a dose-dependent fashion (Figure 4.7D,E). This compound is now the subject of further analysis.

4.4.6 Assay miniaturization to 1,536-well plates and evaluation of red-shifted peptide probes

The FP assay was further miniaturized to a final volume of 4 μL in 1,536-well plate format by direct volume reduction. Retaining the inclusion of NP-40 in the assay buffer helped prevent peptide and protein absorption to the polystyrene wells due to the increased surface-to-volume ratio and also served to minimize the interfering effect of promiscuous inhibitors acting via colloidal aggregate formation [42, 45]. In a titration experiment using 10 nM FITC-RGS12 probe (hereinafter referred to as *green probe*), a robust FP signal change was observed (Figure 4.8) and a $G\alpha_{i1}$ protein concentration of 50 nM was selected for subsequent validation experiments. When the complex of 10 nM green probe and 50 nM $G\alpha_{i1}$ protein was incubated with varying concentrations of unlabeled peptide in the 1,536-well

plate, a concentration-response curve was observed (Figure 4.8B) whose associated IC_{50} value matched closely that obtained from 96- and 384-well based experiments.

In parallel with the miniaturization of the original green assay, a red-shifted probe was explored. Prior experience and our recent profiling of the NIH Molecular Libraries Small Molecule Repository (MLSMR) compound library with respect to autofluorescence [52] prompted us to seek a red-shifted assay system in order to minimize the fraction of fluorescent compounds interfering with the fluorescent readout. Thus, a peptide of the same RGS12 GoLoco motif sequence was labeled with 5-carboxytetramethyl rhodamine (TAMRA, hereinafter referred to as *red probe*) and subjected to the same assay optimization experiments. In order to maintain robust fluorescence intensity signal with this fluorophore, the red probe concentration was increased slightly to 15 nM. In protein titration experiments, the FP signal change observed with the red-labeled peptide was higher, in the range of 180-190 mP, as previously experienced with this fluorophore [52] (Figure 4.8A). The increased FP window per same protein concentration allowed us to decrease the $G\alpha_{i1}$ protein concentration in the red assay to half that of the green assay (25 nM versus 50 nM) while maintaining a sufficient signal window. Consistent with lowered probe and protein concentrations for the red system (15 nM red probe with 25 nM $G\alpha_{i1}$ protein versus 10 nM green probe and 50 nM $G\alpha_{i1}$ protein), the displacement of the red probe from its complex by the unlabeled competitor peptide resulted in left-shifted concentration-response curve (Figure 4.8B), thus confirming that the lowered protein load resulted in slightly improved assay sensitivity.

During the course of our red probe exploration, we evaluated two red-shifted fluorophores. An RGS12 GoLoco motif peptide of the same sequence labeled with BODIPY

Texas Red failed to yield a change in fluorescence polarization when titrated with $G\alpha_{i1}$ protein (data not shown), presumably due to an adverse effect of the fluorophore on the RGS12 peptide binding affinity and/or increased self-aggregation of the probe due to the hydrophobic nature of the BODIPY moiety. Thus, not every combination of peptide probe and fluorophore should be expected to yield a readily-optimizable binding assay and, as the present limited example suggests, fluorophores of an overly-hydrophobic nature might be problematic when used with peptides (as opposed to oligonucleotide or DNA probes, for example) while those containing a number of ionizable groups such as TAMRA might offer a better chance for developing a good peptide-based FP assay [52]

4.4.7 qHTS robotic validations using the LOPAC^{1280} library

Once the peptide probe and $G\alpha_{i1}$ protein concentrations were optimized for the green and red assays, we proceeded to run fully-automated, 1,536-well based robotic validations. For each fluorophore system, the LOPAC^{1280} collection was screened three consecutive times in concentration-response mode [41]. A total of 30 plates were run per fluorophore assay: 24 compound plates (i.e., three iterations of the LOPAC^{1280} eight-concentrations set) and 6 control DMSO plates,. The assay signal windows, as expressed by the difference between mean FP values for the bound and unbound labeled peptide controls, were stable throughout the robotic validation (Figure 4.9A). Both assays performed robustly, yielding an average Z' factor of 0.84 for the green assay and 0.66 for the red assay, respectively (Figure 4.9B). The intra-plate peptide control titration curves remained nearly overlapping throughout the screen progression (Figure 4.9C), yielding average IC_{50} values of 7.8 mM and 0.6 mM for the green and red assays, respectively. During these qHTS experiments, each library compound was

tested as an eight-point titration, with concentrations ranging from 2 nM to 57 μM, and for each well and each assay system, fluorescence polarization values, as well as parallel- and perpendicular-plane fluorescence intensity values, were collected and stored in the database.

Unlike traditional HTS, qHTS provides concentration responses for all the compounds screened and allows determination of the half-maximal activity concentrations associated with each active compound. Additionally, compound effect can be described with respect to the shape, efficacy, and goodness-of-fit of its concentration-response curve [41]. Our LOPAC^{1280} library validation runs revealed 8 active compounds shared by the green and red screens, some of which were associated with complete concentration-response curves while others showed single-point inhibition at the highest concentration and, as such, the sigmoidal dose-response curves fitted through their data were of the lowest quality and reproducibility. However, for most of the active compounds identified in the LOPAC^{1280} library, there was excellent reproducibility within the triplicate runs, as well as good agreement between the outcomes from the green and red assays. Four examples of triplicate green and red concentration-response curves derived from the validations are shown in Figure 4.10.

4.5 DISCUSSION

4.5.1 Sensitivity of Binding Detection and Screening Window Optimization

In agreement with several previous studies of $G\alpha_i$/GoLoco interactions (reviewed in [16]), the FP assay we have developed clearly demonstrates preferential binding of the GoLoco motif to the inactive, ground state of $G\alpha_i$ (i.e., $G\alpha_{i1}$·GDP) and selective binding of $G\alpha_{i1}$

versus $G\alpha_o$ (Figures 4.3B and 4.4B). The equilibrium binding-based FP assay was also found to detect binding with affinities that are consistent, but higher, than previously published and unpublished results using kinetic measurements (k_{on}, k_{off}) obtained by surface plasmon resonance [7, 9]. These higher observed affinities for the RGS12 and GPSM2 interactions with $G\alpha_{i1}$·GDP are most likely the result of the highly-sensitive probe detection technique being used in the FP assay, allowing use of probe concentrations that are less than the observed K_D values. Additionally, the relatively hydrophobic FITC moiety added to these GoLoco motif peptides is likely to bind to $G\alpha_{i1}$ and thereby increase the overall affinity of the labeled GoLoco motif peptide for its $G\alpha_i$ substrate.

From Equation (4.2), one can see that the Z′-factor is dependent on the standard deviation of the positive and negative controls. We found that the standard deviation could be decreased by increasing the amount of FITC-GoLoco motif probe in the assay as well as increasing the number of excitation flashes per well during fluorescence polarization measurements. However, these two factors must be balanced with competing considerations of increasing reagent consumption and the time to scan plates. An alternative way to increase the screening window would be to increase the $G\alpha_{i1}$ concentration to increase the difference between the minimum and maximum FP signal; however, this change would concomitantly increase the amount of unbound $G\alpha_{i1}$ and thus require more cold competitor peptide or compound to cause inhibition in the signal, resulting in a less sensitive assay.

4.5.2 Small-Scale Library Screens and Strategies for Minimizing Compound Interference

The fundamentally ratiometric nature of the fluorescence polarization measurement theoretically reduces the effects of interference from compounds that have overlapping spectra with the FITC-labeled probe [30]. Interference from compounds with overlapping absorbance spectra should not change an FP reading so long as the absorbance is proportional (*P*) along both axes (Equation 4.5); however, the robustness of this ratiometric measurement cannot compensate for compounds that interfere by increasing or decreasing the signal in an additive (*A*) manner (Eq. 4.5).

$$(4.5)\quad FP_{prop} = \frac{(P)(I_{\parallel}) - (P)(I_{\perp})}{(P)(I_{\parallel}) + (P)(I_{\perp})} = \frac{I_{\parallel} - I_{\perp}}{I_{\parallel} + I_{\perp}} \text{ but } FP_{add} = \frac{(I_{\parallel} + A) - (I_{\perp} + A)}{(I_{\parallel} + A) + (I_{\perp} + A)} \neq \frac{I_{\parallel} - I_{\perp}}{I_{\parallel} + I_{\perp}}$$

While a high tolerance to interference from compound absorbance is an advantage of FP assays, 226 compounds (11.4% of the set) were excluded from our pilot screening data of the NCI Diversity Set, based on FP measurement interference. With the FITC-labeled (green) assay, we developed a systematic way to exclude interfering compounds as shown in Figure 4.6. From the initial raw data, each plate was normalized so that the average of eight positive control wells for inhibition were set to 0% binding and the average of eight negative control wells were set to 100% binding. After this normalization, compounds that resulted in polarization values 5 standard deviations above 100% binding or 5 standard deviations below 0% binding were excluded. Compounds giving readings above the threshold likely interfered by causing aggregation of either probe or substrate. Compounds giving readings significantly below 0% binding were excluded because these compounds clearly interfered with probe

fluorescence. Following this "polarization filter", additional compounds were excluded based on intensity values [30]. While we observed that the fluorescence intensity of the FITC-GoLoco motif probes increased upon binding to Gα, this change in intensity was consistent between wells and across plates. Compounds that resulted in a total intensity value ($2I_{\perp}+I_{||}$) falling 6 standard deviations outside of the intensity window established from the controls were also excluded. As the result of these exclusions, 1690 of 1976 compounds remained within the NCI Diversity Set for consideration as $G\alpha_i$/GoLoco motif binding inhibitors, with 6 of these compounds demonstrating inhibition of greater than 75 percent. From this single-concentration screen of nearly two thousand compounds at 100 μM final concentration and 1% (v/v) DMSO, the Z-factor was 0.66. This FP screen was also conducted at 50 μM final compound concentration and very little improvement in Z-factor was noted (data not shown). While the Z-factor was significantly lower than the Z′-factor calculated from controls, the Z-factor derived from this pilot library screen represents the actual screening window and, at a value of 0.66, still reflects an excellent assay robustness amenable to HTS of larger compound collections.

Another aspect of our optimization of this FP screening strategy was the development and implementation of a red-shifted fluorophore assay employing a TAMRA-labeled version of the RGS12 GoLoco motif peptide. The rationale for this change was to move farther away from the autofluorescence-sensitive regions of the light spectrum. In fact, our recently-completed fluorescent spectroscopic profiling of the NIH Molecular Libraries Small Molecule Repository (MLSMR) and other compound libraries demonstrated that, in blue-shifted fluorophore regions such as the frequently-utilized UV/vis spectrum (excitations near 360 nm and emissions near 450 nm) and fluorescein spectrum (excitations around 480 nm

and emissions near 520 nm), a significant proportion of library compounds are expected to interfere with the fluorescent assay readout (as high as 3% in the UV/vis region and 0.1% in the fluorescein region, respectively) [53]. In the present work, the transition to a red-shifted fluorophore resulted in an additional two-fold benefit of lowering the protein requirement for the screen and improving the sensitivity of the binding assay, both due to the fact that the rhodamine-based probe afforded greater FP signal change for the same protein concentration.

4.5.3 Benefits of the qHTS Approach

The robotic validation screen for inhibitors of the RGS12 GoLoco motif/$G\alpha_{i1}$ complex was performed in qHTS format, with every compound tested over a range of concentrations, spanning from tens of micromolar to low nanomolar, to generate a broad concentration-response profile. Thus, in addition to potencies and efficacies being assigned to each active compound immediately out of the primary screen, false positives and negatives due to single-point outliers are easily identified in the context of compound titration. Stated differently, after performing qHTS, the selection of active compounds is based on the premise that the biological effect of an active compound is a function of its concentration, rather than on pure statistical arguments and application of cutoffs. While the library preparation and the primary screen are "front-loaded" with an increased number of plates, the savings associated with reduced cherry-picking, re-arraying, and retesting steps tend to make up for those elevated initial costs, due to the increased robustness and higher information content of the screening data. Additionally, the higher quality of such screening datasets is expected to make them more valuable for data-mining in recently-established public databases such as PubChem.

In both robotic validations, the green and red assays performed robustly in the 1,536-well plate format, with Z´-factors remaining flat with the screen progression. The intra-plate unlabeled peptide control titration, which can be viewed as a combined internal standard for both the underlying assay biology and the reproducibility of compound transfer, yielded concentration-response curves that remained stable and reproducible throughout the screens (Figure 4.9C). Of note, miniaturization of this and other assays all the way to the 1,536-well plate format not only leads to reagent savings but also allows one to employ *additional* controls such as the intra-plate titration described here. The application of such controls that measure "the pulse" of the assay, while not necessarily required for signal normalization purposes, is made possible by the availability of so many additional wells in the 1,536-well plate. In lower plate densities, such as the 96-well plate, allocating 8 or 16 wells to low and high normalization controls is frequently barely enough to provide good statistics during large-scale screening. In contrast, in 1,536-well plates, the simple propagation of one empty 96-well plate column (equivalent to 8 wells) to the higher density plate leads to the natural creation of 128 wells (sixteen 96-well source plates feeding into one 1,536-well final plate) [42]. This 16-fold increase in the potentially-available wells makes it possible to add information content to each assay plate (by further partitioning the controls area) during large-collection miniaturized screens without placing undue burden on library preparation or otherwise compromising the outcome of the screens.

During our qHTS validations, each library compound was tested at eight concentrations and, for each well and fluorophore-type assay, three measurements were collected for a combined total of ~200,000 data points. The observed top active compounds in the green and red screens reproduced well upon repeated primary screening and across

fluorophores (Figure 4.10). Our successful robotic validation screen suggests that this FP assay is robust and sensitive enough to be utilized in a large-scale, 1,536-well based screen.

4.6 ACKNOWLEDGEMENTS

Work performed at the NCGC was supported by the Molecular Libraries Initiative of the National Institutes of Health Roadmap for Medical Research. Work performed in the Siderovski lab was funded by NIH grants F30 MH074266 (to A.J.K.) and R03 NS053754 (to D.P.S.).

4.7 DATA DEPOSITION

The two 1,536-well plate formatted bioassays reported in this paper, as well as active compounds identified in the LOPAC^{1280} library validation screens, have been deposited in the PubChem database, http://pubchem.ncbi.nlm.nih.gov (AID codes 879 for the green assay and 880 for the red assay).

4.8 REFERENCES

1. Gilman, A.G., *G proteins: transducers of receptor-generated signals.* Annu Rev Biochem, 1987. **56**: p. 615-49.

2. Overington, J.P., B. Al-Lazikani, and A.L. Hopkins, *How many drug targets are there?* Nat Rev Drug Discov, 2006. **5**(12): p. 993-6.

3. Siderovski, D.P., M. Diverse-Pierluissi, and L. De Vries, *The GoLoco motif: a Galphai/o binding motif and potential guanine-nucleotide exchange factor.* Trends Biochem Sci, 1999. **24**(9): p. 340-1.

4. Willard, F.S. and D.P. Siderovski, *Purification and in vitro functional analysis of the Arabidopsis thaliana regulator of G-protein signaling-1.* Methods Enzymol, 2004. **389**: p. 320-38.

5. De Vries, L., T. Fischer, H. Tronchere, G.M. Brothers, B. Strockbine, D.P. Siderovski, and M.G. Farquhar, *Activator of G protein signaling 3 is a guanine dissociation inhibitor for Galpha i subunits.* Proc Natl Acad Sci U S A, 2000. **97**(26): p. 14364-9.

6. Kimple, R.J., L. De Vries, H. Tronchere, C.I. Behe, R.A. Morris, M. Gist Farquhar, and D.P. Siderovski, *RGS12 and RGS14 GoLoco motifs are G alpha(i) interaction sites with guanine nucleotide dissociation inhibitor Activity.* J Biol Chem, 2001. **276**(31): p. 29275-81.

7. Kimple, R.J., M.E. Kimple, L. Betts, J. Sondek, and D.P. Siderovski, *Structural determinants for GoLoco-induced inhibition of nucleotide release by Galpha subunits.* Nature, 2002. **416**(6883): p. 878-81.

8. Kimple, R.J., F.S. Willard, M.D. Hains, M.B. Jones, G.K. Nweke, and D.P. Siderovski, *Guanine nucleotide dissociation inhibitor activity of the triple GoLoco motif protein G18: alanine-to-aspartate mutation restores function to an inactive second GoLoco motif.* Biochem J, 2004. **378**(Pt 3): p. 801-8.

9. McCudden, C.R., F.S. Willard, R.J. Kimple, C.A. Johnston, M.D. Hains, M.B. Jones, and D.P. Siderovski, *G alpha selectivity and inhibitor function of the multiple GoLoco motif protein GPSM2/LGN.* Biochim Biophys Acta, 2005. **1745**(2): p. 254-64.

10. Natochin, M., B. Lester, Y.K. Peterson, M.L. Bernard, S.M. Lanier, and N.O. Artemyev, *AGS3 inhibits GDP dissociation from galpha subunits of the Gi family and rhodopsin-dependent activation of transducin.* J Biol Chem, 2000. **275**(52): p. 40981-5.

11. Peterson, Y.K., M.L. Bernard, H. Ma, S. Hazard, 3rd, S.G. Graber, and S.M. Lanier, *Stabilization of the GDP-bound conformation of Gialpha by a peptide derived from the G-protein regulatory motif of AGS3.* J Biol Chem, 2000. **275**(43): p. 33193-6.

12. Takesono, A., M.J. Cismowski, C. Ribas, M. Bernard, P. Chung, S. Hazard, 3rd, E. Duzic, and S.M. Lanier, *Receptor-independent activators of heterotrimeric G-protein signaling pathways.* J Biol Chem, 1999. **274**(47): p. 33202-5.

13. Willard, M.D., F.S. Willard, X. Li, S.D. Cappell, W.D. Snider, and D.P. Siderovski, *Selective role for RGS12 as a Ras/Raf/MEK scaffold in nerve growth factor-mediated differentiation.* Embo J, 2007. **26**(8): p. 2029-40.

14. Kimple, R.J., F.S. Willard, and D.P. Siderovski, *The GoLoco motif: heralding a new tango between G protein signaling and cell division.* Mol Interv, 2002. **2**(2): p. 88-100.

15. Siderovski, D.P. and F.S. Willard, *The GAPs, GEFs, and GDIs of heterotrimeric G-protein alpha subunits.* Int J Biol Sci, 2005. **1**(2): p. 51-66.

16. Willard, F.S., R.J. Kimple, and D.P. Siderovski, *Return of the GDI: the GoLoco motif in cell division.* Annu Rev Biochem, 2004. **73**: p. 925-51.

17. Hsu, T.M., X. Chen, S. Duan, R.D. Miller, and P.Y. Kwok, *Universal SNP genotyping assay with fluorescence polarization detection.* Biotechniques, 2001. **31**(3): p. 560, 562, 564-8, passim.

18. Afshar, K., F.S. Willard, K. Colombo, C.A. Johnston, C.R. McCudden, D.P. Siderovski, and P. Gonczy, *RIC-8 is required for GPR-1/2-dependent Galpha function during asymmetric division of C. elegans embryos.* Cell, 2004. **119**(2): p. 219-30.

19. Colombo, K., S.W. Grill, R.J. Kimple, F.S. Willard, D.P. Siderovski, and P. Gonczy, *Translation of polarity cues into asymmetric spindle positioning in Caenorhabditis elegans embryos.* Science, 2003. **300**(5627): p. 1957-61.

20. Izumi, Y., N. Ohta, K. Hisata, T. Raabe, and F. Matsuzaki, *Drosophila Pins-binding protein Mud regulates spindle-polarity coupling and centrosome organization.* Nat Cell Biol, 2006. **8**(6): p. 586-93.

21. Nipper, R.W., K.H. Siller, N.R. Smith, C.Q. Doe, and K.E. Prehoda, *Galphai generates multiple Pins activation states to link cortical polarity and spindle orientation in Drosophila neuroblasts.* Proc Natl Acad Sci U S A, 2007. **104**(36): p. 14306-11.

22. Schaefer, M., A. Shevchenko, A. Shevchenko, and J.A. Knoblich, *A protein complex containing Inscuteable and the Galpha-binding protein Pins orients asymmetric cell divisions in Drosophila.* Curr Biol, 2000. **10**(7): p. 353-62.

23. Wiser, O., X. Qian, M. Ehlers, W.W. Ja, R.W. Roberts, E. Reuveny, Y.N. Jan, and L.Y. Jan, *Modulation of basal and receptor-induced GIRK potassium channel activity and neuronal excitability by the mammalian PINS homolog LGN.* Neuron, 2006. **50**(4): p. 561-73.

24. Webb, C.K., C.R. McCudden, F.S. Willard, R.J. Kimple, D.P. Siderovski, and G.S. Oxford, *D2 dopamine receptor activation of potassium channels is selectively decoupled by Galpha-specific GoLoco motif peptides.* J Neurochem, 2005. **92**(6): p. 1408-18.

25. Sambi, B.S., M.D. Hains, C.M. Waters, M.C. Connell, F.S. Willard, A.J. Kimple, S. Pyne, D.P. Siderovski, and N.J. Pyne, *The effect of RGS12 on PDGFbeta receptor signalling to p42/p44 mitogen activated protein kinase in mammalian cells.* Cell Signal, 2006. **18**(7): p. 971-81.

26. Cho, H. and J.H. Kehrl, *Localization of Gi alpha proteins in the centrosomes and at the midbody: implication for their role in cell division.* J Cell Biol, 2007. **178**(2): p. 245-55.

27. Burke, T.J., K.R. Loniello, J.A. Beebe, and K.M. Ervin, *Development and application of fluorescence polarization assays in drug discovery.* Comb Chem High Throughput Screen, 2003. **6**(3): p. 183-94.

28. Drees, B.E., A. Weipert, H. Hudson, C.G. Ferguson, L. Chakravarty, and G.D. Prestwich, *Competitive fluorescence polarization assays for the detection of phosphoinositide kinase and phosphatase activity.* Comb Chem High Throughput Screen, 2003. **6**(4): p. 321-30.

29. Nikiforov, T.T. and A.M. Simeonov, *Application of fluorescence polarization to enzyme assays and single nucleotide polymorphism genotyping: some recent developments.* Comb Chem High Throughput Screen, 2003. **6**(3): p. 201-12.

30. Owicki, J.C., *Fluorescence polarization and anisotropy in high throughput screening: perspectives and primer.* J Biomol Screen, 2000. **5**(5): p. 297-306.

31. Parker, G.J., T.L. Law, F.J. Lenoch, and R.E. Bolger, *Development of high throughput screening assays using fluorescence polarization: nuclear receptor-ligand-binding and kinase/phosphatase assays.* J Biomol Screen, 2000. **5**(2): p. 77-88.

32. Prystay, L., A. Gagne, P. Kasila, L.A. Yeh, and P. Banks, *Homogeneous cell-based fluorescence polarization assay for the direct detection of cAMP.* J Biomol Screen, 2001. **6**(2): p. 75-82.

33. Lakowicz, J.R., *Principles of fluorescence spectroscopy*. 2nd ed. 1999, New York: Kluwer Academic/Plenum. xxiii, 698 p.

34. Szmacinski, H., E. Terpetschnig, and J.R. Lakowicz, *Synthesis and evaluation of Ru-complexes as anisotropy probes for protein hydrodynamics and immunoassays of high-molecular-weight antigens.* Biophys Chem, 1996. **62**(1-3): p. 109-20.

35. Terpetschnig, E., H. Szmacinski, H. Malak, and J.R. Lakowicz, *Metal-ligand complexes as a new class of long-lived fluorophores for protein hydrodynamics.* Biophys J, 1995. **68**(1): p. 342-50.

36. Youn, H.J., E. Terpetschnig, H. Szmacinski, and J.R. Lakowicz, *Fluorescence energy transfer immunoassay based on a long-lifetime luminescent metal-ligand complex.* Anal Biochem, 1995. **232**(1): p. 24-30.

37. Akula, N., Y.S. Chen, K. Hennessy, T.G. Schulze, G. Singh, and F.J. McMahon, *Utility and accuracy of template-directed dye-terminator incorporation with fluorescence-polarization detection for genotyping single nucleotide polymorphisms.* Biotechniques, 2002. **32**(5): p. 1072-6, 1078.

38. Bonin, P.D. and L.A. Erickson, *Development of a fluorescence polarization assay for peptidyl-tRNA hydrolase.* Anal Biochem, 2002. **306**(1): p. 8-16.

39. Duan, W., L. Sun, J. Liu, X. Wu, L. Zhang, and M. Yan, *Establishment and application of a high throughput model for rho kinase inhibitors screening based on fluorescence polarization.* Biol Pharm Bull, 2006. **29**(6): p. 1138-42.

40. Zhang, T.T., Z.T. Huang, Y. Dai, X.P. Chen, P. Zhu, and G.H. Du, *High-throughput fluorescence polarization method for identifying ligands of LOX-1.* Acta Pharmacol Sin, 2006. **27**(4): p. 447-52.

41. Inglese, J., D.S. Auld, A. Jadhav, R.L. Johnson, A. Simeonov, A. Yasgar, W. Zheng, and C.P. Austin, *Quantitative high-throughput screening: a titration-based approach that efficiently identifies biological activities in large chemical libraries.* Proc. Nat. Acad. Sci.USA, 2006. **103**(31): p. 11473-8.

42. Yasgar, A., P. Shinn, S. Michael, W. Zheng, A. Jadhav, D. Auld, C. Austin, J. Inglese, and A. Simeonov, *Compound Management for Quantitative High-Throughput Screening.* JALA, 2008. **13**(2):79-89.

43. Gasteiger, E., C. Hoogland, A. Gattiker, S. Duvaud, M.R. Wilkins, R.D. Appel, and A. Bairoch, *Protein identification and analysis tools on the ExPASy server*, in *The Proteomics Protocols Handbook*, J.M. Walker, Editor. 2005, Humana Press. p. 571-607.

44. Willard, F.S., A.J. Kimple, C.A. Johnston, and D.P. Siderovski, *A direct fluorescence-based assay for RGS domain GTPase accelerating activity.* Anal Biochem, 2005. **340**(2): p. 341-51.

45. Cleveland, P.H. and P.J. Koutz, *Nanoliter dispensing for uHTS using pin tools.* Assay Drug Dev Technol, 2005. **3**(2): p. 213-25.

46. Niles, W.D. and P.J. Coassin, *Piezo- and Solenoid Valve-Based Liquid Dispensing for Miniaturized Assays.* . Assay Drug. Devel. Technol., 2005. **3**: p. 189-202.

47. Hill, A.V., *The Possible Effects of the Aggregation of the Molecule of Haemoglobin on its Dissociation Curves.* J. Physiol. (London), 1910. **40**: p. 4-7.

48. Willard, F.S., A.B. Low, C.R. McCudden, and D.P. Siderovski, *Differential G-alpha interaction capacities of the GoLoco motifs in Rap GTPase activating proteins.* Cell Signal, 2007. **19**(2): p. 428-38.

49. Huang, X., *Fluorescence polarization competition assay: the range of resolvable inhibitor potency is limited by the affinity of the fluorescent ligand.* J Biomol Screen, 2003. **8**(1): p. 34-8.

50. Seethala, R. and P.B. Fernandes, *Handbook of drug screening*. Drugs and the pharmaceutical sciences ; v. 114. 2001, New York: Marcel Dekker. xiii, 597 p.

51. Zhang, J.H., T.D. Chung, and K.R. Oldenburg, *A Simple Statistical Parameter for Use in Evaluation and Validation of High Throughput Screening Assays.* J Biomol Screen, 1999. **4**(2): p. 67-73.

52. Simeonov, A., A. Jadhav, C.J. Thomas, Y. Wang, R. Huang, N.T. Southall, P. Shinn, J. Smith, C.P. Austin, D.S. Auld, and J. Inglese, *Fluorescence spectroscopic profiling of compound libraries.* J Med Chem, 2008. **51**(8): p. 2363-71.

53. Simeonov, A., A. Yasgar, A. Jadhav, G.L. Lokesh, C. Klumpp, S. Michael, C.P. Austin, A. Natarajan, and J. Inglese, *Dual-fluorophore quantitative high-throughput screen for inhibitors of BRCT-phosphoprotein interaction.* Anal Biochem, 2008. **375**(1): p. 60-70.

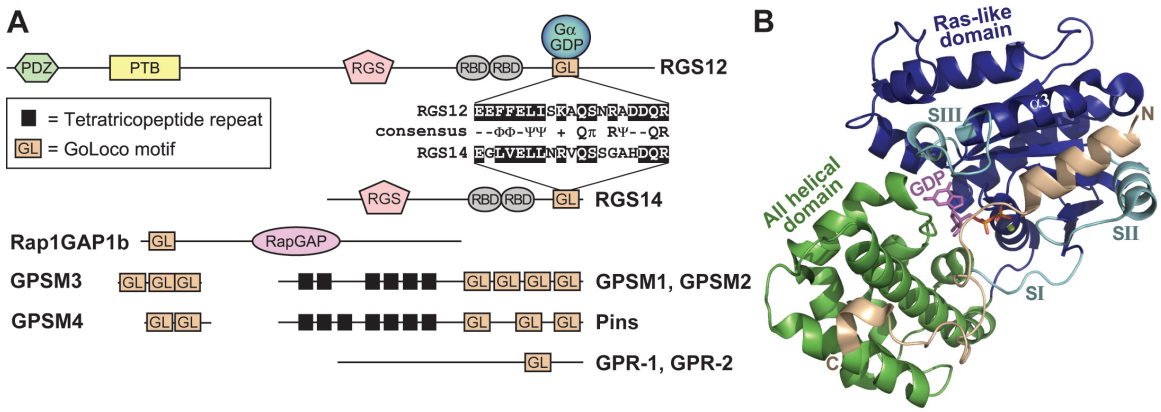

Figure 4.1. The GoLoco motif is a $G\alpha_i$·GDP -interacting polypeptide found singly or in arrays in various proteins. (A) Domain architecture of representative GoLoco motif proteins and a sequence alignment of the conserved core of the RGS12 and RGS14 GoLoco motifs. Domain abbreviations: GPSM, G-protein signaling modulator; PDZ, PSD-95/Discs large/ZO-1 homology; PTB, phosphotyrosine-binding domain; RGS, regulator of G-protein signaling box; RBD, Ras-binding domain; RapGAP, Rap-specific GTPase-activating protein domain. (B) The crystal structure of $G\alpha_{i1}$ (Ras-like domain in *blue*, all α-helical domain in *green*, switch regions in *cyan*) bound to the GoLoco motif of RGS14 (PDB ID 2OM2). The GoLoco motif peptide (*tan*) binds across the Ras-like and all-helical domains of $G\alpha_{i1}$, trapping GDP (*magenta*, with α- and β-phosphates in *orange*) within its binding site. The bound magnesium ion is illustrated in *lime green*.

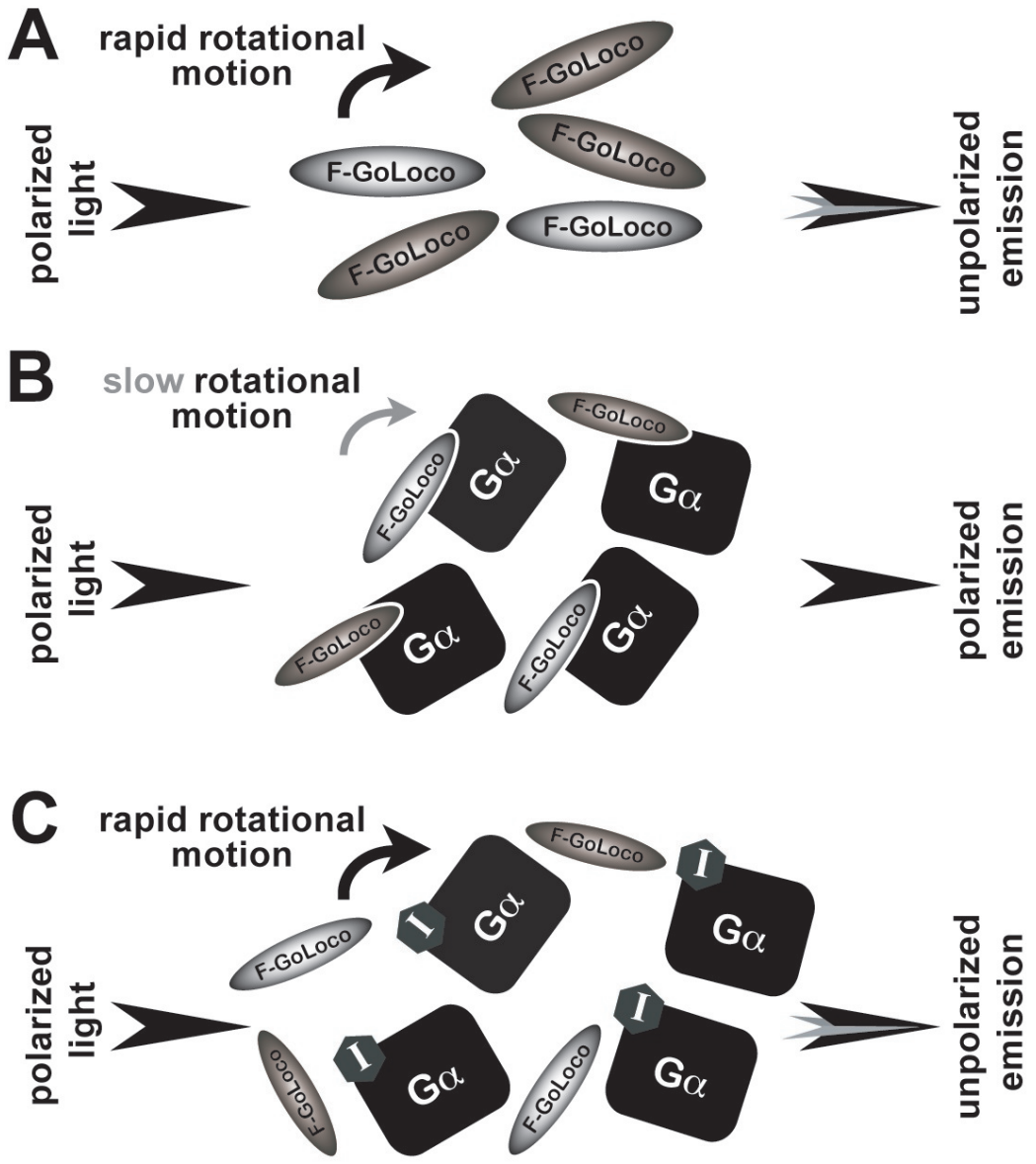

Figure 4.2. Schematic of a fluorescence polarization assay for detection of FITC-GoLoco motif probe binding to its $G\alpha_{i1}$ subunit target. (A) When excited by plane-polarized light, the rapid rotational motion of the unbound FITC-GoLoco motif probe decorrelates the light. (B) The rotational diffusion of the FITC-GoLoco motif probe dramatically decreases as its effective molecular weight changes upon binding to $G\alpha_{i1}$. Consequently, polarized excitation results in polarized emission. (C) A small molecule inhibitor ("I") that binds to $G\alpha_{i1}$ in competition with the FITC-GoLoco motif probe increases the concentration of unbound (and rapidly rotating) probe, resulting in a decreased polarization signal.

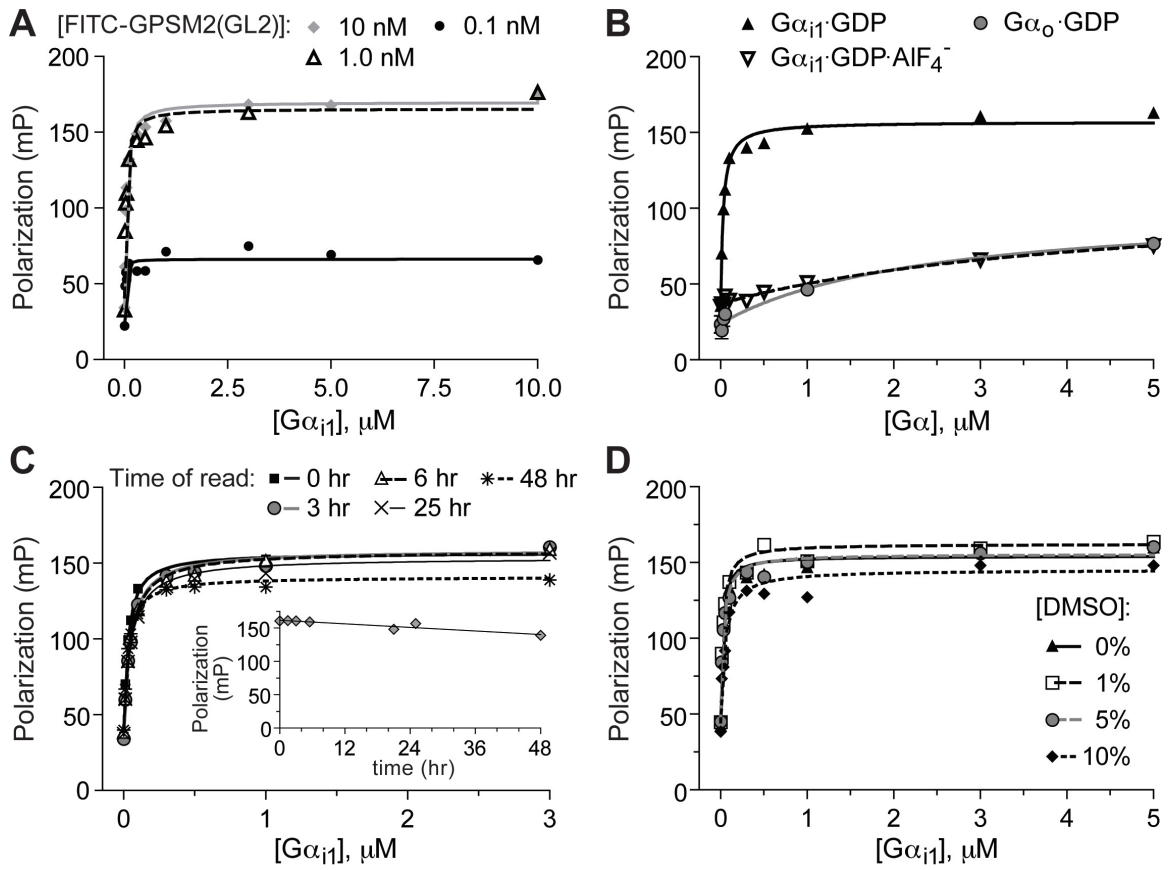

Figure 4.3. 96-well microtiter plate-formatted fluorescence polarization assay for FITC-GPSM2(GL2) probe binding to $G\alpha_{i1}$. (A) Concentration dependence and saturability of binding. Indicated concentrations of FITC-GPSM2(GL2) probe were incubated with indicated concentrations of $G\alpha_{i1}$·GDP prior to measuring fluorescence polarization at equilibrium. (B) Nucleotide and Gα subunit dependence of polarization signal. 1 nM of FITC-GPSM2(GL2) probe was incubated with indicated concentrations of $G\alpha_{i1}$·GDP (ground-state), $G\alpha_{i1}$·GDP·AlF_4^- (transition-state-mimetic form), or $G\alpha_o$·GDP prior to measuring fluorescence polarization at equilibrium. (C) Time-stability studies. 1 nM of FITC-GPSM2(GL2) probe was incubated with indicated concentrations of $G\alpha_{i1}$·GDP in 96-well microtiter plate wells for indicated times prior to measuring fluorescence polarization. *Inset*, Time-dependence of polarization signal from 1 nM of FITC-GPSM2(GL2) probe incubated with 3 μM $G\alpha_{i1}$·GDP. (D) DMSO tolerance. 1 nM of FITC-GPSM2(GL2) probe was incubated with indicated concentrations of $G\alpha_{i1}$·GDP and indicated final concentrations (v/v) of DMSO prior to measuring fluorescence polarization.

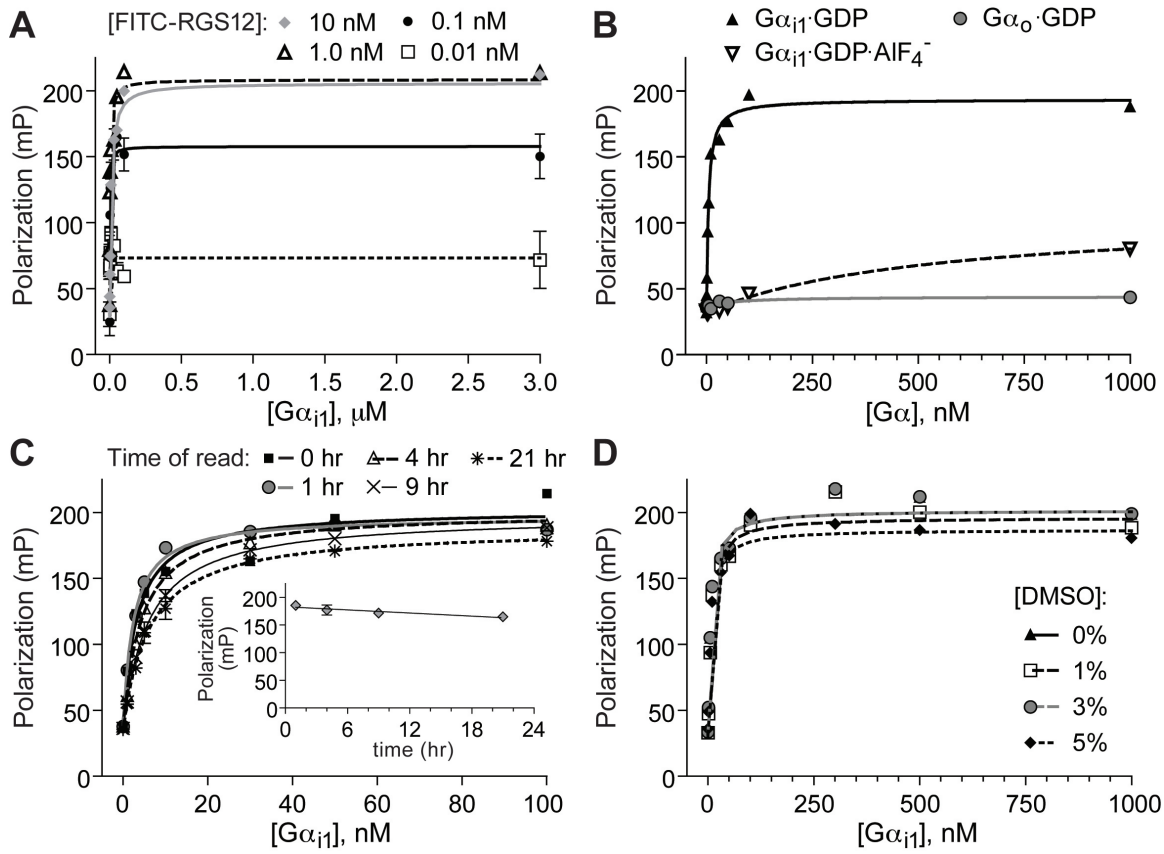

Figure 4.4. 96-well microtiter plate-formatted fluorescence anisotropy assay for FITC-RGS12 GoLoco motif probe binding to $G\alpha_{i1}$. (A) Concentration dependence and saturability of binding. Indicated concentrations of FITC-RGS12 probe were incubated with indicated concentrations of $G\alpha_{i1}$·GDP prior to measuring fluorescence polarization at equilibrium. (B) Nucleotide and Gα subunit dependence of polarization signal. 5 nM of FITC-RGS12 peptide was incubated with indicated concentrations of $G\alpha_{i1}$·GDP (ground-state), $G\alpha_{i1}$·GDP·AlF_4^- (transition-state-mimetic form), or $G\alpha_o$·GDP prior to measuring fluorescence polarization at equilibrium. (C) Time-stability studies. 5 nM of FITC-RGS12 probe was incubated with indicated concentrations of $G\alpha_{i1}$·GDP in 96-well microtiter plate wells for indicated times prior to measuring fluorescence polarization. *Inset*, Time-dependence of polarization signal from 5 nM of FITC-RGS12 probe incubated with 30 nM $G\alpha_{i1}$·GDP. (D) DMSO tolerance. 5 nM of FITC-RGS12 peptide was incubated with indicated concentrations of $G\alpha_{i1}$·GDP and indicated final concentrations (v/v) of DMSO prior to measuring fluorescence polarization. Error bars are mean ± SEM from triplicate samples.

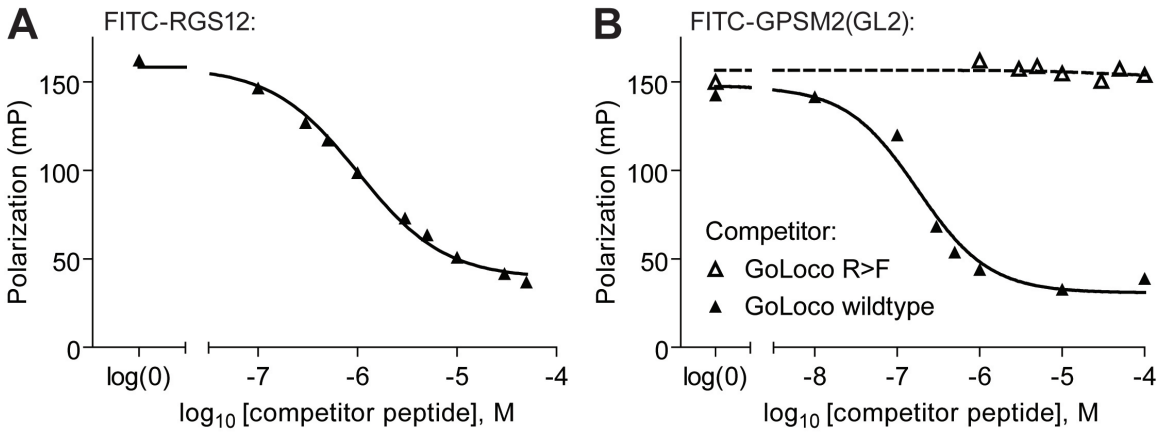

Figure 4.5. Competitive inhibition of fluorescence polarization signal by unlabeled GoLoco motif peptides. (A) Indicated concentrations of the unlabeled GPSM1 GoLoco motif consensus peptide was added to 5 nM FITC-RGS12 probe and 30 nM $G\alpha_{i1}$. (B) Indicated concentrations of the unlabeled GPR-1 GoLoco motif peptide ("GoLoco wildtype) or the same peptide with the critical arginine mutated to phenylalanine ("GoLoco R>F"). Peptides were incubated with 1 nM of FITC-GPSM2(GL2) probe and 600 nM of $G\alpha_{i1}$·GDP protein prior to measuring fluorescence polarization at equilibrium.

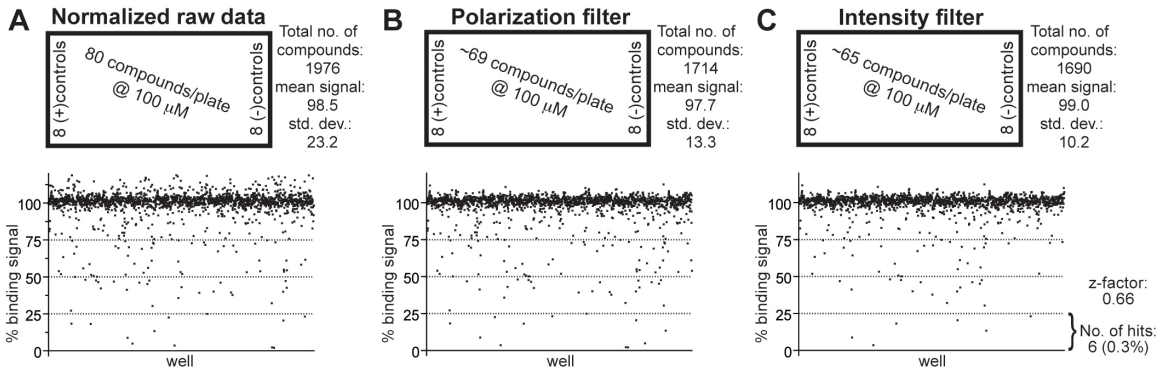

Figure 4.6. Data from pilot screen of the NCI Diversity Set to establish a screening window Z-factor. (A) Plot of normalized fluorescence polarization data from entire 1976 compound set run in 96-well plate format with 5 nM of FITC-RGS12 probe and 30 nM of $G\alpha_{i1}$·GDP protein. Positive control wells contained 30 μM of competitor GPSM1 peptide; negative control wells contained vehicle only (1% (v/v) DMSO). (B) Data after exclusion of wells with polarization values 5 standard deviations outside control values (as described in text). (C) Data after additional exclusion of wells with raw fluorescence intensity values 6 standard deviations outside control values (as described in text).

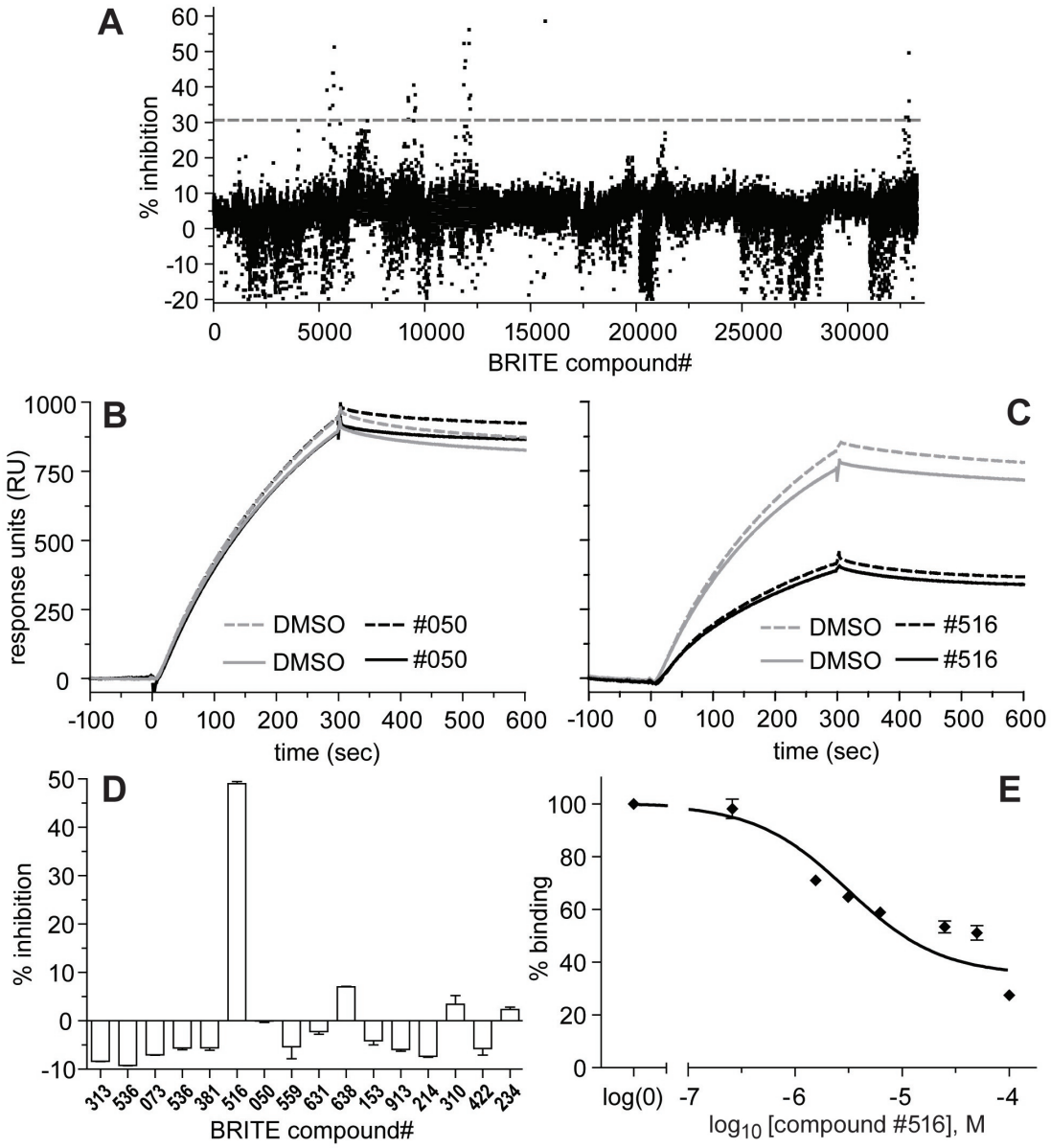

Figure 4.7. Data from pilot primary screen of the BRITE Biogen Idec library subset and hit validation using an SPR-based secondary assay. (A) Plot of percent inhibition for each compound in the 33,600-element BRITE Biogen Idec library subset run at 10 μM final concentration in 384-well plate format with 5 nM of FITC-RGS12 probe and 46 nM of $G\alpha_{i1}$·GDP protein. Note the clustering of inhibitory activity reflecting plate-wise grouping of similar compound chemistry within the 33,600 compound subset of the larger 350,000 Biogen Idec library. Gray dashed line represents cut-off of greater than 30% inhibition used to select compounds for subsequent dose-response testing in the same primary FP assay. (B, C) Representative SPR data from two compounds exhibiting at least partial concentration-dependent responses in the primary FP assay. Panel B represents negative data from

compounds (such as #050) that, after preincubation with $G\alpha_{i1}$·GDP, did not inhibit the latter binding to a GST-RGS12(GoLoco motif) biosensor surface during a 5 minute association phase (0 – 300 seconds). Panel C represents positive data from a confirmed inhibitor of the $G\alpha_{i1}$·GDP / GST-RGS12(GoLoco motif) interaction (compound #516). (D) Results of single-dose testing (13.3 μM final concentration) of 16 hits from the primary FP assay in the SPR-based secondary assay, performed as described in Materials and Methods. (E) Dose-response curve of the sole confirmed hit (compound #516) from the SPR-based secondary assay, performed as described in Materials and Methods, except with 50 μL injections of $G\alpha_{i1}$·GDP at a flow-rate of 20 μL/min and a subsequent 200 second dissociation time.

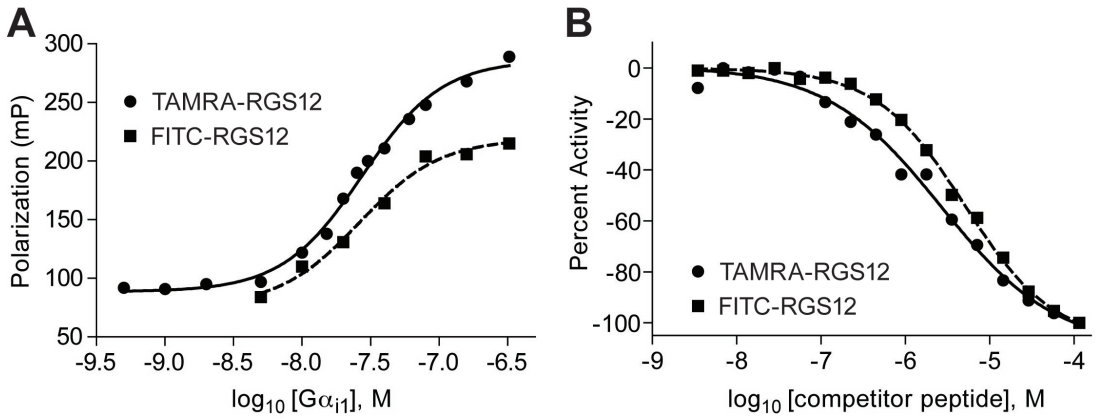

Figure 4.8. Miniaturization of FP assay to 1,536-well plate format and evaluation of FITC- versus TAMRA-labeled RGS12 GoLoco motif peptide probe. (A) Fluorescence polarization signal of FITC- (green) and TAMRA- (red) probes in the 1,536-well plate format. Protein-concentration dependence of the FP signal of 10 nM green probe (solid squares) and 15 nM red probe (solid circles) was measured in titrations with $G\alpha_{i1}$. Evident from the plots is the greater FP signal obtained from the red probe. (B) Probe displacement by unlabeled peptide control in the 1,536-well plate format. Green (solid squares, 10 nM FITC-RGS12 probe plus 50 nM $G\alpha_{i1}$) and red (solid circles, 15 nM TAMRA-RGS12 probe plus 25 nM $G\alpha_{i1}$) protein complexes were allowed to interact with series of concentrations of unlabeled peptide (pin-transferred from DMSO stock solutions) for 15 min at room temperature. The leftward-shift in dose-response of the red probe curve is a reflection of the slight increase in assay sensitivity afforded by the decreased protein concentration.

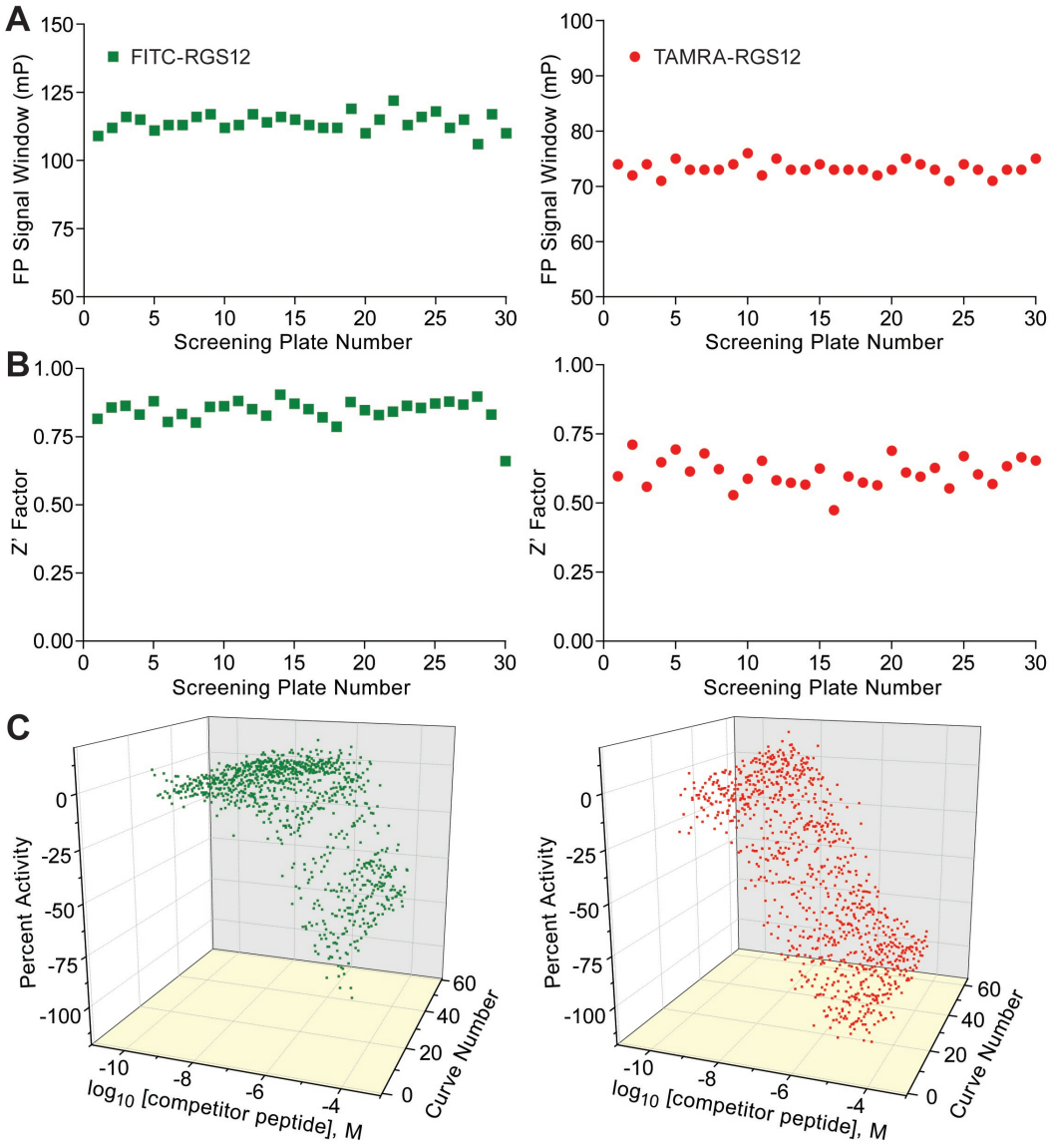

Figure 4.9. qHTS Performance. Shown for both the green and red probe FP assays are the (A) FP signal window, (B) Z' factor trend, and (C) intra-plate control titrations (duplicate curves per plate) as a function of screening plate number.

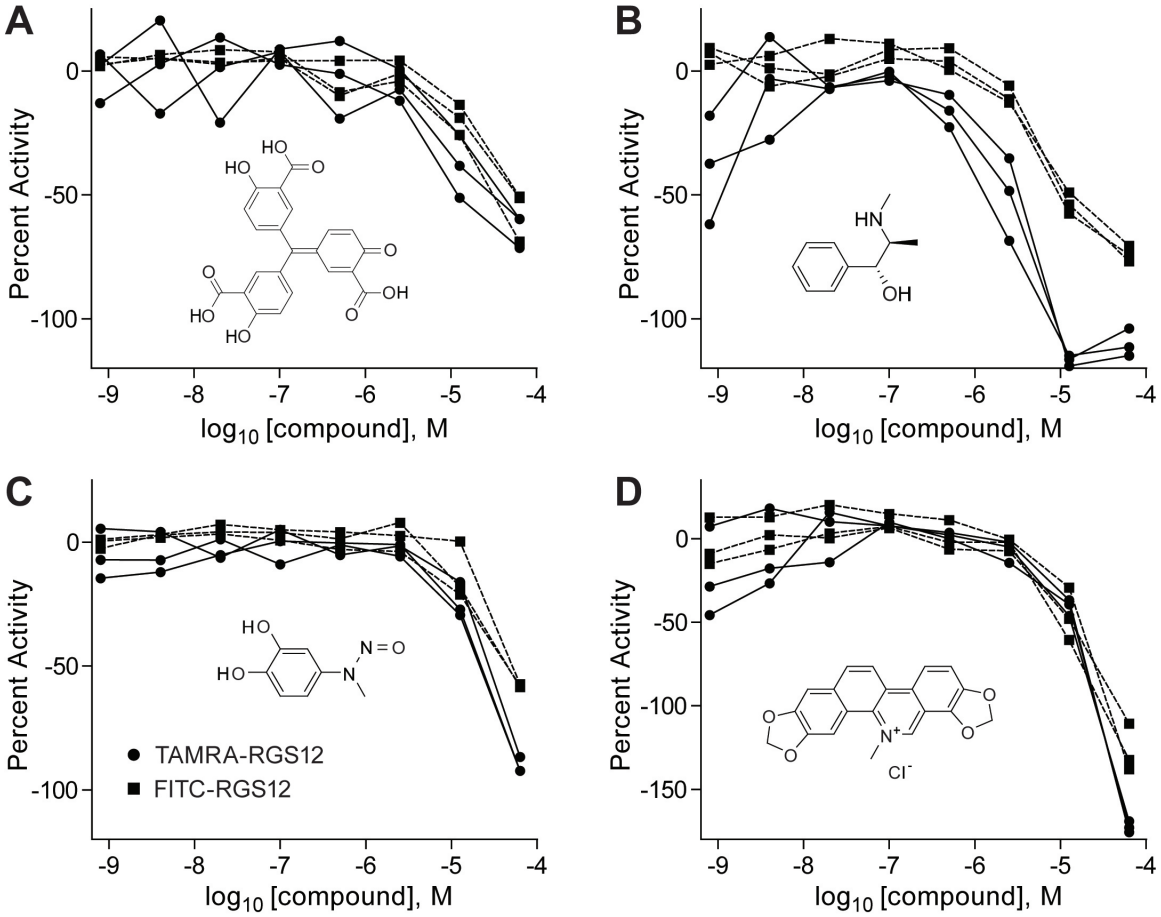

Figure 4.10. Examples of validation-derived active compounds. The concentration-response curves (triplicate runs in both colors, with green probe data in solid squares and red probe data in solid circles) are shown for (A) NCGC00093568 (PubChem SID 11110719), (B) NCGC00093901 (PubChem SID 11111142), (C) NCGC00094195 (PubChem SID 11111500), and (D) NCGC00094379 (PubChem SID 11111810).

CHAPTER 5

TWO $G\alpha_{i1}$ RATE-MODIFYING MUTATIONS ACT IN CONCERT TO ALLOW RECEPTOR-INDEPENDENT, STEADY-STATE MEASUREMENTS OF RGS PROTEIN ACTIVITY

Elements of this work referenced in this chapter have been published in:

Kimple, A. J.*, Zielinski, T.*, Hutsell, S. Q., Koeff, M. D., Siderovski, D. P., Lowery, R. G., Two $G\alpha_{i1}$ Rate-Modifying Mutations Act in Concert to Allow Receptor Independent, Steady-State Measurements of RGS Protein Activity. *J. Biological Screening*. 2009 Dec;14(10):1195-206.

*co-first author

5.1 ABSTRACT

RGS proteins are critical modulators of G protein-coupled receptor (GPCR) signaling given their ability to deactivate Gα subunits via "GTPase-accelerating protein" (GAP) activity. Their selectivity for specific GPCRs makes them attractive therapeutic targets. However, measuring GAP activity is complicated by slow GDP release from Gα and lack of solution-phase assays for detecting free GDP in the presence of excess GTP. To overcome these hurdles, we developed a $G\alpha_{i1}$ mutant with increased GDP dissociation and decreased GTP hydrolysis, enabling detection of GAP activity using steady-state GTP hydrolysis. $G\alpha_{i1}$(R178M/A326S) GTPase activity was stimulated 6~12 fold by RGS proteins known to act on $G\alpha_i$ subunits, and not affected by those unable to act on $G\alpha_i$, demonstrating that the Gα/RGS domain interaction selectivity was not altered by mutation. $G\alpha_{i1}$(R178M/A326S) interacted with RGS proteins with expected binding specificity and affinities. To enable non-radioactive, homogenous detection of RGS protein effects on $G\alpha_{i1}$(R178M/A326S), we developed a Transcreener® fluorescence polarization immunoassay based on a monoclonal antibody that recognizes GDP with greater than 100-fold selectivity over GTP. Combining $G\alpha_{i1}$(R178M/A326S) with a homogenous, fluorescence-based GDP detection assay provides a facile means to explore the targeting of RGS proteins as a new approach for selective modulation of GPCR signaling.

5.2 INTRODUCTION

The standard model of GPCR signal transduction had long been restricted to a three-component system: receptor, G-protein, and effector [1]. The seven-transmembrane domain receptor is coupled to a membrane-associated heterotrimeric complex composed of a GTP-

hydrolyzing Gα subunit and a Gβγ dimeric partner. Agonist-induced conformational changes enhance the guanine nucleotide exchange activity of the receptor, leading to the release of GDP (and subsequent binding of GTP) by the Gα subunit. On binding GTP, conformational changes within the three 'switch' regions of Gα allow the release of Gβγ. Separated Gα·GTP and Gβγ subunits are then free to propagate intracellular signaling via diverse effectors [2]. The intrinsic GTP hydrolysis (GTPase) activity of Gα resets the cycle by forming Gα·GDP which has low affinity for effectors but high affinity for Gβγ. In this way, the inactive, GDP-bound heterotrimer (Gα·GDP/Gβγ) is reformed and capable once again to interact with activated receptor.

Based on this cycle of receptor-catalyzed GTP exchange and intrinsic GTP hydrolysis by Gα, the duration of heterotrimeric G-protein signaling is thought to be controlled by the lifetime of the Gα subunit in its GTP-bound state. After the establishment of this basic model [1], RGS proteins ("regulators of G-protein signaling") were subsequently discovered [3-5] to bind Gα subunits (via a conserved ~120 amino-acid RGS domain) and dramatically accelerate their intrinsic GTPase activity [6], thereby attenuating heterotrimer-linked signaling. Nearly 40 human proteins contain at least one RGS domain, with many of these proteins (*e.g.*, RGS4, RGS16) serving as GTPase-accelerating proteins (GAPs) for $G\alpha_{i/o}$ subunits, yet others such as RGS2 and p115-RhoGEF being particularly attuned to $G\alpha_{q/11}$ and $G\alpha_{12/13}$ substrates, respectively [7]. The discovery of this superfamily of Gα-directed GAPs resolved apparent timing paradoxes between observed rapid physiological responses mediated by GPCRs and the slow hydrolysis activity of the cognate G-proteins seen *in vitro*. Thus, in this capacity as negative regulators of GPCR signal transduction, the RGS proteins present themselves as excellent potential drug discovery targets [7]. For example,

pharmacological inhibition of RGS domain GAP activity should lead to prolonged signaling from G-proteins activated by agonist-bound GPCRs.

The most direct way to detect RGS protein function is by measuring the increased GTPase activity exhibited by its target Gα protein. However, accurate *in vitro* measurements of Gα-catalyzed GTP hydrolysis are difficult to obtain without laborious biochemical reconstitutions with purified Gβγ and an activated GPCR (*e.g.*, ref. [8]). In the absence of GPCR-mediated nucleotide exchange, it is GDP release (rather than GTP hydrolysis) that is the rate-limiting step in the Gα nucleotide cycle [9]. Thus, to examine the effect of an RGS protein in accelerating GTP hydrolysis by an isolated Gα subunit *in vitro*, a single round of hydrolysis of radiolabelled GTP is usually performed (*a.k.a.* the "single-turnover GTPase assay"; ref. [6]). This standard assay for measuring RGS domain-mediated GAP activity is low-throughput and requires discrete steps of [γ-^{32}P]GTP loading onto Gα, protein reactant admixture (with addition of the critical cofactor Mg^{2+} to initiate hydrolysis), isolation (in discrete time intervals) of released [^{32}P]phosphate with activated charcoal precipitation and centrifugation, and finally scintillation counting. We have described an alternative single-turnover GTPase assay [10] using a coumarin-labeled, phosphate-binding protein to facilitate fluorescence-based detection of inorganic phosphate production; however, this method demands stringent controls on multiple experimental steps to eliminate phosphate contaminants that interfere with the detection of GTPase activity. Such convoluted protocols of inorganic phosphate detection are difficult for the non-specialist and especially not suited for high-throughput screening (HTS) of large compound libraries for RGS domain inhibitors. We and others have reported alternative, fluorescence-based strategies for detecting the

binding between RGS protein and Gα substrate [10-12], but none has specifically facilitated a discrete endpoint measurement of RGS domain-mediated GAP activity *per se*.

In order to develop a facile steady-state GTPase assay for RGS domain GAP activity, we first set out to increase the spontaneous GDP release rate of Gα ($k_{off(GDP)}$) while also decreasing its intrinsic rate of GTP hydrolysis ($k_{cat(GTPase)}$), thereby allowing detection of at least a five-fold enhancement of steady-state GTP hydrolysis by RGS proteins to provide an adequate signal-to-noise ratio. $G\alpha_{i1}$ and closely related Gα proteins have been the focus of extensive structure/function studies [13-16], and point mutations that affect both $k_{off(GDP)}$ and $k_{cat(GTPase)}$ without affecting functional interaction with the RGS domain have been identified previously [13-15, 17] (*e.g.*, Figure 5.1A). Two of the most striking Gα mutations have been made to the highly-conserved active-site arginine (R178C; ref. [13]), which causes a ~100-fold reduction in GTPase activity, and to the alanine residue within the conserved TCAT loop that contacts the guanine ring (A326S; ref. [15] which results in a ~25-fold increase in $k_{off(GDP)}$ relative to wildtype yet an identical $k_{cat(GTPase)}$.

To detect RGS protein-accelerated GTPase activity, we adapted a monoclonal antibody and fluorescent tracer, previously developed for the Transcreener ADP assay [18], for selective immunodetection of GDP with a fluorescence polarization readout. Measurement of GTPase activity using this Transcreener GDP assay overcomes the signal-to-noise limitations of phosphate detection methods and has been validated as a robust HTS method in the case of ADP detection for kinases and ATPases [19-21]. Moreover, because it is a catalytic assay rather than a substrate binding assay, it should enable detection of all types of modulators of RGS protein GAP activity, including those that bind at allosteric sites

and affect RGS protein catalytic activity without directly targeting the RGS domain Gα binding-site [22].

In this present study, we tested multiple point-mutant $G\alpha_{i1}$ proteins with increased GDP dissociation and/or decreased GTP hydrolysis rates for their ability to enable detection of RGS domain GAP activity using a steady-state GTPase assay format (*i.e.*, multiple rounds of turnover of GTP to GDP). Coupling one of these variants, $G\alpha_{i1}$(R178M/A326S), to the Transcreener GDP detection system has not only allowed facile detection of RGS protein GAP activity, but was useful in helping establish (along with surface plasmon resonance spectroscopy) that the mutant $G\alpha_{i1}$ interacted with RGS proteins with the same specificity and affinity as the wildtype $G\alpha_{i1}$ protein.

5.3 MATERIALS AND METHODS

5.3.1 Chemicals and assay materials

GDP and GTP were purchased from USB Corp. (Cleveland, OH). The monoclonal antibody and tracer used for GDP detection were developed at BellBrook Labs (Madison, WI) as described [18], with the tracer comprising ADP conjugated to Alexa Fluor 633 (Invitrogen/Molecular Probes). Unless otherwise specified, all additional reagents were of the highest quality obtainable from Sigma (St. Louis, MO) or Fisher Scientific (Hampton, NH).

5.3.2 Protein expression and purification

Wildtype, full-length human $G\alpha_{i1}$ and various RGS proteins used in these studies were expressed in *E. coli* and purified as previously described [23]. $G\alpha_{i1}$ point mutants were created using PCR-based site-directed mutagenesis (QuikChange® II, Stratagene; La Jolla,

CA) on the wildtype pProEXHTb-$G\alpha_{i1}$ expression vector; mutagenesis primers were designed using Stratagene's QuikChange primer-design program and synthesized/PAGE-purified by Sigma-Genosys. All mutant constructs were sequence verified at Functional Biosciences LLC (Madison, WI) before protein expression, purification, concentration, quantitation, and cryopreservation using established protocols [10, 23].

5.3.3 Radiolabeled nucleotide binding and single turnover GTPase assays

Assessments of spontaneous GDP release and single-turnover GTP hydrolysis rates by wildtype and mutant $G\alpha_{i1}$ subunits, using measurements of [^{35}S]GTPγS binding and [γ-^{32}P]GTP hydrolysis respectively, were conducted exactly as previously described [23, 24]. Briefly, for [^{35}S]GTPγS binding by 100 nM of $G\alpha_{i1}$ subunits at 20 °C, timed aliquots were removed, filtered through nitrocellulose, and washed four times with 10 ml of wash buffer before scintillation counting. Assays were conducted in duplicate, counts were subtracted from analogous reactions in "non-specific binding" buffer [23], and normalized data plotted as mean ± S.E.M. For single-turnover [γ-^{32}P]GTP hydrolysis assays, $G\alpha_{i1}$ subunits (100 nM) were pre-bound to [γ-^{32}P]GTP in the absence of Mg^{2+} for 10 minutes at 30 °C. Reactions were then initiated by the addition of 10 mM $MgCl_2$ (final concentration) and the production of $^{32}P_i$ was measured by activated charcoal filtration and liquid scintillation counting [9],[24]. Initial rates obtained by data analysis using GraphPad Prism (La Jolla, CA).

5.3.4 Radiolabeled nucleotide steady-state GTPase assays

Assessments of steady-state [γ-^{32}P]GTP hydrolysis rates by wildtype and mutant $G\alpha_{i1}$ subunits were conducted essentially as previously described [25]. Briefly, $G\alpha_{i1}$ protein was diluted to 50 nM in a buffer containing 50 mM Tris pH 7.5, 100 mM NaCl, 0.05% $C_{12}E_{10}$, 1 mM DTT, 5 mM EDTA, 10 mM $MgCl_2$, and 5 μg/ml BSA. Assays were initiated with the addition of [γ-^{32}P]GTP (and RGS4 if used), aliquots stopped at indicated time intervals, and free [γ-^{32}P]Pi quantified as previously described [25].

5.3.5 Transcreener GDP assays

Standard curves and GTPase reactions were both run at 30 ^{o}C in kinetic mode on a Tecan Safire^2 multiwell reader in Corning® 384-well black round-bottom low-volume polystyrene non-binding surface microplates (Part # 3676). Fluorescence polarization was read using 635 nm excitation (20 flashes per well) and 670 nm emission. A free tracer reference was set to 20 mP by adjusting the photomultiplier tubes, and buffer containing GDP antibody alone was used as a blank for sample and reference wells. EC_{50} and EC_{85} values, Hill slopes, and curves were generated by GraphPad Prism (La Jolla, CA). Unless otherwise indicated, reactions were run in 20 mM Tris 7.5 pH, 1 mM EDTA, 10 mM $MgCl_2$, 10 μM GTP, 8 μg/ml GDP antibody, and 2 nM tracer in a final 20 μl volume. GDP antibody was used at a concentration 85% of the amount required for saturated binding to tracer (*i.e.*, the EC_{85}). Where shown, polarization data was converted to the amount of GDP produced using standard curves. Reaction rates were then determined in GraphPad Prism using linear

regression to estimate slope. For GTPase and GAP assays, reactions were started with the addition of GTP with or without RGS protein.

5.3.6 Compound interference test

To assess the robustness of the Transcreener GDP assay for practical screening applications, we performed a control screen using the GenPlus library of 960 bioactive molecules from Microsource Discovery Systems, many of which are approved drugs. GDP assay reagents (as denoted above) were added to duplicate wells containing 10 μM compound and either 10 μM GTP to mimic no-enzyme control reactions or 9 μM GTP plus 1 μM GDP to mimic completed enzyme reactions in 1% DMSO.

5.3.7 Pilot screen and counterscreen of GenPlus Library

Screens of the GenPlus library with the Transcreener GDP assay (10 μM final compound concentration) for modulators of RGS4 GAP activity on $G\alpha_{i1}$(R178M/A326S), as well as for non-specific modulators of intrinsic GTPase activity of $G\alpha_{i1}$(R178M/A326S) alone, were conducted as mentioned above with the following changes. GTPase reactions containing 50 nM $G\alpha_{i1}$(R178M/A326S) with or without 250 nM RGS4 were run in Corning® 384-well microplates at 30 °C in 20 mM Tris pH 7.5, 1 mM EDTA, 10 mM $MgCl_2$, 10 μM GTP, 12 μg/μl GDP antibody, 2 nM tracer, and 0.5% DMSO (v/v) in a final volume of 20 μl. Fluorescence polarization was read at 60, 90, 120, and 180 minutes of elapsed reaction time on a Tecan Safire^2 multiwell reader as described above.

5.3.8 Surface plasmon resonance (SPR) spectroscopy

Optical detection of surface plasmon resonance (SPR) was performed using a BIAcore 3000 (GE Healthcare; Piscataway, NJ). Wildtype and mutant $G\alpha_{i1}$ proteins were immobilized onto nickel-nitrilotriacetic acid SPR sensor chips (GE Healthcare) by hexahistidine tag-mediated capture-coupling as previously described [26]. Affinities of RGS proteins for immobilized $G\alpha_{i1}$ proteins were obtained from dose-response sensorgrams using equilibrium saturation binding analyses as previously described [23].

5.4 RESULTS AND DISCUSSION

5.4.1 Profiling multiple $G\alpha_{i1}$ point-mutations for nucleotide cycling rate alterations

Using PCR-based site-directed mutagenesis, we created several amino-acid substitutions at various positions within $G\alpha_{i1}$ known to affect $k_{off(GDP)}$ and/or $k_{cat(GTPase)}$ (*e.g.*, Figure 5.1). These mutants included: aspartate, serine, or threonine replacing Ala-326; cysteine, lysine, or methionine replacing Arg-178; alanine, serine, or valine replacing Thr-181; single mutants K192A and F336A; and double mutants K192A/F336A, R178C/A326S, R178C/A326T, R178M/A326S, R178C/A326T, and T181A/A326S. Note that multiple different substitutions were made at several sites, including amino-acids intended to be more or less disruptive than the original reported mutation. For instance, R178K and R178M were tested as more conservative substitutions at the catalytic arginine position relative to the original R178C variant; it was thought that either of these alternative substitutions might result in a smaller decrease in $k_{cat(GTPase)}$ than the cysteine replacement which reduces $k_{cat(GTPase)}$ by two orders of magnitude [13]. While the R178C mutation leads to a substantial decrease in $k_{cat(GTPase)}$, Berman *et al.* [6] have shown that the single-turnover GTPase rate of

this Gα mutant can still be increased by RGS domain-mediated GAP activity, whereas the more conventional GTPase-crippling mutation of Q204L renders $G\alpha_{i1}$ truly dead in terms of responsiveness to RGS proteins. Thus, the $G\alpha_{i1}$(Q204L) mutant was not pursued in this study.

$G\alpha_{i1}$ mutants were initially profiled for enhanced GDP release and/or reduced GTPase rate sufficient to see a change in steady-state GTP hydrolysis upon RGS protein addition. This initial profiling led us to focus on two positions: Arg-178 and Ala-326. Binding of the non-hydrolyzable GTP analog, [^{35}S]GTPγS, to $G\alpha_{i1}$·GDP was used to measure the rate of GDP dissociation (*e.g.*, Figure 5.1B); the prevailing assumption for Gα subunits is that k_{on} for [^{35}S]GTPγS binding is much more rapid than $k_{off(GDP)}$ [27]. Single turnover GTP hydrolysis measuring $^{32}P_i$ released from Gα-bound [γ-^{32}P]GTP – an assay format which is not rate-limited by GDP dissociation [9] – was used to assess intrinsic k_{cat} rates for the $G\alpha_{i1}$ mutants (*e.g.*, Figure 5.1C).

As expected, $G\alpha_{i1}$ variants with mutation to the active-site catalytic residue Arg-178 had very low or undetectable levels of GTP hydrolysis, whereas $G\alpha_{i1}$(A326S), the single mutation reported to only affect GDP dissociation, had a GTPase rate similar to wildtype $G\alpha_{i1}$ (Figure 5.1C-D). [^{35}S]GTPγS binding assays showed that two variants with mutations only at the catalytic site, R178M and R178C, had GDP dissociation rates similar to wildtype $G\alpha_{i1}$, whereas introduction of the A326S mutation, either alone or in combination with R178C, caused a three-fold acceleration in GDP dissociation (Figure 5.1B,D). When the A326S mutation was combined with methionine at Arg-178 (instead of cysteine), the GDP dissociation rate increased more than ten-fold over wildtype: from 0.008 min^{-1} to 0.130 min^{-1} (Figure 5.1D). We currently do not have a precise structural explanation for why the

particular combination of R178M and A326S mutations results in more rapid GDP release than the single A326S mutation alone; it is not an additive effect, since the singly-mutated $G\alpha_{i1}$(R178M) variant exhibits wildtype GDP dissociation (Figure 5.1B). It is interesting to note that Posner and colleagues, when reporting the crystal structure of the $G\alpha_{i1}$(A326S) mutant [15], suggested the presence of an indirect interaction between the Arg-178 and Ser-326 residues (via contacts with nucleotide and Gly-45), thereby providing a possible mechanism for the functional interaction we have observed here between the R178M and A326S mutations.

5.4.2 Combined action of two $G\alpha_{i1}$ mutations allows steady-state measurement of GAP activity

With the R178M/A326S mutant of $G\alpha_{i1}$ demonstrating the largest change in GDP release rate of all mutants tested, we next examined whether this particular $G\alpha_{i1}$ variant would be affected by RGS domain-mediated GAP activity in steady-state [γ-^{32}P]GTP hydrolysis assays. Addition of purified RGS4 protein to the $G\alpha_{i1}$(R178M/A326S) variant (in the presence of free [γ-^{32}P]GTP and Mg^{2+}) resulted in a dramatic increase in [^{32}P]Pi detected over time. In contrast, there was no effect of RGS4 on wildtype $G\alpha_{i1}$ in this steady-state assay (Figure 5.2A *vs* B), as expected given the original report by Berman *et al.* [6].

5.4.3 Development of a Transcreener GDP assay

The Transcreener platform relies upon highly selective antibodies for detection of nucleotides produced in enzyme reactions [28]. To allow measurement of RGS protein-mediated acceleration of steady-state GTP hydrolysis in a homogenous format without

radioactivity, a Transcreener assay for GDP was developed (Figure 5.3A) using a competitive fluorescence polarization immunoassay format. For this method, a recently-developed monoclonal antibody that recognizes GDP with >100-fold higher affinity than GTP [18] is added to the reaction, along with a fluorescent tracer which binds to the antibody with high affinity. When no free, unlabeled GDP is present in the reaction, the fluorescent tracer remains antibody-bound and exhibits a high polarization given its high apparent molecular weight. GDP produced in the reaction displaces the tracer from the antibody, thereby reducing its apparent molecular weight, increasing its rotational motion, and thus reducing the degree of polarization of emitted light. A similar Transcreener assay has been widely used for detection of ADP produced by kinases and other ATP-hydrolyzing proteins (*e.g.*, refs. [19-21]; reviewed in [28]).

Figure 5.3B shows typical fluorescence polarization standard curves mimicking the conversion of GTP to GDP by a GTPase. An important aspect of flexibility for a GTPase assay is the ability to accommodate a range of initial GTP concentrations, so that diverse enzymes and screening strategies can be employed; therefore, these studies were performed using different GTP concentrations of 1, 10 and 100 μM. Because the antibody cross-reacts to some degree with GTP, its concentration must be increased as higher GTP concentrations are used, in order to buffer for the total guanine nucleotide pool. Thus, for this analysis, the EC_{85} concentrations of monoclonal antibody were first determined in the presence of the indicated initial GTP concentrations (2.2, 12 and 64 μg/ml Ab for 1, 10 and 100 μM GTP, respectively) and the standard curves for GTP to GDP conversion were performed with 16 replicates at those antibody concentrations. At a GDP concentration equivalent to 10% conversion of GTP, which is generally considered to be well within the initial velocity

region, polarization shifts of 108, 134, and 148 mP were observed for the 1, 10, and 100 μM GTP concentration curves, respectively (Figure 5.3B). Acceptable Z'-factor values (ref. [29]) of greater than 0.5 were observed down to 2% conversion for the two higher initial GTP concentrations, and to 5% for the 1 μM initial GTP curve (Figure 5.3C), suggesting that the Transcreener GDP assay should be capable of very robust detection of GTPase enzyme initial velocity over at least a 100-fold range of initial GTP concentration.

To assess the potential for compound interference with the Transcreener GDP assay readout, we performed a control screen (Figure 5.3D) with the GenPlus library of 960 bioactive molecules, many of which are approved drugs. This control screen was done under conditions mimicking 10% conversion to GDP for a GTPase reaction run at 10 μM initial GTP concentration. All wells were run in duplicate. The vast majority of the compounds clustered very tightly around the means for the 10 μM GTP and the 9 μM GTP/1 μM GDP conditions; the Z'-factor for the no-compound controls in this screen was 0.93. There were only three compounds in the control screen that caused the signal to vary more than three standard deviations from the mean: dirithromycin, metazolamide, and lonidamin (Figure 5.3D). There is no obvious structural similarity between them nor are any of them similar in structure to guanine nucleotide. These data suggests that compound interference with the Transcreener GDP assay readout will be minimal.

5.4.4 FP-based detection of RGS protein GAP activity is dependent on two rate-altering mutations

Having validated the utility of the Transcreener assay in detecting GDP in the presence of GTP, we next tested its use in measuring RGS protein GAP activity on several rate-altered $G\alpha_{i1}$ variants (Figure 5.4). In these experiments, the $G\alpha_{i1}$ proteins were

incubated with and without the well-characterized, $G\alpha_i$-directed RGS protein RGS4 [30] in the presence of the Transcreener GDP assay reagents, and plates were read at intervals starting at 15 minutes. The change in the absolute value of polarization at each time-point ($\Delta mP_t = | mP_t(G\alpha_{i1}) - mP_t(\text{no } G\alpha_{i1}) |$) was plotted over a time-course of 6 hours; in addition, the plotted change in polarization that occurred in the linear region (over the first hour) was converted to GDP formation using standard curves (akin to those of Figure 5.3B) and normalized to the amount of $G\alpha_{i1}$ protein present in the reaction, with the resultant initial rates of GTP hydrolysis calculated from these data shown in Figure 5.4E.

The two $G\alpha_{i1}$ variants with single mutations at the catalytic arginine only, R178C or R178M, each had lower steady-state GTPase activity than wildtype $G\alpha_{i1}$ and, like wildtype, were unaffected by RGS4 (GAP factors of 0.9 and 1.2, respectively; Figure 5.4E). These results are expected because their steady-state GTPase rate is limited by slow GDP dissociation. Conversely, the A326S variant exhibited a much higher steady-state GTPase rate than wildtype, as expected from its higher $k_{off(GDP)}$ (Figure 5.1); however, its steady-state GTPase rate was unaffected by RGS4 (GAP ratio of 1.1; Figure 5.4E), presumably because a further rate increase in GTPase is limited by $k_{off(GDP)}$. Most importantly, the two double mutants, R178C/A326S and R178M/A326S, had very low basal steady-state GTPase activities that became demonstrably higher in the presence of RGS4 (*e.g.*, Figure 5.4A-B); the GAP effect on $G\alpha_{i1}$(R178M/A326S) was greater than with the $G\alpha_{i1}$(R178C/A326S) variant (GAP factors of 5.5 and 3.6, respectively; Figure 5.4E). Given its high GAP factor response in both the steady-state [γ-^{32}P]GTP hydrolysis assay (Figure 5.2) and the

Transcreener GDP assay (Figure 5.4), the $G\alpha_{i1}$(R178M/A326S) variant was used in subsequent analyses.

5.4.5 $G\alpha_{i1}$(R178M/A326S) interacts with RGS proteins with same affinity and specificity as wildtype

A possible concern about the use of a mutated Gα protein for RGS protein GAP assays is that the mutation(s) could disrupt the global fold of Gα or, at the very least, affect the disposition of the switch regions and other surface contact points to which RGS proteins interact [23, 30], thereby altering the normal affinity and specificity that RGS proteins show for their various Gα substrates. The two point mutations of R178M and A326S are interior to the guanine nucleotide binding pocket (Figure 5.5), but could nevertheless affect the RGS domain interaction surface.

To test for this possibility, we used SPR to compare the binding interactions of RGS2 and RGS16 with wildtype $G\alpha_{i1}$ *versus* the $G\alpha_{i1}$(R178M/A326S) variant. Multiple previous studies [8, 23, 31] have established that RGS2, a potent GAP for $G\alpha_q$, does not interact with wildtype $G\alpha_{i1}$ *in vitro*; this same lack of interaction was observed with the $G\alpha_{i1}$(R178M/A326S) mutant (data not shown). Conversely, RGS16 is known to be a $G\alpha_i$-interacting RGS protein [23], and was found by SPR to bind equivalently to immobilized wildtype $G\alpha_{i1}$ and $G\alpha_{i1}$(R178M/A326S) proteins (Figure 5.6). This equivalence included RGS16 only interacting with high affinity to the Gα subunits in their transition state-mimetic form (namely, Gα in complex with GDP and aluminum tetrafluoride [30]). These binding results suggest that no long-range perturbations have been made to the RGS domain interaction sites on $G\alpha_{i1}$ by the two rate-altering mutations of R178M and A326S.

Using the Transcreener GDP assay, we performed an additional test of the $G\alpha_{i1}$(R178M/A326S) variant to control for any unintended changes the two point mutations could have engendered within $G\alpha$ to alter its interaction specificity with various RGS proteins. With the same RGS protein spectrum used in the SPR binding experiments, we found that RGS2 (highly selective for $G\alpha_q$ over $G\alpha_i$ substrates) had no effect on increasing steady-state GTPase activity of $G\alpha_{i1}$(R178M/A326S), whereas RGS16 increased steady-state GTPase activity 12-fold over the basal rate (Figure 5.7).

5.4.6 Pilot screen for inhibitors of RGS4 GAP activity on $G\alpha_{i1}$(R178M/A326S)

Given the robust performance of the Transcreener GDP assay in the control screen for potential compound interference (Figure 5.3D) and evidence that the two mutations to $G\alpha_{i1}$ affected neither the affinity nor specificity of the $G\alpha$/RGS domain interaction (Figs. 6 and 7), we proceeded to a pilot screen with $G\alpha_{i1}$(R178M/A326S) and RGS4 using the GenPlus library of 960 bioactive molecules (Figure 5.8). The screening window was first optimized by varying the concentrations of $G\alpha$ and RGS protein inputs; at 50 nM $G\alpha_{i1}$(R178M/A326S) and 250 nM RGS4, a maximal signal to background difference of 112 mP units was obtained after 120 minutes of elapsed reaction time before FP measurement. The thiol-reactive compound CCG-4986 was used in the screen as a positive control for RGS4 inhibition [11, 32]. The GenPlus library screen was conducted with $G\alpha_{i1}$(R178M/A326S) and RGS4 (Figure 5.8A); a separate counterscreen of the library was performed with $G\alpha_{i1}$(R178M/A326S) and no RGS4 (Figure 5.8B) to identify compounds having either non-specific effects or modifying $G\alpha_{i1}$ GTPase activity (rather than RGS4 GAP activity *per se*).

Z'-factors of 0.60, 0.83, 0.83, and 0.82 were obtained at 60, 90, 120, and 180 minutes elapsed reaction time, as calculated based on data from control wells containing either

$G\alpha_{i1}$(R178M/A326S) only or $G\alpha_{i1}$(R178M/A326S) plus RGS4. Note that these Z'-factor values reflect only the RGS4-dependent increase in GTPase activity, and not the total observed GTPase activity relative to no-enzyme controls. The Z-factor for the GenPlus library screen at the 120 minute time point (shown in Figure 5.8A) was 0.73, which was calculated by excluding values from wells containing hit compounds. Of the 960 compounds in the GenPlus library, 17 compounds were initially considered hits in the RGS4/Gα screen: *i.e.*, those data points that fell outside the $\mu \pm 3\sigma$ range. However, ten of these 17 hits also resulted in a greater than $\pm 3\sigma$ change in the mean signal within the Gα-only counterscreen and thus were excluded because these compounds are likely either affecting the Gα subunit or otherwise interfering with the assay. Thus the RGS4-specific hit rate was 0.7%: seven compounds from the 960 compound library exhibited an modulatory effect on GDP production that was specific to RGS4-stimulated GTPase activity (Figure 5.8A *vs* 5.8B). Six compounds (id # 62, 63, 244, 413, 524, 812) exhibited an RGS4-specific inhibitory effect (*i.e.*, a change in polarization greater than the [mean + 3 S.D.] signal threshold) and one compound (#596) exhibited an RGS4-specific activating effect on GDP production (*i.e.*, a change in polarization less than the [mean - 3 S.D.] signal threshold). This hit rate may be artificially high in this pilot screen given that the collection of compounds surveyed (GenPlus library) is not a diverse sampling of chemical space but a collection of US, European, and Japanese approved drugs and other bioactive compounds. As expected [11, 32], the thiol-reactive RGS4 inhibitor CCG-4986 consistently exhibited inhibition of RGS4-stimulated GDP production (Figure 5.8A).

To our knowledge, the combined use of a GDP detection assay with a rate-altered Gα subunit represents a unique strategy to the detection of RGS protein GAP activity. Even

though the two primary components of Gα catalysis, GTP hydrolysis rate and product release, were altered significantly by mutation, the resultant Gα subunits still served as functional substrates for the GTPase-accelerating activity of RGS proteins. Using this double mutation strategy to develop a steady-state RGS protein GAP assay that is easy for the non-specialist to perform, and is well-suited for HTS, removes a major technical barrier preventing the exploration of RGS proteins as therapeutic targets. Moreover, $G\alpha_{i1}$ is a substrate for the GAP activity of several RGS protein family members [23] in addition to those we have tested here; thus, the reagents and methods that we have described should have broad applicability across the protein family. Employing the rate-altered $G\alpha_{i1}$(R178M/A326S) mutant in a homogeneous, end-point-based, enzymatic HTS assay will not only be useful in screening for RGS protein inhibitors but, unlike existing assays based on the RGS domain/Gα binding interaction [10-12], this enzymatic assay should also facilitate identification of small molecule *activators* of RGS domain-mediated GAP activity. The lipid moiety phosphatidylinositol-3,4,5-trisphophate (PIP_3) has been shown to bind to, and thereby inhibit in an allosteric fashion, the GAP activity of select RGS domains such as that of RGS4 [22]; Ca^{2+}/calmodulin reverses this PIP_3-mediated inhibition by competing for the PIP_3-binding site [22]. A small molecule targeting this site of allosteric modulation over RGS domain GAP activity could potentially be quite valuable therapeutically in pathophysiological situations which may arise from a loss of RGS protein activity, such as RGS2 in hypertension [33] and RGS4 in schizophrenia [34].

5.5 ACKNOWLEDGMENTS

Thanks to Drs. Christopher Johnston and Francis Willard (UNC) for initial discussions regarding rate-altering Gα mutations, and Dr. Steve Hayes (BellBrook Labs) for discussion and critical appraisal of the manuscript. Work at BellBrook Labs was supported by NIH SBIR grant R43 NS059082 and work in the Siderovski lab was funded by NIH grant R01 GM082892. A.J.K. acknowledges early support from NIH training grant T32 GM008719 and current support from NIH fellowship F30 MH074266.

5.6 REFERENCES

1. Gilman, A.G., *G proteins: transducers of receptor-generated signals.* Annu Rev Biochem, 1987. **56**: p. 615-49.

2. McCudden, C.R., M.D. Hains, R.J. Kimple, D.P. Siderovski, and F.S. Willard, *G-protein signaling: back to the future.* Cell Mol Life Sci, 2005. **62**(5): p. 551-77.

3. Druey, K.M., K.J. Blumer, V.H. Kang, and J.H. Kehrl, *Inhibition of G-protein-mediated MAP kinase activation by a new mammalian gene family.* Nature, 1996. **379**(6567): p. 742-6.

4. Koelle, M.R. and H.R. Horvitz, *EGL-10 regulates G protein signaling in the C. elegans nervous system and shares a conserved domain with many mammalian proteins.* Cell, 1996. **84**(1): p. 115-25.

5. Siderovski, D.P., A. Hessel, S. Chung, T.W. Mak, and M. Tyers, *A new family of regulators of G-protein-coupled receptors?* Curr Biol, 1996. **6**(2): p. 211-2.

6. Berman, D.M., T.M. Wilkie, and A.G. Gilman, *GAIP and RGS4 are GTPase-activating proteins for the Gi subfamily of G protein alpha subunits.* Cell, 1996. **86**(3): p. 445-52.

7. Neubig, R.R. and D.P. Siderovski, *Regulators of G-protein signalling as new central nervous system drug targets.* Nat Rev Drug Discov, 2002. **1**(3): p. 187-97.

8. Ingi, T., A.M. Krumins, P. Chidiac, G.M. Brothers, S. Chung, B.E. Snow, C.A. Barnes, A.A. Lanahan, D.P. Siderovski, E.M. Ross, A.G. Gilman, and P.F. Worley, *Dynamic regulation of RGS2 suggests a novel mechanism in G-protein signaling and neuronal plasticity.* J Neurosci, 1998. **18**(18): p. 7178-88.

9. Ross, E.M., *Quantitative assays for GTPase-activating proteins.* Methods Enzymol, 2002. **344**: p. 601-17.

10. Willard, F.S., R.J. Kimple, A.J. Kimple, C.A. Johnston, and D.P. Siderovski, *Fluorescence-based assays for RGS box function.* Methods Enzymol, 2004. **389**: p. 56-71.

11. Roman, D.L., J.N. Talbot, R.A. Roof, R.K. Sunahara, J.R. Traynor, and R.R. Neubig, *Identification of small-molecule inhibitors of RGS4 using a high-throughput flow cytometry protein interaction assay.* Mol Pharmacol, 2007. **71**(1): p. 169-75.

12. Willard, F.S., A.J. Kimple, C.A. Johnston, and D.P. Siderovski, *A direct fluorescence-based assay for RGS domain GTPase accelerating activity.* Anal Biochem, 2005. **340**(2): p. 341-51.

13. Coleman, D.E., A.M. Berghuis, E. Lee, M.E. Linder, A.G. Gilman, and S.R. Sprang, *Structures of active conformations of Gi alpha 1 and the mechanism of GTP hydrolysis.* Science, 1994. **265**(5177): p. 1405-12.

14. Nishina, H., K. Nimota, I. Kukimoto, T. Maehama, K. Takahashi, S. Hoshino, Y. Kanaho, and T. Katada, *Significance of Thr182 in the nucleotide-exchange and GTP-hydrolysis reactions of the alpha subunit of GTP-binding protein Gi2.* J Biochem (Tokyo), 1995. **118**(5): p. 1083-9.

15. Posner, B.A., M.B. Mixon, M.A. Wall, S.R. Sprang, and A.G. Gilman, *The A326S mutant of Gialpha1 as an approximation of the receptor-bound state.* J Biol Chem, 1998. **273**(34): p. 21752-8.

16. Sondek, J., D.G. Lambright, J.P. Noel, H.E. Hamm, and P.B. Sigler, *GTPase mechanism of Gproteins from the 1.7-A crystal structure of transducin alpha-GDP-AIF-4.* Nature, 1994. **372**(6503): p. 276-9.

17. Marin, E.P., A.G. Krishna, and T.P. Sakmar, *Rapid activation of transducin by mutations distant from the nucleotide-binding site: evidence for a mechanistic model of receptor-catalyzed nucleotide exchange by G proteins.* J Biol Chem, 2001. **276**(29): p. 27400-5.

18. Kleman-Leyer, K.M., T.A. Klink, A.L. Kopp, T.A. Westermeyer, M.D. Koeff, B.R. Larson, T.J. Worzella, S.A.T. van de Kar, G.J.R. Zaman, J.J. Hornberg, and R.G. Lowery, *Characterization and Optimization of a Red-shifted Fluorescence Polarization ADP Detection Assay.* Assay and Drug Development Technologies, 2009. **7**(1): p. 56-67.

19. Huss, K.L., P.E. Blonigen, and R.M. Campbell, *Development of a Transcreener kinase assay for protein kinase A and demonstration of concordance of data with a filter-binding assay format.* J Biomol Screen, 2007. **12**(4): p. 578-84.

20. Klink, T.A., K.M. Kleman-Leyer, A. Kopp, T.A. Westermeyer, and R.G. Lowery, *Evaluating PI3 kinase isoforms using Transcreener ADP assays.* J Biomol Screen, 2008. **13**(6): p. 476-85.

21. Liu, Y., L. Zalameda, K.W. Kim, M. Wang, and J.D. McCarter, *Discovery of acetyl-coenzyme A carboxylase 2 inhibitors: comparison of a fluorescence intensity-based phosphate assay and a fluorescence polarization-based ADP Assay for high-throughput screening.* Assay Drug Dev Technol, 2007. **5**(2): p. 225-35.

22. Popov, S.G., U.M. Krishna, J.R. Falck, and T.M. Wilkie, *Ca2+/Calmodulin reverses phosphatidylinositol 3,4, 5-trisphosphate-dependent inhibition of regulators of G protein-signaling GTPase-activating protein activity.* J Biol Chem, 2000. **275**(25): p. 18962-8.

23. Soundararajan, M., F.S. Willard, A.J. Kimple, A.P. Turnbull, L.J. Ball, G.A. Schoch, C. Gileadi, O.Y. Fedorov, E.F. Dowler, V.A. Higman, S.Q. Hutsell, M. Sundstrom,

D.A. Doyle, and D.P. Siderovski, *Structural diversity in the RGS domain and its interaction with heterotrimeric G protein alpha-subunits.* Proc Natl Acad Sci U S A, 2008. **105**(17): p. 6457-62.

24. Johnston, C.A., E.S. Lobanova, A.S. Shavkunov, J. Low, J.K. Ramer, R. Blaesius, Z. Fredericks, F.S. Willard, B. Kuhlman, V.Y. Arshavsky, and D.P. Siderovski, *Minimal determinants for binding activated G alpha from the structure of a G alpha(i1)-peptide dimer.* Biochemistry, 2006. **45**(38): p. 11390-400.

25. Afshar, K., F.S. Willard, K. Colombo, C.A. Johnston, C.R. McCudden, D.P. Siderovski, and P. Gonczy, *RIC-8 is required for GPR-1/2-dependent Galpha function during asymmetric division of C. elegans embryos.* Cell, 2004. **119**(2): p. 219-30.

26. Willard, F.S. and D.P. Siderovski, *Covalent immobilization of histidine-tagged proteins for surface plasmon resonance.* Anal Biochem, 2006. **353**(1): p. 147-9.

27. Ferguson, K.M., T. Higashijima, M.D. Smigel, and A.G. Gilman, *The influence of bound GDP on the kinetics of guanine nucleotide binding to G proteins.* J Biol Chem, 1986. **261**(16): p. 7393-9.

28. Lowery, R.G. and K. Kleman-Leyer, *Transcreener: screening enzymes involved in covalent regulation.* Expert Opin Ther Targets, 2006. **10**(1): p. 179-90.

29. Zhang, J.H., T.D. Chung, and K.R. Oldenburg, *A Simple Statistical Parameter for Use in Evaluation and Validation of High Throughput Screening Assays.* J Biomol Screen, 1999. **4**(2): p. 67-73.

30. Tesmer, J.J., D.M. Berman, A.G. Gilman, and S.R. Sprang, *Structure of RGS4 bound to AlF4--activated G(i alpha1): stabilization of the transition state for GTP hydrolysis.* Cell, 1997. **89**(2): p. 251-61.

31. Heximer, S.P., N. Watson, M.E. Linder, K.J. Blumer, and J.R. Hepler, *RGS2/G0S8 is a selective inhibitor of Gqalpha function.* Proc Natl Acad Sci U S A, 1997. **94**(26): p. 14389-93.

32. Kimple, A.J., F.S. Willard, P.M. Giguere, C.A. Johnston, V. Mocanu, and D.P. Siderovski, *The RGS protein inhibitor CCG-4986 is a covalent modifier of the RGS4 Galpha-interaction face.* Biochim Biophys Acta, 2007. **1774**(9): p. 1213-20.

33. Heximer, S.P., R.H. Knutsen, X. Sun, K.M. Kaltenbronn, M.H. Rhee, N. Peng, A. Oliveira-dos-Santos, J.M. Penninger, A.J. Muslin, T.H. Steinberg, J.M. Wyss, R.P. Mecham, and K.J. Blumer, *Hypertension and prolonged vasoconstrictor signaling in RGS2-deficient mice.* J Clin Invest, 2003. **111**(4): p. 445-52.

34. Mirnics, K., F.A. Middleton, G.D. Stanwood, D.A. Lewis, and P. Levitt, *Disease-specific changes in regulator of G-protein signaling 4 (RGS4) expression in schizophrenia.* Mol Psychiatry, 2001. **6**(3): p. 293-301.

A

Mutation (*ref.*)	Gα protein mutated	Increase in $k_{off(GDP)}$	Decrease in $k_{cat(GTPase)}$	Equivalent site in $G\alpha_{i1}$	RGS protein interaction?
A326S (*16*)	$G\alpha_{i1}$	25x	none	A326	RGS4
R178C (*15*)	$G\alpha_{i1}$	Reported, not quantified	>100x	R178	RGS4
T182A (*17*)	$G\alpha_{i2}$	2x	>100x	T181	n.d.
K188A (*18*)	$G\alpha_{t}$	6x	n.d.	K192	n.d.
F332A (*18*)	$G\alpha_{t}$	>150x	n.d.	F336	n.d.

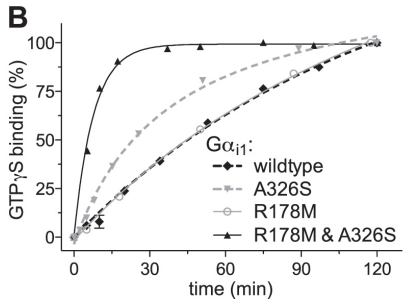

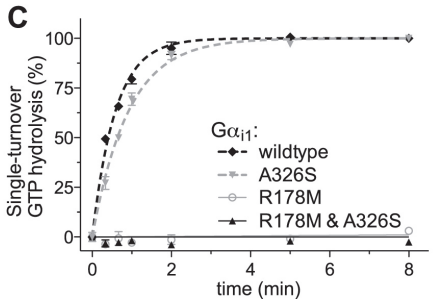

D

$G\alpha_{i1}$ species:	GTP binding (min^{-1})	GTP hydrolysis (min^{-1})
wildtype	0.009	1.7
A326S	0.027	1.1
R178M	0.008	0.001
R178C	0.009	0.008
R178C/ A326S	0.025	0.000
R178M/ A236S	0.130	0.000

Figure 5.1. Increased GDP release and decreased GTP hydrolysis of the $G\alpha_{i1}$(R178M/A326S) mutant compared to wildtype $G\alpha_{i1}$ and single point-mutants, as measured by [^{35}S]GTPγS binding and single-turnover [γ-^{32}P]GTP hydrolysis, respectively. (A) Point mutations to $G\alpha_{i}$-family subunits previously reported in the literature [15-18] to alter intrinsic GTP hydrolysis and GDP dissociation rates. (**B**) Binding of [^{35}S]GTPγS to wildtype or indicated mutant $G\alpha_{i1}$ subunits. (**C**) Single-turnover GTP hydrolysis activities of wildtype or indicated mutant $G\alpha_{i1}$ subunits. (**D**) Initial rates of GTP binding and hydrolysis for the $G\alpha_{i1}$(R178M/A326S) mutant, as well as other $G\alpha_{i1}$ point mutants derived from data similar to that of panels B and C.

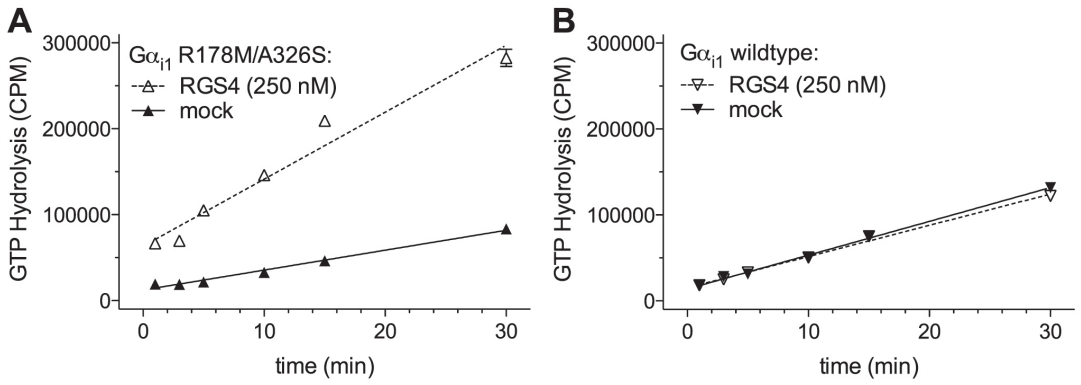

Figure 5.2. RGS4 GAP activity is observed as an increase in steady-state GTP hydrolysis only for the rate-altered $G\alpha_{i1}$(R178M/A326S) variant. Time courses of steady-state [γ-^{32}P]GTP hydrolysis by 50 nM $G\alpha_{i1}$(R178M/A326S) mutant (A) or 50 nM wildtype $G\alpha_{i1}$ (B) in the presence or absence of 250 nM RGS4 at 20°C. Results are the mean (± S.E.M.) of duplicate samples.

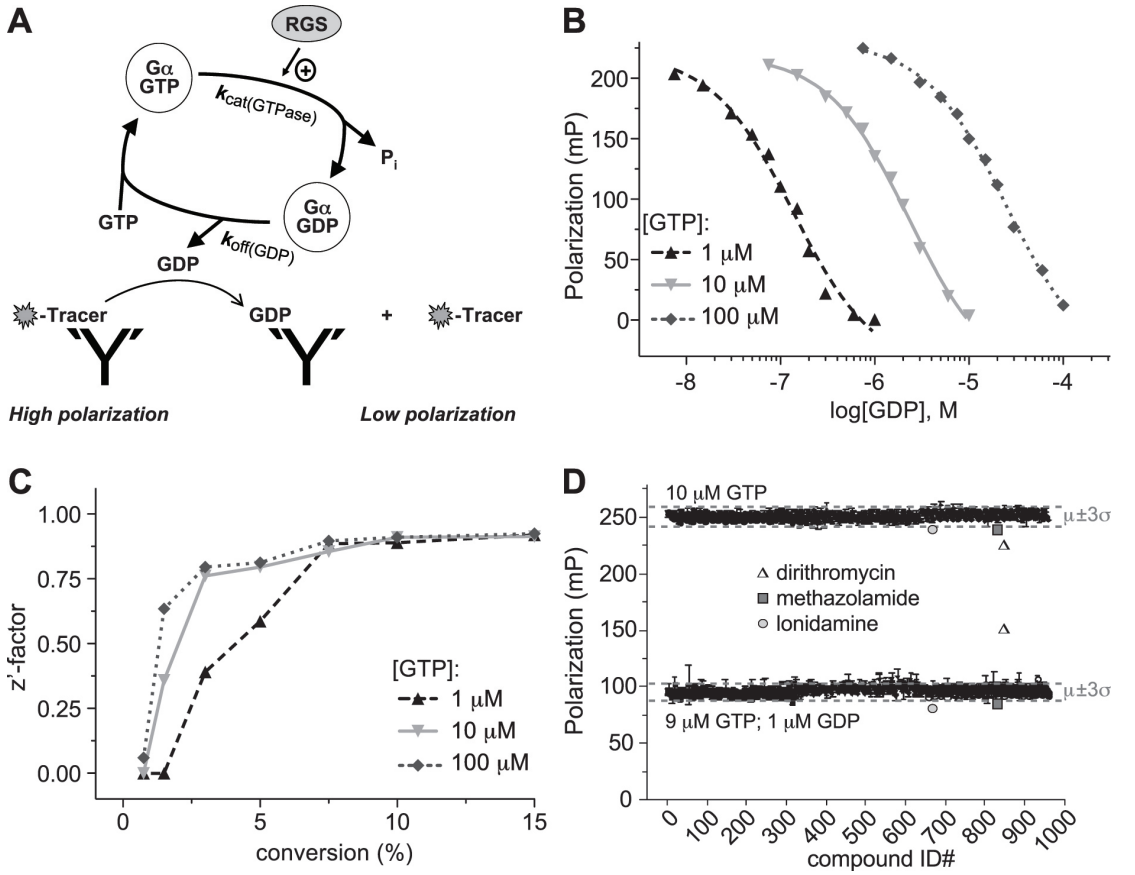

Figure 5.3. Fluorescence polarization immunoassay for the detection of GDP. (**A**) Schematic representation of methodology underlying the Transcreener GDP assay as applied to steady-state GTP hydrolysis (and resultant GDP production) by a rate-altered Gα protein. Fluorescent tracer is illustrated with a jagged oval; when bound to the GDP-selective monoclonal antibody, emitted light remains polarized, whereas there is low polarization of emitted light when tracer is displaced by free GDP. (**B**) The Transcreener GDP assay was used to generate standard curves for conversion of GTP into GDP at initial GTP concentrations of 1, 10, and 100 μM using appropriate EC_{85} concentrations of GDP antibody established for these initial GTP concentrations (2.2, 12, and 64 μg/mL, respectively). (**C**) Z'-factor values, reflecting both assay signal window and signal variability [30], were determined in 16 replicates for each of the points in the GDP-detection standard curves presented in panel B. Although the assay window was reduced at lower percent conversions (*e.g.*, 57 mP for 3% conversion to GDP of 10 μM initial GTP; panel B), acceptable Z'-factors [30] of >0.5 were observed down to 2% conversion for the two higher initial GTP concentrations and to 5% for the 1 μM initial GTP curve, given the very low signal variability. (**D**) Control screen using the 960 compound GenPlus library. Assay components were added to duplicate wells containing 10 μM compound and either 10 μM GTP (to mimic no-enzyme control reactions) or 9 μM GTP plus 1 μM GTP (to mimic completed GTPase reactions). The range of signal observed (3 standard deviations about the mean; "μ±3σ") in each condition is demarked with a dotted grey line.

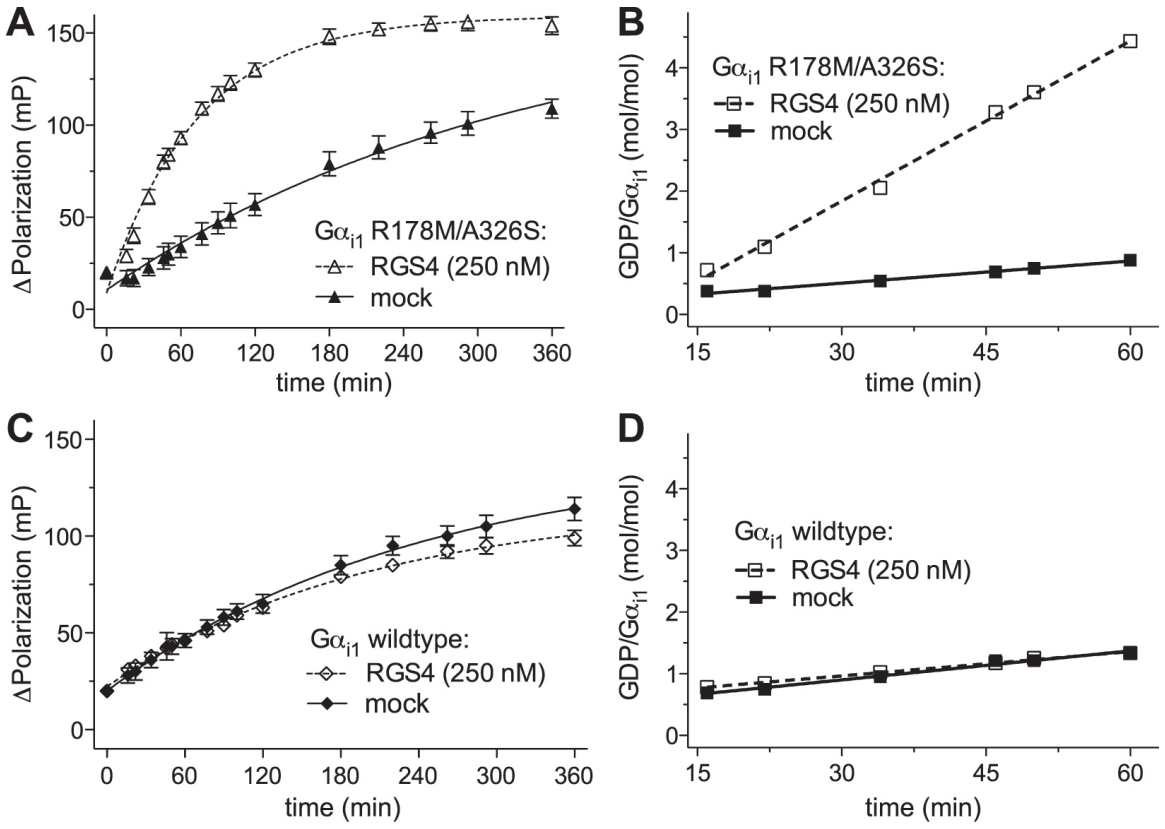

E

$G\alpha_{i1}$ species:	GTPase rate (min^{-1})		GAP factor
	No RGS4	250 nM RGS4	
wildtype	0.016	0.013	0.81
A326S	0.10	0.11	1.10
R178M	0.0059	0.007	1.19
R178C	0.00038	0.00035	0.92
R178C/A326S	0.019	0.069	3.63
R178M/A326S	0.015	0.097	6.47

Figure 5.4. RGS4 increases the steady-state GTPase activity of $G\alpha_{i1}$(R178M/A326S) but not wildtype $G\alpha_{i1}$, as measured using the Transcreener GDP assay and reported in absolute change in polarization (*left panels*) and GDP produced per Gα protein in reaction (*right panels*). R178M/A326S double-mutant (**A,B**) and wildtype (**C,D**) $G\alpha_{i1}$ proteins were present at 50 nM final concentration. Dashed lines represent reactions conducted in the presence, and solid lines ("mock") in the absence, of 250 nM RGS4 protein. (**A,C**) Change in polarization (ΔmP) at each time-point for indicated $G\alpha_{i1}$ protein was calculated as ΔmP = |mP($G\alpha_{i1}$) - mP(no $G\alpha_{i1}$)|. (**B,D**) Data from panels A and C were converted to GDP produced per mol of input $G\alpha_{i1}$ using previously established standard curves for GDP detection in the presence of GTP (*e.g.*, Figure 5.3B). (**E**) Summary of initial rates obtained by the Transcreener GDP assay for each $G\alpha_{i1}$ mutant tested. "GAP factor" is defined as the ratio between steady-state GTPase rate in the presence of RGS protein and steady-state GTPase rate in the absence of RGS protein.

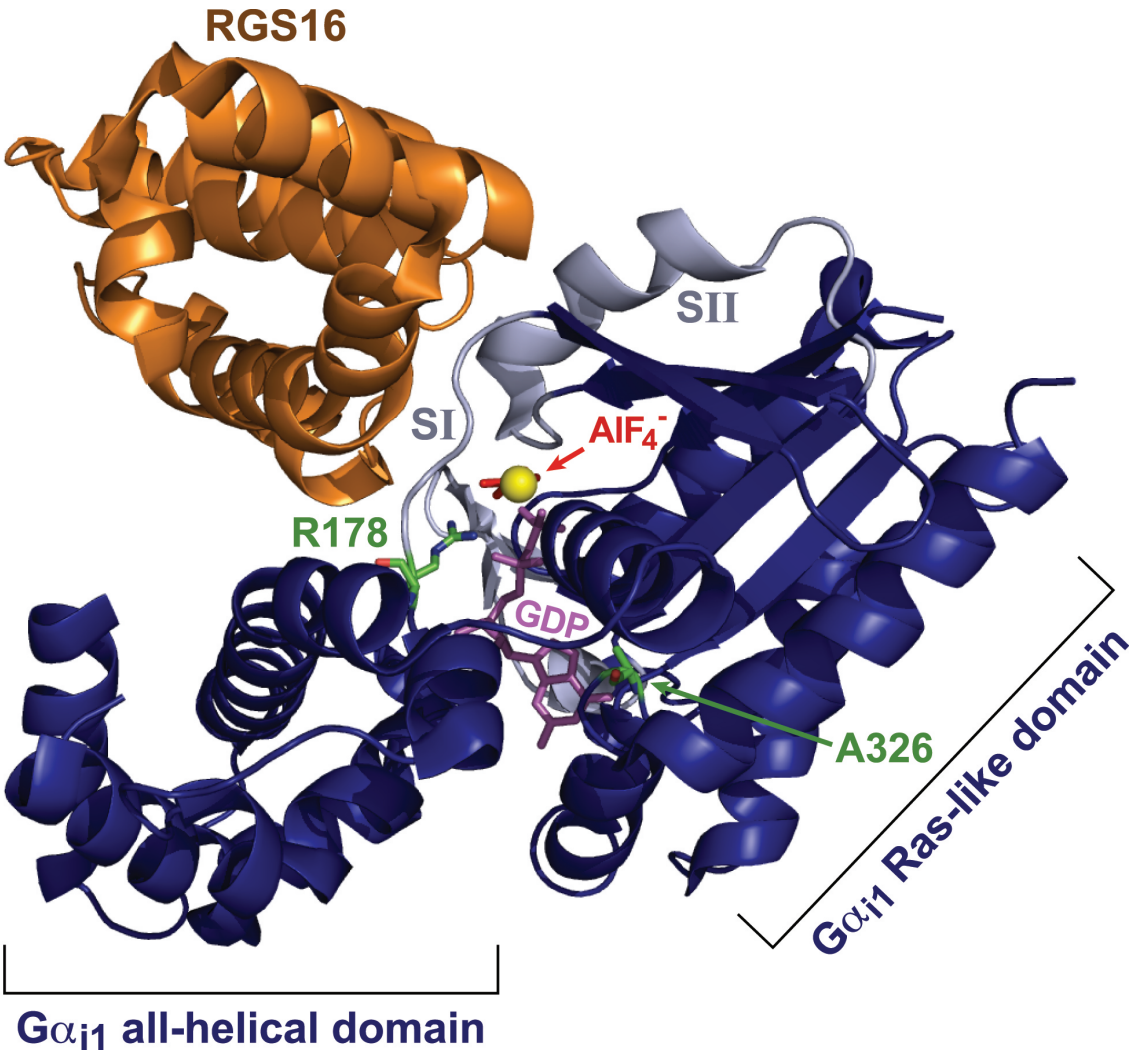

Figure 5.5. Structural features of the RGS16/Gα_{i1}·GDP·AlF_4^- complex highlighting the locations of Arg-178 and Ala-326 residue positions mutated in the Gα_{i1}(R178M/A326S) variant. The RGS16/Gα_{i1} complex (PDB id 2IK8; ref. [24]), was rendered using PyMOL with the RGS16 RGS domain in *orange* and Gα_{i1} protein in *blue*, respectively. Gα_{i1} switch regions are depicted in *grey*; switches one and two (SI, SII) are visible in the foreground, whereas switch three is in the background and thus unlabeled. GDP is shown in *magenta*, the AlF_4^- ion is *red*, and Mg^{2+} ion is depicted as a *yellow* sphere. Residues arginine-178 and alanine-326 are rendered as 'sticks' in *green* with CPK atomic coloring (nitrogen = *blue*, oxygen = *red*).

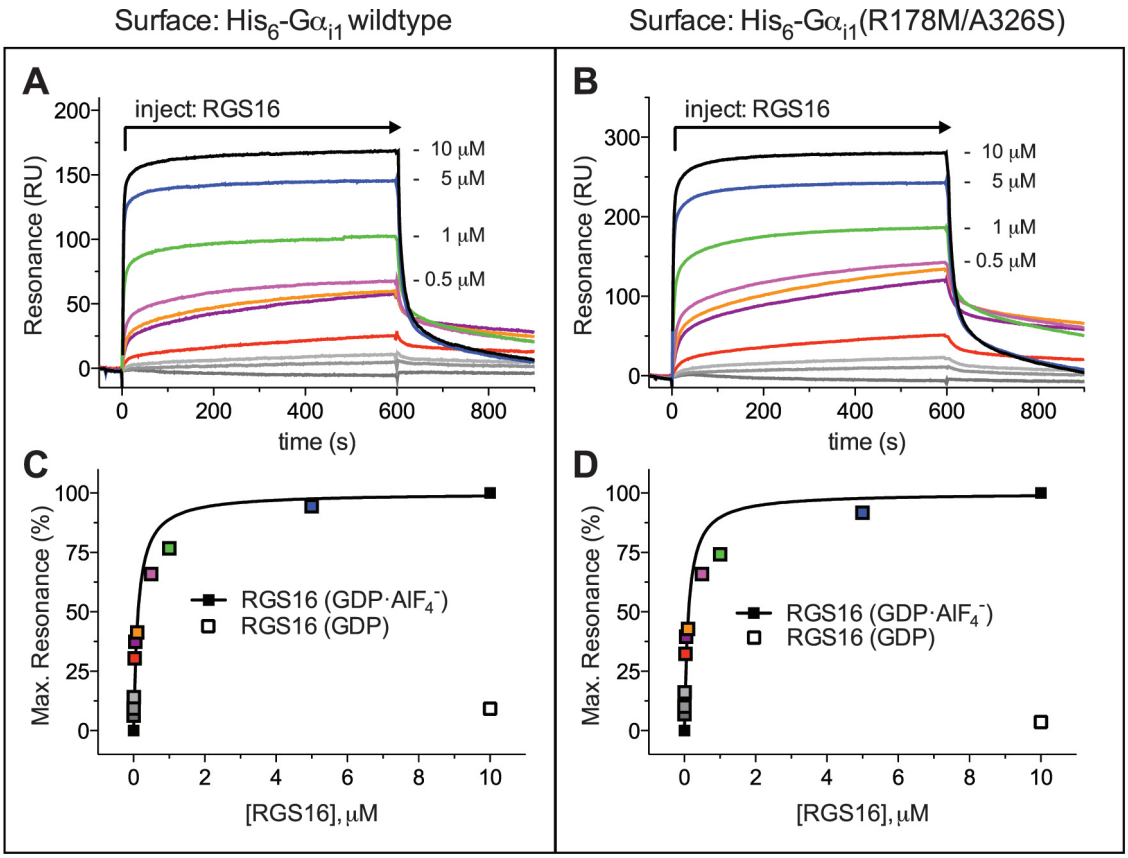

Figure 5.6. RGS16 binds equivalently to wildtype $G\alpha_{i1}$ and the rate-altered $G\alpha_{i1}$(R178M/A326S) mutant. (**A,B**) Sensorgrams derived from 600 second injections of various concentrations (3 nM to 10 μM) of RGS16 over SPR biosensors of immobilized (**A**) wildtype $G\alpha_{i1}$·GDP·AlF_4^- or (**B**) $G\alpha_{i1}$(R178M/A326S)·GDP·AlF_4^-. SPR experiments were also conducted with both $G\alpha_{i1}$ subunits in their inactive, GDP-bound state (data not shown). (**C,D**) Resultant sensorgrams were used in equilibrium saturation binding analyses (as previously described [24]) to derive dissociation constants (K_D values). RGS16 bound to wildtype $G\alpha_{i1}$·GDP·AlF_4^- with a dissociation constant of 124 nM (95% C.I. of 76-174 nM; panel **C**), whereas RGS16 bound to $G\alpha_{i1}$(R178M/A326S)·GDP·AlF_4^- with a dissociation constant of 115 nM (64-166 nM; panel **D**). Note that interactions were not observed (for either Gα subunit) when the Gα was GDP-bound (as expected; refs. [24,31]), nor when RGS2 was injected (data not shown).

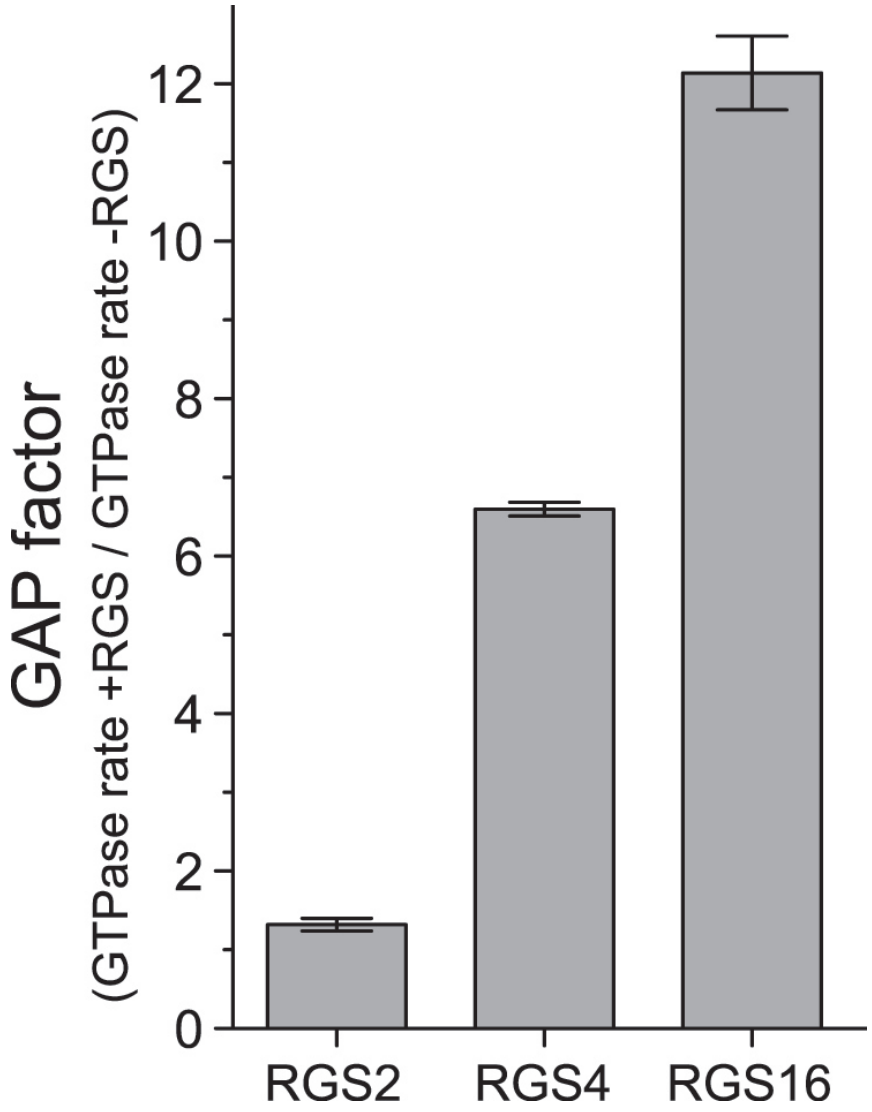

Figure 5.7. The steady-state GTPase activity of $G\alpha_{i1}$(R178M/A326S) is increased by RGS4 and RGS16, but not by the $G\alpha_q$-selective RGS2. Transcreener GDP assays were performed as in Figure 5.4, using 250 nM of the indicated RGS protein. Moles of GDP produced per mol input $G\alpha_{i1}$(R178M/A326S) protein were first plotted over time using GraphPad Prism and linear regression performed to determine steady-state GTPase rates. Presented bar graph denotes GAP factors derived from these steady-state GTPase rates.

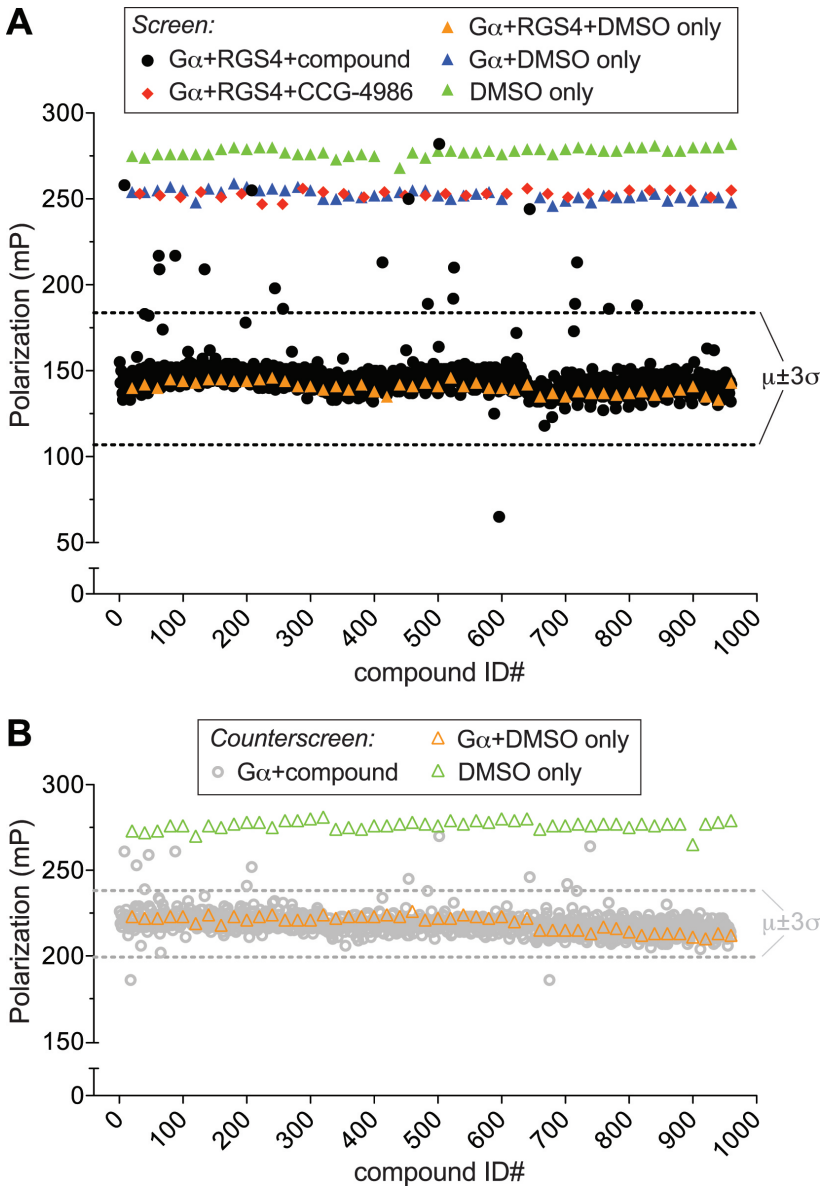

Figure 5.8. Pilot screen and counterscreen using the 960 compound GenPlus library. Transcreener GDP assay components were added to wells containing 50 nM $G\alpha_{i1}$ (R178M/A326S) with (panel **A**) or without (panel **B**) 250 nM RGS4 protein and either 10 μM compound (in 0.5% [v/v] final concentration of DMSO), 150 μM of reactive RGS4 inhibitor CCG-4986, or 0.5% DMSO only, as indicated in the legends. The range of signal observed (three standard deviations [σ] about the mean [μ]) is denoted by the dashed lines for the 960 compound library screen using RGS4 and $G\alpha_{i1}$ (R178M/A326S) (*black;* panel **A**, coefficient of variation [CV%] = 8.8%) and library counterscreen using $G\alpha_{i1}$ (R178M/A326S) alone (*gray;* panel **B**, CV% = 3.0%). Data in panel **A** was obtained at 120 minutes of elapsed reaction time; data in panel **B** was obtained after 210 minutes of elapsed reaction time, given the slower GTPase (and GDP production) rate of $G\alpha_{i1}$ (R178M/A326S) in the absence of RGS4 GAP activity.

CHAPTER 6

RGS21: A NOVEL REGULATOR OF GUSTATION

6.1. INTRODUCTION

The biological process of signal transduction controls a wide variety of cellular activities, ranging from transmembrane ion flux to regulation of gene transcription. One major class of signal transduction pathways is controlled by heterotrimeric guanine nucleotide-binding proteins ("G-proteins") [1, 2]. In addition to being the largest target of currently prescribed pharmaceuticals [3], GPCRs allow us to see, smell and taste the world in which we live. While gustation may seem a luxury, evolutionarily this sense has allowed animals to distinguish between nourishing foods and poisonous toxins.

Mammalian taste can be divided into five components: bitter, sweet, umami (Japanese for savory), salty, and sour. Three of these tastes, bitter, sweet and umami, are directly mediated through GPCRs [4-6]. Radioligand binding experiments, cellular work, and mouse knockouts have provided strong evidence that the T2R family of taste receptors is responsible for the transduction of bitter taste. Some members of the T2R family, such as T2R9, demonstrate remarkable selectivity for one agonist, (e.g., cycloheximide), while others, such as the T2R14 receptor, can be activated by a wide array of bitter compounds [7, 8]. In contrast to the T2R receptors which are functional when expressed individually, T1R taste receptors only function when expressed as heterodimers. Knockout animals and heterologous expression experiments have demonstrated that L-amino acids (umami compounds) signal through a T1R1/T1R3 heterodimer [6, 9, 10]. In the absence of either T1R1 or T1R3 expression, L-amino acids cannot initiate signaling. Similarly, sweet compounds bind to a T1R2/T1R3 heterodimer to initiate taste [5]. As expected, T1R3 knockout mice are able to taste bitter compounds at normal levels but are significantly less sensitive to appetitive effects of sweet and

umami compounds [6, 11]. If the T1R1 or T1R2 receptor is individually knocked out, mice respond normally to bitter compounds but exhibit no response to umami or sweet compounds, respectively [5, 6].

Upon tastant binding to a taste receptor, the receptor acts as a guanine nucleotide exchange factor (GEF), promoting release of GDP by Gα subunits [4, 8, 12]. The heterotrimeric G-proteins involved in gustation are those that classically inhibit adenylyl cyclase; based on Gα deficient animals, the Gα subunits of gustducin and transducin are considered the primary mediators of taste signaling [13-15]. Upon the receptor-mediated exchange of nucleotide, the GTP bound Gα subunit releases Gβγ. The free Gα(GTP) and Gβγ are then capable of modulating downstream effectors. In gustatory signaling, the primary effector of the GTP-bound Gα subunit is adenylyl cyclase [16, 17] and the primary effector of the Gβγ heterodimer is PLC-β2 [18-20]. Of these two downstream effectors, PLC-β2 appears to be the principal effector in mediating the appetitive and aversive effects of tastants in mouse models [20]. The activation of PLC-β2 by Gβγ leads to an increase in intracellular calcium (via IP_3R activation [21]) and subsequent gating of the taste-transduction channel TRPM5 [20, 22]. While the soluble Gα-GEF Ric-8A was recently shown to affect T2R16 signaling in over-expression studies [23], currently no modulators of GPCR signaling -- neither GTPase accelerating proteins (GAPs), guanine nucleotide dissociation inhibitors (GDIs), nor non-receptor GEFs -- are known to affect taste signaling in an endogenous context; however, based on other work, it has been shown that the rate of GTP hydrolysis by Gα is critical to proper perception of the environment (*e.g.*, the critical role of RGS9, the Gα-transducin GAP, in the vertebrate visual system [24, 25]).

The duration of activation of the GPCR-initiated signaling cascade is controlled by the hydrolysis rate of GTP by the Gα subunit which can be greatly accelerated by Regulators of G-protein Signaling (RGS proteins) that serve as GTPase-accelerating proteins [26-30]. The physiological effects of RGS proteins are illustrated in the retinal photoreceptor paradigm. In RGS9-deficient mice [24], the rate-limiting time constant of retinal recovery from flash response increases from 0.2 seconds (wildtype) to 9 seconds (RGS9-null), clearly implicating the importance of these regulators in proper signal transduction timing [31]. Recently, two independent groups have identified a novel member of the RGS protein superfamily, RGS21 [32, 33], as being a potential GAP for taste receptor signaling in analogy to the role of RGS9 in the visual system. Using *in situ* hybridization and RT-PCR analyses, von Buchholtz and colleagues characterized *Rgs21* as having a highly selective distribution in the rat, namely only in lingual epithelium taste cells [33]; however, Li and colleagues described *Rgs21* as being ubiquitously expressed (as detected by RT-PCR in 16 different human tissues) [32]. In this chapter, we resolve this discrepancy regarding the expression pattern of the *Rgs21* transcript, characterize RGS21 biochemically, and provide evidence of the cellular function of this unique RGS protein in tastant receptor signal transduction.

6.2. MATERIALS AND METHODS

6.2.1 Chemicals and assay materials

Unless otherwise noted, all chemicals were the highest grade available from Sigma Aldrich (St. Louis, MO) or Fisher Scientific (Pittsburgh, PA).

6.2.2 Quantitative, real-time reverse transcription-polymerase chain reaction (qRT-PCR) assays

For qRT-PCR experiments to determine expression of human *RGS21* and mouse *Rgs21*, isolation of RNA and subsequent RT-PCR reactions were performed in triplicate exactly as previously described [34] using gene-specific primers and 6-carboxyfluorescein (FAM) and 6-carboxytetramethylrhodamine (TAMRA) dual labeled probes. Primer sequences: Human *RGS21*: forward, 5'-TGC-TGT-TTC-TAC-AGG-TCA-CC-3'; reverse 5'-GTT-GGC-TAA-AAG-CGT-GTC-CA-3'; probe, 5'-FAM-CTG-CGG-AAA-CAA-TGA-CAT-GGT-CTG-TAMRA-3'; human 18S: forward 5'-AGA AAC GGC TAC CAC ATC CA-3'; reverse, 5'-CTC GAA AGA GTC CTG TAT TGT-3'; Probe 5'-FAM-AG GCA GCA GGC GCG CAA ATT ACQ-TAMRA-3'. Mouse *Rgs21*: forward, 5'-GTA-GCT-GAT-GCA CCA-AAA-GAG-3'; reverse, 5'-TGG-AGT-TGG-TTC-AGC-AAT-ATT-C-3'; probe, 5'-FAM-CAT-TGA-CTT-CAG-TAC-CAG-AGA-CCT-CA-TAMRA-3'; mouse 18S: forward, 5'-AGA-AAC-GGC-TAC-CAC-ATC-CA-3'; reverse, 5'-CTC-GAA-AGA-GTC-CTG-TAT-TGT-3'; probe 5'-FAM-AGG-CAG-CAG-GCG-CGC-AAA-TTA-C-TAMRA-3'. The number of cycles until threshold (C_t) was determined using an ABI Prism 7700 Sequence Detector System (Applied Biosystems, Foster City, CA). To normalize for the efficiency of mRNA extraction, the C_t value of 18S was subtracted from the C_t of *Rgs21*. The relative expression of *RGS21* transcript in shRNA lentivirus-transfected stable cell lines *vs* the control lentivirus-transfected 16-HBE cell line was then calculated using the $2^{-(\Delta\Delta C_t)}$ method [35] as shown below:

$$\left[RGS21\right] = 100 \times 2^{-\left(\Delta C_t(shRNA\_Line) - \Delta C_t(control\_line)\right)}$$

where:

$\Delta C_t(shRNA\_line) = C_t(shRNA\_line) - C_t(18S)$ and

$\Delta C_t(control\_line) = C_t(control\_line) - C_t(18S)$.

6.2.3 *In situ* hybridization

Full length mouse RGS21, PLCβ2 (nucleotides 227 -740), and Gustducin (nucleotides 83 - 610) were cloned into pBluescript II SK (Stratagene) using the KpnI and NotI digestion sites. Digoxygenin labeled riboprobes were generated using T7 RNA polymerase and a dig-RNAlabeling mix (Roche). Hybridization was performed by the UNC Neuroscience Center *In Situ* Hybridization Core according to standard protocols (UNC-Chapel Hill).

6.2.4 Cloning

The RGS21 open-reading frame (ORF) was cloned from cDNA isolated from rat taste bud cell cDNA (a gift from Lars von Buchholtz) using the sense primer 5'-CCAGTGAAATGCTGTTTCTAC-3' and antisense primer 5'-CAGGAAAGGCAGCCATC-3' using an annealing temperature of 52 °C and an extension time of 22 s with Phusion thermostable DNA polymerase (New England Biolabs, Ipswich, MA). Following amplification, a 453 bp band was resolved using agarose electrophoresis and isolated by Qiagen Gel Extraction (Qiagen). A second round of PCR, using primers to extend the ORF sequence, was used to subclone the isolated fragment into our pET-based (Novagen) ligation-independent cloning vector to make a

tobacco etch virus protease (TEV) cleavable His_6-fusion protein for protein production in *E. coli,* as well as into a pcDNA3.1-based (Invitrogen) ligation-independent cloning vector to make an hemagglutinin (HA)-epitope fusion protein for expression in mammalian cells, both as previously described [36, 37]. Quick Change site-directed mutagenesis (Stratagene) was used to mutate Arg-126 of the RGS21 ORF to a glutamic acid residue with the sense primer: 5'-GTCTCATGGCCAAGGATTCCTTCCCTGAGTTTCTAAAGTCAGAAATTTATAAGAAA-3' and the antisense primer: 5'-TTTCTTATAAATTTCTGACTTTAGAAACTCAGGGAAGGAATCCTTGGCCATGAGAC-3'.

6.2.5 Protein expression and purification

The vector encoding the His_6-rRGS21(wildtype) or -RGS21(R126E) was transformed into *E. coli* BL21(DE3) cells (Novagen) and grown at 37°C in Luria broth until a culture density of OD_{600} = 0.75 was reached. Protein expression was then induced by the addition of 0.75 mM isopropyl-β-D-thiogalactopyranoside. After culture for 14-16 hours at 20°C, cells were pelleted by centrifugation and frozen at -80°C. Prior to purification, bacterial cell pellets were resuspended in N1 buffer (50 mM Tris pH 7.5, 300 mM NaCl, 30 mM imidazole, 5% (w/v) glycerol) for lysis using high-pressure homogenization with an Emulsiflex (Avestin; Ottawa, Canada). Cellular lysates were clarified by centrifugation for 45 minute at 100,000 x g at 4°C before the supernatant was applied to a nickel-nitrilotriacetic acid resin FPLC column (FF HisTrap; GE Healthcare). The column was washed with 7 column volumes of N1 lacking imidazole then 3 column

volumes of N1 containing 30 mM imidazole, 5 column volumes of N1 containing 300 mM imidazole, and 5 column volumes of N1 containing 700 mM imidazole. Soluble RGS21 was found in the 300 mM imidazole-containing fractions. The column flow-through was pooled and resolved using a calibrated 150 ml size exclusion column (Sephacryl S200, GE Healthcare) with S200 buffer (50 mM Tris pH 7.5, 150 mM NaCl, 5% (w/v) glycerol). Protein was concentrated to approximately 1 mM as determined by A_{280nm} measurements upon denaturation in guanidine hydrochloride.

His_6-$G\alpha_{oA}$ was purified using similar chromatographic methods as previously described [38]. His_6-$G\alpha_{i1,i2,i3}$ and His_6-$G\alpha_{i1}$(G183S) subunits were purified exactly as previously described for the production of $G\alpha_{i1}$ [39]. The His_6-$G\alpha_{t/i1}$ chimeric $G\alpha$ subunit was purified as previously described [40] and transducin was purified from bovine rod outer segments as previously described [41].

6.2.6 NTA pull-down assays

COS7 cells were plated in 6-well dishes and transfected with 1.5 μg of DNA (when at 70% confluency) with Lipofectamine™ 2000 (Invitrogen, Carlsbad, CA) according to manufacturer's instructions. Cells were lysed in lysis buffer containing 20 mM Tris (pH 7.5), 100 mM NaCl, 100 μM GDP, 5 mM GDP, 1 mM EGTA, and 1% Triton-100. To mimic the GTP hydrolysis transition state of the heterotrimeric G-protein α subunit, the lysis buffer was supplemented with 20 mM NaF and 30 μM $AlCl_3$. Cell monolayers were scraped in lysis buffer and incubated at 4 °C for 45 minutes with sonication before insoluble components were separated by centrifugation at 14,000 x g at 4 °C for 10 minutes. Recombinant purified His_6-RGS21 protein (10 μg) was then added

to the clarified cell lysate and rocked at 4°C for 1 hour before the addition of NTA-Agarose and continued incubation overnight at 4°C with rocking. NTA-Agarose was then washed four times with lysis buffer and bound proteins resolved using SDS-PAGE electrophoresis, transferred to nitrocellulose, and detected by chemiluminescence using standard immuno-blotting techniques.

6.2.7 Surface Plasmon Resonance (SPR)

Optical detection of surface plasmon resonance (SPR) was performed using a Biacore 3000 (Biacore Inc., Piscataway, NJ) exactly as previously described [42, 43].

6.2.8 GTP hydrolysis assays

The intrinsic and RGS enhanced GTP hydrolysis rate of Gα subunits was assessed by monitoring the production of ^{32}P-Pi during a single round of GTP hydrolysis. In brief, wild-type $G\alpha_{i1}$ or $G\alpha_{i1}$ mutants (100 nM) were separately incubated for 10 minutes at 20 °C with 1 x 10^6 cpm of [γ-^{32}P]GTP (Perkin Elmer; specific activity of 6500 dpm/Ci) in reaction buffer lacking Mg^{2+} (50 mM Tris pH 7.5, 0.05% C12E10, 1 mM DTT, 10 mM EDTA, 100 mM NaCl, and 5 μg/ml BSA). The reaction was then chilled on ice for 5 minutes prior to initiation of the reaction by the addition of RGS protein, 10 mM $MgCl_2$ and 100 μM GTPγS (final concentration). At periodic intervals, 100 μl aliquots were quenched in 900 μl of charcoal slurry (i.e., 5% (w/v) activated charcoal in 50 mM H_3PO_4 pH 3.0) and centrifuged at 4 °C for 10 minutes at 3750 RCF. Subsequently, 600 μl aliquots of the supernatant were counted via liquid scintillation to quantify ^{32}P-Pi production.

6.2.9 Transient gene overexpression

16-HBE cells were seeded onto 6 well plates at a density of 3 X 10^5 cells per well and incubated in DMEM supplemented with 10% fetal bovine serum (FBS), 4 mM L-glutamine, 100 U/ml penicillin, and 100 μg/ml streptomycin at 37 ^oC in a 5% CO_2/95% air atmosphere. After 24 hours, media was replaced with fresh media. lasmid DNA (1.5 μg) and FuGENE 6 (Roche; Indianapolis, IN) were complexed and added dropwise to each well, per the manufacturer's instructions. Cell monolayers were incubated an additional 24 hours prior to use in the FLIPR assay for transient intracellular calcium mobilization.

6.2.10 Stable gene underexpression

Stable 16-HBE cell lines were generated *via* lentiviral infection. pLKO.1 plasmids encoding human *RGS21*-directed shRNA (Oligo IDs TRCN0000036859, TRCN0000036861, and TRCN0000036863; generated by The RNAi Consortium and purchased from Open Biosystems as catalog # RHS3979-9604267, RHS3979-98492449, and RHS3979-9604271) were prepared from bacterial stocks *via* maxiprep (Qiagen; Valencia, CA) and packaged into a lentiviral vector by the UNC Lineberger Comprehensive Cancer Center Lenti-shRNA Core Facility (Dr. Tal Kafri, director). A control empty lentiviral vector (Open Biosystems catalog #RHS4080) was also packaged to establish the negative control cell line. These viruses were used to infect separate 16-HBE cell cultures seeded onto 100 mm dishes at 50% confluency. Stably-transfected cell

lines were selected with puromycin (Cellgro; Manassas, VA) and maintained in standard media supplemented with puromycin for several weeks prior to use in the FLIPR assay.

6.2.11 GloSensor cAMP assays

Twenty-four hours post–transfection, cells were re-plated on poly-D-lysine-treated, clear-bottom, white 384-well plates at a density of 15,000 cells/well. Forty-eight hours post-transfection, culture medium was aspirated and cells were washed once with assay medium (DMEM (without FBS or phenol), 15 mM HEPES pH 7.4) before being incubated for 2 hours with 20 μl/well of equilibration medium (assay medium with 4% GloSensor™ substrate [Promega]). After two hours, 10 μl of 3x final concentration denatonium benzoate (diluted in 3 μM forskolin-containing assay medium) was added to each well and allowed to incubate for 10 minutes before GloSensor emission was read on a MicroBeta Plate Counter (PerkinElmer). Before plotting, luminescence counts were normalized to 100% maximal response for each condition to account for variability in GloSensor expression, transfection efficiency, and the exact number of cells per well.

6.2.12 Fluorescence Imaging Plate Reader (FLIPR) calcium flux assays

Calcium flux assays were performed as previously described [44]. 16-HBE cells were trypsinized, counted, and seeded onto clear-bottomed 96 well plates (Greiner Bio-One; Monroe, NC) pre-coated with poly-D-lysine, at a density of 7.5 X 10^5 cells per well. After a 24 hour incubation, media was removed and replaced with a Ca^{2+} assay buffer (20 mM HEPES, 1× HBSS, 2.5 mM probenecid, and Ca^{2+} assay dye, pH 7.4) (FLIPR®

Calcium Assay Kit; Molecular Device Corp, Sunnyvale, CA). After a 1-hour incubation at 37^{o}C, during which the cells were allowed to take up the dye, fluorescence responses of cells were measured with a FLIPR^{TETRA} (Molecular Device Corp; Sunnyvale, CA) device upon the addition of variable concentrations of tastant, or vehicle, in the presence of assay buffer (20 mM HEPES, pH 7.4, 1x Hanks Balanced Salt [Invitrogen; Carlsbad, CA] and 2.5 mM probenecid). After data acquisition, a subsequent addition of 5 mM thapsigargin was injected into each well, and fluorescence was measured again. Net peak responses to tastants were normalized to net peak responses to thapsigargin. Responses were compared with that of wild-type control 16-HBE cells. Statistical and graphical analyses were performed using Prism v. 5.0b (GraphPad Software; La Jolla, CA).

6.3. RESULTS AND DISCUSSION

Given the discrepancy in *RGS21* expression patterns presented by the first two reports on RGS21 [32, 33], we first set out to profile the expression of *RGS21* transcripts by the use of quantitative reverse transcription-PCR on RNA isolated from mouse as well as human tissues. In human tissues, *RGS21* was highly expressed in circumvallate papillae and expressed at lower levels in lung tissue (Figure 6.1A). This same expression pattern was also present in mouse tissue, with the addition that *Rgs21* transcripts were also detected in RNA isolated from whole, homogenized mouse tongue (Figure 6.1C). These results support the expression pattern of rat *Rgs21* that was described by von Buchholtz *et al*. [33]. To identify more specifically the cellular localization of *Rgs21* transcripts within lingual tissue, we performed in situ hybridization on mouse tongue tissue. Using this

approach, we were able to identify *Rgs21* expression in cells that appeared to be chemosensory cells only in the circumvallate papillae (Figure 6.2).

Because of the recent evidence implicating gustatory components in enteroendocrine cells in the digestive tract [45-49], we also analyzed *RGS21* transcript levels in different regions of the human and mouse gastrointestinal tract (Figure 6.1B,D). While *RGS21* transcripts were identified in the human gastrointestinal tract, we were unable to identify *Rgs21* transcripts in the mouse GI tract (Figure 6.1B,D). While this may represent a difference in expression between the two organisms, it may also be due to differential probe sensitivity; however, our results suggest that RGS21 expression is associated with related tastant signaling components known to be expressed in chemosensory cells of the human digestive tract [45-49].

While R4 family RGS domains (Figure 6.3) primarily bind to adenylyl cyclase-inhibitory Gα subunits and $G\alpha_{q/11}$ subunits [50-52], RGS domains in general have also been reported to modulate signaling mediated through $G\alpha_s$ [53, 54], $G\alpha_{olf}$ [55] and $G\alpha_{12/13}$ [56-60]. To identify what subset of Gα proteins RGS21 is capable of binding, we performed pull down assays with recombinant His_6-RGS21 protein and cellular lysates containing overexpressed Gα subunits. RGS21 was observed to bind $G\alpha_{i1}$, $G\alpha_{i2}$, $G\alpha_{i3}$, $G\alpha_o$, gustducin, and $G\alpha_q$ in their transition state form (*e.g.*, bound with GDP/AlF_4^-) and not in their ground-state, GDP-bound form. These results with RGS21 are consistent with other reports that, with the exception of RGS2 [61, 62], all R4 family RGS domains can interact with both $G_{i/o}$ and G_q subfamily Gα subunits [50, 63].

We next used surface plasmon resonance (SPR) spectroscopy to determine if the RGS21/Gα interaction is direct and occurs in a manner consistent with the canonical

RGS domain/Gα interaction [50, 51]. An SPR biosensor surface was generated with either immobilized biotin-$G\alpha_{i1}$ or His_6-$G\alpha_q$ fusion protein, and RGS21 was subsequently injected over both surfaces, either in buffer containing aluminum magnesium tetrafluoride (Mg_2AlF_4 or "AMF"; to create the transition state form) or GDP alone. RGS21 bound selectively to $G\alpha_{i1}$(AMF) and $G\alpha_q$(AMF) with affinities (K_d values) of 64 nM (95% confidence interval [C.I.] of 40 - 87 nM) and 20 nM (95% C.I. 11 -29 nM) respectively (Figure 6.5A,B). These affinities for transition state Gα subunits are consistent with earlier reports from other R4 family RGS proteins using SPR [64]. No binding was observed to either $G\alpha_{i1}$ or $G\alpha_q$ surfaces in their GDP-bound state. A charge reversal of the highly conserved Arg 126 (Figure 6.6 to gluatamic acid (R>E or R126E), previously shown to disrupt RGS domain/Gα interactions [38, 62], was observed to disrupt the RGS21 interaction with $G\alpha_{i1}$(AMF) and $G\alpha_q$(AMF) surfaces. SDS-PAGE electrophoresis and circular dichroism studies were performed to verify that the RGS21(R126E) protein was equivalent in purity to wildtype RGS21 protein, and that the global fold of the mutant protein was preserved (Figures 6.7 & 6.8).

To verify the affinities obtained with immobilized Gα SPR surfaces, and to test additional purified Gα subunits for their interaction with RGS21, a GST-RGS21 fusion protein biosensor surface was generated [42] and the binding affinities (K_d values) of $G\alpha_{i1}$, $G\alpha_{i2}$, $G\alpha_{i3}$, $G\alpha_o$, and transducin (Chi6 chimer; [40]) (all in their AMF-bound transition state form) were determined to be 114 nM (95% C.I. 65 - 163 nM), 63 nM (95% C.I. 30 - 95 nM), 61 nM (95% C.I. 25 - 97 nM), 24 nM (95% C.I. 18 - 32 nM), and 190 nM (95% C.I. 134 - 247 nM) respectively; as previously observed, no binding was detected to GDP-bound Gα subunits.

Next, to assess directly if RGS21 could accelerate the GTPase activity of GTP-bound Gα subunits, we measured a single round of GTP hydrolysis by various Gα subunits. RGS21 was able to accelerate robustly the hydrolysis of GTP by $G\alpha_{i1}$. The intrinsic rate of hydrolysis by $G\alpha_{i1}$ was determined to be 0.009 sec^{-1} (95% C.I. 0.007 - 0.011 sec^{-1}) while the hydrolysis rate of GTP upon the addition of RGS21 (50 nM) was 0.25 sec^{-1} (95% C.I. 0.11 - 0.38 sec^{-1}), over 25 times faster (Figure 6.9A). RGS21-mediated GAP activity was also determined on $G\alpha_{i2}$, $G\alpha_{i3}$, $G\alpha_{o}$, and transducin purified from bovine rod outer segments (Figure 6.9 and summarized in Table 6.1). To ensure that the increase in observed hydrolysis rate was not due to a contaminating GTPase protein in the RGS21 preparation, single turnover assays were repeated with a RGS-insensitive $G\alpha_{i1}$ point mutant, namely $G\alpha_{i1}$(G183S) [65, 66]. The intrinsic hydrolysis rate of $G\alpha_{i1}$(G183S) was not accelerated upon the addition of 250 nM of RGS21 or RGS21(R126E) proteins (Figure 6.9B).

The primary Gα subunits implicated in gustation are gustducin-α (GNAT3) and transducin-α (GNAT1) [13-15]. Based on the RGS9/transducin-α structure and comparisons with other RGS domain/Gα complexes [50, 67], the predicted RGS domain contacts on gustducin-α are 95% identical and 100% similar to transducin-α (Figure 6.10). Because the RGS domain/Gα contacts are predicted to be nearly identical, we expect that RGS21 would act as a GAP equivalently on gustducin and transducin alpha subunits.

To determine if RGS21 is capable of modulating gustatory signaling in an integrated, whole-cell context, we first used quantitative RT-PCR to identify a model cell line expressing components of the gustatory singling cascade well as endogenous RGS21.

While we were unable to identify a enteroendocrine cell line that expressed endogenous RGS21 (data not shown), we were able to identify two pulmonary epithelial cell lines (Calu-3 and 16-HBE) that express mRNA transcripts for taste receptors and RGS21 (Figure 6.11). To test the hypothesis that RGS21 is a negative regulator of gustation, we used the bitter receptor agonist denatonium benzoate and monitored inhibition of intracellular cAMP in the 16-HBE cell line (Figure 6.12). Upon the administration of denatonium, cells overexpressing RGS21 had less inhibition of forskolin-mediated cAMP production than control cells. Overexpression of the loss-of-function RGS21(R126E) mutant did not significantly alter bitter tastant-induced reduction of forskolin-mediated cAMP production (*i.e.*, results were comparable to cells transfected with vector-only control; Figure 6.12). To ensure that the overexpression of RGS21 did not have unanticipated, global consequences on GPCR-mediated signaling, isoproterenol-activated production of cAMP was also monitored in 16-HBE cells overexpressing RGS21, RGS21(R126E), or vector alone. No significant alteration in the potency (EC_{50} values) of isoproterenol upon RGS21 overexpression was observed (Figure 6.15).

While bitter taste receptor activation of $G_{i/o}$ subfamily Gα subunits results in the inhibition of adenylyl cyclase activity (Figure 6.12), in the prevailing model of gustatory signal transduction, it is the released Gβγ heterodimer that is thought to have the primary role in signaling, via PLC-β2 activation that results in production of IP_3 and DAG and a subsequent increase in intracellular calcium [68]. To determine if RGS21 is also able to inhibit the activation of PLC-β2-mediated Ca^{2+} release, we monitored intracellular calcium in 16-HBE cells upon the addition of denatonium. A significant decrease in Ca^{2+}

release was observed in RGS21-overexpressing 16-HBE cells, as compared to cells overexpressing the RGS21(R126E) mutant or vector only (Figure 6.14).

While both the cAMP accumulation and Ca^{2+} mobilization data suggest that RGS21 can act as a negative regulator of bitter taste signaling upon its ectopic overexpression in cells, we wanted to test whether endogenous RGS21 expression serves to negatively regulate denatonium signaling. We generated three stable 16-HBE cell lines with decreased *RGS21* expression using lentiviral shRNA-mediated knockdown (Figure 6.15). No difference was seen in levels of forskolin-stimulated cAMP production in the absence of denatonium or upon the addition of 5 mM denatonium; however, at higher concentrations of denatonium (up to 14 mM tested), a significant ($p<0.01$) decrease in cAMP generation was observed in all three cell lines with reduced *RGS21* expression *versus* the control lentivirus-treated cell line (Figure 6.16). To confirm that the generation of the stable *RGS21* knockdown cell lines had not disrupted GPCR-mediated cAMP signaling in a non-specific fashion, we tested isoproterenol responses in these cell lines. No significant different in potency or maximal efficacy was observed; specifically, we determined the EC_{50} values of each cell line for isoproterenol-induced cAMP production to be 4.4 nM (95% C.I. 3.6 - 5.5 nM), 3.7 nM (95% C.I. 2.9 – 4.8 nM), 5.2 nM (95% C.I. 4.4-6.1 nM), and 3.2 nM (95% C.I. 2.4-4.1 nM) for vector control, shRNA#59, shRNA#61, and shRNA#63 stable lines, respectively (Figure 6.17). Intracellular Ca^{2+} responses were also measured in the stable *RGS21* knockdown cell lines upon denatonium addition. At all concentrations tested, decreased *RGS21* expression was observed to result in an increase in denatonium-induced Ca^{2+} release (Figure 6.18). While the unique distribution of RGS21 in lingual gustatory tissue was

originally described by von Buchholtz *et al.* [33], leading to the possibility that RGS21 could be a regulator of gustatory signal transduction, our work has demonstrated the ability of RGS21 to act as a GAP for multiple Gα subunits known to be involved in tastant receptor signaling, as well as provides the first evidence of a non-receptor, G-protein regulatory component to the signal transduction pathway that alters the sensitivity of tastant responsiveness in an endogenous, cellular context.

6.4 REFERENCES

1. Gilman, A.G., *G proteins: transducers of receptor-generated signals.* Annu Rev Biochem, 1987. **56**: p. 615-649.

2. Offermanns, S., *G-proteins as transducers in transmembrane signalling.* Prog Biophys Mol Biol, 2003. **83**(2): p. 101-30.

3. Jacoby, E., R. Bouhelal, M. Gerspacher, and K. Seuwen, *The 7 TM G-protein-coupled receptor target family.* ChemMedChem, 2006. **1**(8): p. 761-82.

4. Chandrashekar, J., K.L. Mueller, M.A. Hoon, E. Adler, L. Feng, W. Guo, C.S. Zuker, and N.J. Ryba, *T2Rs function as bitter taste receptors.* Cell, 2000. **100**(6): p. 703-11.

5. Nelson, G., M.A. Hoon, J. Chandrashekar, Y. Zhang, N.J. Ryba, and C.S. Zuker, *Mammalian sweet taste receptors.* Cell, 2001. **106**(3): p. 381-90.

6. Zhao, G.Q., Y. Zhang, M.A. Hoon, J. Chandrashekar, I. Erlenbach, N.J. Ryba, and C.S. Zuker, *The receptors for mammalian sweet and umami taste.* Cell, 2003. **115**(3): p. 255-66.

7. Meyerhof, W., M. Behrens, A. Brockhoff, B. Bufe, and C. Kuhn, *Human bitter taste perception.* Chem Senses, 2005. **30 Suppl 1**: p. i14-i15.

8. Sainz, E., M.M. Cavenagh, J. Gutierrez, J.F. Battey, J.K. Northup, and S.L. Sullivan, *Functional characterization of human bitter taste receptors.* Biochem J, 2007. **403**(3): p. 537-43.

9. Nelson, G., J. Chandrashekar, M.A. Hoon, L. Feng, G. Zhao, N.J. Ryba, and C.S. Zuker, *An amino-acid taste receptor.* Nature, 2002. **416**(6877): p. 199-202.

10. Li, X., L. Staszewski, H. Xu, K. Durick, M. Zoller, and E. Adler, *Human receptors for sweet and umami taste.* Proc Natl Acad Sci U S A, 2002. **99**(7): p. 4692-6.

11. Damak, S., M. Rong, K. Yasumatsu, Z. Kokrashvili, V. Varadarajan, S. Zou, P. Jiang, Y. Ninomiya, and R.F. Margolskee, *Detection of sweet and umami taste in the absence of taste receptor T1r3.* Science, 2003. **301**(5634): p. 850-3.

12. Bourne, H.R., *How receptors talk to trimeric G proteins.* Curr Opin Cell Biol, 1997. **9**(2): p. 134-42.

13. Wong, G.T., K.S. Gannon, and R.F. Margolskee, *Transduction of bitter and sweet taste by gustducin.* Nature, 1996. **381**(6585): p. 796-800.

14. He, W., K. Yasumatsu, V. Varadarajan, A. Yamada, J. Lem, Y. Ninomiya, R.F. Margolskee, and S. Damak, *Umami taste responses are mediated by alpha-transducin and alpha-gustducin.* J Neurosci, 2004. **24**(35): p. 7674-80.

15. Kusakabe, Y., A. Yasuoka, M. Asano-Miyoshi, K. Iwabuchi, I. Matsumoto, S. Arai, Y. Emori, and K. Abe, *Comprehensive study on G protein alpha-subunits in taste bud cells, with special reference to the occurrence of Galphai2 as a major Galpha species.* Chem Senses, 2000. **25**(5): p. 525-31.

16. Yan, W., G. Sunavala, S. Rosenzweig, M. Dasso, J.G. Brand, and A.I. Spielman, *Bitter taste transduced by PLC-beta(2)-dependent rise in IP(3) and alpha-gustducin-dependent fall in cyclic nucleotides.* Am J Physiol Cell Physiol, 2001. **280**(4): p. C742-51.

17. Abaffy, T., K.R. Trubey, and N. Chaudhari, *Adenylyl cyclase expression and modulation of cAMP in rat taste cells.* Am J Physiol Cell Physiol, 2003. **284**(6): p. C1420-8.

18. Rossler, P., C. Kroner, J. Freitag, J. Noe, and H. Breer, *Identification of a phospholipase C beta subtype in rat taste cells.* Eur J Cell Biol, 1998. **77**(3): p. 253-61.

19. Dotson, C.D., S.D. Roper, and A.C. Spector, *PLCbeta2-independent behavioral avoidance of prototypical bitter-tasting ligands.* Chem Senses, 2005. **30**(7): p. 593-600.

20. Zhang, Y., M.A. Hoon, J. Chandrashekar, K.L. Mueller, B. Cook, D. Wu, C.S. Zuker, and N.J. Ryba, *Coding of sweet, bitter, and umami tastes: different receptor cells sharing similar signaling pathways.* Cell, 2003. **112**(3): p. 293-301.

21. Hisatsune, C., K. Yasumatsu, H. Takahashi-Iwanaga, N. Ogawa, Y. Kuroda, R. Yoshida, Y. Ninomiya, and K. Mikoshiba, *Abnormal taste perception in mice lacking the type 3 inositol 1,4,5-trisphosphate receptor.* J Biol Chem, 2007. **282**(51): p. 37225-31.

22. Damak, S., M. Rong, K. Yasumatsu, Z. Kokrashvili, C.A. Perez, N. Shigemura, R. Yoshida, B. Mosinger, Jr., J.I. Glendinning, Y. Ninomiya, and R.F. Margolskee, *Trpm5 null mice respond to bitter, sweet, and umami compounds.* Chem Senses, 2006. **31**(3): p. 253-64.

23. Fenech, C., L. Patrikainen, D.S. Kerr, S. Grall, Z. Liu, F. Laugerette, B. Malnic, and J.P. Montmayeur, *Ric-8A, a Galpha protein guanine*

nucleotide exchange factor potentiates taste receptor signaling. Front Cell Neurosci, 2009. **3**: p. 11.

24. Chen, C.K., M.E. Burns, W. He, T.G. Wensel, D.A. Baylor, and M.I. Simon, *Slowed recovery of rod photoresponse in mice lacking the GTPase accelerating protein RGS9-1.* Nature, 2000. **403**(6769): p. 557-60.

25. He, W., C.W. Cowan, and T.G. Wensel, *RGS9, a GTPase accelerator for phototransduction.* Neuron, 1998. **20**(1): p. 95-102.

26. Berman, D.M., T.M. Wilkie, and A.G. Gilman, *GAIP and RGS4 are GTPase-activating proteins for the Gi subfamily of G protein alpha subunits.* Cell, 1996. **86**(3): p. 445-52.

27. Druey, K.M., K.J. Blumer, V.H. Kang, and J.H. Kehrl, *Inhibition of G-protein-mediated MAP kinase activation by a new mammalian gene family.* Nature, 1996. **379**(6567): p. 742-6.

28. Koelle, M.R. and H.R. Horvitz, *EGL-10 regulates G protein signaling in the C. elegans nervous system and shares a conserved domain with many mammalian proteins.* Cell, 1996. **84**(1): p. 115-25.

29. Siderovski, D.P., A. Hessel, S. Chung, T.W. Mak, and M. Tyers, *A new family of regulators of G-protein-coupled receptors?* Curr Biol, 1996. **6**(2): p. 211-2.

30. Watson, N., M.E. Linder, K.M. Druey, J.H. Kehrl, and K.J. Blumer, *RGS family members: GTPase-activating proteins for heterotrimeric G-protein alpha-subunits.* Nature, 1996. **383**(6596): p. 172-5.

31. Arshavsky, V.Y., T.D. Lamb, and E.N. Pugh, Jr., *G proteins and phototransduction.* Annu Rev Physiol, 2002. **64**: p. 153-87.

32. Li, X., L. Chen, C. Ji, B. Liu, J. Gu, J. Xu, X. Zou, S. Gu, and Y. Mao, *Isolation and expression pattern of RGS21 gene, a novel RGS member.* Acta Biochim Pol, 2005. **52**(4): p. 943-6.

33. von Buchholtz, L., A. Elischer, E. Tareilus, R. Gouka, C. Kaiser, H. Breer, and S. Conzelmann, *RGS21 is a novel regulator of G protein signalling selectively expressed in subpopulations of taste bud cells.* Eur J Neurosci, 2004. **19**(6): p. 1535-44.

34. Kim, H.S., G. Lee, S.W. John, N. Maeda, and O. Smithies, *Molecular phenotyping for analyzing subtle genetic effects in mice: application to an angiotensinogen gene titration.* Proc Natl Acad Sci U S A, 2002. **99**(7): p. 4602-7.

35. Livak, K.J. and T.D. Schmittgen, *Analysis of relative gene expression data using real-time quantitative PCR and the 2(-Delta Delta C(T)) Method.* Methods, 2001. **25**(4): p. 402-8.

36. Kimple, A.J., F.S. Willard, P.M. Giguere, C.A. Johnston, V. Mocanu, and D.P. Siderovski, *The RGS protein inhibitor CCG-4986 is a covalent modifier of the RGS4 Galpha-interaction face.* Biochim Biophys Acta, 2007.

37. Stols, L., M. Gu, L. Dieckman, R. Raffen, F.R. Collart, and M.I. Donnelly, *A new vector for high-throughput, ligation-independent cloning encoding a tobacco etch virus protease cleavage site.* Protein Expr Purif, 2002. **25**(1): p. 8-15.

38. Willard, F.S., A.J. Kimple, C.A. Johnston, and D.P. Siderovski, *A direct fluorescence-based assay for RGS domain GTPase accelerating activity.* Anal Biochem, 2005. **340**(2): p. 341-51.

39. Kimple, A.J., A. Yasgar, M. Hughes, A. Jadhav, F.S. Willard, R.E. Muller, C.P. Austin, J. Inglese, G.C. Ibeanu, D.P. Siderovski, and A. Simeonov, *A high throughput fluorescence polarization assay for inhibitors of the GoLoco motif/G-alpha interaction.* Comb Chem High Throughput Screen, 2008. **11**(5): p. 396-409.

40. Skiba, N.P., H. Bae, and H.E. Hamm, *Mapping of effector binding sites of transducin alpha-subunit using G alpha t/G alpha i1 chimeras.* J Biol Chem, 1996. **271**(1): p. 413-24.

41. Yamanaka, G., F. Eckstein, and L. Stryer, *Stereochemistry of the guanyl nucleotide binding site of transducin probed by phosphorothioate analogues of GTP and GDP.* Biochemistry, 1985. **24**(27): p. 8094-101.

42. Hutsell, S.Q., R.J. Kimple, D.P. Siderovski, F.S. Willard, and A.J. Kimple, *High-affinity immobilization of proteins using biotin- and GST-based coupling strategies.* Methods Mol Biol. **627**: p. 75-90.

43. Kimple, A.J., R.E. Muller, D.P. Siderovski, and F.S. Willard, *A capture coupling method for the covalent immobilization of hexahistidine tagged proteins for surface plasmon resonance.* Methods Mol Biol. **627**: p. 91-100.

44. Strachan, R.T., D.J. Sheffler, B. Willard, M. Kinter, J.G. Kiselar, and B.L. Roth, *Ribosomal S6 kinase 2 directly phosphorylates the 5-hydroxytryptamine 2A (5-HT2A) serotonin receptor, thereby modulating 5-HT2A signaling.* J Biol Chem, 2009. **284**(9): p. 5557-73.

45. Chen, M.C., S.V. Wu, J.R. Reeve, Jr., and E. Rozengurt, *Bitter stimuli induce Ca2+ signaling and CCK release in enteroendocrine STC-1 cells:*

role of L-type voltage-sensitive Ca2+ channels. Am J Physiol Cell Physiol, 2006. **291**(4): p. C726-39.

46. Dyer, J., K. Daly, K.S. Salmon, D.K. Arora, Z. Kokrashvili, R.F. Margolskee, and S.P. Shirazi-Beechey, *Intestinal glucose sensing and regulation of intestinal glucose absorption.* Biochem Soc Trans, 2007. **35**(Pt 5): p. 1191-4.

47. Margolskee, R.F., J. Dyer, Z. Kokrashvili, K.S. Salmon, E. Ilegems, K. Daly, E.L. Maillet, Y. Ninomiya, B. Mosinger, and S.P. Shirazi-Beechey, *T1R3 and gustducin in gut sense sugars to regulate expression of Na+-glucose cotransporter 1.* Proc Natl Acad Sci U S A, 2007. **104**(38): p. 15075-80.

48. Rozengurt, N., S.V. Wu, M.C. Chen, C. Huang, C. Sternini, and E. Rozengurt, *Colocalization of the alpha-subunit of gustducin with PYY and GLP-1 in L cells of human colon.* Am J Physiol Gastrointest Liver Physiol, 2006. **291**(5): p. G792-802.

49. Wu, S.V., M.C. Chen, and E. Rozengurt, *Genomic organization, expression, and function of bitter taste receptors (T2R) in mouse and rat.* Physiol Genomics, 2005. **22**(2): p. 139-49.

50. Soundararajan, M., F.S. Willard, A.J. Kimple, A.P. Turnbull, L.J. Ball, G.A. Schoch, C. Gileadi, O.Y. Fedorov, E.F. Dowler, V.A. Higman, S.Q. Hutsell, M. Sundstrom, D.A. Doyle, and D.P. Siderovski, *Structural diversity in the RGS domain and its interaction with heterotrimeric G protein alpha-subunits.* Proc Natl Acad Sci U S A, 2008. **105**(17): p. 6457-62.

51. Tesmer, J.J., D.M. Berman, A.G. Gilman, and S.R. Sprang, *Structure of RGS4 bound to AlF4--activated G(i alpha1): stabilization of the transition state for GTP hydrolysis.* Cell, 1997. **89**(2): p. 251-61.

52. Xu, X., W. Zeng, S. Popov, D.M. Berman, I. Davignon, K. Yu, D. Yowe, S. Offermanns, S. Muallem, and T.M. Wilkie, *RGS proteins determine signaling specificity of Gq-coupled receptors.* J Biol Chem, 1999. **274**(6): p. 3549-56.

53. Zheng, B., Y.C. Ma, R.S. Ostrom, C. Lavoie, G.N. Gill, P.A. Insel, X.Y. Huang, and M.G. Farquhar, *RGS-PX1, a GAP for GalphaS and sorting nexin in vesicular trafficking.* Science, 2001. **294**(5548): p. 1939-42.

54. Castellone, M.D., H. Teramoto, B.O. Williams, K.M. Druey, and J.S. Gutkind, *Prostaglandin E2 promotes colon cancer cell growth through a Gs-axin-beta-catenin signaling axis.* Science, 2005. **310**(5753): p. 1504-10.

55. Sinnarajah, S., C.W. Dessauer, D. Srikumar, J. Chen, J. Yuen, S. Yilma, J.C. Dennis, E.E. Morrison, V. Vodyanoy, and J.H. Kehrl, *RGS2 regulates signal transduction in olfactory neurons by attenuating activation of adenylyl cyclase III.* Nature, 2001. **409**(6823): p. 1051-5.

56. Hart, M.J., X. Jiang, T. Kozasa, W. Roscoe, W.D. Singer, A.G. Gilman, P.C. Sternweis, and G. Bollag, *Direct stimulation of the guanine nucleotide exchange activity of p115 RhoGEF by Galpha13.* Science, 1998. **280**(5372): p. 2112-4.

57. Kozasa, T., X. Jiang, M.J. Hart, P.M. Sternweis, W.D. Singer, A.G. Gilman, G. Bollag, and P.C. Sternweis, *p115 RhoGEF, a GTPase activating protein for Galpha12 and Galpha13.* Science, 1998. **280**(5372): p. 2109-11.

58. Booden, M.A., D.P. Siderovski, and C.J. Der, *Leukemia-associated Rho guanine nucleotide exchange factor promotes G alpha q-coupled activation of RhoA.* Mol Cell Biol, 2002. **22**(12): p. 4053-61.

59. Fukuhara, S., H. Chikumi, and J.S. Gutkind, *Leukemia-associated Rho guanine nucleotide exchange factor (LARG) links heterotrimeric G proteins of the G(12) family to Rho.* FEBS Lett, 2000. **485**(2-3): p. 183-8.

60. Suzuki, N., S. Nakamura, H. Mano, and T. Kozasa, *Galpha 12 activates Rho GTPase through tyrosine-phosphorylated leukemia-associated RhoGEF.* Proc Natl Acad Sci U S A, 2003. **100**(2): p. 733-8.

61. Heximer, S.P., N. Watson, M.E. Linder, K.J. Blumer, and J.R. Hepler, *RGS2/G0S8 is a selective inhibitor of Gqalpha function.* Proc Natl Acad Sci U S A, 1997. **94**(26): p. 14389-93.

62. Kimple, A.J., M. Soundararajan, S.Q. Hutsell, A.K. Roos, D.J. Urban, V. Setola, B.R. Temple, B.L. Roth, S. Knapp, F.S. Willard, and D.P. Siderovski, *Structural determinants of G-protein alpha subunit selectivity by regulator of G-protein signaling 2 (RGS2).* J Biol Chem, 2009. **284**(29): p. 19402-11.

63. Bansal, G., K.M. Druey, and Z. Xie, *R4 RGS proteins: regulation of G-protein signaling and beyond.* Pharmacol Ther, 2007. **116**(3): p. 473-95.

64. Popov, S., K. Yu, T. Kozasa, and T.M. Wilkie, *The regulators of G protein signaling (RGS) domains of RGS4, RGS10, and GAIP retain GTPase activating protein activity in vitro.* Proc Natl Acad Sci U S A, 1997. **94**(14): p. 7216-20.

65. DiBello, P.R., T.R. Garrison, D.M. Apanovitch, G. Hoffman, D.J. Shuey, K. Mason, M.I. Cockett, and H.G. Dohlman, *Selective uncoupling of RGS*

action by a single point mutation in the G protein alpha-subunit. J Biol Chem, 1998. **273**(10): p. 5780-4.

66. Lan, K.L., N.A. Sarvazyan, R. Taussig, R.G. Mackenzie, P.R. DiBello, H.G. Dohlman, and R.R. Neubig, *A point mutation in Galphao and Galphai1 blocks interaction with regulator of G protein signaling proteins.* J Biol Chem, 1998. **273**(21): p. 12794-7.

67. Slep, K.C., M.A. Kercher, W. He, C.W. Cowan, T.G. Wensel, and P.B. Sigler, *Structural determinants for regulation of phosphodiesterase by a G protein at 2.0 A.* Nature, 2001. **409**(6823): p. 1071-7.

68. Chandrashekar, J., M.A. Hoon, N.J. Ryba, and C.S. Zuker, *The receptors and cells for mammalian taste.* Nature, 2006. **444**(7117): p. 288-94.

69. Chenna, R., H. Sugawara, T. Koike, R. Lopez, T.J. Gibson, D.G. Higgins, and J.D. Thompson, *Multiple sequence alignment with the Clustal series of programs.* Nucleic Acids Res, 2003. **31**(13): p. 3497-500.

70. Page, R.D., *TreeView: an application to display phylogenetic trees on personal computers.* Comput Appl Biosci, 1996. **12**(4): p. 357-8.

71. Cowan, C.W., T.G. Wensel, and V.Y. Arshavsky, *Enzymology of GTPase acceleration in phototransduction.* Methods Enzymol, 2000. **315**: p. 524-38.

72. Sobolev, V., E. Eyal, S. Gerzon, V. Potapov, M. Babor, J. Prilusky, and M. Edelman, *SPACE: a suite of tools for protein structure prediction and analysis based on complementarity and environment.* Nucleic Acids Res, 2005. **33**(Web Server issue): p. W39-43.

FIGURES

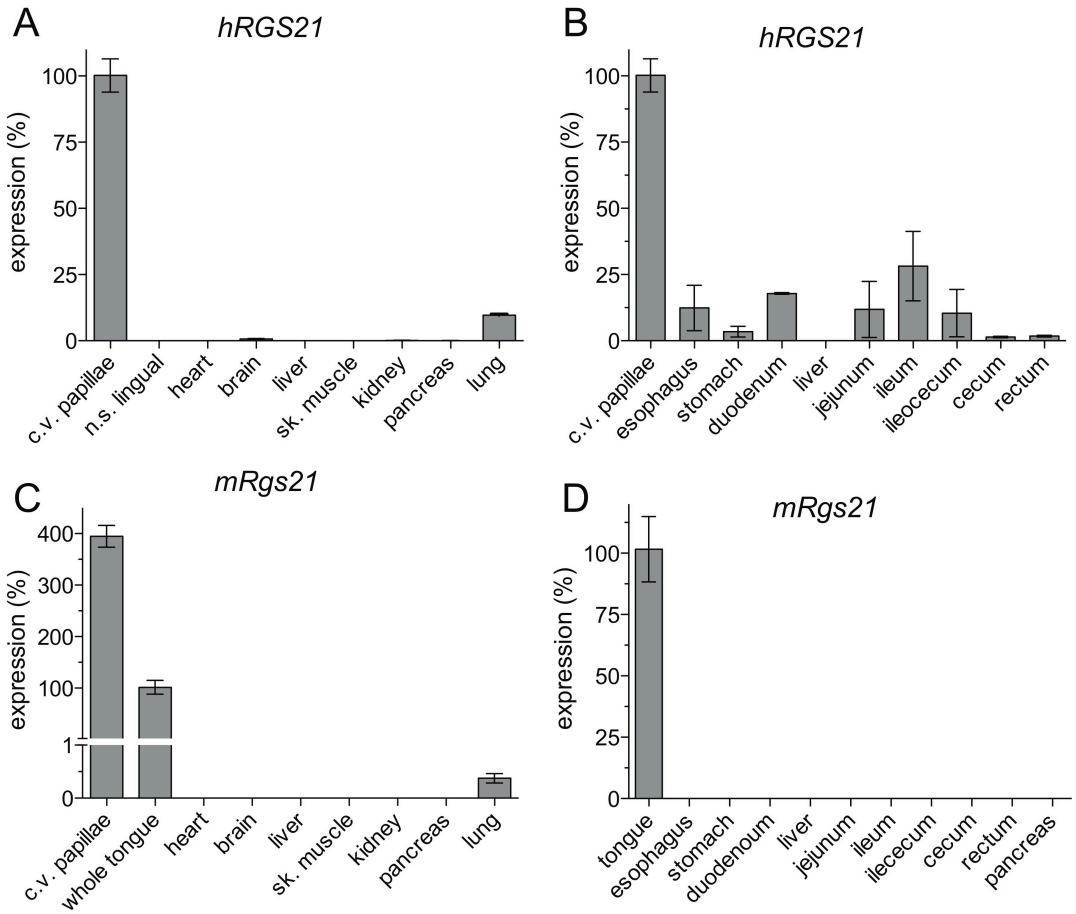

Figure 6.1. ***RGS21*** **transcripts are highly expressed in human and mouse chemosensory tissues as well as in the lung and human gastrointestinal tissues – (A,B)** Real-time, quantitative PCR using fluorogenic probe detection was performed on total RNA from indicated human organs. Variable quantities of RNA were normalized by comparison to *18S* ribosomal RNA and expression of *RGS21* was set to 100% in the circumvallate (c.v.) papillae using the $2^{-(\Delta\Delta C_t)}$ method [35]. **(C,D)** Total RNA was extracted from indicated mouse organs prior to quantitative RT-PCR. Variation in total amounts of RNA isolated were normalized to *18S* ribosomal RNA and were normalized using the $2^{-(\Delta\Delta C_t)}$ method [35] so that expression of mouse *Rgs21* in the tongue was set to 100%.

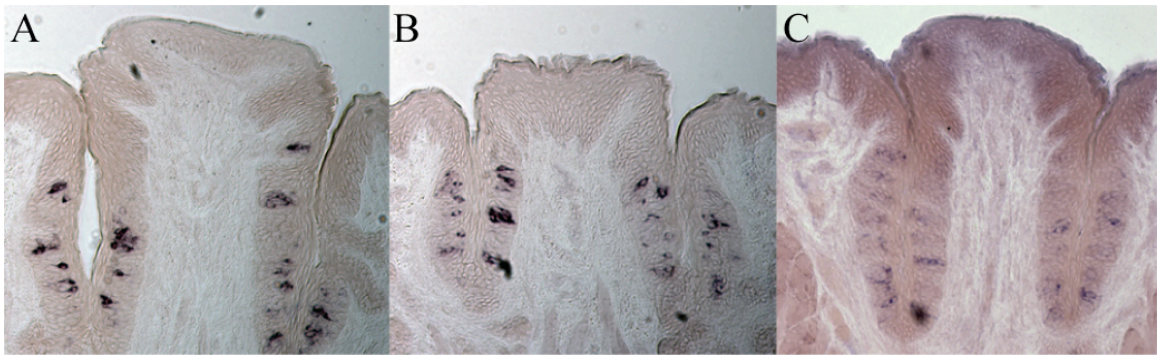

Figure 6.2. *PLC-β2*, *Gustducin*-α, and *RGS21* transcripts are expressed in chemosensory cells in the mouse circumvallate papillae. Sections of mouse circumvallate papillae were hybridized with digoxigenin riboprobes for (A) PLC-β2, (B) Gustducin-α, and (C) RGS21. Following hybridization and washes, probes were detected using an alkaline phosphatase labeled anti-digoxigenin antibody and BCIP/NBT (5-Bromo-4-Chloro-3'-Indolyphosphate p-Toluidine Salt / Nitro-Blue Tetrazolium Chloride) chromogenic detection.

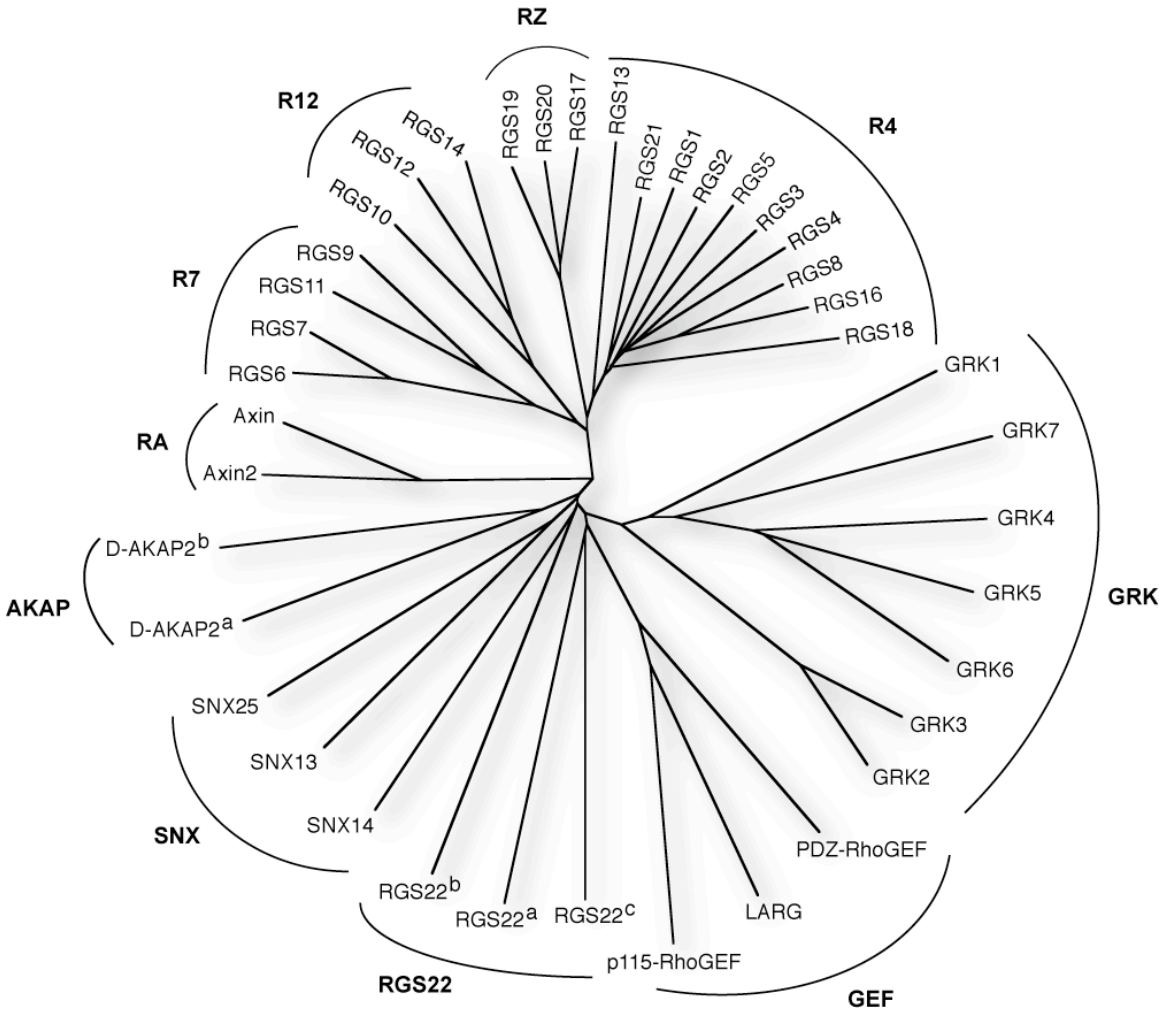

Figure 6.3. Phylogenetic relationship of the 37 RGS domain-containing proteins identified in humans. An unrooted dendrogram, based on the RGS domain polypeptide sequence of the indicated proteins, was generated using ClustalW [69] and visualized using TreeView [70]. Based on this sequence homology analysis, RGS21 is categorized as a member of the R4 subfamily of RGS proteins.

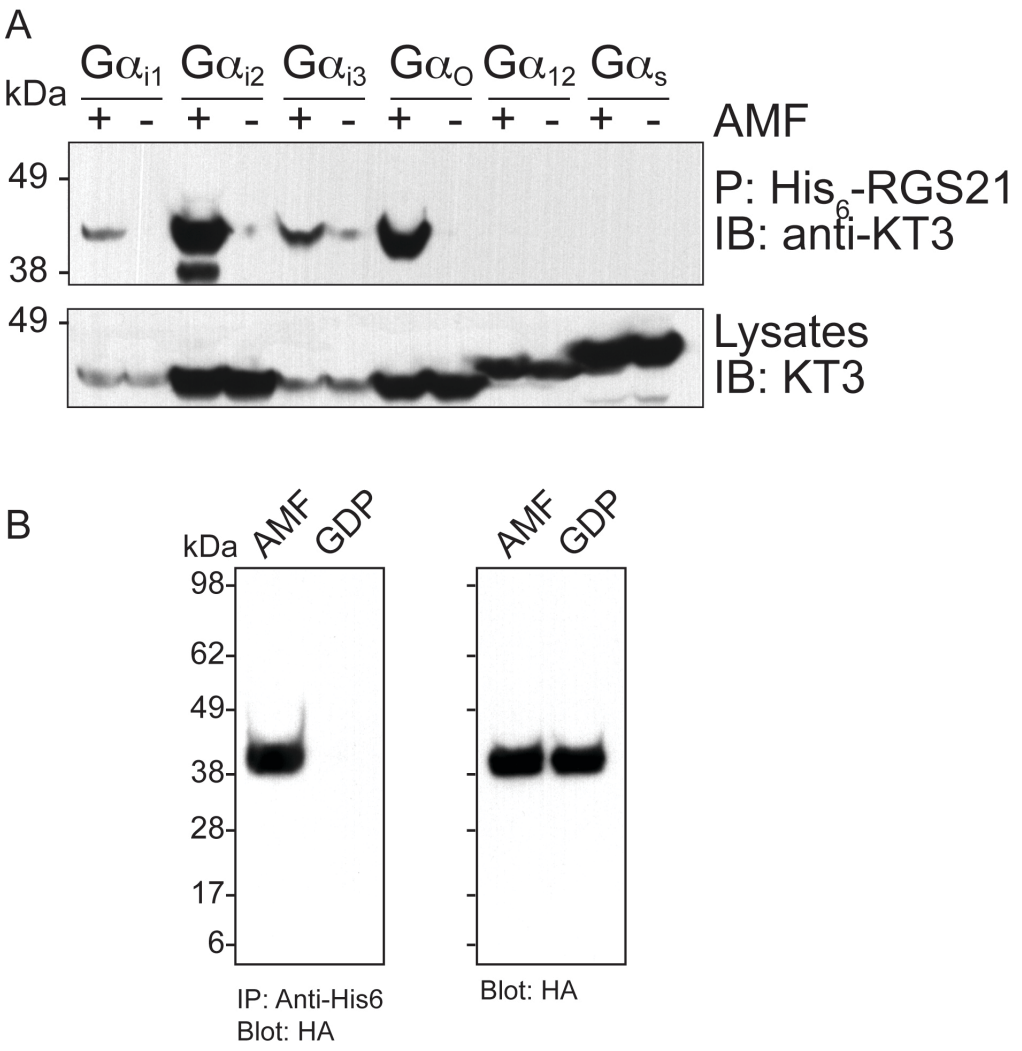

Figure 6.4. RGS21 interacts with $G_{i/o}$ subfamily Gα subunits only in their transition state for GTP hydrolysis. **(A)** COS7 cells were separately transfected using Fugene 6 with 1.5 μg of DNA encoding one of the indicated Gα subunits fused to the KT3 epitope. Forty-eight hours post transfection, cells were lysed in lysis buffer containing GDP, Mg^{2+} and AlF_4^- ("AMF") or GDP alone. Clarified cell lysates were incubated with 10 μg of purified His_6-RGS21 protein at 4 °C overnight with NTA-Agarose. Samples were centrifuged, agarose beads washed four times in lysis buffer, and precipitated proteins eluted by boiling for 5 minutes in loading buffer prior to being resolved by SDS-PAGE electrophoresis, transferred to a nitrocellulose membrane, and detected using anti-KT3 antibody and chemiluminescence. **(B)** COS7 cells were transfected with 1.5 μg of DNA encoding an HA-gustducin-α fusion protein using Fugene 6. The pulldown experiment was then conducted exactly as described for panel A.

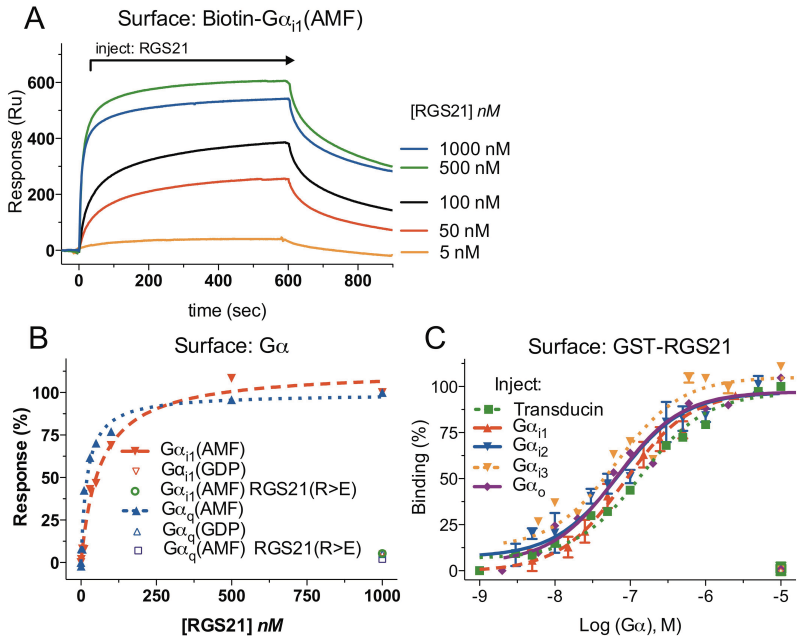

Figure 6.5. RGS21 interacts with transition state forms of $G\alpha_{i/o}$ subunits and $G\alpha_q$ with nanomolar affinities. **(A)** Biotin-$G\alpha_{i1}$ and alkaline-denatured biotin-$G\alpha_{i1}$ were immobilized on separate streptavidin biosensor surfaces for SPR binding analyses. Indicated concentrations of recombinant RGS21 protein were injected over both surfaces at 20 µl/min for 600 sec (injection start at t=0) with a subsequent 300 s dissociation time. Non-specific binding to the alkaline-denatured biotin-$G\alpha_{i1}$ surface was subtracted using BiaEvaluation software. **(B)** Sensorgrams derived from experiments as illustrated in panel A were used for equilibrium saturation binding analyses to determine the affinity of wild-type RGS21 or RGS21(R126E) proteins for $G\alpha_{i1}$ or $G\alpha_q$ in both their transition state (AMF) and ground state (GDP) forms. $G\alpha_q$ biosensor sensorgrams were obtained by immobilizing His_6-$G\alpha_q$ using capture coupling exactly as previously described [43]. The affinity of the $G\alpha_{i1}$(AMF)/RGS21 interaction was determined to be 64 nM (95% C.I. 40-87 nM) and the $G\alpha_q$(AMF)/RGS21 affinity was determined to be 20 nM (95% C.I. 11-29 nM). No specific binding was observed for the loss-of-function RGS21(R126E) protein toward $G\alpha_{i1}$ or $G\alpha_q$ nor for wild-type RGS21 toward GDP-bound $G\alpha_{i1}$ or $G\alpha_q$. **(C)** GST-RGS21 fusion protein or GST alone was immobilized on a biosensor surface exactly as previously described [42]. 200 µl of indicated concentrations of various Gα subunits (in their transition state form) were injected over the biosensor surface. Non-specific binding toward GST alone was subtracted using BiaEvaluation. The binding at t = 590 s was plotted and used for equilibrium binding analyses. The affinities of $G\alpha_{i1}$, $G\alpha_{i2}$, $G\alpha_{i3}$, $G\alpha_o$, and transducin for immobilized RGS21 were determined to be 114 nM (95% C.I. 65-163 nM), 63 nM (95% C.I. 30-95 nM), 61 nM (95% C.I. 25-97 nM), 24 nM (95% C.I. 18-32 nM), and 190 nM (95% C.I. 134-247 nM), respectively. Open symbols denote no binding was detected when the various Gα subunits were in their ground-state, GDP-loaded form.

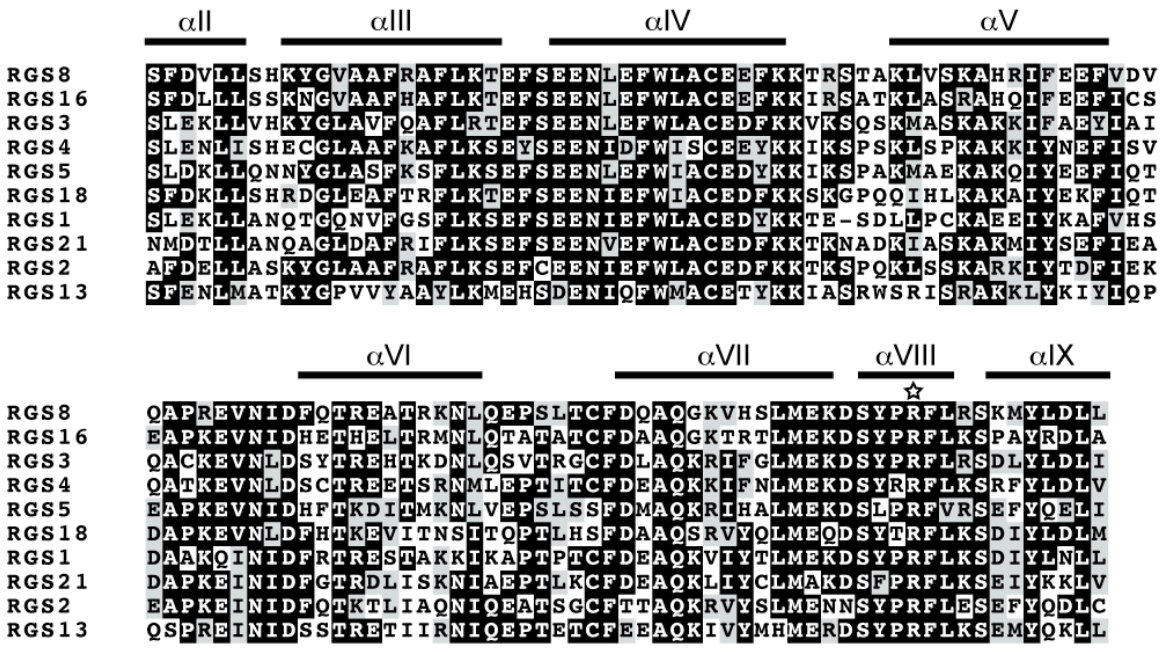

Figure 6.6. Multiple sequence alignment of the RGS domains of all human R4 family members. Sequence alignment of the indicated RGS domains was made using ClustalW [69]. Secondary structure assignments (alpha-helices denoted in Roman numerals) are based on the structure of RGS1 (PDB id 2BV1; [50]). Arg-126 is highlighted with a star; this residue is known to be a highly-conserved, surface-exposed constituent of the Gα-binding "A-site" of RGS domains [50] and its charge-reversal to glutamic acid results in a loss of Gα binding affinity and GAP activity.

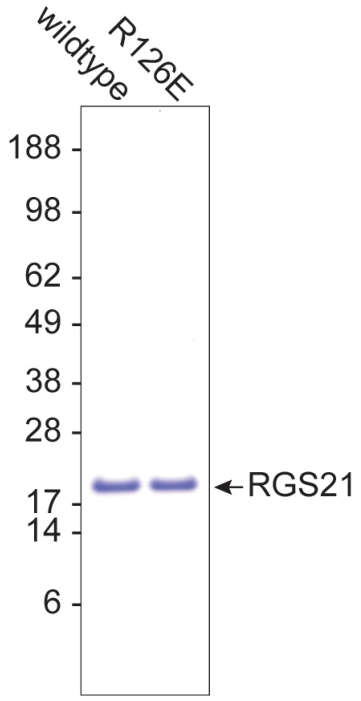

Figure 6.7. Equivalent purification of wildtype RGS21 and RGS21 point-mutant (Arg-126-to-Glu; "R126E"). Proteins used for biochemical analyses in this study are highlighted by Coomassie blue staining after being resolved by SDS-PAGE.

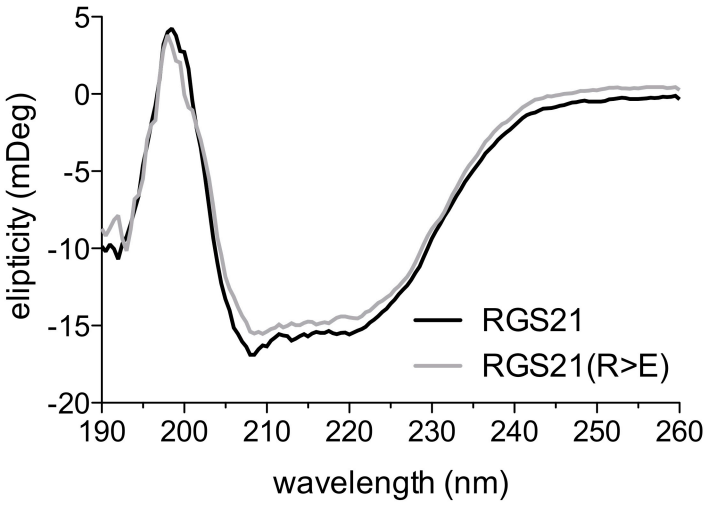

Figure 6.8. Wild-type RGS21 and RGS21(R126E) have similar overall secondary structure. Circular dichroism spectra were separately collected using 0.1 mg/ml of RGS21 and RGS21(R126E) proteins, each diluted in 10 mM potassium phosphate salt (pH 7.5) at 25 °C using a PiStar-180 spectrophotometer (Applied Photophysics, UK). Spectra were collected from 185 nm – 260 nm in 0.5 nm steps with a bandwidth of 2 nm.

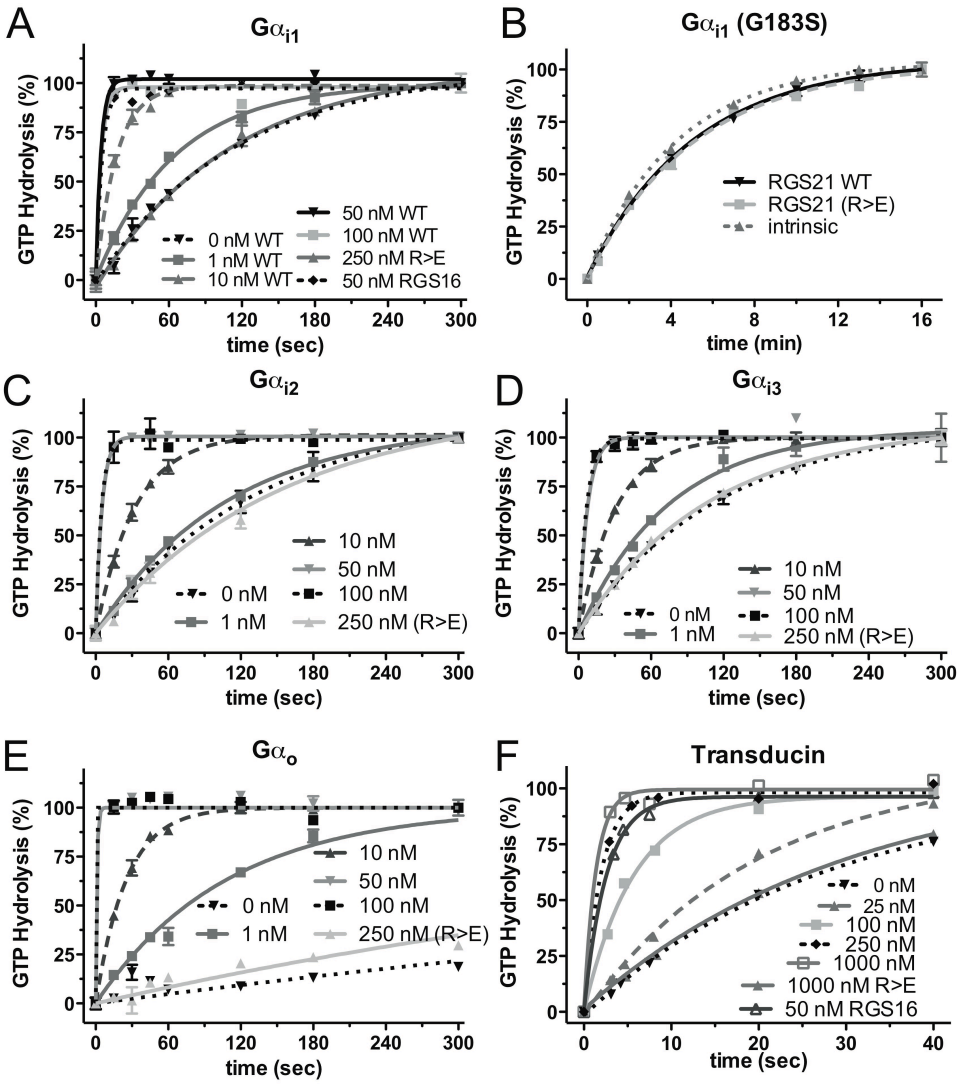

Figure 6.9. RGS21 acts as a GAP for $G_{i/o}$ subfamily Gα subunits. Intrinsic GTPase activity of indicated Gα subunits, as well as RGS protein acceleration of this activity, was determined using [γ-^{32}P]GTP single turnover assays. In the absence of Mg^{2+}, 100 nM of **(A)** $G\alpha_{i1}$, **(B)** RGS-insensitive $G\alpha_{i1}$(G183S), **(C)** $G\alpha_{i2}$, **(D)** $G\alpha_{i3}$, and **(E)** $G\alpha_{oA}$ was preincubated with [γ-^{32}P] GTP at 30 °C for 10 minutes. The reaction was then initiated by the addition of $MgCl_2$ (10 mM), indicated concentration of recombinant RGS protein, and GTPγS (400 μM). At indicated time points, the production of inorganic phosphate was quantified by activated charcoal filtration and subsequent liquid scintillation. **(F)** Transducin assays were conducted on a preformed complex between the G-protein heterotrimer (transducin-αβγ; 2 μM) and rhodopsin (20 μM) and were initiated by the addition of [γ-^{32}P]GTP supplemented with GTP (250 nM) [71]. Nonlinear regression was used to fit the data to a single exponential function using GraphPad PRISM; observed rates are presented in Table 7.1.

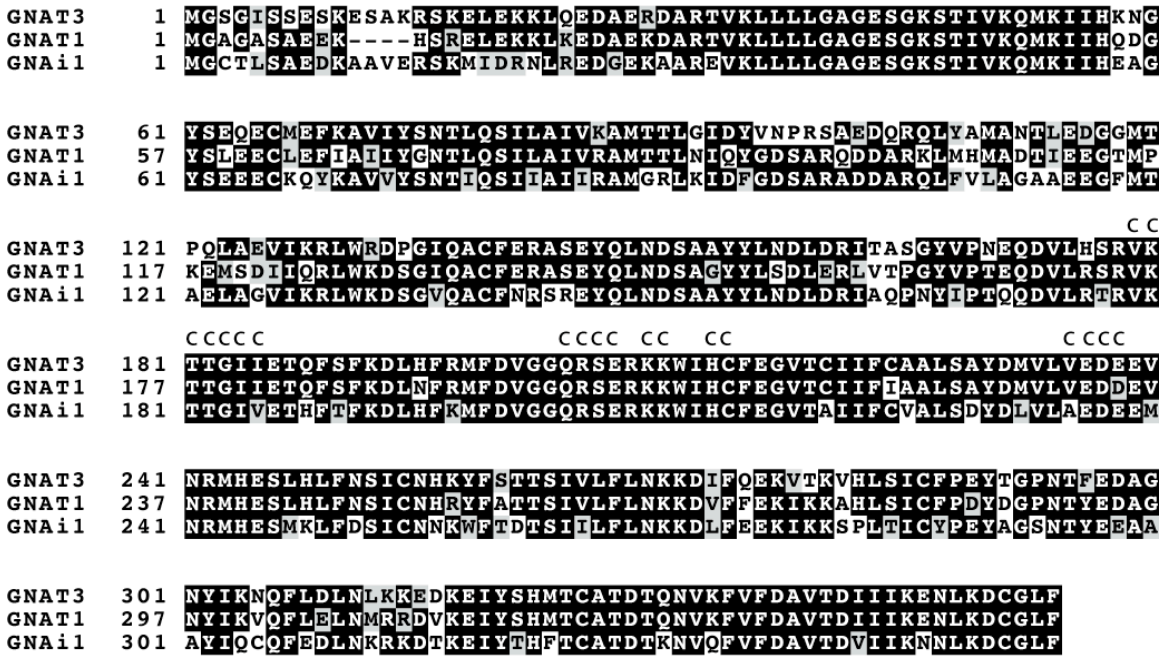

Figure 6.10. Gustducin and transducin Gα subunits have nearly identical interfaces for RGS domains. A protein sequence alignment of human gustducin-α ("GNAT3"; GenBank accession number NP_001095856.1), transducin-α ("GNAT1"; GenBank NP_653082.1), and $G\alpha_{i1}$ ("GNAi1"; GenBank NP_002060.4) was generated using ClustalW [69]. Contacts between the Ras-like domain of transducin-α (Chain A) and the RGS9 RGS domain (Chain B) from the RGS9/transducin structure (PDB ID: 1FQK; ref. [67]) were identified using contact map analysis [72] and are denoted with a "C" above the alignment.

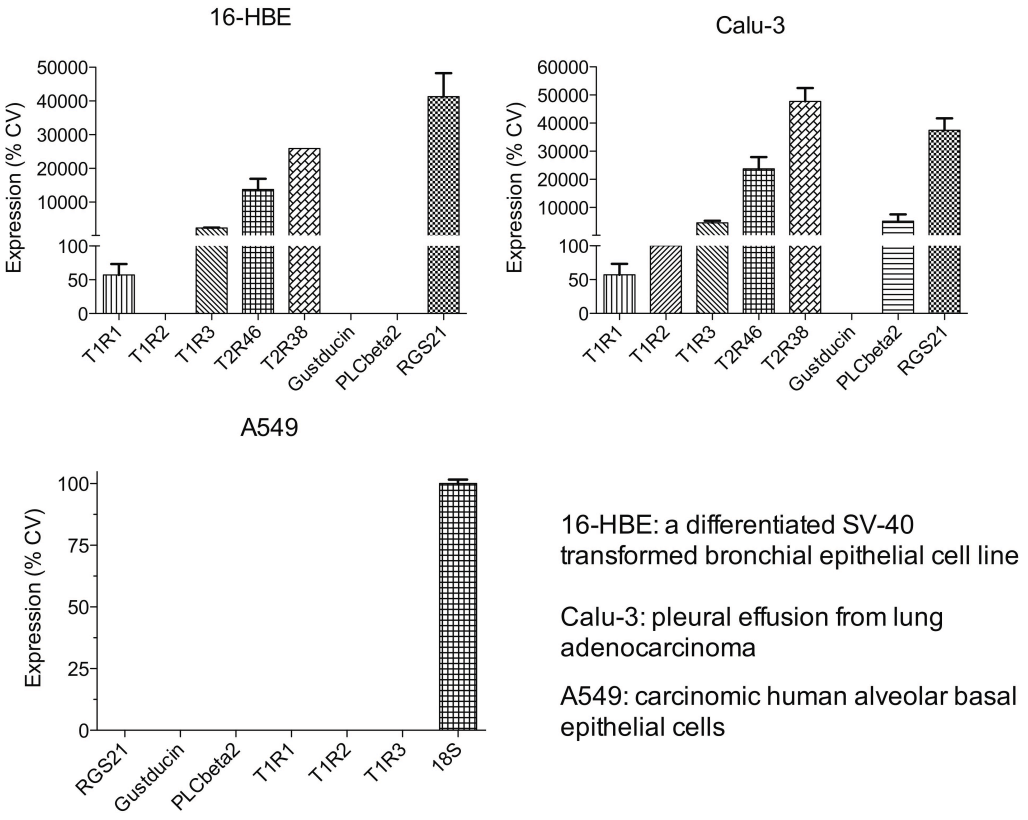

Figure 6.11. Quantitative RT-PCR results demonstrating expression of tastant signaling component transcripts within pulmonary epithelial cell lines 16-HBE and Calu-3, but not the human alveolar epithelium carcinoma cell line A549. Real-time, quantitative RT-PCR using fluorogenic probe detection was performed for the indicated transcripts and normalized to *18S* rRNA signal.

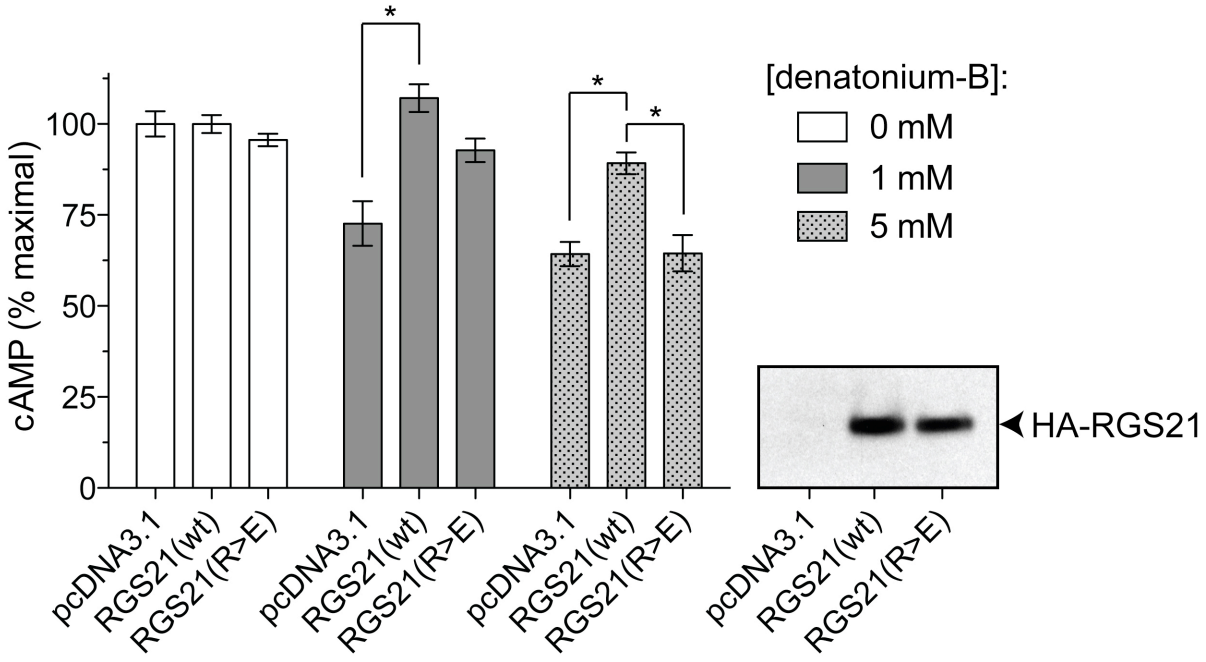

Figure 6.12. Overexpression of wild-type RGS21, but not a loss-of-function, point-mutant RGS21, leads to inhibition of bitter tastant signaling to reduction of cAMP levels in the human airway epithelial cell line 16-HBE. Cultures of the 16-HBE cell line were transiently transfected with Fugene 6 (Roche), the Promega GloSensor cAMP-biosensor cDNA, and expression plasmids containing HA-epitope-tagged open reading frames for wildtype (wt) rat RGS21, or Arg-126-to-Glu point mutated (R>E) rat RGS21, or empty pcDNA3.1 (Invitrogen), as indicated. Inhibition of forskolin-stimulated cAMP production by treatment with indicated concentrations of denatonium-B was determined 24 hours post-transfection by detection of GloSensor-dependent luminescence. *Inset*, Western blot of whole cell lysates of transfected cell cultures with anti-HA-epitope antibody and chemiluminescence detection, demonstrating equivalent expression of wildtype and point-mutant RGS21 proteins. Asterisks denote statistically significant differences, $p < 0.05$ (one-way ANOVA with Bonferroni's post-test).

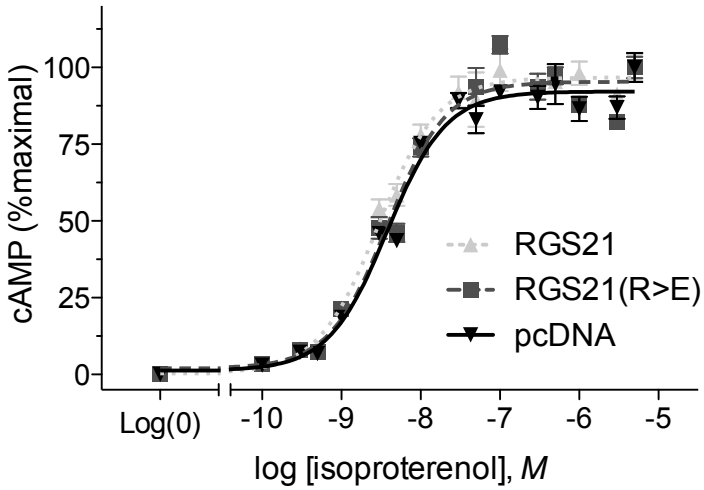

Figure 6.13. Isoproterenol-stimulated production of cAMP is not perturbed by overexpression of RGS21 or RGS21(R126E) in 16-HBE cells. Cells were transfected exactly as described in Figure 6.12. Isoproterenol-induced cAMP production was detected by GloSensor-dependent luminescence. EC_{50} values for isoproterenol were 2.9 nM (95% C.I. 2.3 - 3.7 nM), 3.8 nM (95% C.I. 3.1 - 4.7 nM), and 3.8 nM (95% C.I. 3.1 - 4.7 nM) for 16-HBE cells overexpressing RGS21, RGS21(R126E), and pcDNA3.1 empty vector, respectively.

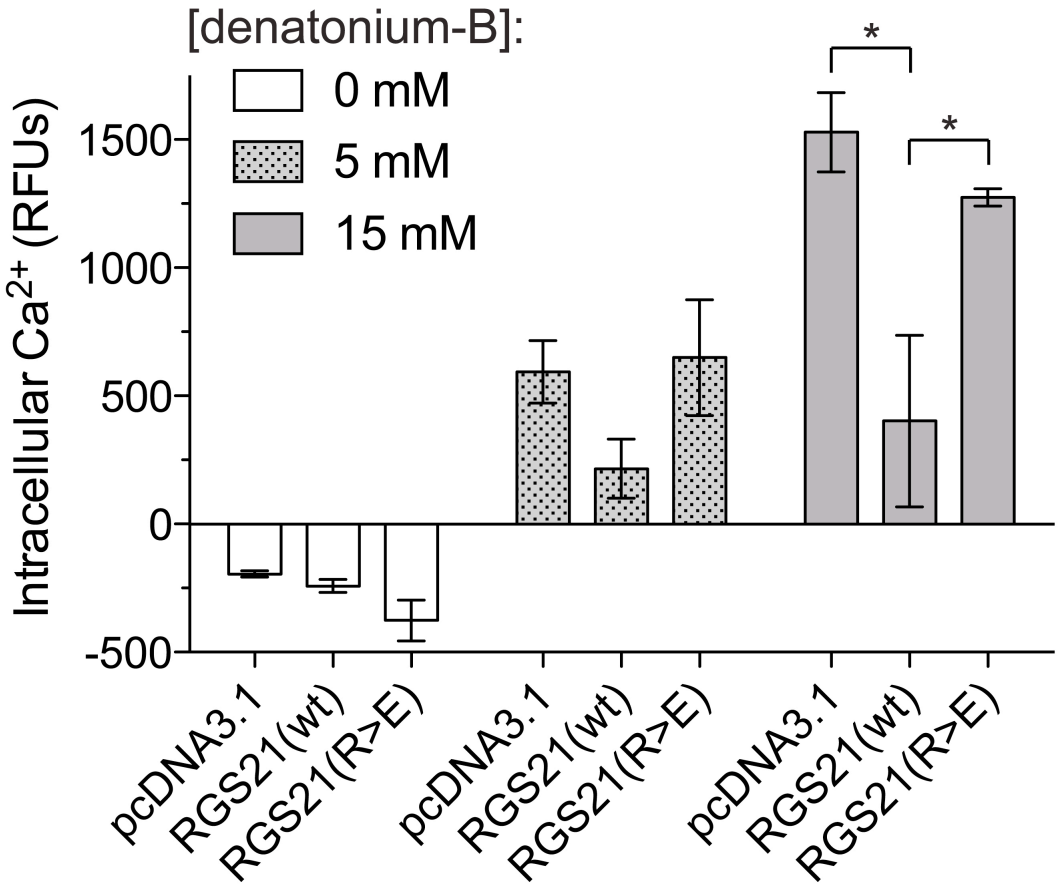

Figure 6.14. Overexpression of wild-type RGS21, but not a loss-of-function, point-mutant RGS21, leads to inhibition of bitter tastant signaling to increased intracellular calcium in the human airway epithelial cell line 16-HBE. Cultures of the 16-HBE cell line were transiently transfected with Fugene 6 (Roche) and expression plasmids containing HA-epitope-tagged open reading frames for wildtype (wt) human RGS21, or Arg-126-to-Glu point mutated (R>E) rat RGS21, or empty pcDNA3.1 (Invitrogen), as indicated. Net peak intracellular calcium production, as elicited by treatment with indicated concentrations of denatonium-B, was determined using calcium indicator dye and FLIPR detection (relative fluorescence units, RFUs), 48 hours post-transfection. Asterisks denote statistically significant differences, $p < 0.05$ (one-way ANOVA with Newman-Keuls post-test).

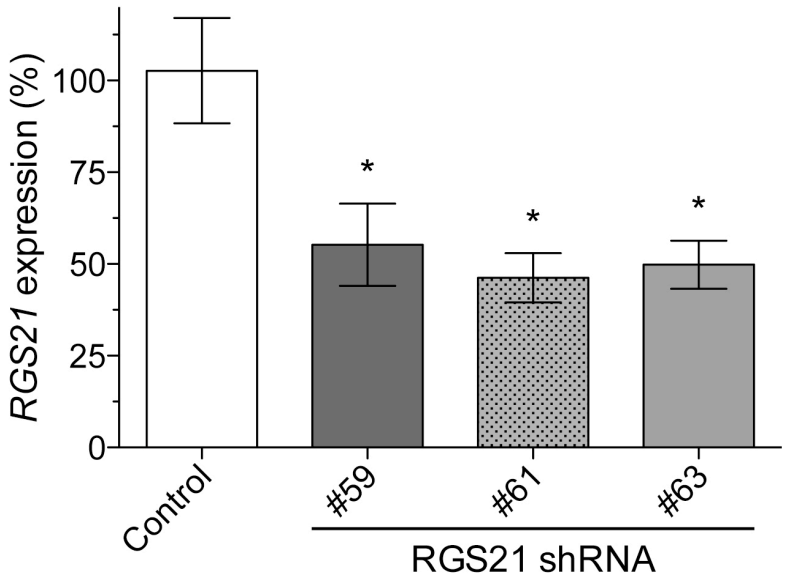

Figure 6.15. Quantitative RT-PCR demonstrating shRNA-mediated knockdown of *RGS21* transcript levels in the stable, lentivirus-transfected variants of the human airway epithelial cell line 16-HBE. Real-time, quantitative PCR using fluorogenic probe detection was performed for the *RGS21* transcript and normalized to *18S* rRNA signal.

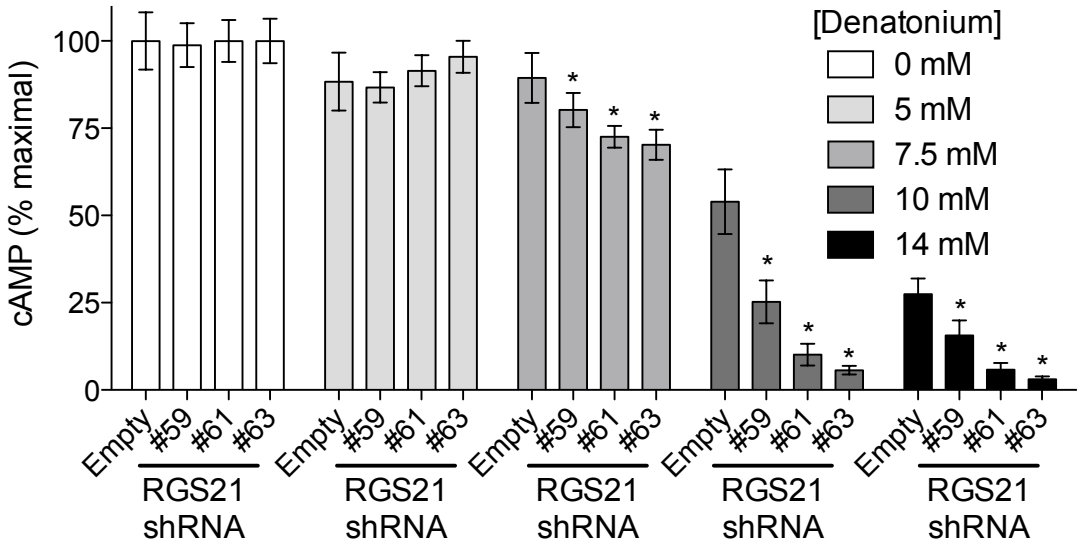

Figure 6.16. shRNA-mediated knockdown of endogenous *RGS21* potentiates bitter tastant signaling to inhibition of cAMP accumulation in the human airway epithelial cell line 16-HBE. The 16-HBE human airway epithelial cell line was stably-transfected with either empty lentivirus ("Empty") or one of three, *RGS21*-directed shRNA-expressing lentiviruses (#59, #61, #63), as indicated. Inhibition of forskolin-stimulated cAMP production by treatment with indicated concentrations of denatonium-B was determined 24 hours post-transfection by detection of GloSensor-dependent luminescence. Asterisks denote statistically significant differences, $p < 0.01$ (one-way ANOVA with Dunnett's Multiple Comparison Test).

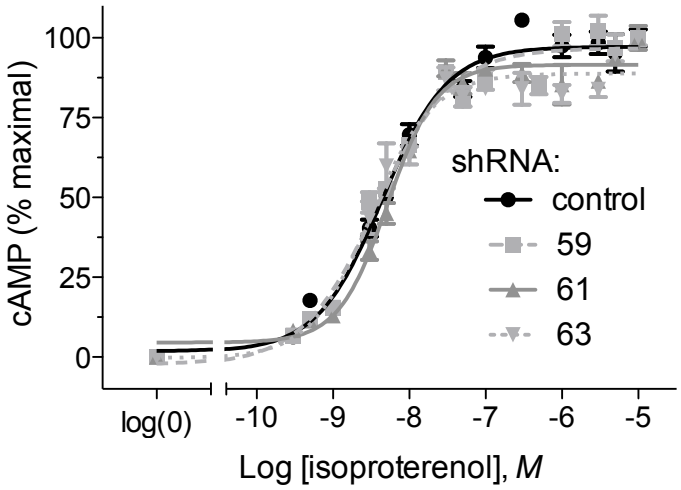

Figure 6.17. Isoproterenol-stimulated production of cAMP is not perturbed by shRNA-mediated knockdown of *RGS21* in 16-HBE cells. Cells were treated exactly as described in Figure 6.13. Stimulation of isoproterenol-induced cAMP production was detected by GloSensor-dependent luminescence. EC_{50} values for isoproterenol were 4.4 nM (95% C.I. 3.6 - 5.5 nM), 3.7 nM (95% C.I. 2.9 - 4.8 nM), 5.2 nM (95% C.I. 4.4 - 6.1 nM), and 3.2 nM (95% C.I. 2.4 - 4.1 nM) for 16HBE cells expressing empty vector control, shRNA#59, shRNA#61, or shRNA#63, respectively.

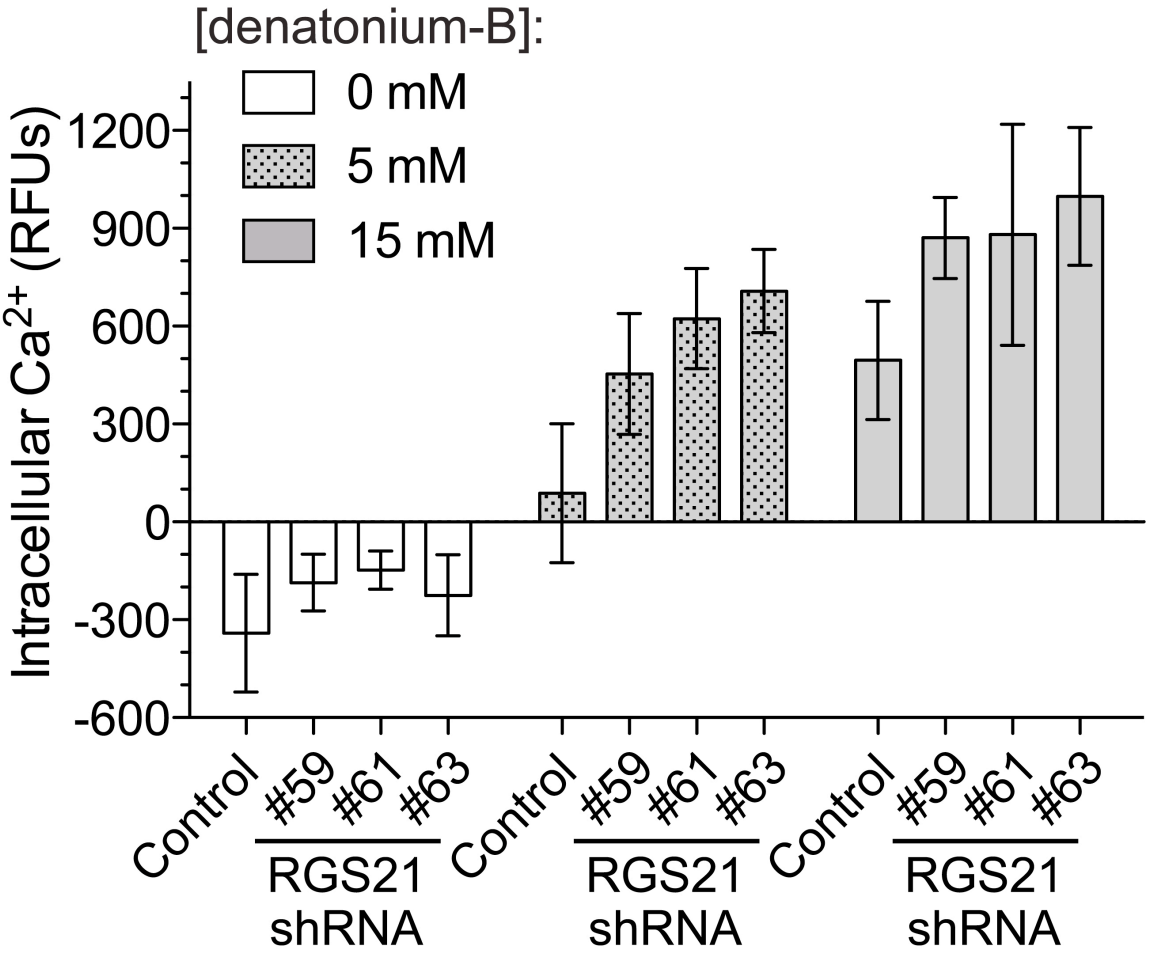

Figure 6.18. shRNA-mediated knockdown of endogenous *RGS21* potentiates bitter tastant signaling to increased intracellular calcium in the human airway epithelial cell line 16-HBE. The 16-HBE human airway epithelial cell line was stably-transfected with either empty lentivirus ("Control") or one of three, *RGS21*-directed shRNA-expressing lentiviruses (#59, #61, #63), as indicated. Net peak intracellular calcium production, as elicited by treatment with indicated concentrations of denatonium-B, was determined using calcium indicator dye and FLIPR detection (relative fluorescence units, RFUs).

Table 6.1. GTP hydrolysis rates observed in single turnover assays. Rates were determined using non-linear regression using GraphPad Prism 5.0 and are expressed in sec^{-1}. 95% confidence intervals are shown in brackets.

RGS21 (nM)	$G\alpha_{i1}$	$G\alpha_{i1}$(G183S)	$G\alpha_{i2}$	$G\alpha_{i3}$	Transducin
0	0.0090 (0.0071-0.011)	0.0039 (0.0036-0.0042)	0.0074 (0.0058-0.0091)	0.0088 (0.0079-0.0097)	0.036 (0.020-0.051)
1	0.015 0.013-0.018	n.d.	0.0092 0.0081-0.010	0.013 (0.010-0.016)	n.d.
10	0.060 (0.051-0.068)	n.d.	0.031 (0.028-0.034)	0.033 (0.030-0.036)	n.d.
25	n.d.	n.d.	n.d.	n.d.	0.051 (0.034-0.067)
50	0.25 (0.11-0.38)	n.d.	0.20 (0.14-0.25)	0.14 (0.10-0.17)	n.d.
100	0.23 (0.078-0.38)	n.d.	0.22 (0.065-0.37)	0.16 (0.12-0.19)	0.18 (0.12-0.23)
250	n.d.	.0033 (0.0029-0.0036)	n.d.	n.d.	0.51 0.35-0.67
250; R126E	0.0090 (0.0071-0.011)	.0033 (0.0029-.0037)	0.0065 (0.0048-0.0082)	0.0093 (0.0083-0.010)	n.d.
1000	n.d.	n.d.	n.d.	n.d.	0.74 0.25-1.2
1000; R126E	n.d.	n.d.	n.d.	n.d.	0.033 (0.013-0.053)

CHAPTER 7

CLINICAL IMPLICATIONS AND FUTURE DIRECTIONS

7.1 GAPS IN THE STRUCTURAL KNOWLEDGE OF RGS PROTEIN / Gα ENGAGEMENT

The original report of the RGS4/$G\alpha_{i1}$ structure by Dr. John Tesmer and colleagues in 1997 initiated a frenzy of structure biology directed towards the RGS protein superfamily [1]. The work of the laboratories of Dr. Sprang, Dr. Tesmer, and Dr. Sigler as well as Natural Science Research Institute in Japan (RIKEN) and the international Structural Genomics Consortium has provided the public domain with nearly 40 NMR and x-ray crystallographic structures of isolated RGS domains and RGS/Gα complexes (Table 7.1). Remarkably, the archetypal RGS/Gα interaction, originally described by the RGS4/$G\alpha_{i1}$ structure, is highly conserved in all complexes of R4 and R7 family members binding $G\alpha_{i1}$, $G\alpha_{i3}$, $G\alpha_{o}$, and transducin-$G\alpha_{i1}$ chimeras [1-4]. While subtle differences can be identified among the complexes, primarily within the Gα all-helical domain/RGS domain interactions [4], the overall mechanism of action and stabilization of the Switch I region of Gα is highly conserved [1-4]. It is doubtful that additional structures of the RGS/$G\alpha_{i}$ family members will provide any novel structural insights. However, there currently is a dearth of structural information regarding how canonical (*i.e.*, GAP-competent) RGS proteins interact with $G\alpha_{q}$, despite the fact that specific RGS domains can interact selectively with $G\alpha_{q}$ (i.e., RGS2) or selectively with $G\alpha_{i}$ and not $G\alpha_{q}$ (e.g., RGS10, RGS12, RGS14, RGS6, RGS7, and RGS20) (Figure 1.8) [4-9]. Complexes of GRK2/$G\alpha_{q}$/Gβγ have been solved; however, the "RGS-homology" domain of GRK2 binds as a $G\alpha_{q}$ effector, using a surface that is distinct from the binding site of canonical RGS domains [10, 11]. Based on the model of $G\alpha_{q}$ from the GRK2/$G\alpha_{q}$/Gβγ structure and the p63RhoGEF/$G\alpha_{q}$/RhoA structure [10, 12], the canonical RGS domain-binding

interface is highly conserved; however, the αB-αC loop of the all helical region of Gα is reoriented in $G\alpha_q$ as compared to $G\alpha_i$ subunits [10]. This perturbation in the all-helical region of $G\alpha_q$ may be a mechanism by which RGS proteins selectively bind Gα subunits. A structure of $G\alpha_q$ in complex with an R4 family RGS protein (*i.e.*, one with canonical GAP activity and no effector function) could therefore help explain the role of the all-helical region in Gα subfamily binding specificity. Chimera and mutagenesis studies have identified critical amino acids within the $G\alpha_q$-selective RGS2 that inhibit its binding to $G\alpha_i$ subunits [13, 14]; in addition, our laboratory has solved a structure of a mutant RGS2 that can bind $G\alpha_i$ (Chapter 2). However, little is known about how wild-type RGS2 selectively engages and accelerates GTP hydrolysis by its native substrate of $G\alpha_q$(GTP).

While the primary binding partner of RGS proteins is the heterotrimeric G-protein α subunit, RGS4 has been demonstrated to bind to phosphatidylinositol-3,4,5-trisphosphate (PIP_3) and Ca^{2+}/calmodulin, in a competitive, mutually exclusive manner, at a distinct site from the Gα-binding interface (Figure 1.10) [15, 16]. Structural information from an RGS domain with PIP_3 or Ca^{2+}/calmodulin bound at this allosteric B-site could provide novel insight into how binding a completely distinct site modifies the catalytic activity of the RGS protein. This information could be used to help design small molecules that could mimic the inhibition or activation by PIP_3 or Ca^{2+}/calmodulin, respectively; such B-site-targeted molecules would be valuable in those clinical or pathological indications where activation of RGS domain GAP activity (rather than inhibition) is desired (*e.g.*, RGS4 function in schizophrenia).

In addition to the PIP_3/Ca^{2+}/calmodulin B-site of R4 family members, RGS proteins are thought to either bind receptors directly [17-19], or through adaptor proteins such as spinophilin [20]. While co-immunoprecipitation studies and pull down assays using cellular lysates have demonstrated that RGS2 interacts with spinophilin [20], it has yet to be shown whether spinophilin can interact directly with RGS2 or if the binding is dependent on other cellular components. A comprehensive biochemical study of RGS/spinophilin and RGS/receptor complexes would help to identify additional targets for NMR or x-ray crystallographic structure determinations that could reveal the molecular mechanism(s) by which RGS proteins engage specific receptors and thereby act in receptor-selective manners in the context of the intact cell.

In addition to future studies investigating the structural basis of RGS domain/$G\alpha_q$ interactions and allosteric modulation of RGS proteins by PIP_3 and Ca^{2+}/calmodulin, an understanding of how RGS12 and RGS14 assemble multiple components of the Ras/Raf/MEK/ERK signaling cascade would broaden our structural understanding of how RGS12 and RGS14 facilitate activation of the MAPK system. Our lab has been at the forefront of understanding how RGS12 and RGS14 use their multi-domain architectures to act as signaling scaffolds (Figure 1.7). In addition to their RGS domain and GoLoco motif (Figure 1.9), both of which interact with adenylyl-cyclase inhibitory $G\alpha$ subunits, RGS12 and RGS14 also contain tandem Ras-binding domains (RBD). Furthermore, RGS12 contains an additional phosphotyrosine binding domain (PTB) and a PSD-95/Dlg/ZO-1 (PDZ) domain [21-23]. In 2007, we reported that RGS12 can bind the nerve growth factor receptor tyrosine kinase TrkA, as well as the downstream signaling components of H-Ras, B-Raf, and MEK2, in an *in vivo* context. By assembling

these components, RGS12 promotes nerve growth factor-mediated neuritogenesis in PC12 cells and axonogenesis in explanted embryonic dorsal root ganglion neurons [23]. Currently, we do not understand the physiological consequences of the seemingly divergent roles of RGS12, which acts as a Gα guanine nucleotide dissociation inhibitor (potentially prolonging signaling from Gβγ subunits), a Gα GAP (terminating heterotrimeric G-protein signaling), and a scaffolding protein (assembling TrkA with H-Ras, B-Raf, and MEK2). Our lab has demonstrated that the GoLoco motif of RGS12 is necessary for the endosomal sub-cellular localization of RGS12 [24]; however, it is not known how the Gα-interacting domains (*i.e.*, RGS domain and GoLoco motif) and the scaffolding domains (*i.e.*, PDZ, PTB, RBD1 and RBD2) allow for RGS12 to integrate signaling from these two signal transduction pathways. Structural information of RGS12 bound to heterotrimeric G-protein binding partners and scaffolding partners would provide insight into whether the binding of components from one signaling system (GPCR *vs* RTK) affects the other system. It is possible that association of Gα with RGS12 via its RGS domain or GoLoco motif inhibits or facilitates the binding of TrkA, H-Ras, B-Raf, and/or MEK2. An additional question to resolve is the nature of the binding exhibited by RGS12 both to activated H-Ras and to B-Raf. It is known that the N-terminal RBD of B-Raf binds H-Ras(GTP) [25]. Our lab has subsequently demonstrated that RGS12 directly binds H-Ras(GTP) via its first RBD and overexpresion of activated H-Ras enhances precipitation of a B-Raf/H-Ras(GTP)/RGS12 complex [23]. However the particular mode of engagement by which two RBD-containing proteins (B-Raf & RGS12) bind to activated H-Ras simultaneously remains enigmatic; thus, future

biochemical and structural studies will be required to allow us to define the mechanism of this binding.

None of the approximately 40 structures of RGS proteins currently in the public domain are of non-mammalian RGS proteins. Our laboratory is well suited to solve structures of non-mammalian RGS domain/Gα pairs. For example, our lab has described a unique seven-transmembrane domain RGS protein in the model plant organism Arabidopsis [26-28] and a unique RGS domain-containing RhoGEF in *Entamoeba histolytica*, as well as its cognate Gα (manuscript in preparation). Structures of unique and evolutionarily divergent RGS protein/Gα complexes would provide an understanding of how RGS proteins have evolved. Based on mutagenesis studies of the *Arabidopsis thaliana* Gα subunit, it is likely that the RGS domain/Gα interaction does not occur in the canonical manner depicted by the known mammalian RGS domain/Gα structures; specifically, mutation of the switch I glycine in Arabidopsis Gα (analogous to G183S in human $G\alpha_{i1}$) does not result in a RGS-insensitive Gα subunit (Dr. Francis Willard, personal communication). The RGS-RhoGEF of *E. histolytica* also appears to bind its EhGα partner in a unique manner. The RGS-insensitive mutation to the switch I glycine that is used to produce RGS-insensitive Gα subunits (e.g., mammalian $G\alpha_{i1}$, $G\alpha_{i2}$, $G\alpha_{o}$, $G\alpha_{q}$; yeast Gpa1 [29-32]) does not result in a loss of binding between $G\alpha_{13}$ and p115RhoGEF, the archetypal mammalian RGS-RhoGEF [33]; in contrast to these mammalian proteins, the RGS-insensitivity mutation is able to abolish binding between EhGα and EhRGS-RhoGEF (manuscript in preparation), indicating that this *E. histolytica* RGS-RhoGEF engages heterotrimeric G-protein subunits by a mechanism distinct from its mammalian counterparts.

7.2 THE PROMISE OF SMALL MOLECULE MODULATORS OF RGS PROTEINS

Even with a significant amount of effort from the pharmaceutical industry and academic laboratories trying to identify small molecule inhibitors of RGS domain GAP activity, the field still has a dearth of validated small molecule inhibitors that function *in vivo.* Despite this, we remain committed to identifying small molecule modulators of RGS proteins and validating RGS proteins as viable therapeutic targets. All *in vitro* high throughput screens that have been performed have been dependent on identifying small molecules that disrupt the binding of the RGS protein to the Gα [34, 35] and, by their very design, cannot identify small molecules that bind allosterically and potentiate GAP activity, nor could they identify small molecules that trap the RGS domain/Gα interaction in a stable complex. The adoption of measuring RGS domain/Gα binding as a proxy for RGS domain-accelerated GTP hydrolysis in screening assays arose because the gold standard assay used to quantify RGS activity involves multiple discrete steps difficult to miniaturize and automate for high-throughput screening campaigns. First the Gα is loaded with ^{32}P-GTP in the absence of Mg^{2+}, then the assay is initiated by the addition of Mg^{2+}, an RGS protein, and excess GTPγS, and finally timed aliquots starting at zero seconds are sampled, which requires centrifugation, separation of the supernatants, and then liquid scintillation. This "single turnover" assay design was required because GDP release (instead of GTP hydrolysis) was always the rate-limiting step of the guanine nucleotide cycle (Figure 1.1). In Chapter 4, we described development of a fluorescent, homogeneous assay that can be used to measure GAP activity of RGS proteins using an

automatable, high-throughput design. It is our hope that, in the future, the Transcreener GDP assay will be used to identify both inhibitory and potentiating small molecules and will provide higher sensitivity than traditional binding assays.

While we have previously stressed the desire to identify small molecules that interact with either the A-site or B-site of RGS domains (Figure 1.10), another possible interaction point exists to target with small molecules. The N-terminal helices, which lay outside of the canonical RGS domain on most R4 RGS proteins, have been demonstrated to provide receptor selectivity to RGS-mediated negative regulation of GPCR signaling [19, 36] and evidence exists that these N-terminal helices can engage receptors either directly or via adaptor proteins [17, 20]. While the molecular mechanisms and structural details of these interactions remain to be elucidated (see Section 7.1 above), targeting the RGS protein/GPCR interaction with small molecules may provide a valuable alternative to targeting the RGS domain/Gα interface. Such an approach is supported by the observation that RGS2 is mislocalized because of a single, SNP-induced point mutation in its N-terminus, a region outside of the canonical catalytic domain; this SNP results in enhanced vasoconstrictive signaling and subsequent hypertension in humans, reminiscent of the phenotype that is observed in RGS2-deficient mice [37, 38]. The possibility that RGS proteins are interacting with the third intracellular loop of GPCRs [17, 39] also suggests that a small molecule that interacts with the GPCR at its intracytosolic interface could perhaps destabilize (or conversely stabilize) the RGS protein/GPCR interaction and thereby inhibit (or enhance) the negative regulatory activity of the RGS protein on GPCR signal transduction.

The yeast-based high-throughput screen [40-42] for small molecule inhibitors of RGS protein activity is the only screen in the literature to date that was directed at identifying RGS protein inhibitors without using purified components *in vitro*. We have actively avoided using cellular systems to screen for small molecule RGS protein modulators because of the high day-to-day variability, the convoluted manner of quantifying the RGS protein $G\alpha_i$-directed GAP activity on an inhibitory system (*i.e.*, measuring compound inhibition of RGS protein inhibition of $G\alpha_i$-mediated inhibition of adenylyl cyclase activity), and the inherent difficulty in identifying the ultimate molecular target of a small molecule that is first discovered in a cellular screen; however, the advent of robust non-radioactive assays to quantify intracellular Ca^{2+} (*e.g.*, FLIPR assays) and cAMP content (*e.g.*, Promega GloSensor) should encourage us to reconsider cell-based assays.

Because many RGS proteins act on adenylyl-cyclase inhibitory $G\alpha$ subunits ($G\alpha_i$ subfamily members), quantification of forskolin-induced cAMP accumulation has been a common cellular assay to quantify the activity of RGS proteins [43, 44]; however, historically these assays have been low-throughput, radioactive assays [45-47]. The advent of robust, luminescence screens for real-time quantification of cAMP levels opens the possibility of performing screens for RGS protein inhibitors using cell lines. Currently there are a wide variety of commercial, non-radioactive assays for quantifying cAMP including "CatchPoint cyclic-AMP" (Molecular Devices; Sunnyvale, CA), "HitHunter™ cAMP" (DiscoverRX; Fremont, CA), "MSD® cAMP" (Meso Scale Discovery; Gaither, MD), and "GloSensor™" (Promega; Madison, WI). (For a more complete review of available cAMP assay, we refer the reader to: [48]). We have

successfully used the GloSensor™, a luminescence-based cAMP assay, in live cells to quantify changes in cAMP levels in response to overexpressed, mutant RGS2 (*i.e.*, mutated to act on $G\alpha_i$ subunits; Figure 2.8). It may be possible, with optimization, to configure this assay to be used to detect small molecule modulators of RGS protein $G\alpha_i$-directed GAP activity. One of the advantages of using such an approach is that the candidate molecules identified will likely be cell-permeable and thus will not require extensive medicinal chemistry efforts to make primary hits cell-permeable.

The benefits of many therapeutic drugs are often not without negative consequences. For example, many patients undergoing chemotherapy experience severe neutropenia or anemia and therefore treatment with adjuvant drugs such as granulocyte stimulating factor or erythropoietin has been formulated to allow patients to maintain their chemotherapeutic regimens [49, 50]. Currently the primary therapeutic option for cognitive impairment, such as Alzheimer's disease, increases acetylcholine levels by targeting acetylcholine esterase activity [51]. However, increased acetylcholine levels results in increased signaling at all muscarinic and nicotinic receptors and, while the improvement in cognition is mediated by $G\alpha_q$-coupled muscarinic receptors, adverse effects such as bradycardia result from agonism of $G\alpha_i$-coupled muscarinic receptors. Up to 15% of patients report discontinuing the use of acetylcholine esterase inhibitors because of the side effects [52, 53]. Given the highly selective RGS2/$G\alpha_q$ interaction (Chapter 2), administration of a subtherapeutic dose of an acetylcholine esterase inhibitor along with an RGS2-selective inhibitor could enhance the cognition improving effects of the additional acetylcholine generated on $G\alpha_q$-muscarinic receptors while minimizing the $G\alpha_i$-muscarinic receptor-mediated nausea and diarrhea.

While the challenge of identifying a new drug class is daunting -- there are potentially hundreds of Gα/RGS protein interactions that could be targeted (not even considering receptor/Gα/RGS protein combinations) -- there must be at least one compound in all of chemical space that can modulate RGS protein activity. We just have to find it.

7.3 RGS21, A NOVEL REGULATOR OF GUSTATION?

The work presented in Chapter 6 has comprehensively characterized the biochemical properties of RGS21; however, there remains a myriad of experimental questions regarding the role of RGS21 in the perception of taste. To more fully understand the role of RGS21 in gustation, it seems essential to develop a mouse deficient in RGS21 expression and assess the changes in gustation that result from this deficiency. Even with the knowledge that RGS21 can act as a GAP *in vitro* for $G\alpha_{i1,i2,i3,o}$ and transducin subunits, and inhibits bitter signaling in cellular assays (Chapter 6), it is difficult to predict *a priori* how RGS21 may affect the perception of bitter, sweet, and/or umami compounds in an entire organism. An example of an RGS protein with an unexpected chemosensory phenotype comes from *C. elegans,* which has a sensory-specific RGS protein: Rgs-3. *C. elegans* worms deficient in Rgs-3 expression have normal development and motor function, but are unable to respond to chemoattractants such as isoamyl alcohol at levels which would ordinarily invoke a response in *C. elegans* [54]. Interestingly, as the concentration of isoamyl alcohol is decreased, Rgs-3 deficient worms regain the ability to respond to isoamyl alcohol [54]. It is plausible that RGS21 plays a similar role by which it dampens tastant signaling so that the gustatory system is not

overwhelmed when molecules are overly abundant on the lingual epithelium. To test how RGS21 might act to regulate taste, I would initially use a two-bottle taste test on wildtype mice and RGS21-deficient mice. In one bottle, normal water is present and, in the second bottle, water with a known concentration of either a bitter, sweet, or umami compound is present. Over a 24-hour period, the consumption of each bottle is recorded, and the preference can be calculated based on consumption of the experimental water (containing bitter, sweet, or umami) compared to the total consumption of water during the time period. It seems likely that the removal of a negative regulator of taste would allow RGS21-deficient mouse strains to detect the appetitive effects of sweeteners at concentrations below the detection limit of wild-type animals. This apparent increase in potency of appetitive compounds would result in a left-shift of the dose-response curve; however, based upon the results seen with Rgs-3 in *C. elegans*, it may be possible to have a left-shift at lower concentrations of an appetitive compound but also a total loss of perception at high concentrations. This could occur if RGS21 is crucial to preventing the gustatory system from being saturated by high tastant concentrations.

It is possible that the taste perception phenotype of RGS21-deficient mice may be too subtle to be observed using such a method; in that case, recordings from the chorda tympani (the nerve responsible for the transduction of lingual chemosensory signal to the brain) could be used to monitor action potentials generated upon administration of bitter, sweet, or umami compounds directly to the circumvallate papillae. The advantage of conducting this type of study is that it removes the integration of other complex inputs that occur once tastant-induced action potentials reach the brain.

In addition to having a negative regulatory role in gustation, we expect RGS21 could also be regulating "local gustation" in the digestive tract. While conscious perception of taste is mediated only through lingual chemosensory cells, evidence is rapidly emerging that bitter and sweet taste receptors are also expressed in enteroendocrine cells and modulate glucagon-like peptide (GLP-1) and insulin levels in response to ingested bitter and sweet compounds [55-57]. I hypothesize that RGS21 suppresses basal activation of taste receptors in enteroendocrine cells. If this hypothesis is true, I expect that RGS21-deficient mice would have a higher fasting insulin levels; chronically, this condition could result in the development of insulin resistance. In contrast to the previous report of *Rgs21* transcripts being expressed exclusively in the circumvallate papillae [58], we have identified *Rgs21* transcripts in digestive and pulmonary tissues using RNA isolated from these organs; however, these results need to be followed up with work defining the particular subset(s) of cells in the lungs and in the digestive tract that express RGS21. We have unsuccessfully attempted to make monoclonal antibodies against two different RGS21-derived immunogens, and *in situ* hybridization has proven difficult in lung tissue slides derived from rodents; thus, it would be useful to develop a transgenic animal that used the *Rgs21* promoter to drive the expression of a fluorescent protein marker (e.g., mCherry). The creation of a mouse line that expressed a fluorescent reporter would allow us to perform cross-breeding with T1R3/YFP, Gustducin/GFP, PLCβ2/GFP, and/or TRPM5/GFP transgenic mouse strains that have been created by other labs [59-61]. These initial crosses, in conjunction with fluorescence-based detection of markers indicating expression of tastant signaling components, would provide conclusive evidence as to what subset(s) of taste cells

express RGS21 in lingual epithelium and also allow us to identify RGS21-expressing chemosensory cells in pulmonary and digestive epithelia.

Our discovery that mRNA transcripts for RGS21 and taste receptors are expressed in a human bronchial epithelial cell line (16-HBE) and a human pulmonary epithelial cell line (Calu-3) was initially surprising, as these cell lines are typically used as a model for cystic fibrosis research; however, contemporaneous with our discovery of *RGS21* expression in 16-HBE cells, Shah and colleagues reported that bitter compounds increase the ciliary beat frequency of airway cells [62]. This published report was the first evidence of gustatory components having a functional role in pulmonary epithelium. Both 16-HBE and Calu-3 cell lines are frequently used in cystic fibrosis research because of their native expression of Cystic Fibrosis Transmembrane conductance Regulator (CFTR). This anion channel is expressed in epithelial cells in the lungs, pancreas, intestines, reproductive tract, and sweat glands [63]. Classically, upon phosphorylation of the CFTR regulatory "R" domain by Protein Kinase A (PKA) in an ATP-dependent manner, the CFTR channel opens to allow the movement of chloride ions onto the apical epithelial surface [64, 65]. The excess negative charge generated by the CFTR on the epithelial surface results in the movement of sodium ions to neutralize the electrical gradient. The excess sodium chloride on the epithelial surfaces causes the movement of water – decreasing the viscosity of the mucus [66]. While the PKA activation of CFTR chloride conductance is well established, the mechanism of CFTR activation *in vivo* is much more complex. In addition to cAMP activation of PKA, activation of the $G\alpha_q$ coupled P2-puringeric receptor ($P2Y_2$) results in a transient increase in intracellular Ca^{2+} mediating a protein kinase C (PKC)-dependent activation of the CFTR [67, 68] and

activation of the Ca^{2+}-dependent Cl^- channels [69, 70]. Given that gustatory signaling can both inhibit adenylyl cyclase via the G-protein α subunit and stimulate Ca^{2+} release by Gβγ activation of PLC-β2 I hypothesize that activation of bitter receptors in lung epithelial cell lines (and the native pulmonary epithelium) modulates CFTR-driven chloride efflux. In order to protect the airway from the inhalation of potentially toxic substances, it would be logical for T2R activation by bitter compounds to result in increased CFTR function to facilitate clearance of the toxic substance from the lung. This type of response would be consistent with the increased ciliary beat frequency observed in pulmonary epithelial cells in response to bitter substances [62] and would also be consistent with the observation that bitter compounds, when applied to *ex vivo* intestinal tissue, results in an increased Cl^- and HCO_3^- secretions [71]. If bitter receptors play a protective role in the airway, I would expect that endogenous RGS21 levels serve to antagonize the effects of bitter compounds on T2Rs. Specifically, in a RGS21-deficient mouse, the administration of bitter compounds should result in an exaggerated mucociliary clearance compared to wild-type mice; however, it is possible that the decreased level of cAMP production, mediated by adenylyl-cyclase inhibitory Gα subunits left unchecked by RGS21 GAP activity, could result in deactivation of CFTR function – a counterproductive response for the RGS21-deficient mouse to exhibit to a bitter inhalant challenge.

While the work presented in this dissertation has provided convincing evidence that RGS21 is a biochemically active negative regulator of Gα subunits and that RGS21 is expressed selectively in chemosensory cells, this work has resulted in more

unanswered questions regarding the physiological role of RGS21 in the protection of airways and in the perception of taste.

While the ability to enjoy savory foods or the bitterness of a cup of coffee may seem like a unnecessary luxury, it has been noted that taste is the only external sensory system that is necessary for life [72]. Individuals born with a complete loss of vision, hearing, or smell are able to adapt and function in society; however few, if any, reports of congenital ageusia (loss of taste) in humans exist [72]. A significant proportion (35-70%) of patients who undergo radiation therapy for head and neck cancers report a loss of taste that remains after a year, and this loss of taste correlates with weight loss [73, 74]. When the loss of the pleasurable experience of consuming caloric (sweet) food is removed patients must be vigilant to maintain body mass.

In addition to clinicians working with patients with head and neck cancers, pediatricians are well aware of the clinical consequences of gustation. One of the main factors of non-compliance among pediatric populations is the predominant bitter taste of many xenobiotics [75-77]. Additional research into blocking the activation of bitter receptors by xenobiotics would allow prescribed pharmaceuticals to be taken more consistently and allow their full therapeutic potential to be realized.

7.4 REFERENCES

1. Tesmer, J.J., D.M. Berman, A.G. Gilman, and S.R. Sprang, *Structure of RGS4 bound to AlF4--activated G(i alpha1): stabilization of the transition state for GTP hydrolysis.* Cell, 1997. 89(2): p. 251-61.

2. Slep, K.C., M.A. Kercher, W. He, C.W. Cowan, T.G. Wensel, and P.B. Sigler, *Structural determinants for regulation of phosphodiesterase by a G protein at 2.0 A.* Nature, 2001. 409(6823): p. 1071-7.

3. Slep, K.C., M.A. Kercher, T. Wieland, C.K. Chen, M.I. Simon, and P.B. Sigler, *Molecular architecture of Galphao and the structural basis for RGS16-mediated deactivation.* Proc Natl Acad Sci U S A, 2008. 105(17): p. 6243-8.

4. Soundararajan, M., F.S. Willard, A.J. Kimple, A.P. Turnbull, L.J. Ball, G.A. Schoch, C. Gileadi, O.Y. Fedorov, E.F. Dowler, V.A. Higman, S.Q. Hutsell, M. Sundstrom, D.A. Doyle, and D.P. Siderovski, *Structural diversity in the RGS domain and its interaction with heterotrimeric G protein alpha-subunits.* Proc Natl Acad Sci U S A, 2008. 105(17): p. 6457-62.

5. Posner, B.A., A.G. Gilman, and B.A. Harris, *Regulators of G protein signaling 6 and 7. Purification of complexes with gbeta5 and assessment of their effects on g protein-mediated signaling pathways.* J Biol Chem, 1999. 274(43): p. 31087-93.

6. Snow, B.E., A.M. Krumins, G.M. Brothers, S.F. Lee, M.A. Wall, S. Chung, J. Mangion, S. Arya, A.G. Gilman, and D.P. Siderovski, *A G protein gamma subunit-like domain shared between RGS11 and other RGS proteins specifies binding to Gbeta5 subunits.* Proc Natl Acad Sci U S A, 1998. 95(22): p. 13307-12.

7. Hollinger, S., J.B. Taylor, E.H. Goldman, and J.R. Hepler, *RGS14 is a bifunctional regulator of Galphai/o activity that exists in multiple populations in brain.* J Neurochem, 2001. 79(5): p. 941-9.

8. Hunt, T.W., T.A. Fields, P.J. Casey, and E.G. Peralta, *RGS10 is a selective activator of G alpha i GTPase activity.* Nature, 1996. 383(6596): p. 175-7.

9. Snow, B.E., R.A. Hall, A.M. Krumins, G.M. Brothers, D. Bouchard, C.A. Brothers, S. Chung, J. Mangion, A.G. Gilman, R.J. Lefkowitz, and D.P. Siderovski, *GTPase activating specificity of RGS12 and binding specificity of an alternatively spliced PDZ (PSD-95/Dlg/ZO-1) domain.* J Biol Chem, 1998. 273(28): p. 17749-55.

10. Tesmer, V.M., T. Kawano, A. Shankaranarayanan, T. Kozasa, and J.J. Tesmer, *Snapshot of activated G proteins at the membrane: the Galphaq-GRK2-Gbetagamma complex.* Science, 2005. 310(5754): p. 1686-90.

11. Shankaranarayanan, A., D.M. Thal, V.M. Tesmer, D.L. Roman, R.R. Neubig, T. Kozasa, and J.J. Tesmer, *Assembly of high order G alpha q-effector complexes with RGS proteins.* J Biol Chem, 2008. 283(50): p. 34923-34.

12. Lutz, S., A. Shankaranarayanan, C. Coco, M. Ridilla, M.R. Nance, C. Vettel, D. Baltus, C.R. Evelyn, R.R. Neubig, T. Wieland, and J.J. Tesmer, *Structure of Galphaq-p63RhoGEF-RhoA complex reveals a pathway for the activation of RhoA by GPCRs.* Science, 2007. 318(5858): p. 1923-7.

13. Heximer, S.P., S.P. Srinivasa, L.S. Bernstein, J.L. Bernard, M.E. Linder, J.R. Hepler, and K.J. Blumer, *G protein selectivity is a determinant of RGS2 function.* J Biol Chem, 1999. 274(48): p. 34253-9.

14. Kimple, A.J., M. Soundararajan, S.Q. Hutsell, A.K. Roos, D.J. Urban, V. Setola, B.R. Temple, B.L. Roth, S. Knapp, F.S. Willard, and D.P. Siderovski, *Structural determinants of G-protein alpha subunit selectivity by regulator of G-protein signaling 2 (RGS2).* J Biol Chem, 2009. 284(29): p. 19402-11.

15. Sowa, M.E., W. He, T.G. Wensel, and O. Lichtarge, *A regulator of G protein signaling interaction surface linked to effector specificity.* Proc Natl Acad Sci U S A, 2000. 97(4): p. 1483-8.

16. Popov, S.G., U.M. Krishna, J.R. Falck, and T.M. Wilkie, *Ca2+/Calmodulin reverses phosphatidylinositol 3,4, 5-trisphosphate-dependent inhibition of regulators of G protein-signaling GTPase-activating protein activity.* J Biol Chem, 2000. 275(25): p. 18962-8.

17. Bernstein, L.S., S. Ramineni, C. Hague, W. Cladman, P. Chidiac, A.I. Levey, and J.R. Hepler, *RGS2 binds directly and selectively to the M1 muscarinic acetylcholine receptor third intracellular loop to modulate Gq/11alpha signaling.* J Biol Chem, 2004. 279(20): p. 21248-56.

18. Wang, Q., L.Y. Liu-Chen, and J.R. Traynor, *Differential modulation of mu- and delta-opioid receptor agonists by endogenous RGS4 protein in SH-SY5Y cells.* J Biol Chem, 2009. 284(27): p. 18357-67.

19. Xu, X., W. Zeng, S. Popov, D.M. Berman, I. Davignon, K. Yu, D. Yowe, S. Offermanns, S. Muallem, and T.M. Wilkie, *RGS proteins determine signaling specificity of Gq-coupled receptors.* J Biol Chem, 1999. 274(6): p. 3549-56.

20. Wang, X., W. Zeng, A.A. Soyombo, W. Tang, E.M. Ross, A.P. Barnes, S.L. Milgram, J.M. Penninger, P.B. Allen, P. Greengard, and S. Muallem, *Spinophilin regulates Ca2+ signalling by binding the N-terminal domain of RGS2 and the third intracellular loop of G-protein-coupled receptors.* Nat Cell Biol, 2005. 7(4): p. 405-11.

21. Shu, F.J., S. Ramineni, and J.R. Hepler, *RGS14 is a multifunctional scaffold that integrates G protein and Ras/Raf MAPkinase signalling pathways.* Cell Signal. 22(3): p. 366-76.

22. Willard, F.S., M.D. Willard, A.J. Kimple, M. Soundararajan, E.A. Oestreich, X. Li, N.A. Sowa, R.J. Kimple, D.A. Doyle, C.J. Der, M.J. Zylka, W.D. Snider, and D.P. Siderovski, *Regulator of G-protein signaling 14 (RGS14) is a selective H-Ras effector.* PLoS One, 2009. 4(3): p. e4884.

23. Willard, M.D., F.S. Willard, X. Li, S.D. Cappell, W.D. Snider, and D.P. Siderovski, *Selective role for RGS12 as a Ras/Raf/MEK scaffold in nerve growth factor-mediated differentiation.* EMBO J, 2007. 26(8): p. 2029-40.

24. Sambi, B.S., M.D. Hains, C.M. Waters, M.C. Connell, F.S. Willard, A.J. Kimple, S. Pyne, D.P. Siderovski, and N.J. Pyne, *The effect of RGS12 on PDGFbeta receptor signalling to p42/p44 mitogen activated protein kinase in mammalian cells.* Cell Signal, 2006. 18(7): p. 971-81.

25. Wittinghofer, A. and C. Herrmann, *Ras-effector interactions, the problem of specificity.* FEBS Lett, 1995. 369(1): p. 52-6.

26. Chen, J.G., F.S. Willard, J. Huang, J. Liang, S.A. Chasse, A.M. Jones, and D.P. Siderovski, *A seven-transmembrane RGS protein that modulates plant cell proliferation.* Science, 2003. 301(5640): p. 1728-31.

27. Johnston, C.A., J.P. Taylor, Y. Gao, A.J. Kimple, J.C. Grigston, J.G. Chen, D.P. Siderovski, A.M. Jones, and F.S. Willard, *GTPase acceleration as the rate-limiting step in Arabidopsis G protein-coupled sugar signaling.* Proc Natl Acad Sci U S A, 2007. 104(44): p. 17317-22.

28. Willard, F.S. and D.P. Siderovski, *Purification and in vitro functional analysis of the Arabidopsis thaliana regulator of G-protein signaling-1.* Methods Enzymol, 2004. 389: p. 320-38.

29. Apanovitch, D.M., K.C. Slep, P.B. Sigler, and H.G. Dohlman, *Sst2 is a GTPase-activating protein for Gpa1: purification and characterization of a cognate RGS-Galpha protein pair in yeast.* Biochemistry, 1998. 37(14): p. 4815-22.

30. DiBello, P.R., T.R. Garrison, D.M. Apanovitch, G. Hoffman, D.J. Shuey, K. Mason, M.I. Cockett, and H.G. Dohlman, *Selective uncoupling of RGS action by a single point mutation in the G protein alpha-subunit.* J Biol Chem, 1998. 273(10): p. 5780-4.

31. Howland, D.S., Y. She, J. Kulik, C. Culpepper, L.J. DeGennaro, X. Khawaja, Rosenzweig-Lipson, K. Marquis, H.G. Dohlman, M.I. Cockett, and K.H. Young, *Transgenic expression of an RGS-resistant Gqα mutant (G188S) in rat brain.*, in *Society for Neuroscience*. 2000: New Orleans.

32. Lan, K.L., N.A. Sarvazyan, R. Taussig, R.G. Mackenzie, P.R. DiBello, H.G. Dohlman, and R.R. Neubig, *A point mutation in Galphao and Galphai1 blocks interaction with regulator of G protein signaling proteins.* J Biol Chem, 1998. 273(21): p. 12794-7.

33. Grabocka, E. and P.B. Wedegaertner, *Functional consequences of G alpha 13 mutations that disrupt interaction with p115RhoGEF.* Oncogene, 2005. 24(13): p. 2155-65.

34. Kimple, A.J., A. Yasgar, M. Hughes, A. Jadhav, F.S. Willard, R.E. Muller, C.P. Austin, J. Inglese, G.C. Ibeanu, D.P. Siderovski, and A. Simeonov, *A high throughput fluorescence polarization assay for inhibitors of the GoLoco motif/G-alpha interaction.* Comb Chem High Throughput Screen, 2008. 11(5): p. 396-409.

35. Roman, D.L., J.N. Talbot, R.A. Roof, R.K. Sunahara, J.R. Traynor, and R.R. Neubig, *Identification of small-molecule inhibitors of RGS4 using a high-throughput flow cytometry protein interaction assay.* Mol Pharmacol, 2007. 71(1): p. 169-75.

36. Zeng, W., X. Xu, S. Popov, S. Mukhopadhyay, P. Chidiac, J. Swistok, W. Danho, K.A. Yagaloff, S.L. Fisher, E.M. Ross, S. Muallem, and T.M. Wilkie, *The N-terminal domain of RGS4 confers receptor-selective inhibition of G protein signaling.* J Biol Chem, 1998. 273(52): p. 34687-90.

37. Gu, S., S. Tirgari, and S.P. Heximer, *The RGS2 gene product from a candidate hypertension allele shows decreased plasma membrane association and inhibition of Gq.* Mol Pharmacol, 2008. 73(4): p. 1037-43.

38. Yang, J., K. Kamide, Y. Kokubo, S. Takiuchi, C. Tanaka, M. Banno, Y. Miwa, M. Yoshii, T. Horio, A. Okayama, H. Tomoike, Y. Kawano, and T. Miyata, *Genetic variations of regulator of G-protein signaling 2 in hypertensive patients and in the general population.* J Hypertens, 2005. 23(8): p. 1497-505.

39. Hague, C., L.S. Bernstein, S. Ramineni, Z. Chen, K.P. Minneman, and J.R. Hepler, *Selective inhibition of alpha1A-adrenergic receptor signaling by RGS2 association with the receptor third intracellular loop.* J Biol Chem, 2005. 280(29): p. 27289-95.

40. Nieuwenhuijsen, B.W., Y. Huang, Y. Wang, F. Ramirez, G. Kalgaonkar, and K.H. Young, *A dual luciferase multiplexed high-throughput screening platform for protein-protein interactions.* J Biomol Screen, 2003. 8(6): p. 676-84.

41. Wang, Y. and K.H. Young, *Analysis of RGSZ1 protein interaction with Galphai subunits.* Methods Enzymol, 2004. 390: p. 31-52.

42. Young, K.H., Y. Wang, C. Bender, S. Ajit, F. Ramirez, A. Gilbert, and B.W. Nieuwenhuijsen, *Yeast-based screening for inhibitors of RGS proteins.* Methods Enzymol, 2004. 389: p. 277-301.

43. Huang, C., J.R. Hepler, A.G. Gilman, and S.M. Mumby, *Attenuation of Gi- and Gq-mediated signaling by expression of RGS4 or GAIP in mammalian cells.* Proc Natl Acad Sci U S A, 1997. 94(12): p. 6159-63.

44. Takesono, A., J. Zahner, K.J. Blumer, T. Nagao, and H. Kurose, *Negative regulation of alpha2-adrenergic receptor-mediated Gi signalling by a novel pathway.* Biochem J, 1999. 343 Pt 1: p. 77-85.

45. Gilman, A.G. and J.D. Minna, *Expression of genes for metabolism of cyclic adenosine 3':5'-monophosphate in somatic cells. I. Responses to catecholamines in parental and hybrid cells.* J Biol Chem, 1973. 248(19): p. 6610-7.

46. Gilman, A.G. and F. Murad, *Assay of cyclic nucleotides by receptor protein binding displacement.* Methods Enzymol, 1974. 38: p. 49-61.

47. Salomon, Y., C. Londos, and M. Rodbell, *A highly sensitive adenylate cyclase assay.* Anal Biochem, 1974. 58(2): p. 541-8.

48. Williams, C., *cAMP detection methods in HTS: selecting the best from the rest.* Nat Rev Drug Discov, 2004. 3(2): p. 125-35.

49. Renwick, W., R. Pettengell, and M. Green, *Use of filgrastim and pegfilgrastim to support delivery of chemotherapy: twenty years of clinical experience.* BioDrugs, 2009. 23(3): p. 175-86.

50. Spivak, J.L., P. Gascon, and H. Ludwig, *Anemia management in oncology and hematology.* Oncologist, 2009. 14 Suppl 1: p. 43-56.

51. Lockhart, I.A., S.A. Mitchell, and S. Kelly, *Safety and tolerability of donepezil, rivastigmine and galantamine for patients with Alzheimer's disease: systematic review of the 'real-world' evidence.* Dement Geriatr Cogn Disord, 2009. 28(5): p. 389-403.

52. Mossello, E., E. Tonon, V. Caleri, S. Tilli, C. Cantini, M.C. Cavallini, F. Bencini, R. Mecacci, M. Marini, F. Bardelli, E. Sarcone, E. Razzi, C.A. Biagini, and G. Masotti, *Effectiveness and safety of cholinesterase inhibitors in elderly subjects with Alzheimer's disease: a "real world" study.* Arch Gerontol Geriatr Suppl, 2004(9): p. 297-307.

53. Pakrasi, S., E.B. Mukaetova-Ladinska, I.G. McKeith, and J.T. O'Brien, *Clinical predictors of response to Acetyl Cholinesterase Inhibitors: experience from routine clinical use in Newcastle.* Int J Geriatr Psychiatry, 2003. 18(10): p. 879-86.

54. Ferkey, D.M., R. Hyde, G. Haspel, H.M. Dionne, H.A. Hess, H. Suzuki, W.R. Schafer, M.R. Koelle, and A.C. Hart, *C. elegans G protein regulator RGS-3 controls sensitivity to sensory stimuli.* Neuron, 2007. 53(1): p. 39-52.

55. Jang, H.J., Z. Kokrashvili, M.J. Theodorakis, O.D. Carlson, B.J. Kim, J. Zhou, H.H. Kim, X. Xu, S.L. Chan, M. Juhaszova, M. Bernier, B. Mosinger, R.F. Margolskee, and J.M. Egan, *Gut-expressed gustducin and taste receptors regulate secretion of glucagon-like peptide-1.* Proc Natl Acad Sci U S A, 2007. 104(38): p. 15069-74.

56. Nakagawa, Y., M. Nagasawa, S. Yamada, A. Hara, H. Mogami, V.O. Nikolaev, M.J. Lohse, N. Shigemura, Y. Ninomiya, and I. Kojima, *Sweet taste receptor expressed in pancreatic beta-cells activates the calcium and cyclic AMP signaling systems and stimulates insulin secretion.* PLoS One, 2009. 4(4): p. e5106.

57. Rozengurt, E. and C. Sternini, *Taste receptor signaling in the mammalian gut.* Curr Opin Pharmacol, 2007. 7(6): p. 557-62.

58. von Buchholtz, L., A. Elischer, E. Tareilus, R. Gouka, C. Kaiser, H. Breer, and S. Conzelmann, *RGS21 is a novel regulator of G protein signalling selectively expressed in subpopulations of taste bud cells.* Eur J Neurosci, 2004. 19(6): p. 1535-44.

59. Damak, S., B. Mosinger, and R.F. Margolskee, *Transsynaptic transport of wheat germ agglutinin expressed in a subset of type II taste cells of transgenic mice.* BMC Neurosci, 2008. 9: p. 96.

60. Gulbransen, B.D., T.R. Clapp, T.E. Finger, and S.C. Kinnamon, *Nasal solitary chemoreceptor cell responses to bitter and trigeminal stimulants in vitro.* J Neurophysiol, 2008. 99(6): p. 2929-37.

61. Kim, J.W., C. Roberts, Y. Maruyama, S. Berg, S. Roper, and N. Chaudhari, *Faithful expression of GFP from the PLCbeta2 promoter in a functional class of taste receptor cells.* Chem Senses, 2006. 31(3): p. 213-9.

62. Shah, A.S., Y. Ben-Shahar, T.O. Moninger, J.N. Kline, and M.J. Welsh, *Motile cilia of human airway epithelia are chemosensory.* Science, 2009. 325(5944): p. 1131-4.

63. Tizzano, E.F. and M. Buchwald, *CFTR expression and organ damage in cystic fibrosis.* Ann Intern Med, 1995. 123(4): p. 305-8.

64. Gadsby, D.C., P. Vergani, and L. Csanady, *The ABC protein turned chloride channel whose failure causes cystic fibrosis.* Nature, 2006. 440(7083): p. 477-83.

65. Riordan, J.R., *Assembly of functional CFTR chloride channels.* Annu Rev Physiol, 2005. 67: p. 701-18.

66. Hwang, T.C. and D.N. Sheppard, *Gating of the CFTR Cl- channel by ATP-driven nucleotide-binding domain dimerisation.* J Physiol, 2009. 587(Pt 10): p. 2151-61.

67. Seavilleklein, G., N. Amer, A. Evagelidis, F. Chappe, T. Irvine, J.W. Hanrahan, and V. Chappe, *PKC phosphorylation modulates PKA-dependent binding of the R domain to other domains of CFTR.* Am J Physiol Cell Physiol, 2008. 295(5): p. C1366-75.

68. Chappe, V., D.A. Hinkson, T. Zhu, X.B. Chang, J.R. Riordan, and J.W. Hanrahan, *Phosphorylation of protein kinase C sites in NBD1 and the R domain control CFTR channel activation by PKA.* J Physiol, 2003. 548(Pt 1): p. 39-52.

69. Faria, D., R. Schreiber, and K. Kunzelmann, *CFTR is activated through stimulation of purinergic P2Y2 receptors.* Pflugers Arch, 2009. 457(6): p. 1373-80.

70. Hwang, T.H., E.M. Schwiebert, and W.B. Guggino, *Apical and basolateral ATP stimulates tracheal epithelial chloride secretion via multiple purinergic receptors.* Am J Physiol, 1996. 270(6 Pt 1): p. C1611-23.

71. Kaji, I., S. Karaki, Y. Fukami, M. Terasaki, and A. Kuwahara, *Secretory effects of a luminal bitter tastant and expressions of bitter taste receptors, T2Rs, in the human and rat large intestine.* Am J Physiol Gastrointest Liver Physiol, 2009. 296(5): p. G971-81.

72. Hummel, T. and A. Welge-Lüssen, *Taste and smell : an update*. Advances in oto-rhino-laryngology. 2006, Basel ; New York: Karger. vii, 294 p.

73. Bolze, M.S., G.J. Fosmire, J.A. Stryker, C.K. Chung, and B.G. Flipse, *Taste acuity, plasma zinc levels, and weight loss during radiotherapy: a study of relationships.* Radiology, 1982. 144(1): p. 163-9.

74. Maes, A., I. Huygh, C. Weltens, G. Vandevelde, P. Delaere, G. Evers, and W. Van den Bogaert, *De Gustibus: time scale of loss and recovery of tastes caused by radiotherapy.* Radiother Oncol, 2002. 63(2): p. 195-201.

75. Saito, M., M. Hoshi, A. Igarashi, H. Ogata, and K. Edo, *The marked inhibition of the bitter taste of Polymyxin B sulfate and trimethoprim x sulfamethoxazole by flavored BMI-60 in pediatric patients.* Biol Pharm Bull, 1999. 22(9): p. 997-8.

76. Shah, P.P. and R.C. Mashru, *Palatable reconstitutable dry suspension of artemether for flexible pediatric dosing using cyclodextrin inclusion complexation.* Pharm Dev Technol, 2009.

77. Sohi, H., Y. Sultana, and R.K. Khar, *Taste masking technologies in oral pharmaceuticals: recent developments and approaches.* Drug Dev Ind Pharm, 2004. 30(5): p. 429-48.

Table 7.1: Database of apo- and Gα-complexed RGS domain structures

RGS protein family	PDB code [a]	Description	Method of structure determination [b]	Reference [c]
R4	2BV1	RGS1	X-ray crystallography	18434541
R4	2AF0	RGS2	X-ray crystallography	18434541
R4	none	RGS3	NMR (BMRB# 15178)	18434541
R4	2OJ4	RGS3	X-ray crystallography	Unpublished
R4	1EZT, 1EZY	RGS4	NMR (BMRB# 4386)	10852703
R4	2CRP	RGS5	NMR	Unpublished
R4	2IHD	RGS8	X-ray crystallography	18434541
R4	2BT2	RGS16	X-ray crystallography	18434541
R4	3C7L	RGS16	X-ray crystallography	18434540
R4	2OWI, 2JM5	RGS18	NMR (BMRB# 7106)	16964532
R4	2DLV	RGS18	NMR	Unpublished
R7	2ES0	RGS6	X-ray crystallography	18434541
R7	2A72	RGS7	X-ray crystallography	18434541
R7	2D9J	RGS7	NMR	Unpublished
R7	1FQI	RGS9	X-ray crystallography	11234020
RZ	1ZV4	RGS17	X-ray crystallography	18434541
RZ	1CMZ	RGS19	NMR (BMRB# 4407)	10452897
RZ	none	RGS20	NMR (BMRB# 5872)	14872136
R12	2I59	RGS10	NMR (BMRB# 7272)	17180548
R12	2DLR	RGS10	NMR	Unpublished
R12	2JNU	RGS14	NMR (BMRB# 15128)	18434541
RA	1DK8	Axin	X-ray crystallography	10811618
GEF	1HTJ	PDZ-RhoGEF	X-ray crystallography	11470431
GEF	1IAP	p115-RhoGEF	X-ray crystallography	11524686
R4	2GTP	RGS1 bound to $G\alpha_{i1}\cdot GDP\cdot AlF_4^-$	X-ray crystallography	18434541
R4	1AGR	RGS4 bound to $G\alpha_{i1}\cdot GDP\cdot AlF_4^-$	X-ray crystallography	9108480
R4	2ODE	RGS8 bound to $G\alpha_{i3}\cdot GDP\cdot AlF_4^-$	X-ray crystallography	18434541
R4	2IK8	RGS16 bound to $G\alpha_{i1}\cdot GDP\cdot AlF_4^-$	X-ray crystallography	18434541
R4	3C7K	RGS16 bound to $G\alpha_{o}\cdot GDP\cdot AlF_4^-$	X-ray crystallography	18434540
R7	1FQK	RGS9 bound to $G\alpha_{t/i1}\cdot GDP\cdot AlF_4^-$	X-ray crystallography	11234020
R7	1FQJ	RGS9 bound to PDEγ and $G\alpha_{t/i1}\cdot GDP\cdot AlF_4^-$	X-ray crystallography	11234020
R12	2IHB	RGS10 bound to $G\alpha_{i3}\cdot GDP\cdot AlF_4^-$	X-ray crystallography	18434541
GEF	1SHZ	p115-RhoGEF bound to $G\alpha_{13/i1}\cdot GDP\cdot AlF_4^-$	X-ray crystallography	15665872
GRK	2BCJ	GRK2 bound to $G\alpha_{q}\cdot GDP\cdot AlF_4^-$	X-ray crystallography	16339447

[a] Accessible at the Protein Data Bank, www.pdb.org.
[b] Assigned chemical shifts are accessible at the Biological Magnetic Resonance Data Bank (BMRB), www.bmrb.wisc.edu.
[c] Published references are listed as PMID numbers accessible at PubMed, www.pubmed.org.
Adapted from Soundarajaran, Kimple, *et al.* 2008 *Proceedings of the National Academy of Sciences USA*, vol. 105, pgs. 6457-6462.